DEVELOPMENT OF A DESIGN PROCEDURE FOR GREENHOUSE SOLAR HEATING SYSTEMS

by

ANTHONY KA-PONG LAU

B. Sc. (Eng), University of Guelph, Ontario, 1981

M. Sc., University of Guelph, Ontario, 1983

A THESIS SUBMITTED IN PARTIAL FULFILMENT OF

THE REQUIREMENTS FOR THE DEGREE OF

DOCTOR OF PHILOSOPHY

in

FACULTY OF GRADUATE STUDIES

Department of Interdisciplinary Studies

(Field: Bio-Resource Engineering)

We accept this thesis as conforming

to the required standard

THE UNIVERSITY OF BRITISH COLUMBIA

March 1988

39

In presenting this thesis in partial fulfilment of the requirements for an advanced degree at the University of British Columbia, I agree that the Library shall make it freely available for reference and study. I further agree that permission for extensive copying of this thesis for scholarly purposes may be granted by the head of my department or by his or her representatives. It is understood that copying or publication of this thesis for financial gain shall not be allowed without my written permission.

Department of Interdisciplinary Studies (Field: Bio-Resource Engineering)

The University of British Columbia
1956 Main Mall
Vancouver, Canada
V6T 1Y3

Date March, 1988

ABSTRACT

The techniques of computer modeling and simulations are used to develop a design procedure for greenhouse solar heating systems.

In this study a flexible computer program was written based on mathematical models that describe the various subsystems of the solar heating system that uses the greenhouse as the solar collector. Extensive simulation runs were carried out for predicting system thermal performance, and subsequently correlations were established between dimensionless variables and long term system performance.

The combined greenhouse thermal environment – thermal storage model along with the empirical relationships and the values of constants approximated in the simulation yielded reasonably accurate computed results compared to observed data. The computer model was then applied to predict the system behaviour using long-term average climatological data as forcing functions. A parametric study was made to investigate the effects of various factors pertinent to greenhouse construction and thermal energy storage characteristics on system performance. The key performance indices were defined in terms of the 'total solar contribution' and the 'solar heating fraction'.

Correlations were developed between monthly solar load ratio and total solar contribution, and between total solar contribution and solar heating fraction. The result is a simplified design method that covers a number of alternative design options. It requires users to obtain monthly average climatological data and determine the solar heating fraction in a sequence of computational steps.

A crop photosynthesis model was used to compute the net photosynthetic rate of a greenhouse tomato canopy; the result may be used to compare crop performance under different aerial environments in greenhouses equipped with a solar heating system.

This research program had attempted to generate technical information for a number of design alternatives, and as design optimization of greenhouse solar heating is subject to three major criteria of evaluation: thermal performance, crop yield and cost, recommendations were put forward for future work on economic analysis as the final step required for selecting the most cost effective solution for a given design problem.

Table of Contents

LIST OF TABLES

LIST OF FIGURES

ACKNOWLEDGEMENTS

I wish to express my sincere gratitude to my supervisor, Professor L.M. Staley, for his continuous guidance and encouragement throughout the course of this research programme. Professor Staley made himself available from time to time for discussions and gave me timely advice on a number of key points. I would also like to thank him for giving me the opportunity to join the team working on the solar greenhouse research project.

Much appreciation is also due to other members of the supervisory committee for their constructive comments and criticisms at various stages of the thesis development. Dr. N.R. Bulley served on the committee previously and pointed out some practical aspects of concern. I thank Dr. G.W. Eaton for stressing the importance of the clarity of the project objectives at the outset. Dr. M. Iqbal was instrumental in identifying the need of a design procedure for solar heating systems for greenhouses, and was helpful in reminding the author to bring the simulation results down to earth. Dr. P.A. Jolliffe exposed me to the intriguing field of plant physiology, and was supportive of my attempts to model plant response under different aerial environments. I thank Dr. K.V. Lo for participating in the committee to replace Dr. Bulley, and for his assistance in the capacity of former graduate advisor. Dr. M. D. Novak made some valuable suggestions and introduced alternative methods regarding the modeling of the greenhouse thermal environment and soil thermal storage. The author expresses his hearty thanks to each and every one of them for making this interdisciplinary programme more complete and meaningful.

Special thanks are extended to a number of individuals who provided assistance in various ways. Mr. G.J. Monk carried out the engineering management of the greenhouse research facilities, and paved the way for me to acquire additional data. Mr. D. Thomas untiringly updated me with details of the status of sensors and recorded data during the 1983/1984 experimental period. Dr. E.M. van Zinderen Bakker supplied the crop productivity data and other details of the research operation. Mr. E. Charter, Ms. T. DeLaurier, Mr. B. Ewert and Mr. A. Wakelin working in the summer on the greenhouse project have contributed to data collection and analysis. Here at UBC, Dr. T.A. Black of the Soil Science Department has kindly let me use some laboratory equipment. Mr. J. Pehlke has consistently rendered me prompt technical assistance. Ms. C. Moore, Mr. T. Nicol, Mr. D. Townsend and Mr. B. Wong have each given me some good advice on using the packaged programs available from the Computing Center.

Appreciation is also due to Dr. J.M. Molnar, former Director of Agriculture Canada Saanichton Research Station for permission to use the experimental data.

The continuous support and encouragement of my parents is greatly appreciated. And, to my friends and fellow graduate students, my cordial thanks for their companionship and care.

And, as Rome is not built in one day, I am indebted to all my teachers during these years of education and training for laying the foundation which enables me to overcome the obstacles that I encountered on the road, and to accept future challenges.

The financial assistance of the University of British Columbia through the University Graduate Fellowship, and the financial support made available to Professor Staley from the Faculty of Agricultural Sciences Research Fund, and the Natural Sciences and Engineering Research Council of Canada are gratefully acknowledged. Last, but not least, I want to thank Ms. J. Blake for her help in the capacity of administrative assistant.

Chapter 1

INTRODUCTION

1.1 General

The greenhouse industry in Canada is centred primarily in Southern Ontario and secondly in South Western B.C. Salad vegetables and flower crops are the main products followed by ornamentals and tree seedlings. The survival and expansion of a viable commercial greenhouse industry is largely dependent on the production costs, some thirty to forty percent of which are due to heating. To reduce the reliance of greenhouse heating on fossil fuels, research efforts have concentrated along two major paths: developing energy conservation techniques such as double skin coverings, lower operating temperatures and use of thermal screens; and developing alternative energy sources like solar heat and waste heat.

Optimizing the use of solar energy to partially fulfil the heating requirements of greenhouses has stimulated a number of investigations of collection and storage systems in combination since the 1970's. A summary of some greenhouse solar heating systems is shown in Table 1.1.

Solar radiation may be converted into useful heat gain by means of passive or active collections. Passive collection makes use of the greenhouse itself as an existing resource to collect excess heat trapped within the greenhouse during the daytime. On the other hand, active collection usually involves external solar collectors placed near the greenhouse; alternatively, an internal collector can be incorporated as an integral part of the greenhouse design. Furthermore, to match solar energy availability to energy needs requires the provision of sensible or latent heat storage in rock beds, wet soil, water tanks, salt ponds, containers of phase-change materials, and so on. Thus, active systems require additional electrical inputs to facilitate solar heat capture.

TABLE 1.1 Greenhouse solar heating systems

Greenhouse	Cover	Collection	Storage	Solar fraction*	Authors
Brace-style	Double polyethylene	Internal (Q-mats with water)	–	10%	Albright et al. (1979)
Hemispheric	Polyethylene	–	–	93% (estimated)	Bégin et al. (1984)
Quonset	Corrugated fibreglass/ plastic	External air solar collector with reflective wings	Soil	4%	Dale et al. (1980)
Shed-type	Corrugated fibreglass/ Tedlar	External (flat plate air collector)	Soil	43%	Dale et al. (1984)
Quonset	Double polyethylene	Solar pond (brine solution)	Solar pond	62%	Fynn et al. (1980)
Semi-cylindrical	Double acrylic	Internal (solar air heater and fan)	Rock	84%	Garzoli and Shell (1984)
Quonset	Double polyethylene	External (plastic film solar collector)	Rock and water	5%	Ingratta and Blom (1981)
Gutter-connected	Glass	Internal (fan)	$CaCl_2 \cdot 10\ H_2O$	60%	Jaffrin and Cadier (1982)
Brace-style	Double polyethylene	–	–	35%	Lawand et al. (1975)
Quonset	Double polyethylene	External (plastic film solar collector)	Gravel and water	53%	Mears et al. (1977)
Venlo-type	Glass	Internal (fan)	$Na_2SO_4 \cdot 10\ H_2O$ with additives	100%	Nishina and Takakura (1984)
Shed-type	Glass	Internal (solar air heater and fan)	Rock	35%	Staley and Monk (1984)
Conventional	Glass	Internal (fan)	Soil	20%	Staley and Monk (1984)
Quonset	Fibreglass	Internal (fan)	Rock	33%	Willits et al. (1980)

*measured over a period (month, season or annual).

Internal collection has been tested by Albright et al. (1979), Areskoug and Wigstroem (1980), Blackwell et al. (1982), Caffell and MacKay (1981), Garzoli and Shell (1984), Jaffrin and Cadier (1982), Kozai et al. (1986), Milburn and Aldrich (1979), Nishina and Takakura (1984), Portales et al. (1982), Staley et al. (1984), Willits et al. (1980), and Wilson et al. (1977). The collected solar heat was transferred to the storage, and the air returned to the greenhouse generates a closed-loop cooling effect to some extent.

Experiments with an external collection scheme were conducted by Chiapale et al. (1977), Connellan (1985), Dale et al. (1980, 1984), Fynn et al. (1980), Ingratta and Blom (1981), McCormick (1976) and Mears et al. (1977).

Internal greenhouse collection systems have to operate at lower temperatures than external collectors, so that healthy plant growth will not be jeopardized under relatively hot and humid conditions. However, the merits of an internal collection scheme are primarily two-fold. Firstly, it saves on capital cost and secondly, no extra land is required. It was noted by van Die (1980) that if a solar heating system were ever to be used by the greenhouse industry, growers would prefer it to be an integral component.

Greenhouses with shapes quite different from conventional ones have been studied by Ben-Abdallah (1983), Begin et al. (1984), Lawand et al. (1975) and Turkewitsch and Brundrett (1979).

As summarized in Table 1.1, with these active and passive systems, the solar heating fraction, f, defined as the percentage of greenhouse heating load that is supplied by solar energy, was reported to vary from 4% to 100%, measured on a monthly, seasonal or annual basis. It should be noted that some of the high f-values encompassed the contribution from other energy conservation measures such as nighttime use of retractable thermal curtains.

Some researchers (Arinze et al., 1984; Cooper and Fuller, 1983; Duncan et al., 1981; Santamouris and Lefas, 1986, Shah et al., 1981 and Willits et al., 1985) have coordinated their experimental and theoretical works using mathematical models to study the thermal performance of their research greenhouses. Others presented models that are pertinent to the greenhouse thermal environment (Avissar and Mahrer, 1982; Chandra et al., 1981; Froehlich et al., 1979; Kimball, 1973; Kindelan, 1980; Short and Montero, 1984; Soribe and Curry, 1973 and Takakura et al., 1971). Kimball (1981) developed perhaps the most detailed computer model thus far, which is similar to the modular TRNSYS program (Klein et al., 1975) written primarily for residential solar heating systems. His model can couple the thermal environment of greenhouses with some energy-related external devices such as heat exchangers and rock bed thermal storage.

Whereas experimental results indicated that a solar heating system had satisfactory or poor performance at a specific location, it is not known how the same or a similar system with modified design parameters might behave under climatic conditions that prevail in other places. Experiments with each plausible design are too expensive because of the high costs of heating a greenhouse, let alone monitoring full-scale tests over many years to assess the system performance. Computer modeling and simulations can implement a systematic approach to solve these uncertainties and enable designers to evaluate long-term average system behavior for different design alternatives. The simulation results derived from extensive simulations may also be reduced to generate a simplified design procedure, through which designers and engineers serving the greenhouse industry can readily extract the necessary technical information.

While many more innovations are yet to appear and be tested, research work in greenhouse solar heating has provided a reasonably broad base for the development of design methods for greenhouse solar heating systems as an extension to the 'f-chart method' for active solar residential space and water heating systems (Klein, et al., 1976) or the 'solar load ratio method' for similar but passive systems (Balcomb and MacFarland, 1978).

Design optimization of greenhouse solar heating is subject to three major criteria: thermal performance, crop yield and cost. With adequate technical information generated for a number of design alternatives, economic analysis is the final step required for selecting the most cost-effective solution for a given design problem.

1.2 Objectives

The objectives of this research work reflect, in part, the steps leading to the establishment of a simplified design procedure for solar greenhouse design. They are listed as follows:

1. to develop mathematical models that describe the greenhouse thermal environment and thermal storage,
2. to develop a computer program based on the overall mathematical model that is capable of interconnecting various subsystems of the solar heating system,
3. to carry out simulations for validating the models with existing experimental data and predicting long-term system thermal performance,
4. to quantify the effects of important design parameters on system thermal performance and crop net photosynthesis,
5. to develop correlations between dimensionless variables and the system long-term thermal performance.

1.3 Scope of the Study

While enabling a designer to readily predict the solar fraction, the development of the f-chart and solar load ratio methods for systems with standard configurations necessarily put restrictions on their usage. Since no 'standard' greenhouse solar heating system has yet been defined, the present work aims at the establishment of a simplified design method for two generic systems that have each been subjected to intermittent testing at the Agriculture Canada Saanichton Research Station located at Sidney, B.C. (latitude 48.5 °N, longitude 123.3 °W) between 1980 and 1984.

1.4 Organization of the Manuscript

The thesis is organized into five chapters. A brief outline of the rationale for the research programme is presented in chapter 1, where the objectives and scope of the study are also specified.

In chapter 2, a critical review of the work done by other researchers is made. Experiments with greenhouse solar heating systems using the internal and external collection methods are cited and described in detail, followed by a review of mathematical modeling of solar greenhouses, which includes the greenhouse thermal environment and thermal energy storage. An account is also given of the existing design methods for solar heating systems, for residences and greenhouses alike. Finally, effects of environmental factors on greenhouse plant growth are introduced, and research works in the area of modeling crop growth are described.

Chapter 3 presents the simulation models for two generic solar heating systems for greenhouses. System I represents 'augmented internal collection with sensible heat (rockbed) storage' while system II is representative of 'internal collection with sensible heat (wet soil) storage'. Results of model validation with existing experimental data are reported separately for the two systems investigated.

A parametric study is launched in chapter 4 to study the variation of system behaviour under different conditions as affected by parameters pertinent to greenhouse construction and thermal storage characteristics. Modifications to the simulation method employed in chapter 3 are explained, and some uncertainties of the modeling technique are examined by a sensitivity analysis. Results of the parametric study are analyzed and used for the synthesis of a simplified design procedure. An example is given demonstrating the steps to be followed in using the proposed design method. A special section is assigned to study crop performance by means of a net photosynthesis model as derived from literature review.

Lastly, the thesis is concluded with suggestions for future theoretical and experimental research work in chapter 5.

The appendices contain listings of the computer program developed in this project for simulating system performance, as well as a small program that implements the simplified design procedure. Psychrometric equations, and expressions for direct (beam) radiation interception factor and diffuse radiation view factor are also included.

Chapter 2

LITERATURE REVIEW

2.1 Greenhouse Solar Heating Systems

2.1.1 Internal collection

Wilson et al. (1977) adopted the notion of the greenhouse as a solar collector; they attempted to find ways to improve the collection efficiency which for the greenhouse under study at Ithaca, N.Y. was found to be 32%. They proposed to increase this percentage by modifying the greenhouse shape similar to the Brace-style design. For a given floor area, the authors suggested that taller structures will enhance temperature stratification without endangering plants at the bench level.

Albright et al. (1979) tested yet another method of improving the greenhouse as a passive solar collector, whereby a number of 12.2 m long x 0.254 m wide flat polyethylene tubings known as Q-mats were filled with water and laid between rows of potted poinsettias and chrysanthemum plants inside a Brace-type greenhouse. These mats increase the thermal mass within the greenhouse by 9 MJ/$^{\circ}$K. The authors pointed out that regions with severe winter weather cannot expect to have enough excess solar heat during even the best of days to provide a significant portion of the nighttime heat in a conventional greenhouse without adapting other energy conservation techniques. They further noted that if day and night greenhouse temperatures are permitted to vary according to ambient conditions, passive solar systems could be more beneficial. For the Q-mat system, contribution of stored energy to the nighttime heating demand was found to be 10% and it increased to 50% for the same house with highly insulated night cover that has reduced the heating load by 80%.

Milburn and Aldrich (1979) tested a collection system using a plastic tube with perforations along the greenhouse ridge, while a fan helps to circulate the warm air from there to the rockbed heat storage. The authors found that with this method of collection, a single cover greenhouse located in Pennsylvania could have 10 to 20% of the annual heating load met by solar energy. The system performance relied on outdoor temperature, crop zone temperature and air flow rate.

Staley et al. (1982) designed an air-type solar heating system for a shed-type glasshouse (that is, glass greenhouse) located at Sidney, B.C. (Fig. 2.1). The 6.4m x 18.3m structure is formed from one half of a conventional gable roof greenhouse that has had its north roof eliminated and north wall insulated. The greenhouse is used as the collector whereby a 97 m^2 low-cost black thermal shade cloth mounted against its inside north wall surface acts as the absorber plate. The roof and side vents are opened to different extents when inside air temperature reaches 28°C or above in order to cool the greenhouse by way of natural ventilation. Heated air that rises up the absorber plate is drawn by a centrifugal fan into a slotted duct and conveyed downwards to be stored in two parallel underground horizontal rockbeds. Cooled air returns to the greenhouse to complete the closed circuit. At night, the air flow direction is reversed and the stored energy is recovered to heat the greenhouse. This system represents the method of 'augmented internal collection with sensible (rockbed) heat storage'. The annual energy savings amounted to 29% and 35% during the operating periods of 1980-81 and 1983-84 respectively.

All equipment designed to adjust the indoor environment, including the solar heating systems, were controlled by a microprocessor which performed the following tasks:

- to integrate indoor and outdoor climatic information
- to control the greenhouse temperature to precise but flexible set-points
- to adjust ventilation and auxiliary heating systems to conserve energy
- to optimize solar energy collection, storage and recovery
- to control nutrient supplies to plants grown with the Nutrient Film Technique

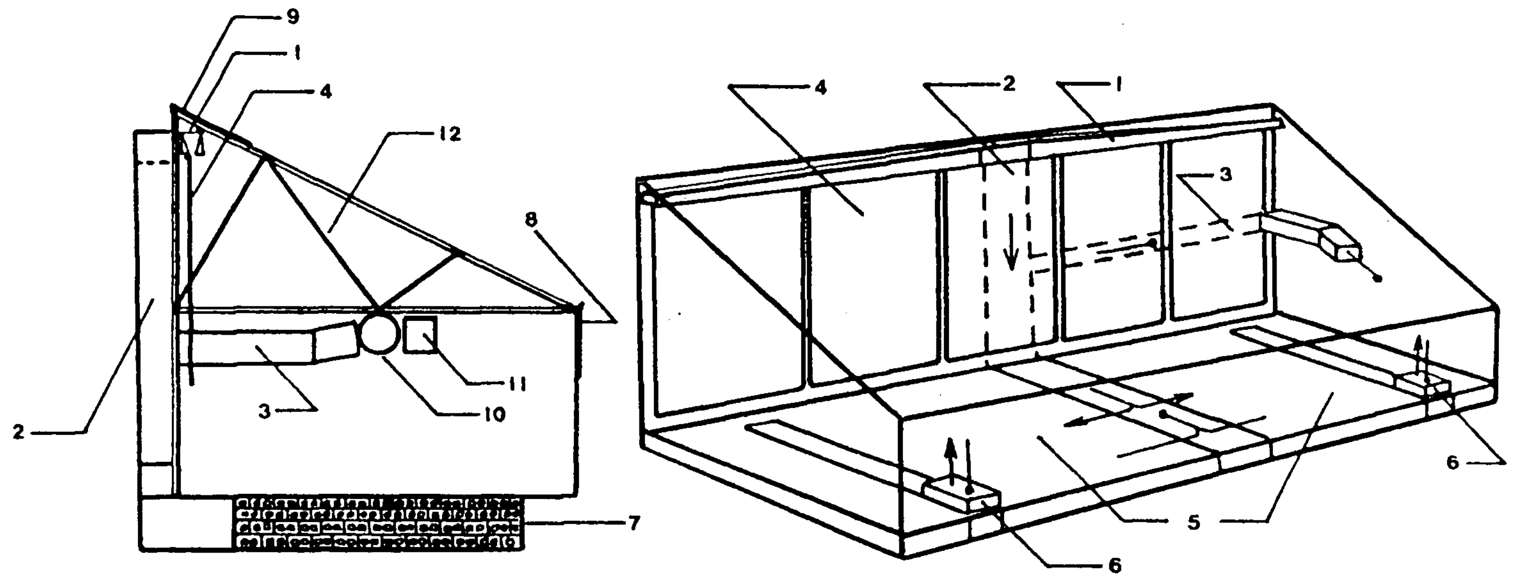

section view toward east wall

schematic diagram

1: tapered air duct   2: vertical air duct   3: horizontal air duct

4: vertical absorber plate   5: rockbed thermal storage   6: storage air inlet/outlet

7: rockbed storage partition   8: side vent   9: roof vent

10: polytube   11: auxilliary heater   12: light weight pipe struts

airflow direction (storage charging)

airflow direction (storage discharging)

Fig. 2.1 Solar heating system for a shed-type greenhouse with rockbed thermal storage

(NFT)

- to collect experimental data on a continuously integrated basis

Blackwell et al. (1982) described a simple system that stores the heat generated within a tunnel-type greenhouse covered with fiberglass reinforced polyester. A solar air heater consisted of ten air channels formed from overlapping five sheets of galvanized roofing materials mounted in the northern side of the apex, thus the angle of inclination of the absorber varies from 21.5° along the northern edge to almost horizontal at the top. During the day, a fan draws the heated air into a rock bed thermal storage, which acts as the solar heat sink. At nighttime, its function is reversed.

Areskoug and Wigstroem (1980) reported findings of experimental investigations of an earth heat accumulation system directly beneath a greenhouse. During July and August in Alnarp, Sweden (62 °N) excess solar heat from the greenhouse was collected by heat pumps. Heat exchange takes place between water that flows through a system of buried polyethylene pipes and the moist soil. The soil temperature at 2 m deep reached 42°C during the loading period. In the rest period of September and October, before unloading actually took place, heat losses through the sides and bottom, as well as heat flow to greenhouse via the soil surface led to a drop of temperature to 28°C. By early January, the temperature fell further to below 10°C. Seasonal storage of solar heat as originally desired did not seem to be feasible with the system studied. They suggested that if the soil storage was intended to capture all excess solar heat during the summer, a network of vertical pipes that extended to a depth of 10–15 m might be necessary.

Staley et al. (1984) monitored the performance of an earth thermal storage coupled to a conventional gable roof glasshouse that collects excess daytime heat (Fig. 2.2). Design and construction details were reported by Monk et al. (1983). When interior air temperature rises above 22°C, warm air is drawn through a network of

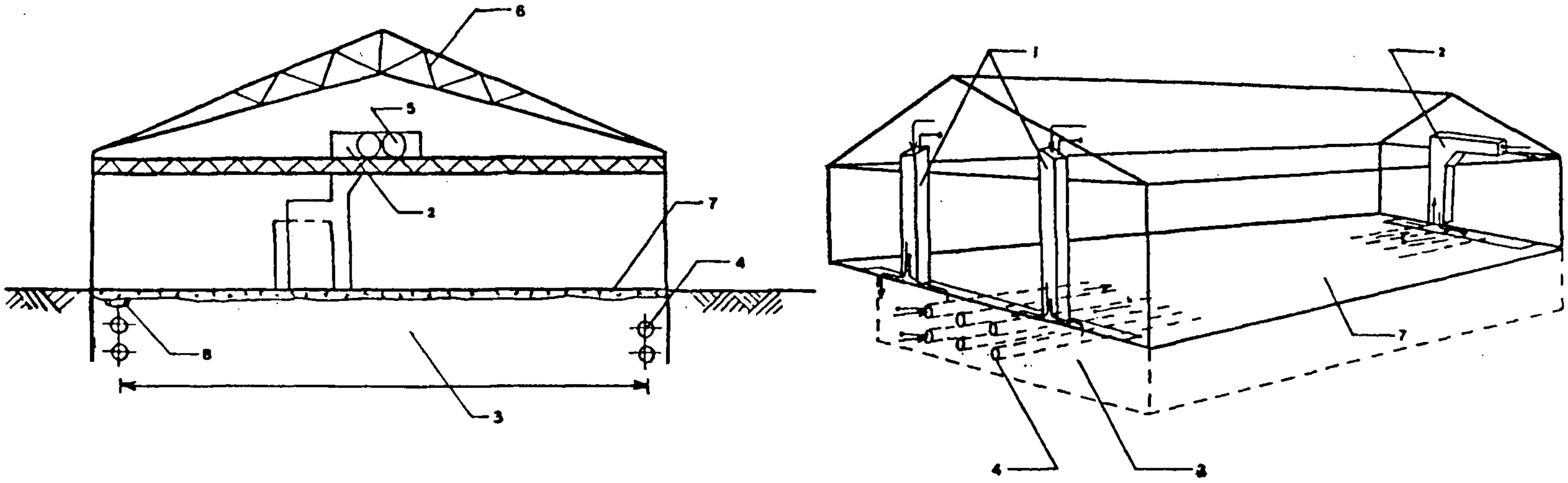

section view towards east gable

schematic diagram

1. vertical air ducts bolted to the top of west gable plenum chamber

2. centrifugal fan housing 3. earth (heavy clay loam) thermal storage

4. 100 mm diameter PVC pipes, total 17 rows on 0.63 m centres

5. polytube 6. energy truss for sloped thermal curtains

7. 75 mm porous concrete floor 8. 50 mm gravel layer

⟶ airflow direction (storage charging)

—• airflow direction (storage discharging)

Fig. 2.2 Solar heating system for a conventional greenhouse with earth thermal storage

34, 0.1m diameter PVC sewer pipes buried in two layers longitudinally in the soil beneath the greenhouse porous concrete floor. Excess irrigation water is allowed to seep through this floor thereby keeping the soil wet. Heat is transferred from the air in the pipe to the soil storage. At night, when greenhouse temperature drops below 17°C, cool air is circulated through the pipes to pick up heat from the storage and deliver it to the greenhouse. This system is representative of 'internal collection with sensible (soil) heat storage'. During the 1983–84 heating seasons, stored heat was able to supply 20% of the heat demand of the greenhouse.

The concept of latent heat storage applied to horticulture was tested at the La Baronne solar greenhouse complex (42°N) in France (Jaffrin and Cadier, 1982). The experiment was run in a 500 m^2 multispan glasshouse devoted to rose production. The excess solar heat available inside the greenhouse is extracted from the top of the roof ridges, thence transferred for storage in an underground network of flat bags made of a polyester–aluminum–polyethylene complex and filled with 13.5 tonnes of Calcium chloride decahydrate ($CaCl_2.10H_2O$) as a phase change material (PCM). This PCM melts at 25°C and half solidification occurs at 15°C. The storage capacity due to the latent (PCM) and sensible (soil) heat of the materials add to a total of 155.4 MJ/m^3. At night, fans forced cool greenhouse air through the storage to recover stored heat. Heat flux across the soil surface also contributed to nighttime heating supply to the insulated greenhouse fitted with inflated polyethylene film. During the December 1979 – April 1980 heating season, this solar greenhouse achieved 60% savings in gas cunsumption compared to the control, and net savings of 50% when electricity is accounted for.

Nishina and Takakura (1984) also presented preliminary results of studies in a solar greenhouse with latent heat storage system at the Kanagawa Horticultural experiment station. The experiments were carried out in a 352 m^2 Venlo type glasshouse. During day time, when the inside temperature was above 22°C, air was drawn by fans into the heat storage unit placed within the greenhouse (Fig. 2.3). Warm air exchanged heat with 2.5 tonnes of sodium sulphate decahydrate ($Na_2SO_4.10H_2O$) with chemical additives that are encapsulated in 200 aluminum laminated polyethylene bags. This PCM has a melting point around 20°C and a heat of fusion of 235.2 MJ/m^3. The roof ventilators were opened when inside air temperature reached 28°C. During the December 1982 - March 1983 period, 50 % of the night time heating requirement was supplied by PCM while the other 50 % was met by heat released from the soil surface. No auxiliary heating was needed since heating load is already reduced by two energy conservation measures: one to two layers of thermal screens depending on outside air temperature, and splitting night time set-point temperatures between 12 and 8°C.

2.1.2 External collection

Mears et al. (1977) developed a low-cost solar collector for greenhouse applications using plastic films (Fig. 2.4). A black polyethylene layer serves as the absorber plate and is sandwiched between four layers of 6 μm clear, ultraviolet stabilized polyethylene films that form two air inflated pillows on each side of the black sheet. The dead air space created by the inflated section acts as a modest insulator. Warm water leaving the collector is stored under the greenhouse porous concrete floor in a stone/water mix. The heat capacity of the stone water mix is about 3550 kJ/m^3K. The composite floor also acts as the primary heat exchanger for transfering heat to the greenhouse. Vertical curtains (double sheets of polyethylene) with warm water in between trickling down from the distribution pipe to the floor are placed between rows of plants and act as secondary heat exchanger units that increase the thermal coupling between the water in the floor storage and the greenhouse environment at night. Over four full heating seasons from 1976 to 1980, the researchers found that stored solar energy met 44.8% of the greenhouse heating

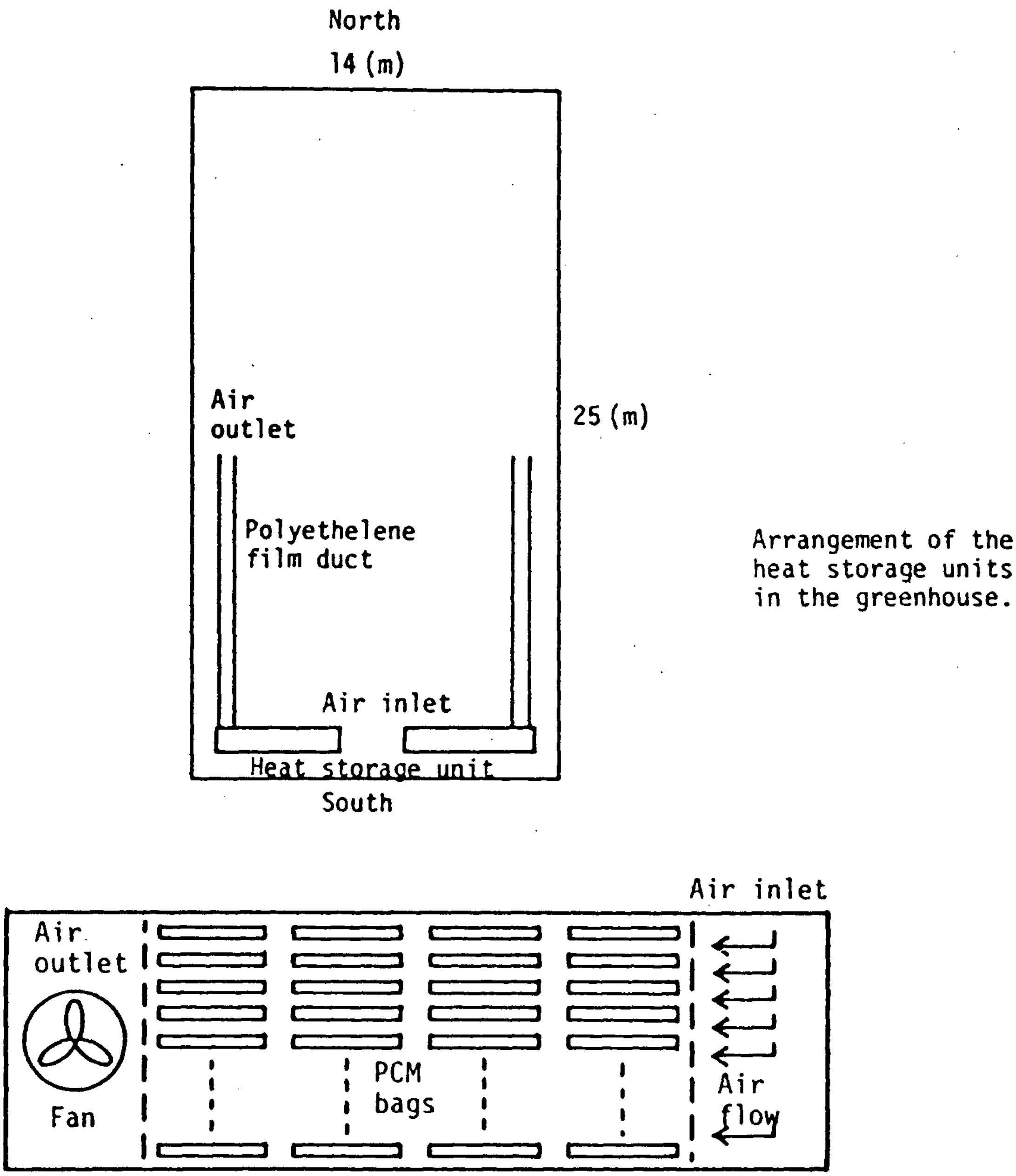

Fig. 2.3 Schematic diagram of the latent heat storage unit

(Nishina and Takakura, 1984)

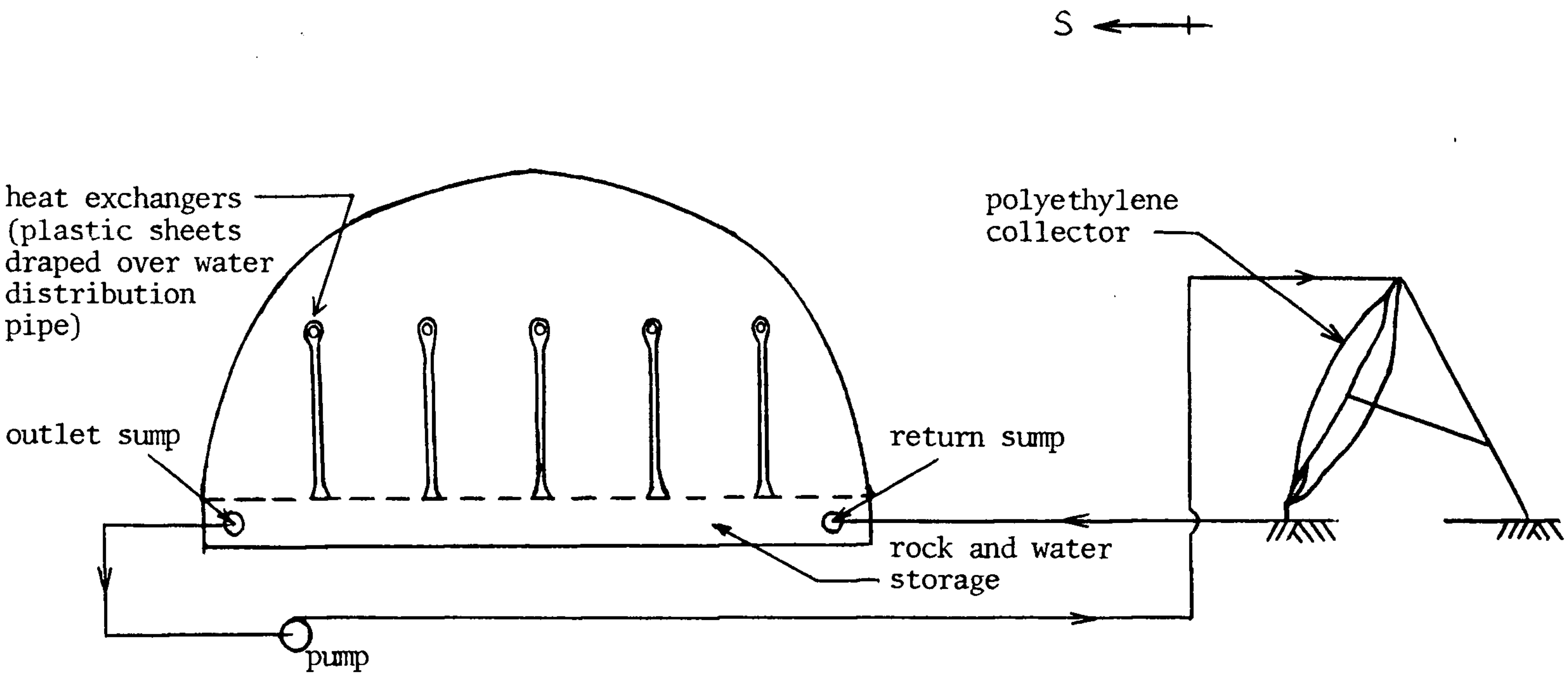

Fig. 2.4 Greenhouse solar heating system with active collector and thermal storage (Mears et al., 1977)

requirement that had been reduced by 44% through nighttime deployment of thermal curtains.

Ingratta and Blom (1981) evaluated the performance of a similar system for the climatic conditions at the Vineland Station of the Horticultural Research Institute of Ontario. No vertical curtains were used to enhance heat transfer between thermal storage and greenhouse environment. The system is comparatively inexpensive, and could be installed for a cost of \$35 to \$40/m^2 (1980 value) of greenhouse floor area. A water flow rate of 1.86 l/s produced a collector efficiency of 49.3%. Yet, only 4.9% savings in fossil fuel consumption was achieved during the period September 1979 to May 1980. Based on these figures alone, the authors suggested that active solar heating of greenhouses in Ontario did not appear to be feasible; however, refinement of collection and long term storage technology may alter this situation.

Another type of active solar collection system is the solar pond (Fig. 2.5). Fynn et al. (1980) carried out experiments using a salt gradient pond for greenhouse heating. An 18.3 m long, 8.5 m wide and 3 m deep pond with vertical walls was constructed. The pond was lined with a layer of high density polyethylene material that was able to meet the stringent physical and biological requirements. The bottom half of the pond is a 20% salt (sodium chloride) solution convective zone (LCZ), whereas the top half is a non-convective zone (NCZ) due to a salt concentration gradient that varies from fresh water at the top to 20% salt at the LCZ/NCZ interface. The gradient zone is transparent to incoming shortwave radiation and opaque to re-radiated thermal energy, and it provides good insulation against conductive losses from the top. Heat was normally extracted from the pond by pumping the hot brine from the LCZ through a shell and tube heat exchanger. When the brine temperature was low (typically between 20 and 40 °C in the middle of winter at Wooster, Ohio), the fresh water leaving the heat exchanger was manually switched to circulate through a heat pump evaporator. The higher source temperature compared to outside air or

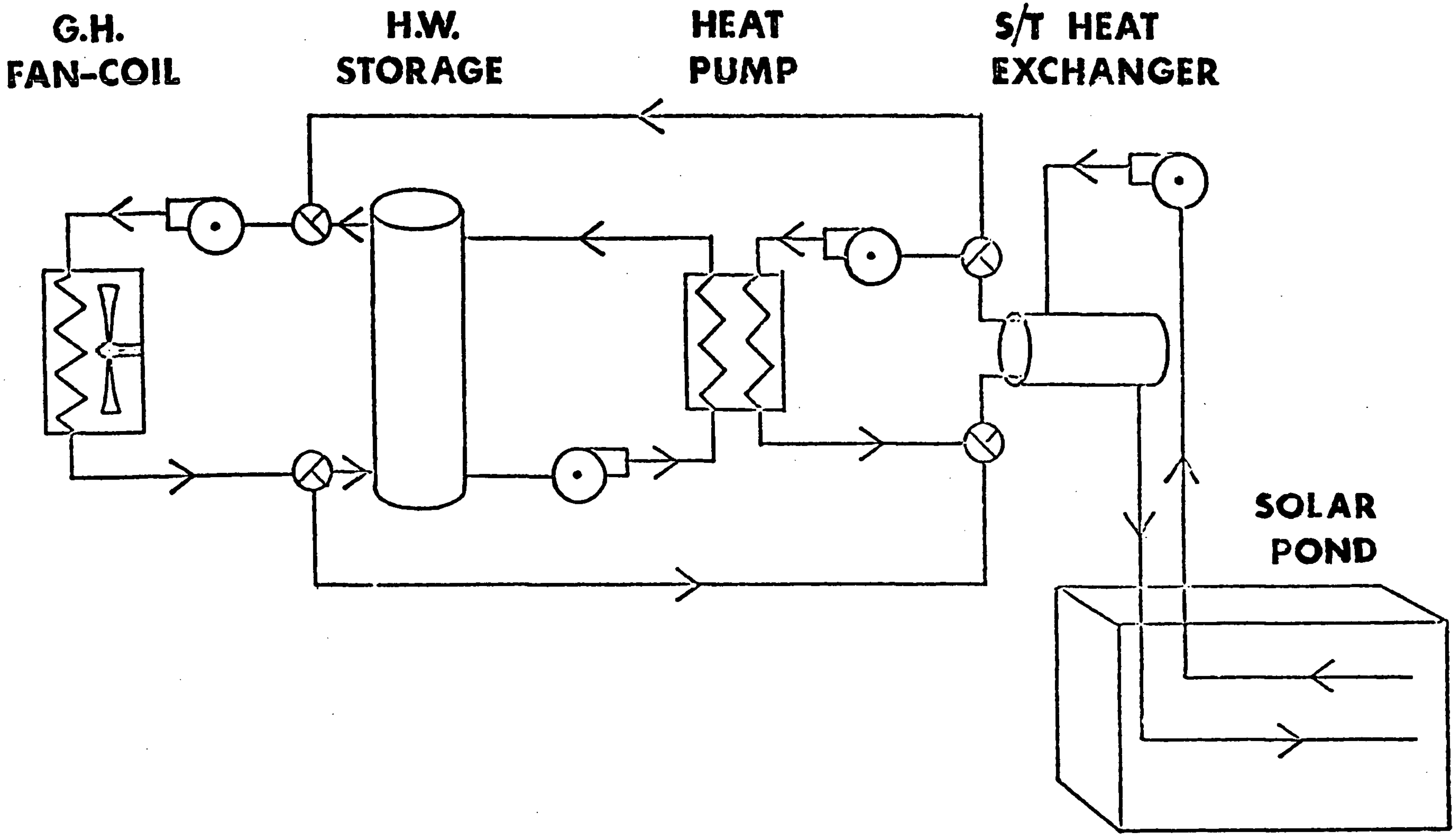

Fig. 2.5 Schematic of the solar pond–greenhouse heating system which included a direct exchange loop and a heat pump loop (Fynn et al., 1980)

well water improves the coefficient of performance of the heat pump. The fresh water circuit transferred heat from the heat exchanger or the heat pump to a storage tank that eventually supplies heat to the greenhouse. The solar pond started to collect and store energy in mid-March of 1979. During the fall period, solar contribution to the greenhouse heating load was found to be 79%, although this amount of solar heat represents merely 4.5% of the solar radiation that fell on the pond in 1979.

Dale et al. (1980) investigated a solar air collection - ground water heat storage system for heating greenhouses. The collector was fabricated with reflective wings at the top and bottom, and its tilt was 30 and 60° for summer and winter months at West Lafayette, Indiana. The subterranean groundwater soil storage unit was enclosed in an impermeable pond liner and sealed to prevent vapor leaks. To reduce heat losses to the surroundings, it was insulated on the sides and top. The warm air from the collector outlet was circulated through a network of corrugated 0.1 m diameter PVC drainage pipes buried in the storage unit, thus heating up the soil. The average soil temperature around mid-September was 32.2°C, but reached only 15.5 °C by late January. Hence, the soil storage subsystem was unable to retain heat for an extended time period. During the winter of 1979-1980, stored solar heat supported barely 4% of the greenhouse heat load. Aside from the soil heat losses, this low percentage could be due to the inefficiency incurred by simultaneously subjecting the soil storage unit to regeneration and extraction modes using two sets of alternating hot and cold pipes.

A similar project was initiated by Dale et al. (1984) in October 1980 with the goal of developing an energy efficient greenhouse, and combined with an air type flat-plate collector (Fig. 2.6). A shed-type greenhouse was constructed with a vertical south wall and a tilted north roof. The north wall is insulated, while the remaining walls and roof are covered with Filon coated corrugated fiberglass on the outside and a layer of tedlar (polyvinylfluoride) on the inside. Thermal curtains were closed at

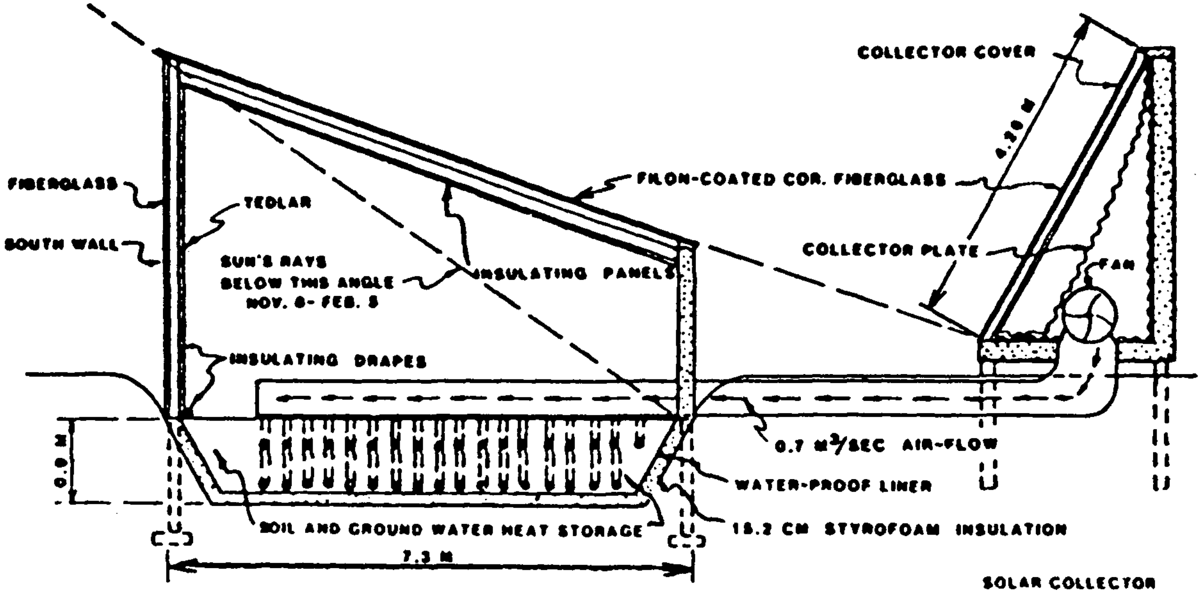

Fig. 2.6 Cross-section through greenhouse and solar energy collector (Dale et al., 1984)

night. The 40.7 m^2 collector is fabricated of the same type of cover materials as the greenhouse roof with a blackened aluminum absorber plate. Collector area to greenhouse floor area ratio is 1:2. Transfer of collected heat to the saturated soil storage underneath the greenhouse is achieved by means of 45, 0.1m diameter non-perforated plastic tiles that extend in two layers through the soil. For the heating season between November 1980 to February 1981, energy contribution from heated soil amounted to 43.4% of total greenhouse heating demand. It should be noted, however, that this percentage is based on reduced heat load brought about by the energy conservation measures mentioned earlier. Without these measures, the solar heating fraction would have been 10.7 %. They suggested that the auxiliary solar collector may be eliminated; instead, air from within the greenhouse during the daylight period can be circulated through the heat transfer pipes when the greenhouse approaches 28 to 30° C.

2.2 Mathematical Modeling of Solar Greenhouses

2.2.1 Greenhouse thermal environment

Very little glasshouse (greenhouse) climate research had been reported during the many years of their use until Businger (1963) gave a detailed description of the energy budget of the glasshouse, which involved the usual heat transfer mechanisms, as well as evaporation, condensation and ventilation. He partitioned the greenhouse into three components: the greenhouse cover, the air and the soil surface.

Walker (1965) presented a single equation for predicting air temperature in ventilated greenhouses as environmental conditions or air flow rate is changed. Neglecting the energy associated with respiration and photosynthesis, and the heat released by equipment, the energy balance for inside air is given as

$$Q_s + Q_{au} + Q_{cn} + Q_g + Q_v + Q_t = 0 \tag{2.1}$$

The symbols used in the above equation are defined in the 'Notation' section placed at the end of this chapter. In subsequent chapters, separate notations are used. Symbols found in figures and tables in the entire manuscript are also explained therein. This expression also permits some preliminary determination of heating and ventilation requirements of greenhouses. However, the impact of changes in design parameters on the microclimate cannot be assessed.

Models that divide the greenhouse into its essential elements started perhaps with Takakura et al. (1971). The authors realised that measured leaf temperature and inside air temperature were not the same, especially during daytime, and as photosynthetic rate depends on the former, they introduced the plant canopy into the heat (energy) and mass (moisture) balance models.

From top to bottom, these components are: the cover (inside and outside surfaces), the inside air, the plant canopy, floor surface and the soil. Heat balances are then given by:

$$Q_{so} + Q_{to} + Q_{cvo} + Q_{cd} = 0 \tag{2.2}$$

$$Q_{si} + Q_{ti} + Q_{cvi} + Q_{cdi} - Q_{cn} = 0 \tag{2.3}$$

$$Q_{cvp} + Q_{cvf} + Q_{au} - Q_{cvi} - Q_v = 0 \tag{2.4}$$

$$Q_{sp} + Q_{tp} - Q_{cvp} - Q_{\lambda p} = Q_{mp} \tag{2.5}$$

$$Q_{sf} + Q_{tf} - Q_{cvf} + Q_{cdf} = Q_{mf} \tag{2.6}$$

$$Q_{t1} - Q_{t2} = Q_{ms} \tag{2.7}$$

and mass balance for the inside air given by

$$M_e - M_v - M_{cdi} = M_{ma} \tag{2.8}$$

Since then, similar models were presented by Kimball (1973), Maher and O'Flaherty

(1973), Takami and Uchijima (1977), Soribe and Curry (1973), Seginer and Levav (1970), Froehlich et al. (1979), Chandra et al. (1981), Kindelan (1980), and Avissar and Mahler (1982). These models differed in the degree of complexity with which they treat the various fluxes involved in the above equations, with some improving on the shortcomings of others. Each model was able to bring about reasonably accurate predictions of the greenhouse environmental conditions that did not deviate considerably from measured data, as collected from experiments that lasted from a three-day to six-month period. This tends to suggest that these models may not be very sensitive to the magnitudes of certain of their parameters, and therefore very complicated models might not be warranted, depending on the objectives of the research.

The extension of these energy balance models to incorporate features of a greenhouse solar heating system was presented by Duncan et al. (1981), Kimball (1981), Cooper and Fuller (1983), Arinze et al. (1984) and Willits et al. (1985). The computer model presented by Kimball was developed for both conventional and solar greenhouses. It couples the greenhouse to energy-related devices such as curtain heat exchangers, rockbeds, infrared heaters, and evaporative coolers. In essence, equations (2.2) through (2.8) are again valid for solar greenhouses, except that the energy balance of inside air must now include the heat transferred to storage during charging or recovered from storage during discharging, thus

$$Q_{cvp} + Q_{cvf} + Q_{au} - Q_{cvi} - Q_v - Q_{td} = 0 \tag{2.9}$$

2.2.1.1 Solar radiation level inside the greenhouse

In the energy budget, solar radiation constitutes the major heat input to the greenhouse and it should be calculated as accurately as possible. The following review is concentrated on solar radiation transmission characteristics of greenhouses. In fact, many studies have been carried out to evaluate the performance of greenhouses in transmitting light, and results were generally presented with regard to the glazing level transmittance, τ, or more frequently the effective transmissivity, τ_e . Whereas τ showed mainly the effects of the optical properties of glazing materials, sky clearness and solar angle of incidence, τ_e is strongly influenced by the greenhouse geometric configuration and internal structures. Though various authors used different terminologies in reporting their research outcomes, τ_e can generally be defined as the amount of solar radiation (broadband or PAR) received on an inside horizontal surface as a percent of that falling on an outside horizontal surface of the same area. The inside horizontal surface may be taken at any height, but the plant canopy level is the most appropriate reference while floor level measurements have also been reported.

Research works pertinent to τ are reviewed first, followed by those that concern τ_e .

Walker and Slack (1970) made a comparative summary of the optical properties of selected rigid and film greenhouse covering materials, including glass, fiberglass, PVC, polyvinyl, polyester, UV-polyethylene and ordinary polyethylene. Spectral transmittance values were measured with a Bausch and Lomb spectrophotometer. Several of the materials, polyvinyl, polyester, fiberglass and rigid PVC show a reduced transparency in the 735 nm wavelength, which would have a significant effect upon flowering and stem elongation of plants. Transmittance of global (direct and diffuse) solar radiation for all materials with the exception of standard fiberglass was about 90 percent; fiberglass exhibited a marked difference between direct and global transmittance.

Later in the decade, Godbey et al. (1979) carried out extensive experimental work to determine values of τ for a variety of glazing materials. Global as well as direct solar energy transmission were measured for six angles of incidence ranging from the normal (0°) to 67°. Results were presented for single-layer samples and two-layer combinations. Measurements of long wavelength transmission were also included in their project.

In his comprehensive study of the greenhouse climate, Businger (1963) introduced a daylight coefficient which related inside and outside short-wave radiations, taking into account the optical losses through glass and the influence of the construction, the orientation and the location of the greenhouse on a lumped basis. This coefficient varies from 0.55 under diffuse light conditions to 0.70 when direct light predominates for glass panes 0.6 m wide in wooden construction greenhouses; a larger size of glasspane (0.72 m) favored a higher value.

Edwards and Lake (1965) measured solar radiation transmission in a large-span 1800 m^2 east-west oriented greenhouse. Outside global and diffuse radiations, as well as the transmission onto an inside horizontal surface were measured at various positions in the greenhouse. Obstructions to diffuse radiation caused by various components of the structure was found by making measurements on overcast days at various stages of construction. The mean daily transmissivity of the diffuse component was found to be 64 to 69%; that of the beam component, 57% in summer and 68% in winter. He pointed out that changes in shape rather than structure could lead to improvements in transmission, particularly that of direct radiation.

Manbeck and Aldrich (1967) were probably the first ones to generalize direct visible solar energy transmission in greenhouses using an analytical procedure. Computations were done with various planar and curvilinear surfaces that represent rigid plastic greenhouses. Results showed that at a latitude of 45 $^{\circ}$N, an E-W oriented gable-roof surface transmitted more solar radiation in the winter months and slightly less in early fall and spring than one oriented N-S. However, a greenhouse with ridge aligned N-S is superior to an E-W one when it is located at a more southern latitude of 35 °N. A latitude of 40.8 °N is about the neutral location where E-W and N-S houses are more or less equally effective in light transmission. These results are similar for the vault-type fiberglass greenhouse.

A more detailed analytical method was outlined by Smith and Kingham (1971) for calculating the solar radiation components falling within a single-span glasshouse located at Kew, England. They introduced an angle-factor F and separately evaluated this factor using geometric and trigonometric analyses for the direct and diffuse radiations transmitted by a glass surface (roof or wall) and subsequently intercepted by the floor of the house. Two glasshouses, one with lumber construction and the other a more modern wide-span metal type were compared in terms of percentage transmission of total radiation at the floor level. For the modern greenhouse aligned E-W, the calculated values of τ_e range from 0.66 in June to 0.70 in January, and were said to be in good agreement to within 5% with the observed values of Edwards and Lake (1965).

Experimental rigid plastic greenhouses ranging in size from 20 m^2 to 40 m^2 were used by Aldrich and White (1973) to study the relationship between structural form and quality and quantity of transmitted solar energy in such greenhouses. Measurements were taken on selected days during two winter growing seasons. Results showed that there is an insignificant difference in τ_e due to single acrylic sheet cover or glass, with values ranging from 0.64 to 0.84, compared to that of a fiberglass cylindrical vault which varied from 0.58 to 0.74.

The Brace Research Institute style greenhouse was proposed by Lawand et al. (1975) as an unconventionally shaped greenhouse for colder (northern) regions. The basis for the new design was to maximize solar radiation input while reducing high heat losses associated with conventional greenhouse designs. As illustrated in Fig. 2.7, the greenhouse is oriented on an east-west axis, the

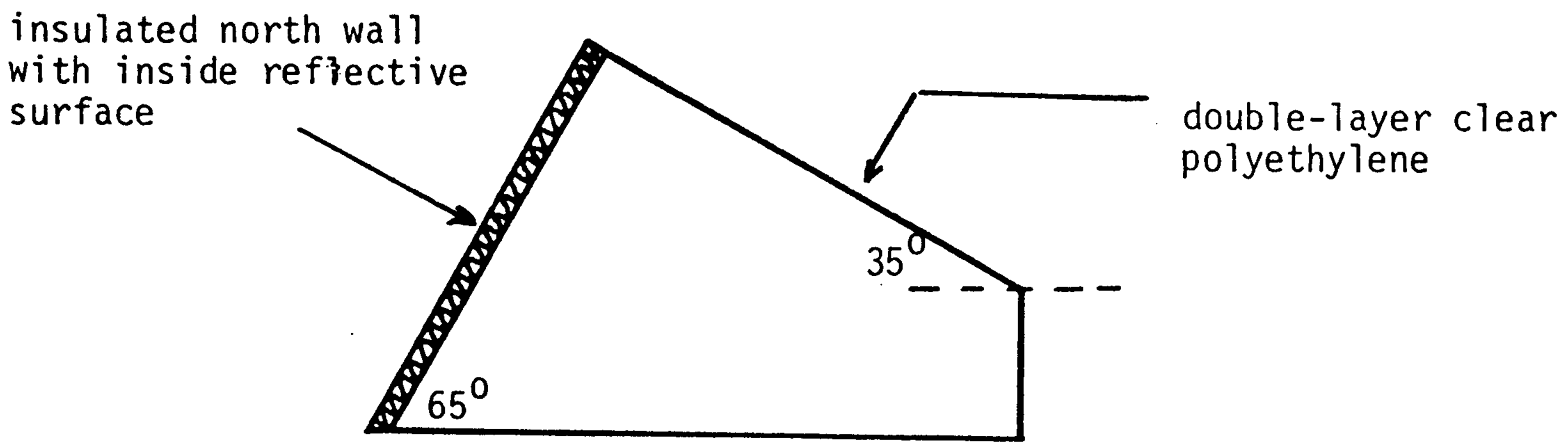

Fig. 2.7 Brace–style greenhouse (Lawand et al., 1975)

south-facing roof and wall is transparent, and the inclined north wall is insulated with a reflective cover on the interior face. The angle of the transparent roof and the inclined wall are chosen to meet the design criteria. Tests with an experimental unit with 40 m^2 floor area showed that a 30 to 40% reduction in heating requirements was achieved compared to conventional double layered plastic greenhouses. Solar irradiance incident on north side of the house was observed to be higher than that on south side, giving an average τ_e value of 0.54 in April and 0.90 in December. They further reported higher yields of tomato and lettuce grown in the new design greenhouse, possibly due to increased luminosity in winter.

Kozai et al. (1977) developed a computer model to predict the effects of orientation and latitude on the overall transmissivity of a free-standing conventional glasshouse. He concluded that the difference in greenhouse direct transmissivity (the ratio of daily integrated direct solar light at floor level to that outside) between east-west and north-south oriented greenhouses is larger at higher latitudes; when comparing Amsterdam (52.3 $^\circ$N) to Tokyo (35.7 $^\circ$N), the E-W orientation was greater by 22% for the former and 7% for the latter locations. That the E-W oriented greenhouse performs better than the N-S oriented one at the more southern latitude of Tokyo contradicts somewhat with the calculated results of Manbeck and Aldrich (1967) as mentioned earlier.

Turkewitsch and Brundrett (1979) used the computer simulation technique to predict solar energy admission of four single-span glasshouses: two conventional (E-W and N-S oriented), one Brace style and an asymmetrical glasshouse ('Greensol') retaining the north roof and insulating only the north wall (Fig. 2.8). Floor level or plant canopy level irradiance were the outputs of computer simulations, and a 'net transmission factor' was defined accordingly to compare collection efficiency. Their results indicated that reflecting insulation walls

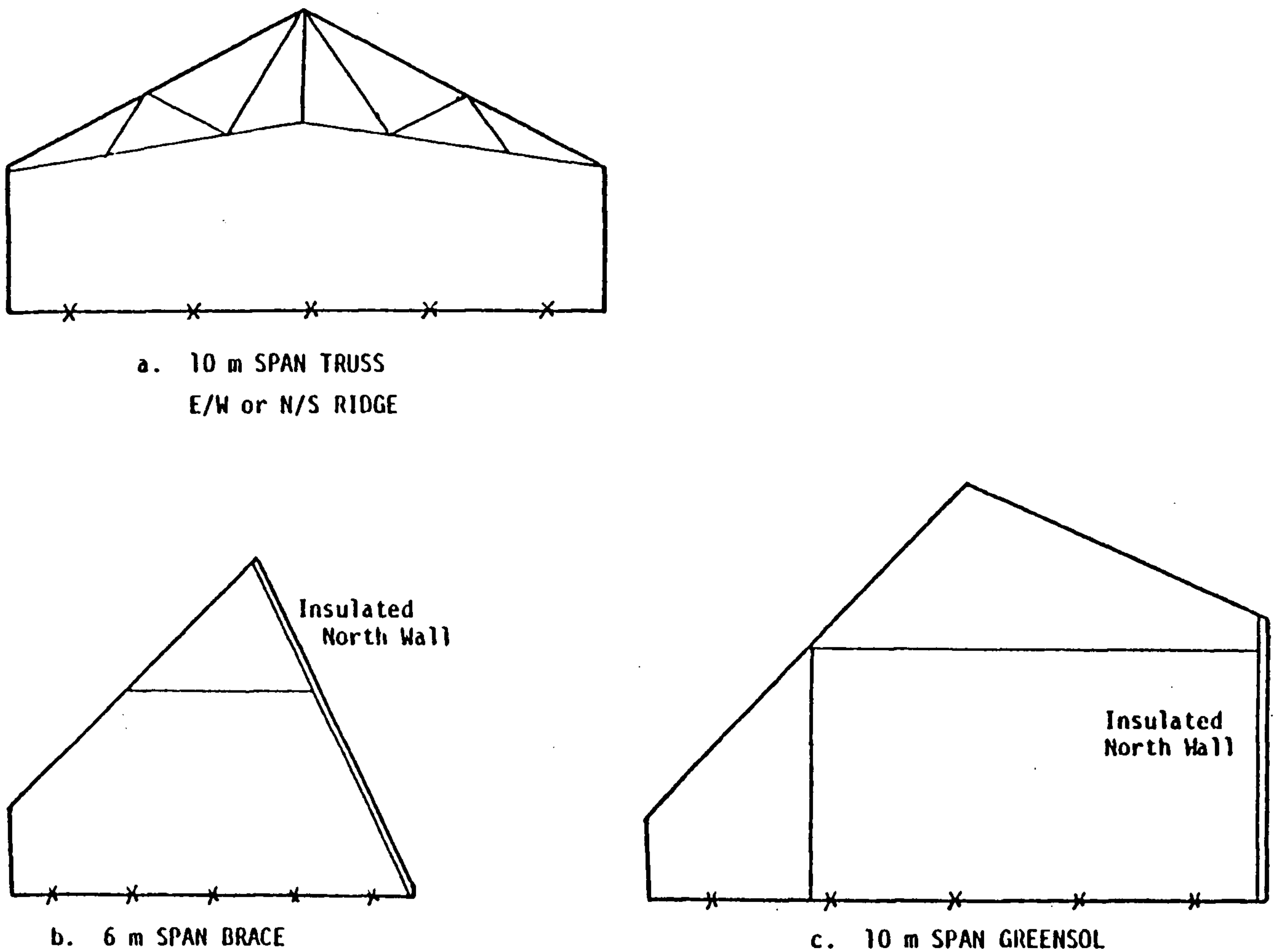

Fig. 2.8 Greenhouse types evaluated by Turkewitsch and Brundrett (1979)

augment winter light levels and reduce summer ventilating heat load. The Brace design was found to have the greatest collection efficiency among the four alternatives during winter months in both locations (Toronto and Winnipeg) studied, whereas transmitted radiation per unit floor area in summer was the lowest. Its disadvantage is the higher penalty under completely overcast conditions compared to Greensol; the latter has a larger transparent cover area to floor area ratio. In this regard, though, Lawand (1975) suggested that new greenhouse designs should have every effort made to reduce the exposed transparent cover surface area and hence the conductive heat loss, while maximizing solar gain. The authors cautioned that care should be taken to ensure a reasonably uniform distribution of the radiation across the greenhouse floor as variations as high as 60% were calculated for the Brace design.

Light intensity measured directly above the top heating pipes was compared by Amsen (1981) for double glass and double acrylic greenhouses with reference to a single glasshouse. No absolute values of τ_e were reported, rather, light level was found to be 20% and 22% less under double glass and double acrylic respectively.

Stoffers, as cited by Critten (1984) showed that transmissivity increased steadily as the roof tilted more from the horizontal. The latter used computer modeling techniques to study the effects of geometric changes in a 'structureless' greenhouse cross section on transmissivity patterns across the greenhouse and hence average greenhouse transmissivity under diffuse and direct irradiance conditions. Parameters investigated were wall height, roof height, and roof symmetry with one to three spans. He concluded that in houses with one or two spans, average direct light transmissivity can exceed unity. under low angle direct sunlight conditions, and a vertical south roof that reflects light downwards instead of upwards as in conventional multispans would also improve this value.

On the other hand, diffuse light transmissivity varied from 0.88 to 0.92 for both the conventional roofed house and the vertical south roofed house.

Ferare and Goldsberry (1984) reported values of τ_e measured at plant level (1m above floor) under double glazings. The percent of global radiation transmitted ranged from 0.55 to 0.65 for double polyethylene (Monsanto 603) and 0.62 to 0.72 for double PVC (4mil) between October and April.

In Hannover (52.5 °N), Bredenbeck (1985) measured light transmissivity at the plant canopy level in three N-S oriented greenhouses each covered with single glass, double glass and double acrylic over a period of two years. The transmissivity of the single glass house was about 0.60 in summer and 0.55 in winter. It was noted that the transmissivity for diffuse radiation in winter time was higher than that for direct radiation, a well known connection between greenhouse orientation and light transmissivity. The corresponding values of the double glass house were about 0.10 less. He suggested that cleaning the glasses in the roof area could increase τ_e by 0.03. On the other hand, double acrylic cover had a transmissivity ranging from 0.60 to 0.64 with no significant difference between summer and winter months. That τ_e for double acrylic is better than double glass was attributed to the placing of less bars (aluminum with rubber profiles) in the roof area and the treatment of the cladding material with a 5% 'SUN-CLEAR' solution.

Ben-Abdallah (1983) analyzed solar radiation input to conventional and shed-type glasshouses by means of two factors, the 'total transmission factor, TTF' and the 'total capture factor, TCF'. TTF was defined as follows:

$$TTF = \frac{\sum_{j=1}^{n} A_j(\tau_b I_{b\beta} + \tau_d I_{d\beta})_j}{A_f I_{oh}} \tag{2.10}$$

The numerator represents the sum of beam and diffuse radiations transmitted through all glazing surfaces, while the denominator is global solar radiation incident on an outside horizontal surface. He used this factor to compare solar input efficiency of greenhouses having different values of construction parameters. Since geometric losses are excluded in this expression, the TTF is not an appropriate indicator of actual solar input efficiency. The author then applied view factors to compute solar radiation absorbed by the plant canopy (similar to τ_e in concept); unfortunately, the values of TCF thus derived are too high compared to standard values for conventional greenhouses because of the assumption that all beam radiation transmitted through the cover is intercepted by an inside horizontal surface. Nevertheless, the concept behind the TTF is important in that the transmitted solar radiation is an essential secondary quantity that leads to the computation of tertiary results such as I_p and I_f.

Another piece of research work that dealt with both τ and τ_e was due to Ting and Giacomelli (1987) who found that air-inflated double polyethylene transmitted a higher percentage when measured in the global solar radiation range (83%) than in the PAR range (76%). Moreover, effective transmissivity based on the PAR range is much reduced at the canopy level, and is only 0.48 (that is, 48%).

A number of greenhouse steady state or unsteady state modeling studies adopted a simple method to estimate the solar radiation level on an inside horizontal surface and incorporated this estimated value in the energy balance, thus

$$I_{ih} = \tau\, I_{oh} \tag{2.11}$$

τ, the transmittance of the greenhouse depends on the type of cover material and is assigned an average value regardless of greenhouse construction, orientation and latitude. While this approach is appropriate for the determination of an adequate ventilation rate required to maintain healthy plant growth (Walker et al., 1983) based on maximum solar heat input at noon, it is not applicable for the purpose of this research work. Not only would large errors be induced in the estimation of solar gain if an average τ value is used throughout the detailed hour-by-hour simulations, but more importantly, τ is by no means equivalent to the effective transmissivity τ_e of the greenhouse as a whole.

All the above experimental and simulation studies have one idea in common despite the use of different terminologies: transmissivity is based on the solar radiation incident on an inside horizontal surface. The knowledge of this property of the greenhouse provides useful information for preliminary greenhouse design. Yet, when the actual amount of solar gain is needed in a detailed greenhouse thermal environment model that incorporates a number of construction parameters, the previous research findings are not readily applicable as they are specific to the greenhouses studied.

2.2.1.2 Convective heat exchange

For the heat convection terms relevant to inside air, several expressions have been reported in the literature, all of which are of the form

$$h_{ka} = a_1 (\Delta T)^{a_2} \tag{2.12}$$

where ΔT denotes the temperature difference between a component surface and greenhouse air. The values of a_1 and a_2 are well established for flat surfaces (Kreith and Black, 1980). They depend on the physical conditions of the heated surface and air flow, and the suggested values are 2.56 $(\Delta T)^{1/4}$ (Sears and Zemansky, 1960); 1.38 $(\Delta T)^{1/3}$ (Jakob, 1949); 4.87 $(\Delta T)^{1/3}$ (Kimball, 1973); 1.52 $(\Delta T)^{1/3}$ for cover and 1.90 $(\Delta T/\ell_p)^{1/4}$ for plant (Seginer and Livne, 1978). The values of a_1 = 1.38 and 1.52 corresponding to turbulent flow (a_2 = 1/3) are representative of the air thermal properties (χ, ν, μ and Pr) whereas the empirical value of a_1 = 4.87 obtained by Kimball is specific to his experimental conditions, which probably includes contribution from forced convection due to ventilation. Seginer and Livne (1978) treated the problem of a ventilated greenhouse with a typical air flow velocity of 0.5 m s^{-1} as one of mixed convection regime; they added the contribution from forced convection to the expressions shown above for free convection. based on principles of momentum transfer across a boundary layer over a flat plate.

A testing of model sensitivity led Avissar and Mahrer (1982) to emphasize the need of accurately determining the inside air transfer coefficients since the computed plant and air temperatures and thus the convective heat fluxes are stongly influenced.

External heat exchange coefficient due to wind governs the heat loss from the greenhouse. Iqbal and Khatry (1977) conducted wind tunnel tests on a pentagonal-shaped model greenhouse to determine the wind-induced transfer coefficients for bluff bodies that are subjected to the flow from the earth's boundary layer. Based on power-law profiles, they presented an empirical relationship

$$h_w = 17.9 u_w^{0.567} \tag{2.13}$$

van Bavel et al. (1980) found that this heat transfer coefficient led to too large a heat loss when compared to actual data for their multispan greenhouse. They adopted Jurges' (cited by McAdams, 1954) expression for a 0.5 x 0.5 m vertical flat plate oriented along the air flow

$$h_w = 5.7 + 3.8 u_w \tag{2.14}$$

However, in their review of heat loss from flat plate solar collectors due to outside winds, Duffie and Beckman (1980) cautioned that it is not reasonable to assume eqn. 2.14 is valid at other plate lengths. Garzoli and Black (1981) and Willits et al. (1985) presented slightly different expressions, which are derived by linear regression on data given in the ASHRAE Handbook of Fundamentals (1981). Calculated h_W values are practically the same as that due to eqn. (2.14).

2.2.1.3 Evapotranspiration

Quantitative description of the evapotranspiration process in greenhouses is one area where authors appeared to differ widely in their approach.

Morris et al. (1957) carried out experiments on tomatoes, lettuce and carnations to determine the relationship of transpiration to the solar radiation impinging upon the crop. Their results indicated a high degree of correlation of transpiration with radiation observed when the water supply is non-limiting. They recommended a ratio of 0.5 for freely transpiring, well-watered crops. Walker et al. (1983) adopted this value in their procedure of evaluating ventilation requirements, but added that it should be reduced by a varying factor when plants are very small or when the ratio of active growing space to aisle space is low.

Businger (1963) suggested that the latent heat flux associated with transpiration may be expressed as a function of net radiation in the greenhouse and the Bowen ratio β (the ratio of sensible heat flux to latent heat flux). Yet, Seginer and Levav (1971) had made a thorough review of the models existing at that time, pointing out the need to develop models which only include primary boundary (environmental) conditions that are easy to measure and unaffected by the existence of the greenhouse. These include, among other climatic factors, outside solar radiation and air temperature. Net radiation should therefore not be used as the driving function. Garzoli and Shell (1973) conducted a series of experiments at the C.S.I.R.O. Division of Irrigation Research, Griffith, and found that the latent heat percentage of the enthalpy increase for a fully developed greenhouse cotton crop varied between 48 and 75% with an average of 57%, under the summer conditions of high solar radiation intensities and ambient temperatures, characteristics of the semi-arid area of inland Australia.

Milburn (1981) stated that for typical greenhouse operations, β ranged from about 0.4 for dense crops, such as roses and tomatoes to 4.0 for very sparse crops, such as bedding plants. If absorbed solar radiation by the plant canopy is partitioned into sensible and latent heat exchanges only, then for β = (0.33, 0.4, 1, 2 and 4), the proportion that is latent heat flux will be $1/(1+\beta)$ = (75%, 70%, 50%, 33% and 20%). A β value of 0.4 therefore seems too high compared to the findings of other authors.

Bello (1982) made an in-depth study of evapotranspiration in a greenhouse, and concluded that a constant Bowen ratio should not be assumed over a seasonal period.

Another way of evaluating transpiration may be called the direct fundamental method, and is used by Takakura et al. (1971), Chandra et al. (1981), Cooper and Fuller (1983), Kindelan (1980), Kimball (1981) and Arinze et al. (1984). Basically it is the Ohm's law approach

$$M_e = \frac{2\nu_a(e^* - e)}{r_p} \tag{2.15}$$

in which the canopy resistance (r_p) to water vapor diffusion is made up of a stomatal resistance in series with a boundary layer air resistance and weighted according to leaf area index. These investigators used very different values for r_p, ranging from 250 to 900 s m^{-1}, and not necessarily depending on the stage of plant growth.

Parameterization of the vapor diffusion process was outlined by Avissar and Mahrer (1982) who introduced an empirical expression for a rose crop, taking into account the effects of environment factors including solar radiation, temperature, vapor pressure gradient, CO_2 concentration and soil water potential. The constants in their expression were specific for rose and not available for other plants in the literature.

2.2.2 Thermal energy storage

There are basically two types of thermal energy storage systems, sensible heat storage and latent heat storage. The latter is outside the scope of this study, and two sensible heat storage media will be covered in this section.

2.2.2.1 Rockbed thermal storage

Rockbed thermal storage is also known as a packed bed, pebble bed or rock pile storage, whereby a fluid (usually air) is circulated through the bed of loosely packed material to add or remove heat. A variety of solids may be used, rock being the most common. Its specific heat ranges within narrow limits from 800 to 920 J/kg.C. With a void ratio of 0.25 to 0.40, the effective density varies from 1600 to 2300 kg m^{-3} (Telkes, 1977).

Schumann (1929) formulated the classic equations for the solid and fluid phases

$$(\nu c)_f \epsilon A_n \frac{\partial T_f}{\partial t} = -(\dot{m}c)_f \frac{\partial T_f}{\partial x} + h_v A_n (T_r - T_f) \tag{2.16}$$

$$(\nu c)_r (1-\epsilon) \frac{\partial T_r}{\partial t} = h_v (T_f - T_r) \tag{2.17}$$

Underlying these governing equations are the following assumptions: one-dimensional fluid plug flow; constant properties; no axial conduction or dispersion; no mass transfer; no temperature gradient within the solid particles; internal heat generation is absent; and radiation effects are negligible. Since then, many studies have been made on the heating and cooling characteristics of packed beds. Works that link with solar applications include transient analysis (Mumma and Marvin, 1976; Hughes et al., 1976; White and Korpela, 1979; Coutier and Farber, 1982; Saez and McCoy, 1982), and pressure drop estimation

(Chandra and Willits, 1981; Parker et al., 1983). In particular, Hughes et al. (1976) found that the long-term performance of a solar air heating system with NTU (number of heat transfer units) equal to 25 is virtually the same as that with NTU equal to infinity, where

$$\begin{aligned} NTU_c &= \frac{h_v A_n L_{rs}}{(\dot{m}c)_a(1+0.2\mathrm{Bi})} \\ \mathrm{Bi} &= h_v d^2/12k_r \\ h_v &= 650(\dot{m}/A_n d)^{0.7} \end{aligned} \tag{2.18}$$

and thus eqns (2.16) and (2.17) can be combined into a single PDE since T_f and T_r are everywhere the same. With the addition of a heat loss term and another one for axial conduction, the simplified equation becomes

$$(\nu c)_r(1-\epsilon)A_n\frac{\partial T_{rs}}{\partial t} = -(\dot{m}c)_a\frac{\partial T_{rs}}{\partial x} + \frac{(UA)_{rs}}{L_{rs}}(T_{amb}-T_{rs}) + k_r A_n\frac{\partial^2 T_{rs}}{\partial x^2} \tag{2.19}$$

where T_{rs} is now the effective storage temperature. It is noted that the empirical expression for heat transfer coefficient h_v is due to Löf and Hawley (1948).

Close et al. (1968, cited by Klein, 1976) observed experimentally that up to 25% more heat could be discharged as pebbles adsorb water, and thus increases the bed's apparent storage capacity. Kimball (1986) attempted to consider condensation of moisture on the rock particles thereby releasing latent heat. It was assumed that no significant absorption of moisture occurs and that all condensed water drains away so evaporation cannot take place during discharging. He did not check his model with actual data, though. Willits et al. (1985) also realized the need to modify the rockbed model to include latent heat exchange since their inspection of the bed at the end of a charging period revealed that condensation has occured. The amount of water condensed in each rock layer in their model was assumed to remain in that layer, and was calculated by means of a mass balance using the humidity ratio of moist air. However, details of the modeling were not given.

2.2.2.2 Soil thermal storage

Theoretical work on heat transfer between a pipe and soil were done by researchers such as Ingersoll et al. (1948) and Pappas and Freberg (1949). They found that heat transfer to the soil became difficult as the soil dried out.

In the area of waste heat utilization, Kendrick and Haven (1973) considered the steady-state radial flow of heat from the water in pipes into a semi-infinite soil body. The key assumption in their work was that the temperature field established by each pipe acting as a line source at an arbitrary cross section is independent of all the other pipes in the field.

Parker et al. (1981) presented a computer model to predict heat and moisture transfer in the soil produced by a subsurface network of warm water pipes. A finite difference scheme was used to implement the soil model on the computer. Soil thermal properties that change with moisture content were updated at each time step. The water flow rate in the pipes was assumed high enough so that the temperature gradient in the longitudinal direction was negligible.

Puri (1984) applied the finite element method to analyze the simultaneous diffusion of moisture and heat in soils. A time-dependent axisymmetric formulation for a single tube was used to evaluate the thermal performance of an earth tube heat exchanger system. Based on numerical results, he concluded that the single tube analysis can be extended to multiple tubes using addition provided a minimum distance of eight tube diameters is maintained between the tubes. The author also noted that for a pipe air temperature of 38°C, the soil-pipe interface volumetric moisture content is reduced from the initial 30% (near saturation) to 28.75% after 12 hours of continuous operation and result in only a 4% change in soil thermal conductivity. This is inconsequential and does not affect the overall system performance. Furthermore, he studied two initial moisture regimes, 30% and 20% and suggested that the preliminary design curves developed for 30% are equally valid for a θ_w of 20%, since C_s varies linearly with moisture content, whereas k_s has an approximately linear variation with the range of moisture content considered; in other words, the thermal diffusivity of soil, α_s, does not change significantly.

The study made by Lei et al. (1985) on the characteristics of a single underground pipe for tempering ventilation air for plant and animal shelters falls along the same line as Puri (1984). They considered more parameters and the combined effects of pipe diameter, pipe length and air velocity were quantified. As experimental data revealed that the soil temperature gradient in the radial direction is on the average at least 100 times greater that that along the pipe's, they restricted the region of interest to a semi-cylindrical section. The latent heat released due to condensation of moist air on the inside of the pipe was handled by calculating the increase in the convective heat transfer coefficient using heat and mass transfer analogy. The simulated data indicated that the overall soil effects on the temperature differential between inlet and outlet air are not significant. Model validation of their work was based on simulated and measured outlet air temperatures, which agreed fairly well with each other.

Areskoug and Wigstroem (1980) used the general heat conduction equation to simulate soil temperatures in an earth thermal storage system directly beneath a greenhouse. The modeled region was constructed with symmetry at the centerline of the greenhouse and was discretized in a two-dimensional finite difference scheme. Predicted values compared favorably with actual data measured at depths up to 7 m on days with charging and discharging operations.

Simulation study of a soil heat storage system for a solar greenhouse was also carried out by Dale et al. (1980) and Boulard and Baille (1986a,b). The former researchers used a three-dimensional finite difference model to predict heat transfer to or from pipes. The standard deviation between predicted and actual hourly soil temperatures on two typical days, one each in summer and winter, was reported to be within 1°C. Boulard and Baille quoted the work of Person: 'At low soil temperatures (30 °C) and with small soil water potential gradients, heat diffusion due to moisture movement can be safely ignored'. This observation agreed with the experimental steady-state silt loam soil temperatures obtained from a controlled laboratory system, as reported by Elwell et al. (1985), where it was shown that a soil/pipe interface temperature of 30.0 °C did not lead to dry core formation while raising it to 43.3 °C caused a dry core region of approximately 9 cm in diameter to form around each electrically heated copper tube 2.5 cm in diameter, and hence steep temperature gradients around the pipes were produced. They adopted Fourier's heat conduction equation as the governing equation and discretized it in two dimensions using the implicit finite difference method. The time-varying boundary conditions were measured values of surface soil temperature, pipe/soil interface temperature and underground water temperature. Of these three sets of data, surface pipe temperature shall be treated as a secondary boundary condition as it is affected by the fluid temperature inside the pipe and conduction process in the soil itself. Hence their model is not suitable for a complete simulation study integrating the soil thermal storage with the greenhouse thermal environment.

2.3 Design Methods

The present research program aims at the establishment of a simplified design procedure for greenhouse solar heating systems, along the lines of the 'f-chart' method for active collection systems or the 'SLR-method' for passive collection systems, both coupling to storage and other equipment in the overall residential solar heating system. Also presented in this section is a discussion of some design-oriented studies related to solar greenhouses that appeared in the literature previous to the proposed design procedure.

2.3.1 f-chart method

The f-chart method proposed by Klein et al. (1976) and Beckman et al. (1977) which is now widely adopted in flat-plate solar collector designs is a generalized design method that results from numerous computer simulations. The conditions of the simulations were varied over appropriate ranges of parameters of practical system designs. For an air heating system, the fraction, f, of the monthly total heating load supplied by the solar heating system is given as a function of X and Y which are respectively the ratio of absorbed solar radiation to total heating load and the ratio of collector loss to total heating load. The relationship between X, Y and f in equation form is

$$f = 1.04Y - 0.063X - 0.159Y^2 + 0.00187X^2 - 0.0095Y^3 \tag{2.20}$$

Fig. 2.9 illustrates the design curves in two graphical forms.

Given the basic design characteristics of the system, such as collector area, the storage size, heat-exchanger parameters, air flow rate, and the collector performance, as well as the monthly climatological averages, solar insolation and heat load data based on the degree-days method (ASHRAE, 1981), the f-chart will predict the monthly and hence annual solar fraction of the system. These can then be used for design decisions

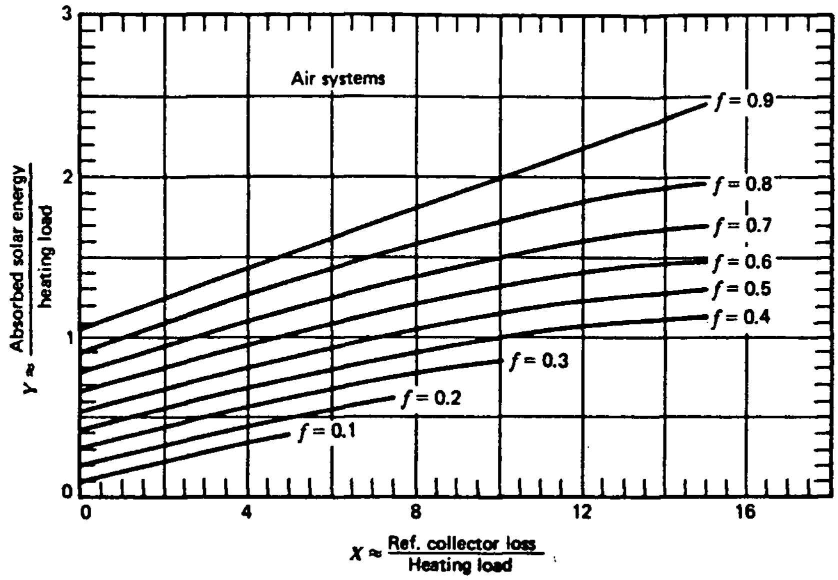

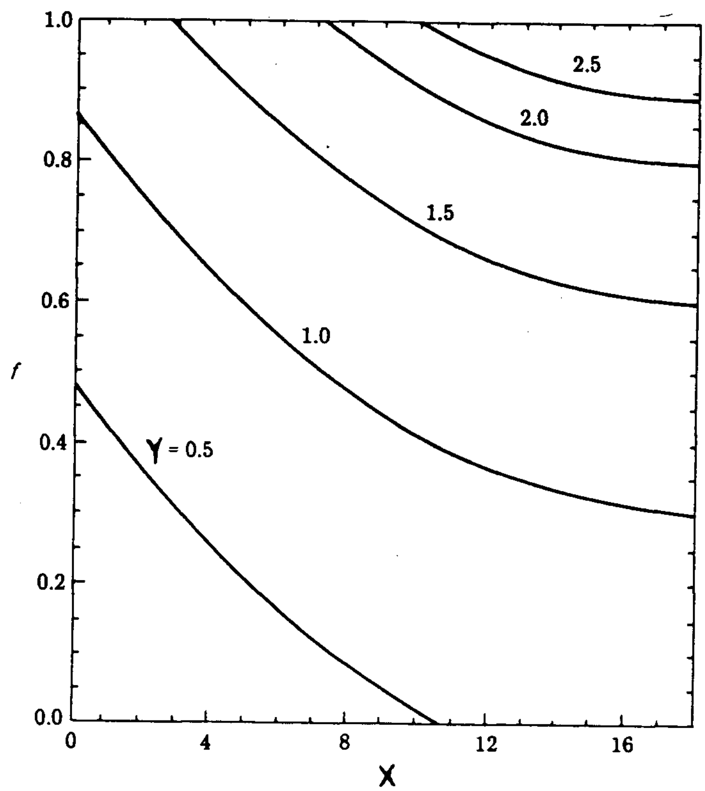

The f-chart for an air system.

Fig. 2.9 The f-chart for an air system (Klein et al., 1976)
above: f as a function of X and Y
below: f versus X with Y as parameter

and economic evaluation.

2.3.2 SLR-method

The SLR (solar load ratio) method devised by Balcomb and McFarland (1978) is a simplified method for estimating the performance of a collector-storage wall (also called Trombe wall or Trombe-Michel wall) passive heating system. The SLR is defined as the ratio of monthly solar energy absorbed on the storage wall surface to the monthly building heat load. It is calculated for each month and a monthly solar heating fraction, SHF, is obtained from Fig. 2.10 for the particular system.

2.3.3 Direct simulations as design method

Both the f-chart and SLR methods allow designers to estimate system performance based on local weather data if they are readily available. However, these methods are not applicable to unconventional designs that involve other system arrangements or when the magnitudes of the design parameters deviate significantly from the specified ranges. Under these conditions, dynamic simulations by means of a computer model are still necessary.

Rotz et al. (1979) extended their computer models written for conventional and solar greenhouses to predict energy requirements for greenhouses equipped with alternative insulating and solar heating systems. Four solar heating systems were modeled, which included a solar water system with uninsulated or insulated external collectors, a solar air system, and an internal greenhouse collection system. Insulation options were: double acrylic cover and thermal blanket. Computer runs were made with only one fixed set of design parameters and for an average location in Pennsylvania, hence results were very specific. They concluded that the system with the least potential (about 9%) for fuel saving was that based on internal greenhouse collection of excess solar heat alone, whereas the most promising one (about 90%) was

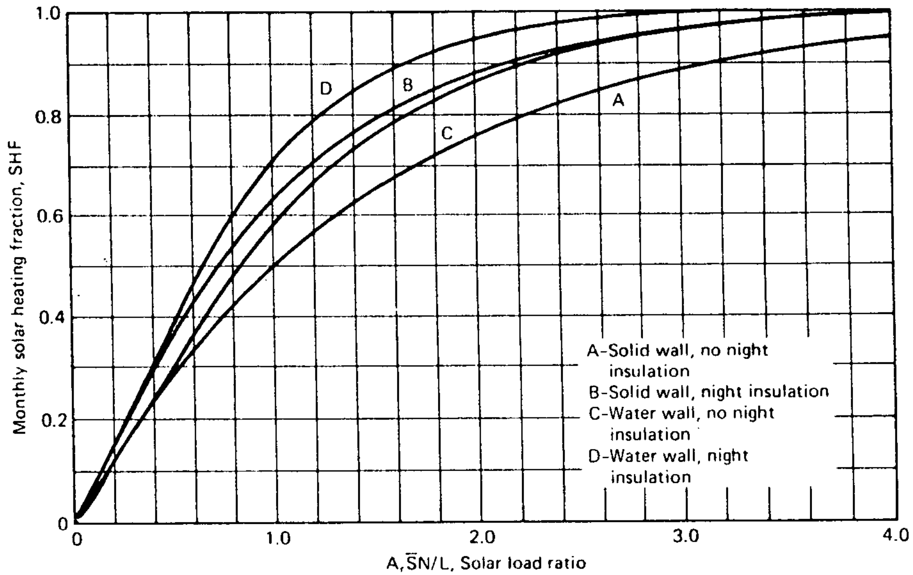

Fig. 2.10 Monthly solar heating fraction versus solar load ratio for buildings with south-facing collector-storage wall systems (Balcomb and McFarland, 1978)

a system that combined heavy thermal blankets, double acrylic cover and external solar collection.

Solar greenhouses with a rockbed thermal storage have been tested by a number of researchers, as pointed out in an earlier section. Puri (1981) presented a few design curves (Fig. 2.11) as a quick means of predicting the long-term thermal performance of a solar heating system that makes use of an external flat-plate collector. The design parameters considered are the ratio of collector to greenhouse areas, the ratio of storage volume to greenhouse area, as well as collector tilt and azimuth angles. Though the results are specific for the location at Lafayette, Indiana, and have limited applications, it was the first of its kind that aims at providing designers with some guidelines in sizing a solar heating system for their customers.

Montero and Short (1984) tested plastic solar collectors similar to the Rutgers design (Mears et al., 1977). After an efficiency curve was established a collector model was combined with a computer simulation program for greenhouses in order to predict the thermal performance of the system in two distinctly different areas - Ohio (USA) and Malaga (Spain), which subsequently led to two sets of curves that may be used as design tools. These charts, as depicted in Fig. 2.12, relate the solar heating fraction to the collector area:greenhouse area ratio for various kinds of greenhouse covers.

2.4 Effects of Environmental Factors on Greenhouse Plant Growth

2.4.1 Environmental factors

The major environmental factors that affect the physiological processes and hence growth and development of greenhouse plants are light, carbon dioxide, temperature, and humidity, which are in turn influenced by cultural and engineering practices.

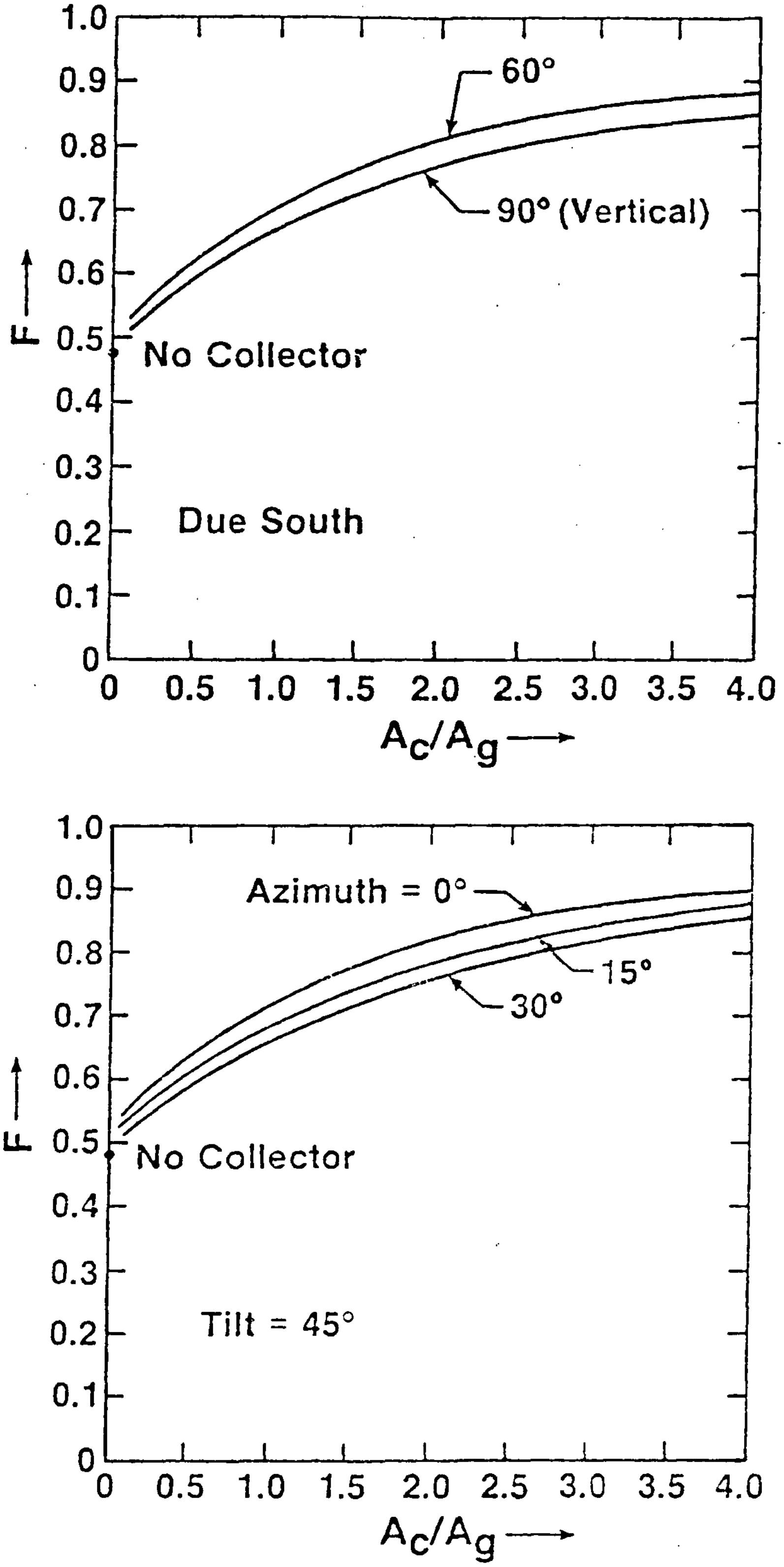

Fig. 2.11 Nomographs for greenhouse–rock storage–collector system (Puri, 1981)
above: for vertical and 60° tilt collectors
below: for 45° tilt collector and various azimuth angles

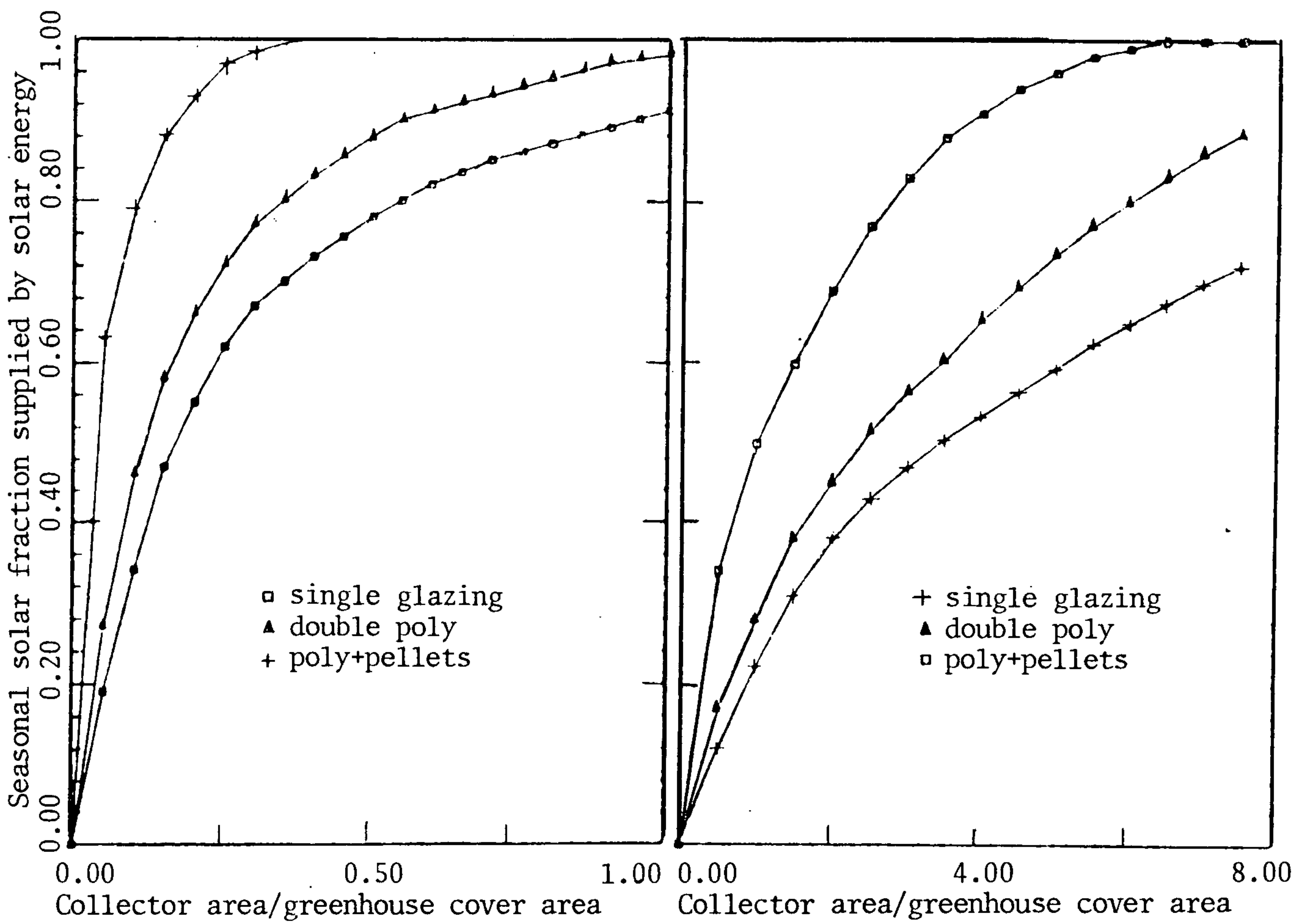

Fig. 2.12 Computer predicted seasonal performance of a solar collector–heating system for three commercial type greenhouses (Short and Montero, 1984)
left: Wooster, Ohio, U.S.A.
right: Malaga, Spain

Blackman (cited by Mastalerz, 1979) stated the 'principle of limiting factors' as follows:

> "When a process is conditioned as to its rapidity by a number of separate factors, the rate of the process is limited by the pace of the slowest factor."

This principle may be illustrated by the photosynthesis of a cucumber leaf at limiting and saturating CO_2 concentrations under 500 W incandescent light (Fig. 2.13). At 300 ppm ($\mu l/l$) CO_2 level, the saturation rate is reached at comparatively lower light level (about 100 W m^{-2} PAR), regardless of air temperature. However, with CO_2 enrichment to 1300 ppm, marked difference is seen under two different temperature regimes.

Looking at this phenomenon from another angle, higher carbon dioxide levels stimulated CO_2 fixation more at increasing light intensities. This relationship, as depicted in Fig. 2.14 for sugar beet (a C-3 dicot), has been well known for many years. At normal CO_2 level of 330 ppm, a drop in PAR level from 308 W/m^2 to 126 W/m^2 leads to a very slight reduction in CO_2 fixation rate, while a further drop in light level to 35 W/m^2 brings about an additional 50 % rate reduction. In other words, photosynthetic rate saturation occurs at a PAR of about 120 W m^{-2}.

For tomato plants (also C-3 dicots) single leaves exposed to normal CO_2 concentration show photosynthetic rate saturation at PAR intensities one-third to one-half full sunlight, that is, 150 - 200 W m^{-2} (or 30 - 40 klx) on an exposed horizontal surface; young tomato plants do not need the light intensities of full sunlight.

For an entire crop, though, light saturation occurs at much higher intensities. For instance, typical values for two C-3 crops, wheat (monocot) and cotton (dicot) are about 280 and 420 W m^{-2} respectively. On the other hand, many experiments have demonstrated that the optimum CO_2 concentration ranges between 1000 and 1500 ppm

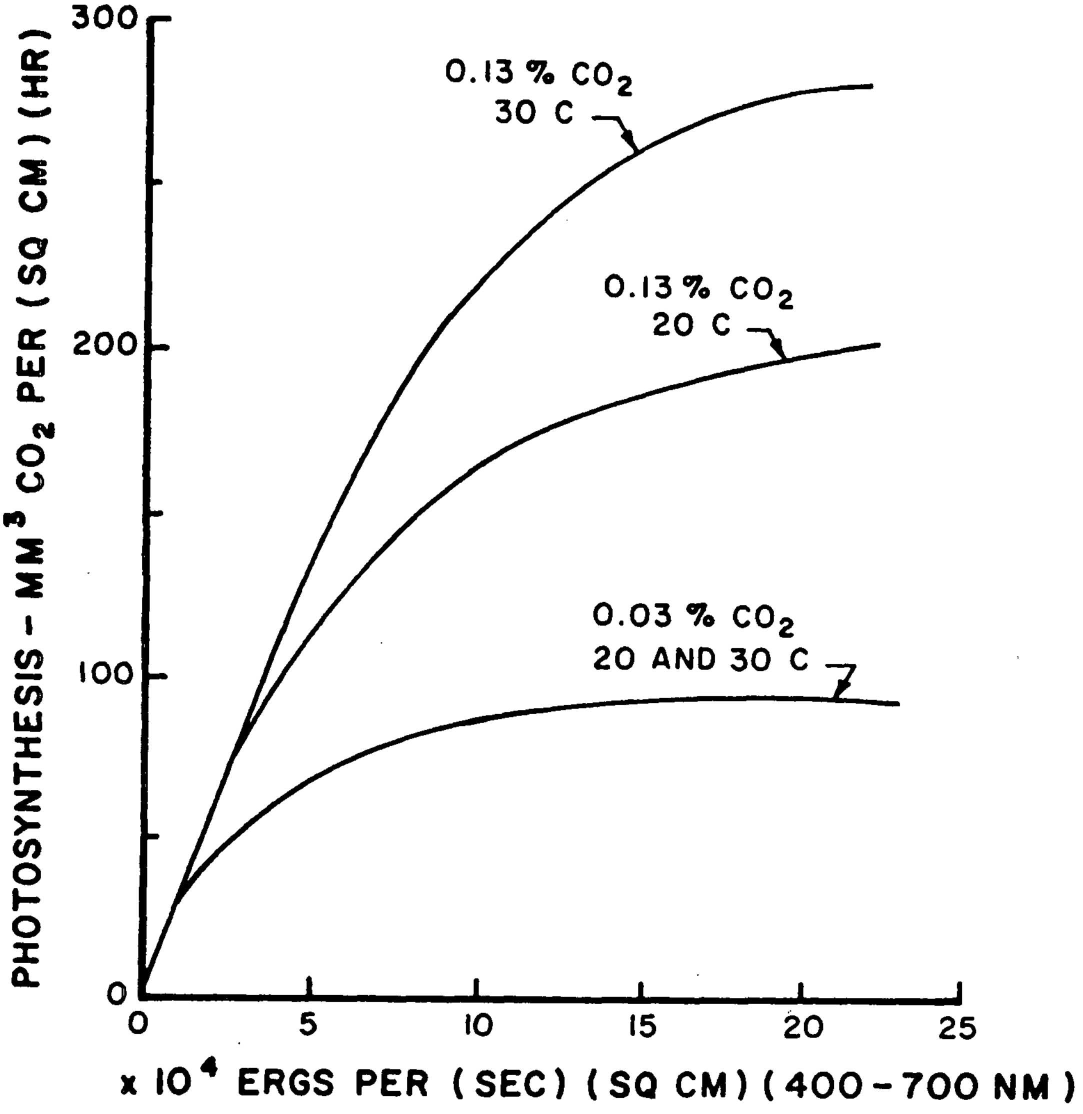

Fig. 2.13 Photosynthesis of a cucumber leaf at limiting and saturating CO_2 concentrations under incandescent light (Gaastra, 1963)

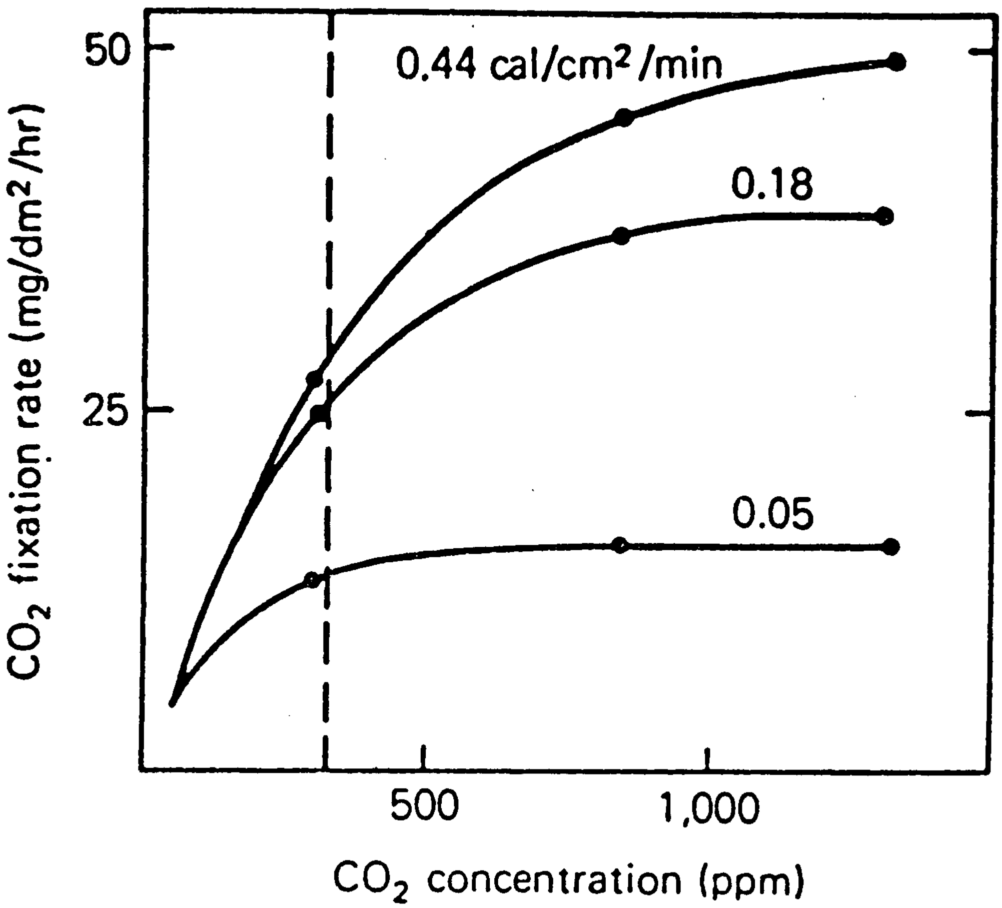

Fig. 2.14 Effects of atmospheric CO_2 enrichment on CO_2 fixation in a sugar beet leaf (Salisbury and Ross, 1982)

(Wittwer and Honma, 1979).

Bauerle and Short (1984) studied the CO_2 depletion effects in energy efficient greenhouses. At 200 ppm CO_2 and 600 PAR light intensity (130 W m^{-2}), net photosynthesis of tomato plants was found to be 35% less than that at 300 ppm CO_2. At the same time, transpiration rate was 4% higher (Fig. 2.15) since stomates open more at low CO_2 concentrations. Larger photosynthesis and transpiration differences occured with increasing light levels. In fact, the phenomenon of transpiration and stomatal opening with changes in CO_2 content of the air had been observed by Pallas (1965) and many other physiologists. Lettuce showed less of a reduction in net photosynthetic rate at reduced CO_2 concentrations than did tomato.

Reduction in net photosynthetic rate would likely lead to reduced fruit size, and even a longer growing season, thus posing scheduling problems. On the other hand, higher transpiration rate means more ventilation is needed for humidity control, and watering should be more frequent.

The temperature range over which plants can photosynthesize is large. Increases in temperature usually stimulate photosynthetic rates until the stomates close or enzyme denaturation begins to occur. Each species or variety has therefore, at any given stage in its life cycle, an optimum range of temperatures that promotes maximum growth rate. For C-3 plants photorespiration activity increases with temperature rise because of a higher ratio of dissolved O_2 compared to CO_2, thus counteracting the stimulating effect of a temperature rise, resulting in a rather flat and broad temperature response curve between 15 and 30 °C when compared to C-4 plants (Salisbury and Ross, 1978). Klapwijk (1987) commented that under unsaturated light conditions, this temperature range can lie between 18 and 35 °C. Very high temperatures usually cause stomatal closure in most plants and therefore affect photosynthetic activity; besides, such conditions destroy proteins, inactivate enzymes and disintegrate cell membranes.

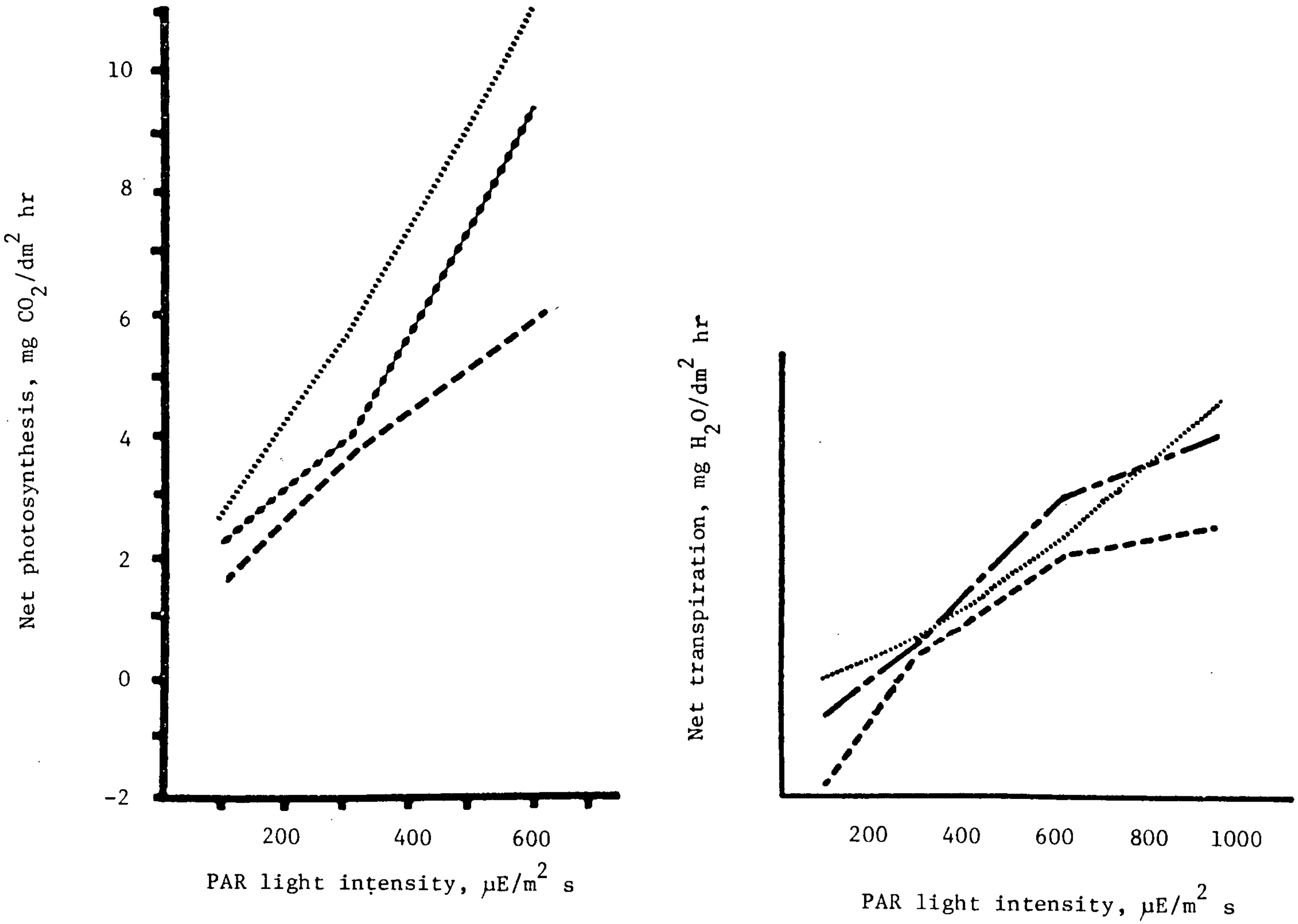

Fig. 2.15 Photosynthetic (above) and transpirational (below) responses of tomato plants to various light intensities and CO_2 levels

Many plants, especially woody ones, grow better when the night temperature is lower than the day temperature. These plants have two optimum temperatures, one during the day and the other and more crucial one at night, for each stage of plant development. Moore (cited by Alrich et al., 1983) reported that the optimum temperature for tomatoes during flowering and fruiting is 15 to 19 °C for cloudy days and at night, and 20 to 27 °C on sunny days, whereas Wittwer and Honma (1979) suggested slightly different ranges of 15° to 17°C, and 18° to 24°C correspondingly. Salisbury and Ross (1978) noted that the relative growth rate of tomatoes is at a maximum when night temperature is around 20 °C for a typical optimum day temperature of 26 °C.

Relative humidity level of 70–80% is considered most desirable for greenhouse plants. This optimum range allows adequate transpiration to take place and effectively cool the leaves. Above 80%, if water vapor condenses on the foliage, disease organisms are more likely to be a problem; the situation could deteriorate when combined with high temperatures. During cold weather, condensation frequently occurs on the inside surface of the greenhouse cover, it does not pose a problem until it builds up to the point of dripping onto the leaves. In plastic-covered structures, more moisture accumulates in the house because of less exchange of air through infiltration. Condensed moisture spreads out into a thin film on glass while it remains in droplet form on the plastic surface. Polyethylene films can now be made with modified surface tension properties that can reduce the size of the droplets thereby bringing the condensation problem under some control.

Aside from these primary environmental factors, air movement is a factor that cannot be overlooked in greenhouse environment control. Greenhouses that are designed to be used as solar collectors for the solar heating system still need ventilation for temperature, CO_2 level and humidity control, while every effort is being made to maximize the collection of trapped solar heat. The ventilation system should be designed to provide adequate air mixing and distribution.

The boundary layer resistance of air moving across a leaf surface decreases with increasing air speed, thus increasing transpiration, heat transfer and CO_2 movement into the leaf. Aldrich et al. (1983) pointed out that air speeds of 0.1 to 0.25 m s^{-1} facilitate CO_2 uptake, as air speed increases above this value, CO_2 uptake is reduced, growth is inhibited and eventually may even cause damages to plants, whereas below this value, uniform mixing in all sections of the greenhouse is not assured (Mastalerz, 1979).

Welles et al. (1983) studied the effect of thermal screens and wall insulation on yield. For an east-west aligned glasshouse, cropping near the north-facing wall was little affected by the cladding materials compared to those grown near the opposite wall, probably due to a reduction in temperature near the walls. Buitelaar et al. (1984) made further investigations on the effects of four insulation materials placed against single-glazed glasshouse walls on growth and production of tomatoes. Materials in the south wall have a more profound effect on the production. It appeared that the less the light is transmitted by the insulating material, the greater is the loss in production; flowering rate was hardly influenced.

Papadopoulos and Jewett (1984) compared tomato growth, development and yield in twin-wall PVC panel and single glass greenhouses. Plant growth and development were found to be better under glass during the light-deficient months of the year. Final marketable yields depend on the season. In all experiments, harvests from the PVC house had larger and higher percent grade #1 fruits.

van Winden et al. (1984) compared the effects of single and double glass greenhouses on production of tomato. In spring and autumn, plants inside the double-glazed house yielded respectively 10-15% and 4-13% less in comparison with single glass.

The above findings indicated that a definite trend could not yet be observed with regard to the effect of double glazing on greenhouse tomato production. They enhanced the conclusion made by Hurd (1983) from his survey of energy saving techniques tested by a number of researchers, that differences in yields between single-skinned and double-skinned plastic or glass greenhouses have not consistently favoured the former houses.

2.4.2 Mathematical models

The variation of greenhouse designs in shape, size, orientation, type and layers of cover may lead to a variety of internal environmental conditions, and it is desirable to work with a crop growth model that incorporates the essential environmental factors such as light, CO_2 and temperature. Other factors (e.g. irrigation and nutrient supplies) are assumed to follow normal practice and sound management assures that they are at their optimal quantities for plant growth so as to reduce the complexity involved in modeling.

France and Thornley (1984) made a critical survey of crop growth models that can be operated over a whole growing season to predict growth and yield. They categorized the models into empirical or mechanistic types, though many models fall somewhere in between. Empirical models attempt to relate crop growth and yield directly to various aspects of climate, weather and environment; the major objectives are to account for observed yield variations and to discover which factors affect yield most greatly. Mechanistic models are constructed by assuming that the system has a certain structure, and assigning to the components of the system properties and processes which can be assembled within a mathematical model. The submodels of a mechanistic model may be either empirical or mechanistic. A simple mechanistic model may just consist of photosynthesis and respiration (for instance, Johnson et al., 1983), while a comprehensive model would attempt to account for all the processes (for instance Meyer et al, 1979). The authors deemed that sound mechanistic models are suitable for applied scientists whose aim is to use current knowledge for their research and development activities.

Soribe and Curry (1973) extended the dynamic modelling established by Curry and Chen (1971) to simulate lettuce growth in an air-supported plastic greenhouse. The major processes considered in their model were photosynthesis and respiration. Modeling of gross photosynthetic rate is based on Monteith (1965a):

$$\frac{dP_g'}{dt} = \left(\frac{A'}{C} + \frac{B'}{\mathrm{PAR}}\right)^{-1} F \tag{2.21}$$

As suggested by Saeki (cited by Charles-Edwards, 1981), the light flux density incident on the surface of a leaf within a canopy can be described by

$$\mathrm{PAR} = \frac{\mathrm{PAR}_p K_p}{1 - \tau_p} \exp(-K_p L_i) \tag{2.22}$$

which is an adaptation of Bouguer's law of light attenuation. The rate of respiration that is made up of two parts, maintenance and conversion (growth) respiration, is temperature dependent and is given by

$$\frac{dR_d'}{dt} = cWQ_{10}^{(T_p - T_o)/10} + a\frac{dW}{dt} \tag{2.23}$$

while the rate of dry matter accumulation is

$$\frac{dW}{dt} = \frac{1}{1+a}\left(\frac{dP_g'}{dt} - cWQ_{10}^{(T_p - T_o)/10}\right) \tag{2.24}$$

which represents the difference between the quantity of carbohydrates synthesized and their consumption during dark respiration. The rate of leaf area expansion may be empirically expressed in terms of increments of leaf weight ratio, LWR and specific leaf area, SLA:

$$\frac{dA_\ell}{dt} = LWR(t).SLA(t).\frac{dW}{dt} \tag{2.25}$$

and it acts as a positive feedback term for photosynthesis, via expanding the base for light interception.

Acock et al. (1978) evaluated two models of canopy net photosynthesis of a tomato crop. Tomato plants were grown in a glasshouse using nutrient culture techniques. The glasshouse was heated to 16.5°C at night and maintained at 20°C during the day. Primarily the gross photosynthesis part of the model for a single leaf takes the form of Monteith's expression except that the temperature function F is removed:

$$P_g = \frac{\alpha \mathrm{PAR} \varsigma C}{\alpha \mathrm{PAR} + \varsigma C} \tag{2.26}$$

where α is the leaf light utilization efficiency and ς is the leaf conductance to CO_2 transfer. The coefficients α and ς are evaluated on the assumption that P_g stands for (P_g - R_l), where R_l is the photorespiration rate and (α , ς) corresponds to (1/B, 1/A) in equation 2.21. The simple model assumed that the canopy was composed of leaves with identical photosynthetic and respiratory characteristics, whereas the more detailed model allows explicitly for variation in ς and R_d within the canopy.

The rate of canopy net photosynthesis per unit ground area, P_n is expressed as

$$P_n = \frac{\varsigma C}{K_p} \ln \left(\frac{\alpha K_p \mathrm{PAR}_p + (1 - \tau_p)\varsigma C}{\alpha K_p \mathrm{PAR}_p \exp(-K_p L_i) + (1 - \tau_p)\varsigma C} \right) - R_d \tag{2.27}$$

where R_d includes 'dark' respiration by stems, fruits and roots besides that of the leaves. Equation 2.27 may be derived by integrating over the entire leaf area of the canopy from the expression of P_g for a single leaf along with eqn (2.22). It differed from Soribe and Curry's procedure of numerically solving their ordinary differential equations.

Experimentally, P_n was measured over a range of natural light flux densities. The canopy with L_i = 8.6 was divided into three layers for progressive defoliation tests. In this way, the uppermost layer, occupying 23% of total leaf area, was found to assimilate 66% of the net CO_2 fixed by the canopy and accounted for a similar percentage of the total leaf respiration. Measured values of the canopy extinction coefficient decreased with depth in the canopy, ranging from 0.63 from the top to 0.52 at the bottom layer, corresponding to L_i of 2.0 and 8.6. Estimated values of α and ζ from fitting experimental data to equation 2.27 were $10.1 \pm 1.0 \times 10^{-3}$ [mg CO_2/J] and $1.6 \pm 0.4 \times 10^{-3}$ [m/s] respectively. A mean value of 0.15 for the leaf transmission coefficient, m, was used in all analyses.

Subsequently, Charles-Edwards (1981) concluded that the simple canopy model (equation 2.27) adequately quantify the photosynthetic response of the canopy to light, and that detailed modeling of leaf photosysthesis by incorporating the photorespiration effect precludes simple analytical solutions upon integration and results in crop models too cumbersome for general use.

Seginer and Albright (1983) worked on an optimization method for equipment operation that can influence the greenhouse climate. The procedure required a reasonably simple growth function, which incorporates the key factors of PAR, CO_2 and temperature. They adopted the model of Acock et al. (1978) for the entire canopy, reintroducing the temperature function that is attached to the gross photosynthesis term, and like Soribe and Curry, they expressed dark respiration in terms of an exponential function in temperature with a Q_{10} of 2.0 for leaf temperatures between 10 and 35 °C (Enoch and Hurd, 1977), thus

$$R_d \quad = \quad R_{20} Q_{10}^{(T_p - T_o)/10} \tag{2.28}$$

where R_{20} is the value of R_d at 20 °C. Charles-Edwards (1981) expressed this variable as

$$R_{20} \quad = \quad \frac{R_{do}}{K_p}[1 - \exp(-K_p L_i)] \tag{2.29}$$

where R_{do} is the dark respiration rate of an unshaded leaf at the top of the canopy.

Their proposed temperature function, F, reflects the optimum temperature relevant to tomato growth in the greenhouse as different from that grown in the field, and is of a parabolic form

$$F = 1.25 - 0.007(T_p - 26)^2 \tag{2.30}$$

This formula suggests that at the optimum temperature of 26 °C for gross photosynthesis, F is at the maximum of 1.25, its value is 1.0 at 20 °C and 32 °C. They therefore claimed that a deviation of 6°C from the optimum results in a loss of production of 20%, which is typical of tomato plants at the vegetative stage (Went, 1945). Yet, they did not hesitate to point out that if net photosynthesis follows a parabolic trend, then gross photosynthesis should not be so, although they did not suggest any modification.

Almost concurrent with the study made by Acock et al. (1978), Enoch and Sacks (1978) presented an empirical model of CO_2 exchange of a C_3 plant (spray carnation) in relation to light, CO_2 concentration and leaf temperature. The model stems from a customary equation for photosynthate balance

$$P_n = P_g - R_\ell - R_d \tag{2.31}$$

In order to minimize the number of parameters, the authors made the following assumptions:

1. P_g is a multiplicative function of PAR, CO_2 and T_l, so that the variables are allowed to modify each other
2. R_l is related to P_g by a function whose value varies between 0 and 1, depending on CO_2 concentration and
3. R_d is the rate during the first hour of dark respiration, and is a function of T_p and PAR in a previous period.

120 combinations of PAR, CO_2 and T_p were tested, with PAR varying from 45 to 450 W/m², CO_2 200 to 3100 ppm and T_p 10 to 35°C. For each combination, measurements of P_n were recorded. Besides, R_d was measured during a one-hour

period of induced darkness when leaf temperature stabilized at 20° C. They fitted a linear logarithmic model to their data, which takes the following form:

$$P_n = \exp(-a')\text{PAR}^{b'}C^{c'}T_p^{d'} - (m' + n' \ln \text{PAR}^*)Q_{10}^{(T_p - T_o)/10} \qquad (2.32)$$

The authors noted that the constants a', b', c', d', m', and n' may be experimentally determined for other C_3 plants using similar methods.

NOTATION

		Dimension
A	Area	m^2
A	Leaf area	m^2
A_n	Area normal to fluid flow	m^2
A', B'	Constants used in eqn. 2.21	-
Bi	Biot number	-
C	CO_2 concentration	$mg\ m^{-3}$
F	Temperature-correction factor	-
I	Hourly solar irradiance	$W\ m^{-2}$
K	Extinction coefficient	m^{-1}
L	Length	m
L_i	Leaf area index	$m^2\ m^{-2}$
LWR	Leaf weight ratio	$g\ g^{-1}$
M	Moisture flow rate	$kg\ s^{-1}$
P_n	Net photosynthetic rate	$mg\ m^{-2}\ s^{-1}$
PAR	Hourly photosynthetically active irradiance	$W\ m^{-2}$
Pr	Prandtl number	-
P_n	Net photosynthetic rate	$mg\ m^{-2}\ s^{-1}$
P_g	Gross photosynthetic rate	$mg\ m^{-2}\ s^{-1}$
P'_g	Gross photosynthesis	$mg\ m^{-2}$
Q_{10}	Respiration ratio	-
Q	Heat flow rate	W
Q_{t1}	Conduction heat gain of a soil layer	W
Q_{t2}	Conduction heat loss of a soil layer	W
R_d	Dark respiration rate	$mg\ m^{-2}\ s^{-1}$
R'_d	Dark respiration	$mg\ m^{-2}$
SLA	Specific leaf area	$m^2\ g^{-1}$
SLR	Solar load ratio	-
T_o	Reference temperature for respiration	°C
W	Dry matter weight	mg
X, Y	Dimensionless variables used in eqn. 2.23	-
TCF	Total capture factor	-
TTF	Total transmission factor	-
U	Overall heat loss coefficient	$W\ m^{-2}\ K^{-1}$
ΔT	Temperature difference	°C
a_1, a_2	Constants used in eqn. 2.12	-
a, c	Constants used in eqn. 2.23	-
a', b') c', d') m', n')	Constants used in eqn. 2.32	-
e	greenhouse air vapor pressure	kPa
f	Monthly solar heating fraction	-
h	Convective (surface) heat transfer coefficient	$W\ m^{-2}\ K^{-1}$

h_v	Convective (volumetric) heat transfer coefficient	$W\ m^{-3}\ K^{-1}$
k	Thermal conductivity	$W\ m^{-1}\ K^{-1}$
$\dot{m}$	Air flow rate	$kg\ s^{-1}$
r_p	Plant resistance to water vapor diffusion	$s\ m^{-1}$
t	Time	s
u_w	Ambient wind velocity	$m\ s^{-1}$
x,y,z	Cartesian coordinates	m
α	Leaf light utilization efficiency	-
ϵ	Void ratio	-
μ	Absolute viscosity	$kg\ m^{-1}\ s^{-1}$
ν	Density	$kg\ m^{-3}$
τ	Solar radiation transmittance	-
τ_e	Effective transmissivity	-
χ	Volumetric thermal expansion coefficient	$^{\circ}K^{-1}$

Subscripts

a	inside air
au	supplemental heat
b	beam radiation
cd	condensation
cn	conduction
cv	convection
d	diffuse radiation
e	transpiration
f	floor, fluid
g	transferred to or from ground
i	inside cover
ih	inside horizontal surface
k	component surface
m	accumulated quantity
o	outside cover
oh	outside horizontal surface
p	plant canopy
r	rock
rs	rockbed storage
s	solar gain
t	thermal radiation
td	transferred to storage
v	ventilation and infiltration
w	wind
λ	latent heat
β	inclined surface

Superscript

*	saturated value

Chapter 3

COMPUTER MODELING AND SIMULATIONS

Computational simplicity is needed in the simulation model intended for the generation of a simplified design procedure to allow an examination of the thermal performance of many system designs in a variety of climates, so that computing time can be minimized. On the other hand, care must be taken in constructing and making simplifications to the mathematical models that any essential processes or mechanisms are not precluded.

Since sufficient experimental data are readily available for model validation purposes, the present study is focused upon the following two generic systems of the internal collection type.

System I - augmented internal collection with rockbed thermal storage

System II - internal collection with wet soil thermal storage

The design and operation of these two systems have been described in Chapter 2, and each system with its key features has been schematically shown in Fig. 2.1 and 2.2.

3.1 System I - Augmented Internal Collection With Rockbed Thermal Storage

3.1.1 Greenhouse thermal environment

The principal components considered to play an important role in the analysis are: the inside air, the plant canopy, the cover, the absorber plate and the concrete floor (Fig. D3.1). During most of the growing period, the latter can be excluded from the model since the vegetation cover shades the floor. At the seedlings and early transplanting stages this assumption may lead to minor errors in predicting the inside temperature since the solar absorptivity and thermal emissivity of concrete differ from those of plant materials.

Energy balances of the cover (inside and outside surfaces), the absorber plate, the plant canopy, the floor and the inside air yield the following equations:

$$(mc)_{ci}\frac{dT_{ci}}{dt} = S_{ci} + h_{cia}A_{ci}(T_a - T_{ci}) + \left(\frac{n_c\vartheta_g}{k_g} + \frac{1}{h_a}\right)^{-1} A_c(T_{co} - T_{ci}) + \lambda\, M_{cd} + Q_{rci} \tag{3.1}$$

$$(mc)_{co}\frac{dT_{co}}{dt} = S_{co} + h_w A_{co}(T_o - T_{co}) + \left(\frac{n_c\vartheta_g}{k_g} + \frac{1}{h_a}\right)^{-1} A_c(T_{ci} - T_{co}) + Q_{rco\psi} \tag{3.2}$$

$$(mc)_q\frac{dT_q}{dt} = S_q + 2h_{qa}A_q(T_a - T_q) + U_qA_q(T_o - T_q) + Q_{rq} + Q_{rq\psi} \tag{3.3}$$

$$(mc)_p\frac{dT_p}{dt} = S_p + 2(1 + \frac{1}{\beta})h_{pa}A_p(T_a - T_p) + Q_{rp} + Q_{rp\psi} \tag{3.4}$$

$$(mc)_f\frac{dT_f}{dt} = S_f + h_{fa}A_f(T_a - T_f) + Q_{rf} + Q_{rf\psi} \tag{3.5}$$

$$(mc)_a\frac{dT_a}{dt} = h_{cia}A_{ci}(T_{ci} - T_a) + 2h_{qa}A_q(T_q - T_a) + 2h_{pa}A_p(T_p - T_a) + Q_{au} - Q_{td} - Q_v \tag{3.6}$$

The mass balance on the inside air gives

$$(\nu V)_a\frac{dW_a}{dt} = M_e - M_{cd} - M_v \tag{3.7}$$

The convective heat transfer coefficient, h_a , for air is included in eqns. (3.1) and (3.2) for analyzing twin-walled covers that are separated by air.

Basic assumptions of the model are:

1. The system is vertically layered.
2. All the component surfaces are homogeneous, having uniform temperature horizontally and vertically.
3. Horizontal fluxes are neglected.
4. The physical properties of the various layers do not vary during the simulation.

5. The air flow in the greenhouse is uniform.
6. Greenhouse crops are grown in hydroponics systems placed on concrete floor.

Of the heat and moisture accumulation terms on the left-hand side of Eqns. (3.1) to (3.7), those for the cover, air, floor and plate are negligible compared to existing fluxes, either due to small mass or small heat capacities. Heat capacity per unit volume of plant materials (4200 kJ/m^3K) as reported by Takakura et al. (1971) is essentially that of water. When solar radiation is high, exceeding 600 W m^{-2} at the plant canopy level, the amount of energy stored over an hour is insignificant in comparison to diurnal energy fluxes. For the situation of moderate to low solar radiation and large change in leaf temperature with time, this storage term cannot be overlooked. However, this condition rarely occurs and hence, energy storage in leaves can also be neglected. Eqns. (3.1) to (3.7) therefore degenerate into steady-state equations that may be solved to predict greenhouse environmental conditions on an hourly basis. A similar approach was used by Kindelan (1980), Kimball (1981) and Avissar and Mahler (1982).

Description of how the various heat fluxes in the model are evaluated follows.

Solar radiation absorbed by the various surfaces are computed from global and diffuse irradiances incident on an outside horizontal surface. Beam irradiance is the difference between the two quantities. Diffuse and beam components were each transposed to radiation incident upon an inclined plane (the greenhouse cover). Transmitted solar irradiance is then calculated for each hour using the incidence angle at mid-hour, by means of Fresnel's relations and Bouguer's law of attenuation that account for reflectance and absorptance respectively. The above computational formulae are presented in detail by Iqbal (1983). The diffuse component is relatively independent of the sun's position and is assumed to be incident at a constant 60 degrees (Duffie and Beckman, 1980). The total primary solar energy input is the sum of beam and diffuse radiations transmitted through the cover (roof, wall and gable ends), $I_{b \beta t}$

and $I_{d\beta t}$. The latter originates from I_d which consists of sky diffuse irradiance and ground reflected irradiance, assumed perfectly diffused. An anisotropic model (Klucher, 1979 cited by Iqbal, 1983) was used to transform I_d to $I_{d\beta}$; this model approximates partly cloudy sky conditions, and may vary from clear skies on one extreme to entirely cloudy skies on the other.

The admitted solar radiation has to be traced further to arrive at quantities of solar energy incident on an inside horizontal surface (plant canopy or floor level) or absorber plate surface. Two separate factors are determined for this end, one being called the 'interception factor (P_{kj})' for beam radiation and the other is the well known 'configuration factor (F_{kj})' for diffuse radiation. The interception factor is necessary because the dimensions of the greenhouse dictate the percentage of transmitted direct sunrays that is captured inside the greenhouse, whereas the configuration factor accounts for diffuse radiation that does not reach the surface in question. Based on the method outlined by Smith and Kingham (1971), P_{kj} was formulated for each of the inside horizontal surface and the absorber plate surface; it is a function of the solar altitude, the solar azimuth, as well as the cover surface azimuth and slope, and the greenhouse dimensions. The expression for F_{kj} between two rectangles having a common edge and forming an arbitrary angle was first derived by Hamilton and Morgan (1952) and later corrected numerically by Feingold (1965). F_{kj} varies with the greenhouse dimensions and the relevant cover surface area involved in the radiation interchange. The equations associated with P_{kj} and F_{kj} are derived or otherwise reproduced in appendix A. Absorbed solar radiations by the plant canopy S_p, and the absorber plate S_q are summarized in the following two expressions:

$$S_p = \alpha_p \sum_k A_k \left[(\tau_b I_{b\beta} P_{kp} + \tau_d I_{d\beta} F_{kp}) + \rho_q F_{qp}(\tau_b I_{b\beta} P_{kq} + \tau_d I_{d\beta} F_{kq})\right] \qquad (3.8)$$

$$S_q = \alpha_q \sum_k A_k \left[(\tau_b I_{b\beta} P_{kq} + \tau_d I_{d\beta} F_{kq}) + \rho_p F_{pq}(\tau_b I_{b\beta} P_{kp} + \tau_d I_{d\beta} F_{kp})\right] \qquad (3.9)$$

where k denotes each cover surface. Two assumptions were made:

1. only one internal reflection is considered, as subsequent multiple reflections are much weakened because of low albedo values of the various participating surfaces
2. a surface reflects radiation diffusely

The evaluation of internal convective heat transfer coefficients follows Seginer and Livre's (1978) rational approach, which considers the combined effects of free and forced convection. Thus

$$h_{qa} = 1.43|T_q - T_a|^{1/3} + 5.2\left(\frac{u_m}{L_c}\right)^{1/2} \tag{3.10}$$

$$h_{cia} = 1.52|T_{ci} - T_a|^{1/3} + 5.2\left(\frac{u_m}{L_c}\right)^{1/2} \tag{3.11}$$

$$h_{pa} = 1.90\left|\frac{T_p - T_a}{\ell_p}\right|^{1/4} + 5.2\left(\frac{u_p}{\ell_p}\right)^{1/2} \tag{3.12}$$

The dimensions of the cover (or the absorber plate) and the larger temperature difference between inside air and the cover (or absorber plate) leads to a large enough Grashof number that in turn causes turbulent free convection between these elements. On the other hand, the much smaller dimension of the leaf and a less pronounced temperature difference between the air and plant canopy would likely result in laminar free convection near the plant canopy. Thus, the forms of the free convection coefficients differ slightly in equations 3.10 to 3.12. The external convective heat transfer coefficient h_w is evaluated using eqn. 2.13 when wind speed is between 4 and 20 m s^{-1}. Below the lower limit, h_w is obtained from eqn. 2.14.

Thermal (long-wave) radiation exchange among the various component surfaces (assumed gray diffuse) is calculated by the two relationships (Siegel and Howell, 1965) for isothermal surfaces that form an enclosure:

$$Q_{rk} = A_k \frac{\varepsilon_k}{1-\varepsilon_k}(\sigma\theta_k^4 - J_k) \tag{3.13}$$

$$Q_{rk} = A_k\left(J_k - \sum_{j=1}^{n} F_{kj} J_j\right) \tag{3.14}$$

The sign convention is such that a negative value of Q_{rk} represents heat gain by the surface k. Eqns. (3.13) and (3.14) are written for the enclosure formed by the absorber plate, the plant canopy and the cover. In addition, thermal radiation exchange between each surface and the sky is treated as a two-body system, thus

$$Q_{rk\psi} = \tau_{\ell w} \frac{A_k \sigma(\theta_k^4 - \theta_\psi^4)}{\frac{1-\epsilon_k}{\epsilon_k} + \frac{1}{F_{k\psi}}} \tag{3.15}$$

where τ_{lw} is the long wavelength transmittance of the cover. Typical values are 0.04 for glass and 0.80 for polyethylene, whereas acrylic material transmits virtually no thermal radiation. This expression excludes the sky emissivity since the surface area A_k is negligibly small compared to the sky dome's thus A_k /A --> 0. The sky temperature, θ_ψ , then is related to outside air temperature (Swinbank, 1963) by

$$\theta_\psi = 0.0552\,\theta_o^{1.5} \tag{3.16}$$

Although it is certain that both the clouds and the ground will tend to increase the effective sky temperature over that for a clear sky, it makes little difference upon evaluating collector long-term performance when their influence is not reflected in Eqn. (3.16) (Duffie and Beckman, 1980).

The terms that are common in both the heat and mass transfer processes include M_{cd} , the rate of the inside air moisture loss by condensation on the cover, M_e , the rate of transpiration and M_v , the rate of moisture transfer due to ventilation and infiltration.

The expression for M_{cd} is

$$M_{cd} = h_D A_c (W_a - W^*_{ci})$$
$$h_D = h_{cia} Le^{0.67} / c_a \tag{3.17}$$

M_{cd} is given a zero value when it is negative. Humidity ratio, W, is evaluated using psychrometric equations obtained by Wilhelm (1976) through curve fitting to data points on the psychrometric chart (appendix B). Implicit calculations are necessary here since it is a function of inside temperatures and relative humidity that are to be solved at the same time. Heat of condensation is then calculated as $\lambda\ M_{cd}$.

M_v is also expressed in terms of humidity ratio as follows:

$$M_v = (\nu V)_a N (W_a - W_o)/3600 \tag{3.18}$$

where N is the number of air changes per hour. When no ventilation is required, N assumes the values pertinent to infiltration, typical values are 0.75 to 1.50 for newly constructed glass structure, and 1 to 2 for well-maintained old glass construction (ASHRAE, 1981). The corresponding rate of sensible heat loss can be determined as

$$Q_v = (\nu c V)_a N (T_a - T_o)/3600 \tag{3.19}$$

M_e is computed from the latent heat transfer due to transpiration as

$$M_e = \frac{2}{\lambda \beta} h_{pa} A_p (T_p - T_a) \tag{3.20}$$

when the humidity ratio of the leaf (assumed at saturation) is greater than that of inside air. But when the reverse condition $W_a > W_p$ is encountered, transpiration will be assigned a zero value, and condensation on the canopy is neglected.

3.1.2 Rockbed thermal storage

Rock size (25–38 mm) and air flow rate (0.11 m^3 s^{-1} per m^2 cross-sectional area) used in the solar shed experiments were within the range of experimental conditions investigated by Lof and Hawley (1948) and hence their empirical expression (eqn. 2.18) for h_v , the volumetric heat transfer coefficient is valid for this study. Moreover, with a cross-sectional area of 4.57 x 0.91 m, NTU_c was calculated to be 56 for each storage chamber. Thus, the necessary condition for using the one-dimensional heat flow equation for packed beds (eqn. 2.19) is met. Another point that has to be addressed before applying this equation to analyze storage of greenhouse excess solar heat concerns the assumption of no occurence of mass transfer and thus release of latent heat possessed by the moist inlet air. Condensed vapor in the storage was in fact drained into a sump so that the rockbed thermal properties are not significantly altered by the presence of water. The amount of condensate was not measured, thus the importance of the latent heat term as compared to the sensible heat cannot be assessed. During the charging operation, the release of latent heat would lead to more heat being stored, and improves the performance of the solar heating system. The assumption of no mass transfer is therefore conservative and this simplified rockbed model is considered sufficient for the present investigation.

Using the finite difference method, the bed may be divided into a numer of segments along the flow direction, as shown in Fig. 3.1. The boundary and initial conditions are:

$$\begin{aligned} T_{rs}(x,t) &= T_a && \text{at } x = 0 && \text{charging} \\ T_{rs}(x,t) &= T_a && \text{at } x = L_{rs} && \text{discharging} \\ T_{rs}(x,0) &= T_{sm} \end{aligned} \tag{3.21}$$

Since airflow direction is reversed during the discharging operation, the first term on the right-hand-side of eqn. 2.19 is negated. Besides, when the rockbed is in neutral

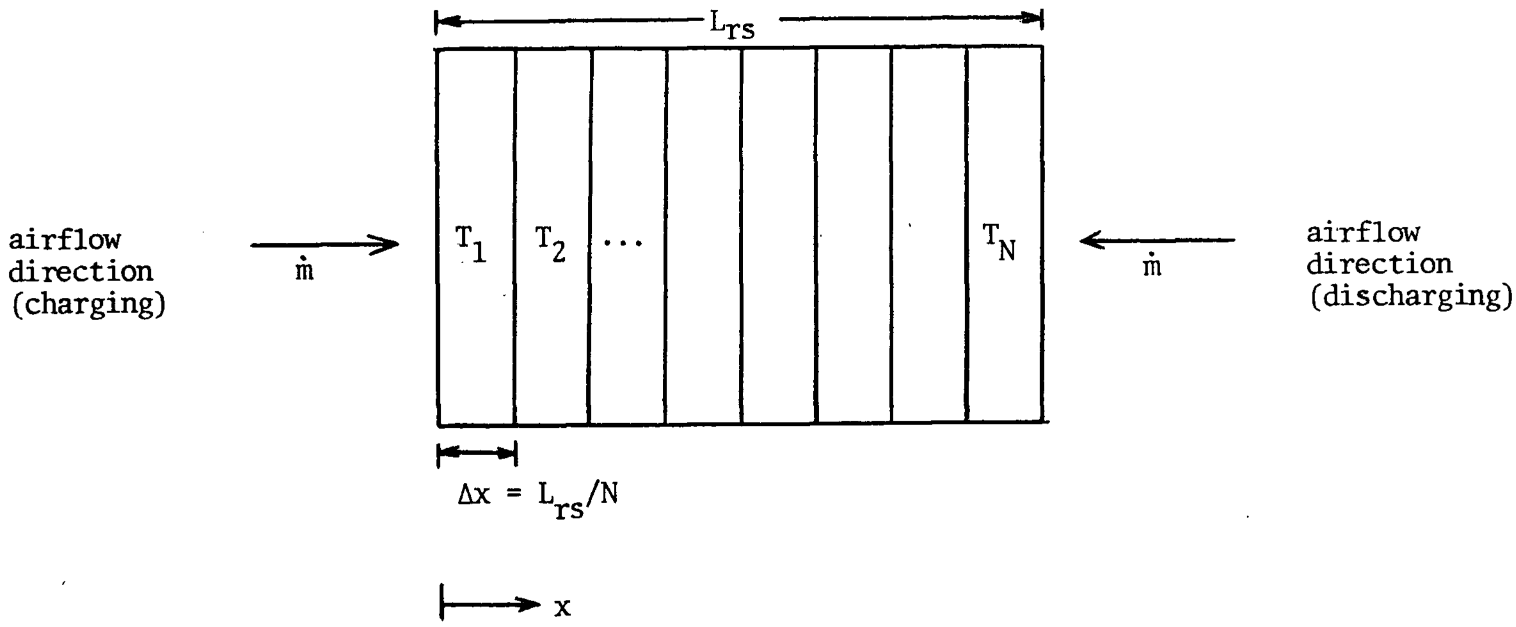

Fig. 3.1 Rocked thermal storage divided into N segments

mode, this term will be omitted in the calculations. The rockbed is assumed to be well insulated such that heat transfer through the greenhouse floor is negligible.

3.2 System II - Internal Collection With Soil Thermal Storage

3.2.1 Greenhouse thermal environment

The heat and mass balances that constitute the greenhouse thermal environment model are similar to those of the solar shed, except for the absence of a vertical absorber plate that will modify the conventional greenhouse climate. Eqns. 3.1 to 3.7 are therefore applicable to this system, with the exception of eqn. 3.3 and excluding terms that are related to the absorber plate.

3.2.2 Soil thermal storage

The choice of an appropriate model for the soil thermal storage with a subsurface pipe system depends on its cost-effectiveness. Three-dimensional (3-D) computer models should give the most accurate results, however, they need much more computing time than either the two-dimensional (2-D) or axisymmetric formulations that require more assumptions. Since many simulation runs are anticipated for model validation and subsequently the prediction of long term system performance, the 3-D method was ruled out. Unfortunately, the more powerful axisymmetric formulation about a single pipe does not appear to suit the existing network of buried pipes, a 2-D scheme was therefore considered most applicable for the present work. Further savings in computational cost can be achieved by neglecting moisture fluxes. The possible problem of soil becoming dried around the pipe is ameliorated by the excess irrigation water that seeps through the porous concrete floor to keep the soil moist. The use of the 2-D model is also justified by observed soil temperature data along the pipes. Thermistors located in the longitudinal direction measured temperature difference in the order of 2 to 4°C, indicating that the thermal gradient and therefore heat transfer was quite small in this direction compared to the lateral (x) and vertical (y) directions.

With the above assumptions, the governing equation of transient heat transfer in the wet soil thermal storage is the Fourier equation for systems that have no heat generation

$$C_s \frac{\partial T_s}{\partial t} = k_s \left(\frac{\partial^2 T_s}{\partial x^2} + \frac{\partial^2 T_s}{\partial y^2} \right) \tag{3.22}$$

$$C_s = (0.315 + \theta_s) \times 4.18$$
$$k_s = a_s \theta_s + b_s$$

The thermal conductivity is assumed to be independent of the x and y coordinates for a homogeneous soil, and its relation with moisture content is approximated by a linear expression. The modeled region of the storage is shown in Fig. 3.2 along with all the boundary conditions. The temperature gradient vanishes ($\partial T/\partial x = 0$) across the axis of symmetry (centerline of the greenhouse, $x=d_2 + w/2$), since the greenhouse with its components is modeled as a one-dimensional entity, and is assumed to be so at the insulation edge. Other boundary conditions are

$$\frac{\partial T_s}{\partial y} = 0 \qquad \text{at } y = d_1 + s_1 + 3d_2$$

$$\frac{\partial T_s}{\partial x} = 0 \qquad \begin{cases} \text{at } x = 0, y > 2d_1 + s_1 \\ \text{at } x = d_2, y \leq 2d_1 + s_1 \end{cases}$$

$$-k_s \frac{\partial T_s}{\partial x} = -k_s \frac{\partial T_s}{\partial y} = U_p (T_a - T_s) \qquad \text{at pipe/soil interface}$$

$$-k_s \frac{\partial T_s}{\partial y} = U_{as} (T_a - T_s) \qquad \text{at } y = 0, x > d_2 \tag{3.23}$$

The diurnal damping depth, d_2, for the clay soil with 30% moisture content was calculated to be 0.124 m, and perturbation was considered insignificant at a depth of three times d_2.

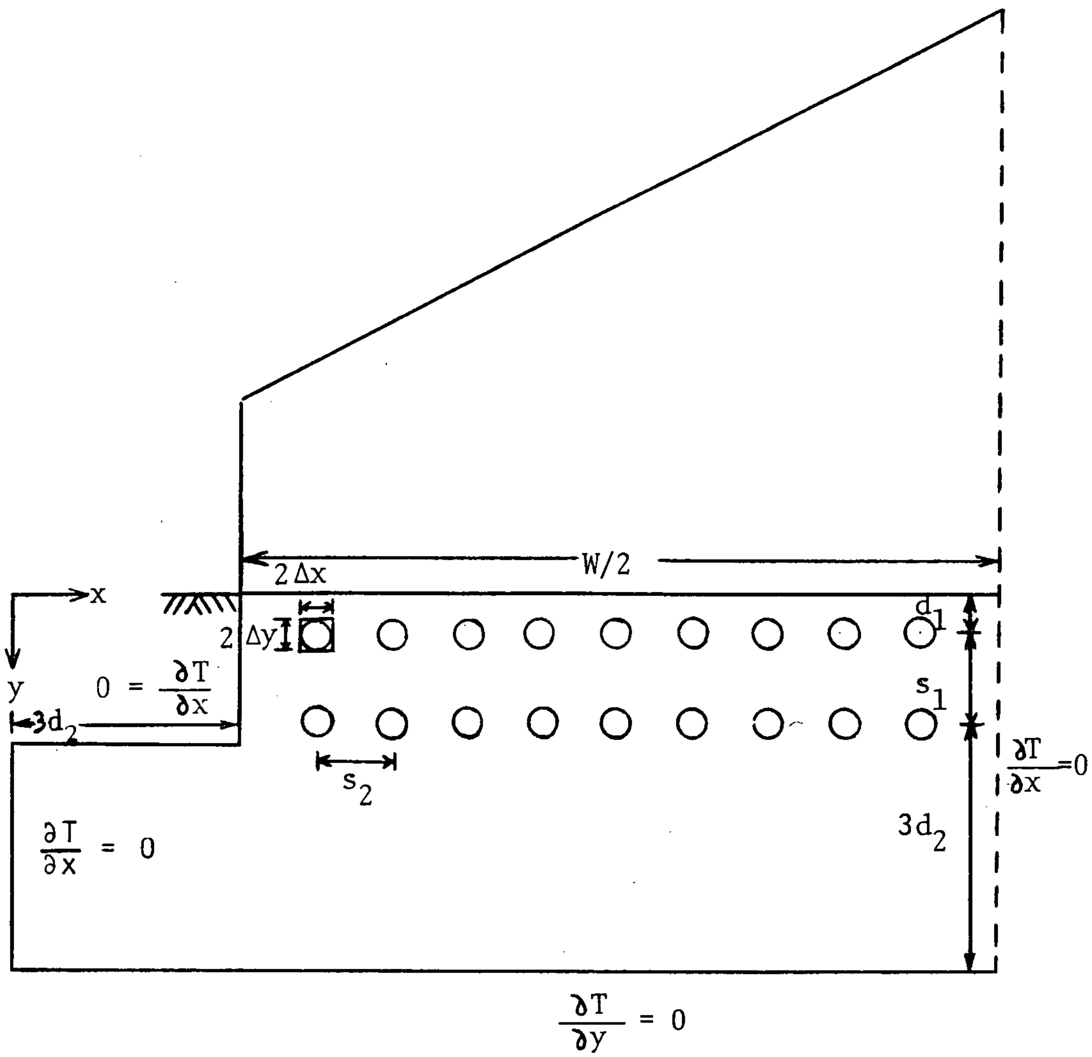

Fig. 3.2 Soil thermal storage - modeled region

w: greenhouse width = 10.8 m
d_1: depth of upper row pipes = 0.35 m
d_2: damping depth of wet clay soil = 0.12 m
s_1: vertical spacing between upper and lower rows = 0.20 m
s_2: horizontal spacing between two neighbouring pipes = 0.65 m

$\Delta x = \Delta y$; finite difference scheme grid size = D/2
D: pipe diameter = 0.10 m

The convective heat transfer coefficient for pipe air, h_p, was evaluated by the Dittus–Boelter empirical equation for turbulent flow in smooth pipes (Sibley and Raghaven, 1984). Preliminary calculations also showed that h_p so calculated was close to experimental values obtained by Eckhoff and Okos (1980) under similar circumstances. Incorporating the thermal resistance of the PVC pipe wall, the overall heat transfer coefficient between pipe air and soil/pipe interface may be expressed as

$$U_p = \left(\frac{1}{h_p} + \frac{\vartheta_p}{k_p}\right)^{-1} \tag{3.25}$$

whereas the overall heat transfer coefficient between greenhouse air and soil surface underneath the porous concrete floor (y = 0) is calculated from

$$U_{as} = \left(\frac{1}{h_{fa}} + \frac{\vartheta_f}{k_f}\right)^{-1} \tag{3.24}$$

This expression for U_p along with the related boundary condition calculates the heat transferred from greenhouse air to the soil, thus bypassing the use of the floor temperature.

Psychrometric equations were applied to determine if condensation would take place inside the pipe which would cause an increase in the convective heat transfer coefficient h_p. An augmented value of h_p can be calculated based on the latent heat removed from the condensate, assuming that the area is the same for both sensible and latent heat transfers. Again, the latent heat is calculated from the Lewis relationship

$$Q_\lambda = \frac{\lambda}{c_a} h_p Le^{0.67} A_w (W_a - W_w^*) \tag{3.26}$$

3.3 The Simulation Method

Computer simulations were performed aiming at validating the mathematical models presented earlier for the two systems. Values of the constants used in the simulations were either measured or approximated from literature, and are listed in Table 3.1.

Actual hourly data collected by Staley et al. (1984) include: global and diffuse solar radiation on an outside horizontal surface, solar radiation transmitted through various greenhouse surfaces, solar radiation striking the absorber plate, photosynthetically active radiation (PAR) at the gutter height level, inside air dry bulb temperature (at various positions) and relative humidity, outdoor dry bulb temperature, absorber plate temperature (at various heights), charging and discharging air flow rates, rock bed temperatures and soil temperatures (at a number of locations), storage inlet and outlet temperatures, supplemental energy consumption and soil temperature outside the rock bed. These measurements were taken regularly and recorded on the control computer. In addition, plant canopy temperature and greenhouse cover temperature were measured separately on a few occasions between February and May 1984. The instruments employed for data acquisition are listed in appendix D, along with the location of relevant sensors. Data for wind speed and outside relative humidity were obtained from the weather records maintained by the Victoria International Airport, located 2 km from the greenhouse research station. Preliminary computer runs used these actual data to calibrate the greenhouse model and the thermal storage model separately, while the two models are subsequently combined during validation runs.

In the greenhouse model, the most difficult variable to be evaluated is the ventilation rate N (number of air changes per hour) due to natural ventilation, which is a function of wind speed, vent location and size of vent opening. Another parameter that was not precisely measured is the Bowen ratio β, which was allowed to assume values between 1.0 and 2.5 for an actively growing crop, and between 2.5

Table 3.1 Values of parameters used in validating the simulation model for systems I and II

Greenhouse

orientarion		E-W
roof tilt		26.6
eave height		2.6 m
length	I:	18.3 m
	II:	19.3 m
width	I:	6.4 m
	II:	10.8 m
ridge height	I:	5.8 m
	II:	5.3 m
volume	I:	490 m^3
	II:	820 m^3

Area

plant canopy	I:	105 m^2
	II:	140 m^2
cover		
roof	I:	131 m^2
	II:	232 m^2
wall	I:	47 m^2
	II:	100 m^2
gable ends	I:	54 m^2
	II:	85 m^2
absorber plate		96 m^2
insulation		106 m^2

Rockbed storage (per chamber)

area normal to flow	4.16 m^2
bed length	4.57 m
mass flow rate	0.56 kg s^{-1}
rock diameter	25-38 mm
bulk density	1760 kg m^{-3}
void ratio	0.37
specific heat	880 J kg^{-1} K^{-1}
thermal conductivuty	0.93 W m^{-1} K^{-1}
heat loss coefficient	0.60 W m^{-2} K^{-1}

Soil storage

pipe	
wall thickness	2.5 mm
thermal conductivity	0.145 W m^{-1} K^{-1}
diameter	0.1 m
length	18 m
number of layers	2
spacing	0.63 m
depths	0.4 and 0.6 m
total mass flow rate	1.78 kg s^{-1}
soil	
thermal conductivity	1.40 W m^{-1} K^{-1}
thermal capacity	2.57 MJ m^{-3} K^{-1}
moisture content	30%

Solar radiation	plant	absorber plate
reflectivity	0.15	0.05
absorptivity	0.75	0.90
transmissivity	0.10	0.05
Thermal radiation		
emissivity	0.95	0.90

Cover

number of layers	1
refraction index	1.526
thickness	3 mm
extinction coefficient	10 m^{-1}

and 4.0 for relatively sparse plants. A checking guideline for N is the values measured by Whittle and Lawrence (1960), which are shown in Table 3.2. The program algorithm was directed to keep checking how much ventilation was needed during each hour to attain the measured inside air temperature and relative humidity level, which put N and β into iterations. During calibration, measured solar radiation incident on the absorber plate and plant canopy were used in eqns. (3.3) and (3.4), while measured storage inlet and outlet temperatures were substituted into eqn. (3.6) during the hour when charging took place for calculating the rate of heat transfer to the storage. The measured external climatic conditions were precribed at each hour. Eqns. (3.1) - (3.7) along with all other expressions for the evaluation of various heat fluxes were simultaneously solved iteratively by the modified secant method as a set of nonlinear algebraic equations. The solving package, NDINVT, is also documented by the UBC computing center (Moore, 1984). Predicted inside air temperature, relative humidity and absorber plate temperature, and occasionally, plant canopy temperature as well as cover temperature will be compared to the actual data. Besides, simulated solar radiation inside the greenhouse will also be verified.

Values of N and β were modified within the allowable limits in order to get more accurate results of greenhouse temperature and relative humidity. Iterations continue until the difference between predicted and measured values of inside air temperature and relative humidity falls within specified tolerance intervals. For temperature, a maximum difference of 10% (from an engineering point of view) was used as the criterion for good prediction accuracy. As relative humidity depends on air temperature, it would likely be less accurately predicted; the tolerance interval for RH_a was set at 15%. At a particular hour when computed and measured values cannot converge, possibly due to factors involved in the greenhouse operation and not indicated in data collection, the model may be deemed unable to yield reasonably accurate results.

TABLE 3.2 THE EFFECT OF WIND SPEED AND VENTILATOR POSITION ON AIR EXCHANGE IN THE GREENHOUSE
(from Whittle and Lawrence, 1960)

Vent position Roof	Sides	Wind speed, kmh	Air exchange per hour
Shut	Shut	21.6	2.9
Lee side ¼ open	Shut	21.4	9.1
Both sides full open	Shut	4.3	14.
Both sides full open	Shut	9.7	20.
Both sides full open	Shut	10.5	34.
Both sides full open	Open	2.3	41.
Both sides full open	Open	3.1	45.

In the rock bed model, measured hourly air inlet temperature was prescribed as the boundary condition at calibration stage. As for initial conditions, spline fitting to the measured rockbed temperatures at various sections was performed to generate continuous values for all rockbed segments. A UBC general purpose program, MOL1D (Nicol, 1987) was used for simulation, it provided a Runge–Kutta integration scheme to solve the differential equation. Rock bed temperatures and the temperature of the air passage outlet during storage charging and discharging are the outputs that are verified with measured data.

For the soil model, soil temperature was assumed to be uniform throughout the storage when the cluster of thermistors placed at two strategic locations all recorded similar temperatures. Eqn. 3.22 together with the various boundary conditions was discretized by an explicit finite difference scheme; details of all representative nodal equations can be found in the computer program listing in appendix C. The explicit scheme is less costly than an implicit one, but the time step Δt has to be selected in such a way that no solution stability criterion is jeopardized. Δt depends on the Fourier number $\alpha\Delta t/\Delta x^2$ which in turn is a function of soil thermal properties (and thus the type of soil and its moisture content) and pipe diameter. Computed hourly soil temperatures and pipe outlet air temperature are checked with actual data.

The two models are then coupled together, whereby the thermal storage models are coded as subroutines in the computer program. Another major subroutine computed the solar radiation striking the glass cover, the plant canopy and the absorber plate. At this stage of simulation, only those environmental conditions unaffected by the presence of the greenhouse were read as inputs to the computer program. Examination of experimental data showed that for system I, the rockbed storage inlet air temperature T_{rsi} was within 1–3 °C of the contemporary greenhouse air temperature T_a , and for system II, the pipe inlet air temperature was lower than the greenhouse air temperature by 2 to 7 °C. The attenuation of air temperature might be associated with the pressure drop as air passes through the vertical ducts before entering the pipe network. For an air flow rate of 0.74 m^3 s^{-1}, calculations show that at constant density, the associated drop of 2.2 kPa in pressure from P_{atm} is sufficient to cause a 6.5 °C decrease in temperature. During each iteration step, the thermal storage subroutine was activated to compute the air outlet temperature and hence the amount of heat transferred to the storage.

3.4 Model Validation - Results and Discussion

3.4.1 Solar radiation transmission and interception

Before making any comparison between simulated and measured data, the latter were analyzed and transformed into two factors, the total transmission factor TTF (eqn. 2.10), and the effective transmissivity τ_e given by

$$\tau_e = \frac{A_p \, \mathrm{PAR}_p / 0.45}{A_f I_{oh}} \tag{3.27}$$

The constant 0.45 is the conversion factor between PAR and broadband solar radiation (Salisbury and Ross, 1978). Values of TTF deduced from measured solar radiation data inside and outside the greenhouse for the shed-type structure are consistently higher than those for the control (conventional gable house). The shed has a TTF ranging from 2.16 in December to 1.03 in June, whereas the control house achieved a value declining from 1.66 in December to 0.93 in July. During the period Oct 83 to Sept 84, solar energy input into the shed with north wall insulated amounted to 5.11 GJ/m^2 compared to 4.22 GJ/m^2 for the conventional house. On a per unit floor area basis, the shed received 32% more radiation than the conventional gable house from Oct 83 to Mar 84, though this margin is reduced to 18% for the months covering Apr to Sept 84. Since the two houses have almost the same transparent cover surface to floor area ratio (1.98 vs. 2.02), the shed-type glasshouse appears to be more efficient in admitting solar radiation than the conventional shape. This may be attributed to the shed's larger area (131 m^2) of the south roof as the major cover surface compared to 110 m^2 for the control house. Simulations were then carried out using one week's data from each month, and results of TTF are plotted in Fig. 3.3. The very good agreement between measured and predicted values may be credited to the well established mathematical relations used for calculating transmitted solar radiation through non-diffusing materials. Values of τ_e derived from experimental data are plotted in Fig. 3.3 along with the TTF values. Two trends that are not possessed by TTF can now be realized. The effective transmissivity of each greenhouse does not vary more than 25% annually, and the shed-type glasshouse has an effective transmissivity insignificantly different from its conventional counterpart. These results are not particularly surprising considering the dimensions of the solar shed that limit the percentage of transmitted beam radiation to be intercepted at the plant canopy level. Simulations produced τ_e values that have a maximum difference of 12% from the experimentally derived values, and these computed results are also plotted in Fig. 3.3. More details about the inside solar radiation that forms the basis of τ_e may be found in the next section.

3.4.2 Greenhouse thermal environment and thermal storage

A number of validation runs have been carried out using the combined greenhouse environment - thermal storage model for the growing period from January to May 1984. In the solar shed, tomato plants were transplanted on February 10 and harvesting started on April 16. During this period, the conventional greenhouse equipped with soil storage had some grape plants. Results for system I and system II are presented in separate sections. Among a large number of observational data that are available for model verification, three weeks with different climatic conditions and system performances were examined in detail for purpose of illustration.

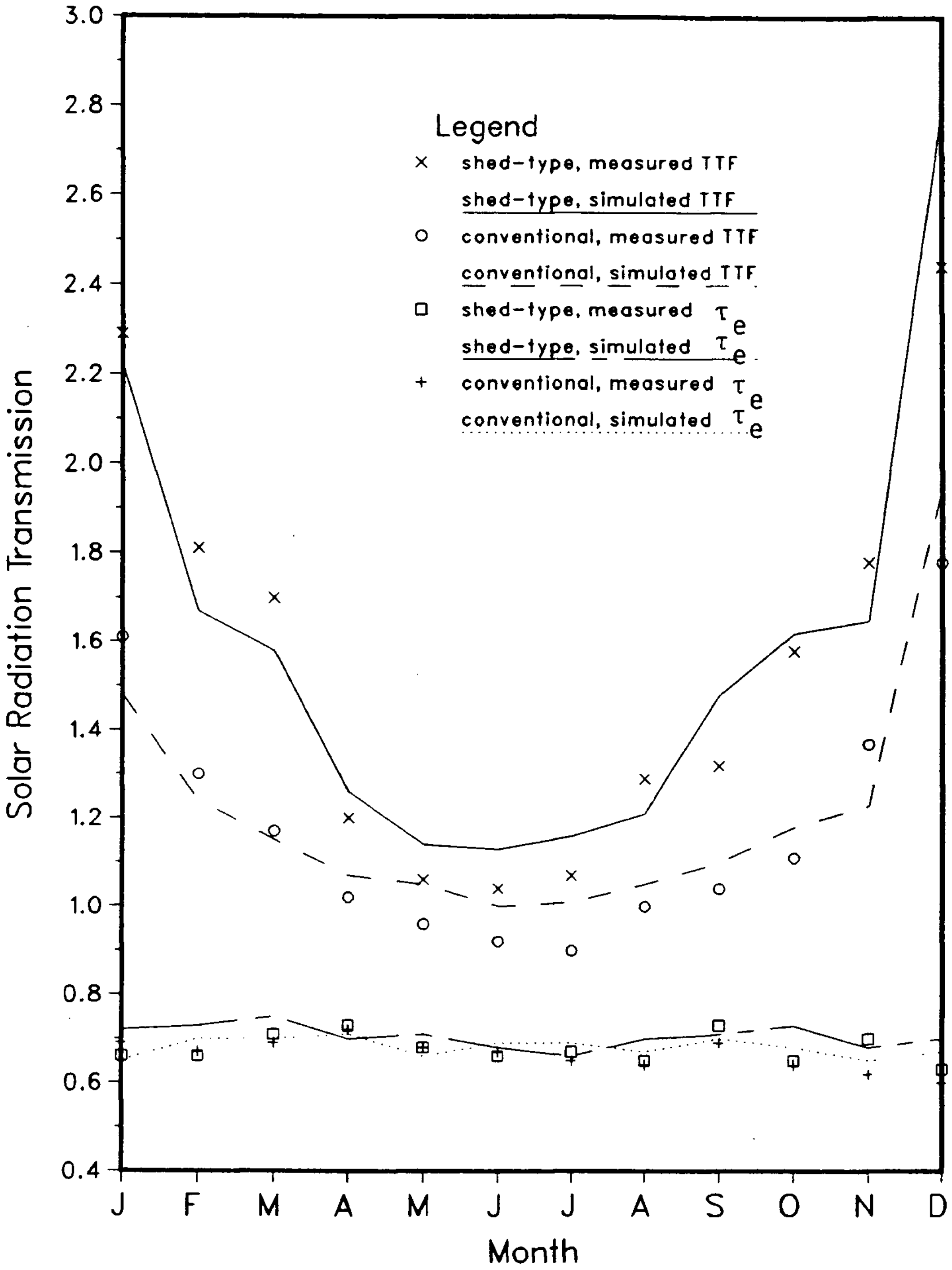

Fig. 3.3 Total transmission factor and effective transmissivity - experimental and simulated results for the period Sept 1983 to Aug 1984

3.4.2.1 System I

Case 1. Feb 18–24

This week recorded a sequence of medium to low hourly solar radiation (I_o = 300 - 500 W m^{-2}), which was mostly (81%) diffuse in nature. Average daily I_o was found to be 6.2 MJ m^{-2}. Other climatic conditions are shown in Fig. 3.4, where diurnal outdoor temperatures are seen to vary from −1 to 10 °C, and the first half of the week was very windy and gusts of up to 60 km h^{-1} were not uncommon.

Predicted values, based on eqns. (3.8) and (3.9), of hourly solar radiation inside the greenhouse are plotted in Fig. 3.5. A day within the week is represented by the interval between two ticks. Since the number of daytime hours with measurable solar radiation varied from day to day, these intervals differ in width. All the figures that illustrate model validation results in this chapter bear this feature. Conversion of PAR to global solar radiation radiation revealed that the magnitude of I_q , solar radiation incident on the absorber plate, was very close to I_p , solar radiation incident on an inside horizontal surface at the plant canopy (gutter height) level, as demonstrated in Fig. 3.6. Weekly total I_p is 8421 MJ and is 5% greater than the measured value of 8015 MJ. As for I_q , simulated and actual data differ by 9%.

Daytime greenhouse environmental temperature regimes and relative humidity are presented in Figs. 3.7 and 3.8. The computed and measured values of inside air temperature T_a , and absorber plate temperature T_q are in very good agreement, with a maximum difference of 4.6 °C for T_a and 3.7 °C for T_q . The means and standard deviations of the differences between simulated and actual greenhouse temperature data are found in Table 3.3. This table also contains statistical results for measured and predicted greenhouse relative humidity and thermal storage temperatures in this case (Feb 18–24) and two others to be

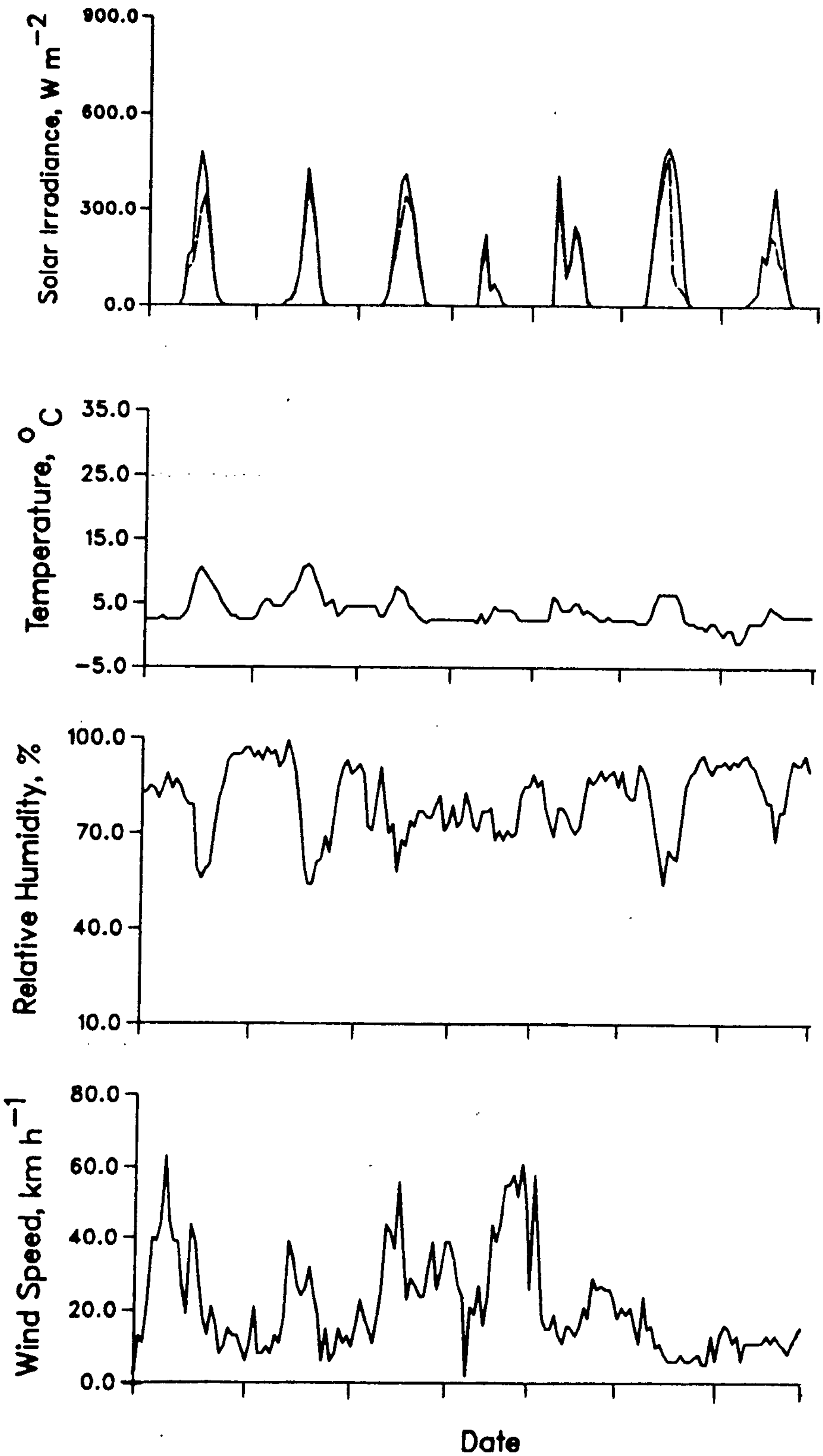

Fig. 3.4 External climatic conditions during the week of Feb 18-24, 1984

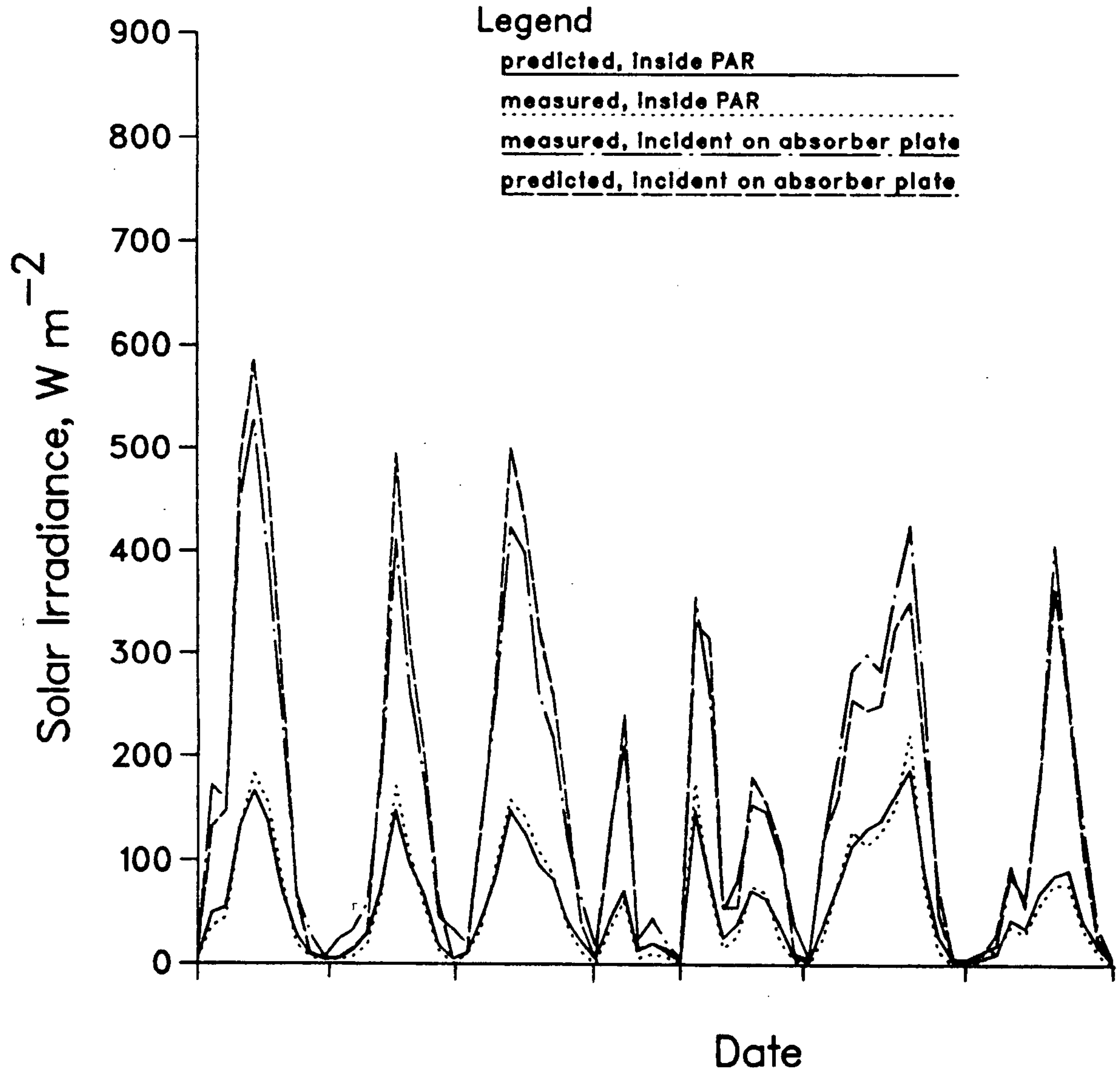

Fig. 3.5 System I - photosynthetically active radiation at plant canopy level, Feb 18-24

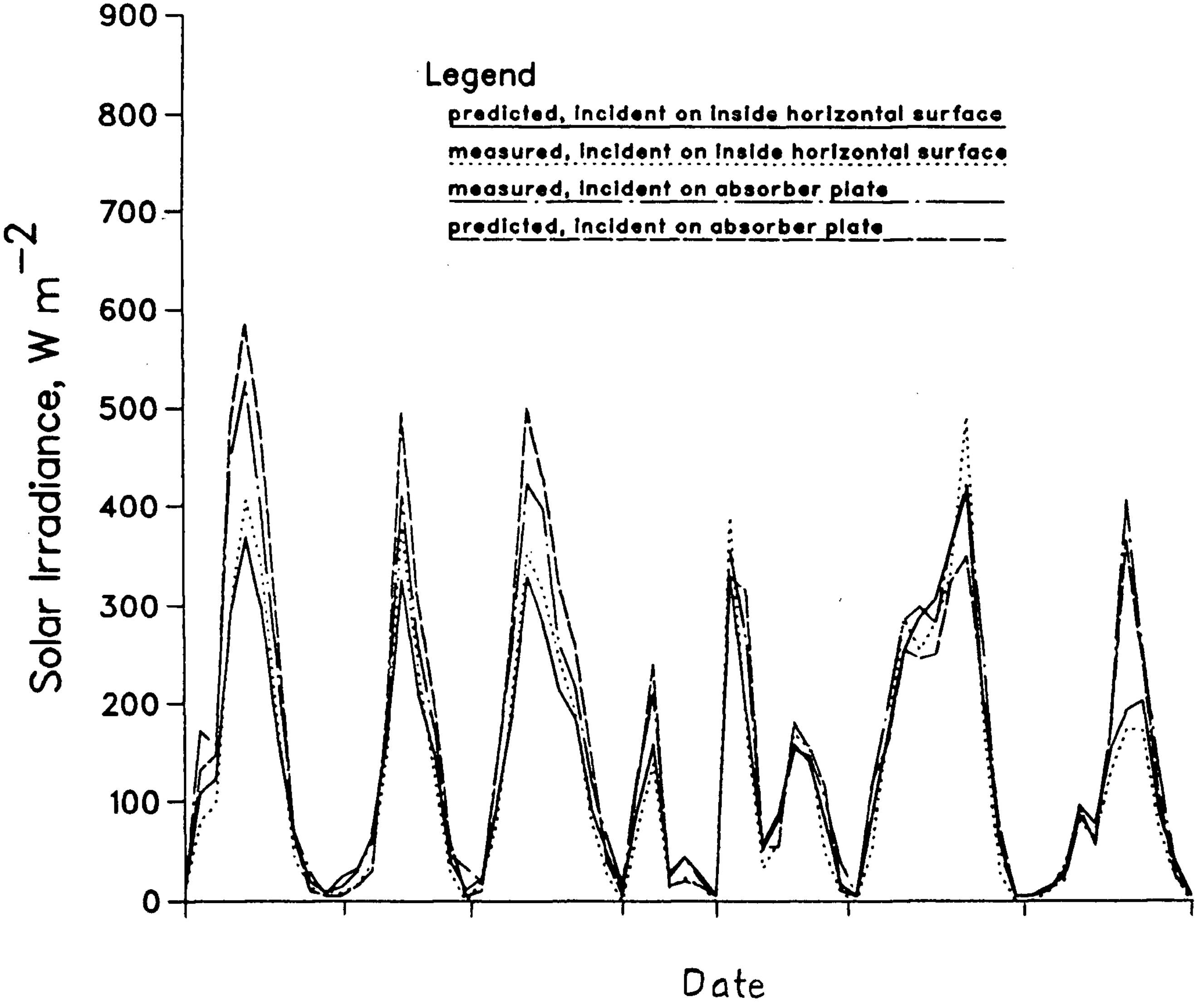

Fig. 3.6 System I - solar radiation incident at plant canopy level and absorber plate, Feb 18–24

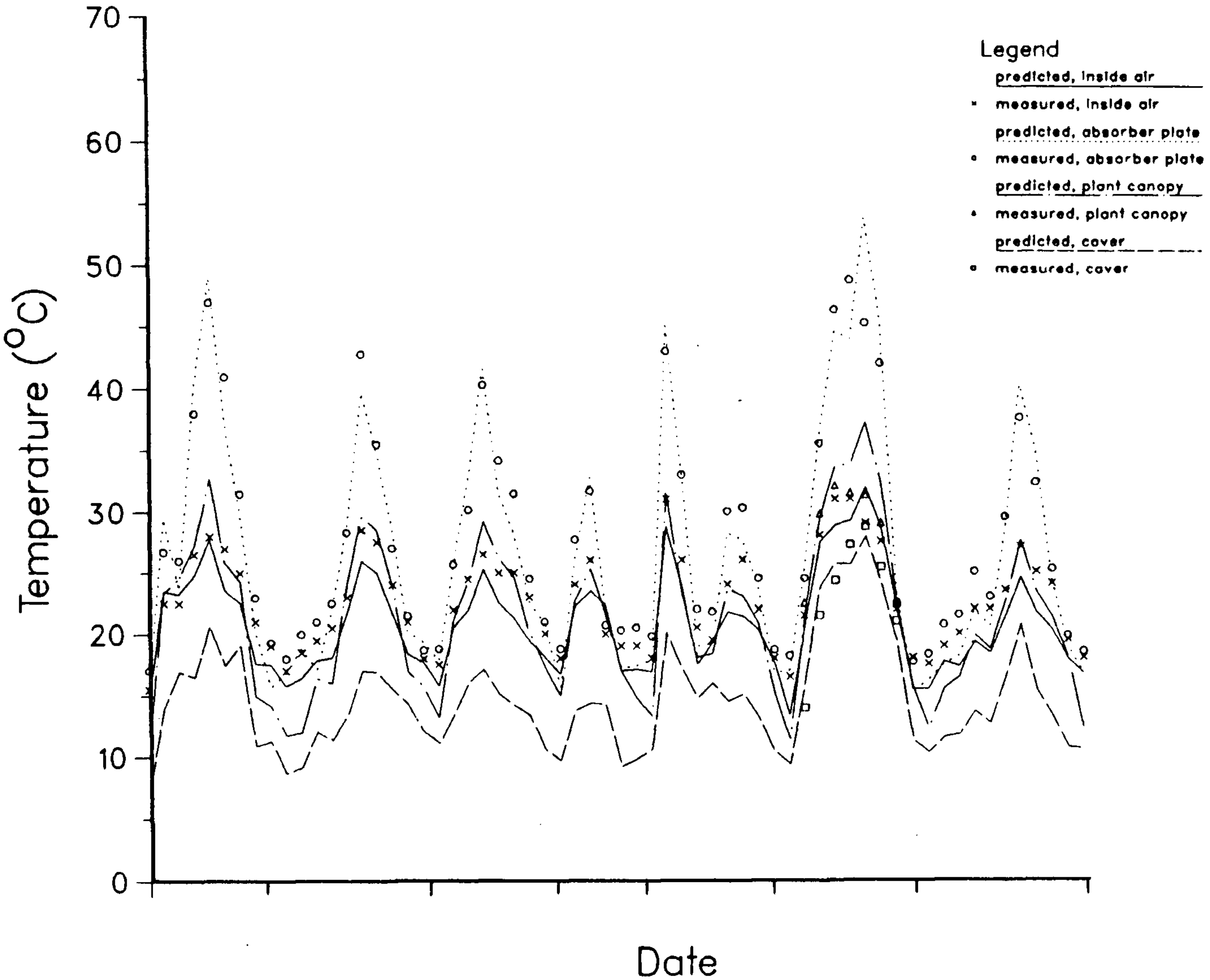

Fig. 3.7 System 1 - temperatures of the greenhouse thermal environment, Feb 18-24

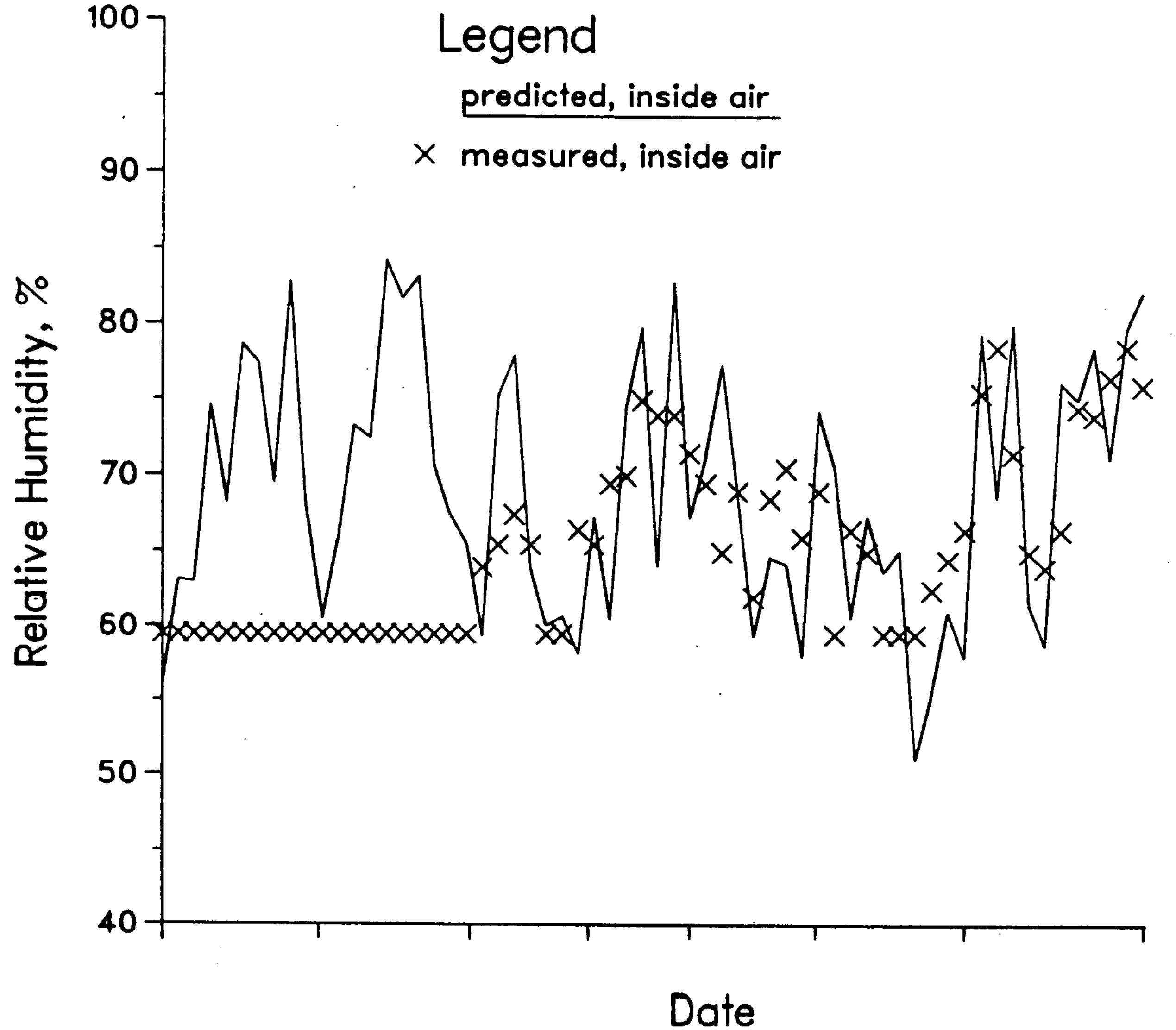

Fig. 3.8 System I - greenhouse relative humidity, Feb 18-24

Table 3.3 Means and standard deviations of differences between predicted/observed temperatures and relative humidities on 3 occasions for 2 systems

Variable		System I			System II		
		Case			Case		
		1	2	3	1	2	3
T_q, ^oC	mean	2.1	3.8	2.3	-	-	-
	S.D.	1.3	2.8	1.6	-	-	-
T_a, ^oC	mean	2.0	1.6	1.6	1.8	1.5	1.6
	S.D.	1.0	1.0	0.9	1.2	1.0	1.3
RH_a, %	mean	3.8	4.7	3.7	3.5	5.3	4.8
	S.D.	3.8	2.2	2.6	2.3	3.7	3.0
T_{rs}, ^oC	mean	1.0	1.0	0.9	-	-	-
	S.D.	0.8	0.9	0.7	-	-	-
T_s, ^oC	mean	-	-	-	0.9	1.0	1.3
	S.D.	-	-	-	0.6	0.7	1.1

discussed later. During the hours with higher solar radiation, plant canopy temperature T_p is greater than T_a by 3 to 5 $^{\circ}$C. Measured leaf temperatures are lower than those calculated, and a difference of up to 6 $^{\circ}$C is obtained. Near sunrise and sunset times when supplemental heating was supplied from the furnace, calculated T_p falls below T_a by 2 to 4 $^{\circ}$C. The highest values of T_a, T_q and T_p occurred on day 6 at 1200 hr (31.0, 48.7 and 33.8 $^{\circ}$C) when I_o rose to 495 W m^{-2} to produce values of (I_q , I_p) as (550, 582 W m^{-2}). The plant canopy receives slightly more solar radiation, but transpiration serves to cool it down substantially while the absorber plate stays at a high temperature.

Relative humidity prediction has a larger error when compared to actual data. Discarding faulty constant-value readings (59.5 percent) on days 1 and 2, a maximum difference of 10 percent is obtained. The statistics of the difference between computed and measured values is also found in Table 3.3. The prediction accuracy is directly linked to the moisture balance of the greenhouse as governed mainly by crop transpiration, which in turn, is a complex function of interacting greenhouse environmental conditions - light, temperature, air velocity and carbon dioxide level. The dominating factor(s) among them would determine the extent of stomatal activity. In the model, transpiration is represented by the Bowen ratio β . Even though β is allowed to vary within reasonable bounds during the simulation runs, it is still not capable of detecting such events on a small time scale. An indirect cause for the discrepancy between measured and predicted values is related to the accuracy in greenhouse air temperature estimation. Assuming constant moisture quantity and hence humidity ratio W_a , the extent of $\Delta T_a = T_a - \tilde{T}_a$ would lead to quite different RH_a values, depending on the magnitude of T_a itself. Table 3.4 gives some typical values of relative humidity as a function of humidity ratio and dry-bulb temperature as derived from the psychrometric chart. The variation of RH with

Table 3.4 Relative humidity as a function of humidity ratio and dry bulb temperature

W, kg/kg	T_{db}, °C	RH, %
0.010	20	68
	25	50
	30	37
	35	28
0.015	20	100
	25	75
	30	56
	35	
0.020	20	100
	25	100
	30	75
	35	

T_{db} diminishes as W becomes smaller. Therefore, as W changes with the moisture balance calculations, the degree of accuracy in predicting RH also varies.

Considering temperature profiles at various positions of the rock bed storage as shown in Fig. 3.9, it is evident that the storage capacity was not fully utilized as some one-quarter of the storage had little rise in temperature during the charging hours to reach its potential value. The low air flow rate of 0.56 kg s^{-1} led to a high NTU and hence transfer to storage was only effective for the anterior portion of the bed. Duncan et al. (1981) noted that long flow paths were inefficient for the typical time-temperature patterns of a greenhouse unless larger air flow rates or heat transfer coefficients could be used. The maximum storage entrance temperature was 33.5 $^{\circ}$C at 1200 hr on day 6 when solar irradiance was at its peak, and was 2.5 $^{\circ}$C higher than the greenhouse air temperature. Energy stored was computed to be 1910 MJ per storage chamber, giving a total of 3820 MJ. Agreement between the predicted and measured rockbed temperatures is better during the charging process, whereas predicted temperatures are generally lower than measured values upon discharging. Although the mean value of the difference between predicted and measured rockbed temperature is only 1.0 $^{\circ}$C with a standard deviation of 0.8 $^{\circ}$C, the temperature of the bed anterior is less accurately predicted compared to either the middle or the posterior section. The means and standard deviations for each of these three sections are (1.5, 0.7), (1.0, 0.9) and (0.6, 0.6) $^{\circ}$C. The whole week had 48 cumulative nighttime hours during which time storage discharging took place and a total of 2960 MJ was recovered. This represents 75% of that stored during daytime. The second half of the nights required supplemental heat when storage exit temperature was lower than or barely reached the greenhouse nighttime setpoint temperature of 18 $^{\circ}$C.

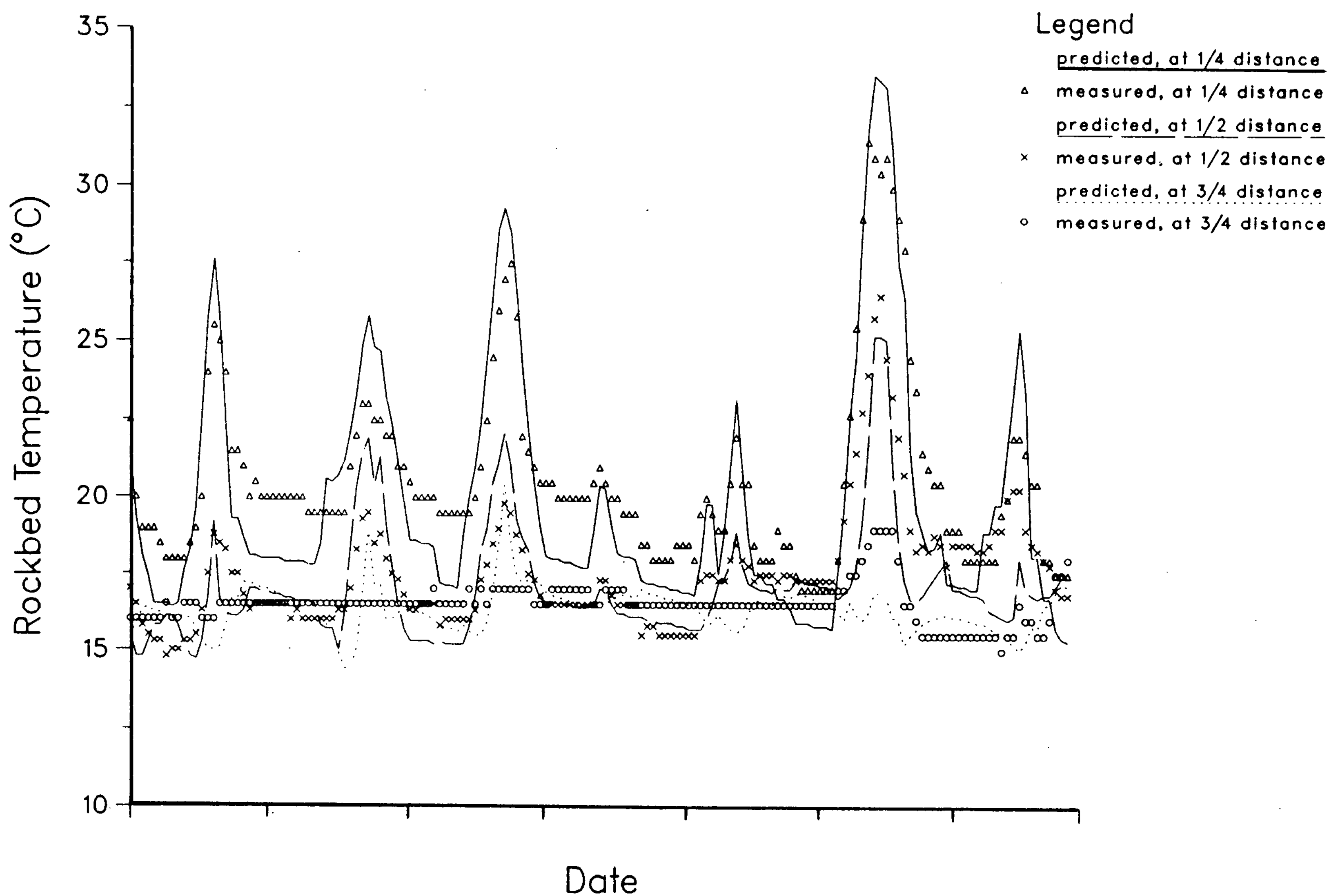

Fig. 3.9 System I - Rockbed temperatures at three sections, Feb 18-24

The thermal stratification of the rockbed based on calculated values on day 3 is shown in Fig. 3.10. Discharging took place between 0000 and 0400 hours while the charging process occured from 0800 to 1500 hours, beyond which the discharging mode resumed. As time progressed, the temperature front passed through the bed and fluctuated in accordance with the operation modes. While the peak charging inlet temperature was 30.5 °C at 1200 and 1300 hours, the subsequent two hours of charging had lower inlet temperatures of 27.5 and 25.5 °C, thus causing a drop in temperature of the anterior rockbed segments. However, effective charging still occured in other parts of the bed. On this day, there was considerable heat discharge between 1600 and 2000 hours as the greenhouse air temperature fell below 18 °C in the evening.

Auxiliary energy requirement for the shed-type greenhouse was recorded to be 3710 MJ. On the other hand, the control house recorded a total heat supply of 60.5 MJ m^{-2}, which translated to 7080 MJ for the solar shed were it operated as a conventional glasshouse without insulation. Hence, energy savings for this week amounted to 3370 MJ and is basically met by the stored solar heat. This value is 410 MJ more than the energy recovered from storage as calculated from the rockbed temperature history. Aside from the slight inside air temperature difference between the two houses, it seems at first glance that the difference could be attributed to the north wall insulation. While it is certain that energy savings may be nullified without the insulation, the $(UA)_h$ value of the shed being 13.9 W $°C^{-1}$ per m^2 floor area is higher than that for the control house with $(UA)_h$ = 13.7 W $°C^{-1}$ m^{-2}. In other words, the shed by itself likely needs as much heating requirement as a conventional greenhouse. Therefore, predicted energy savings for this week is 11% less than the actual data.

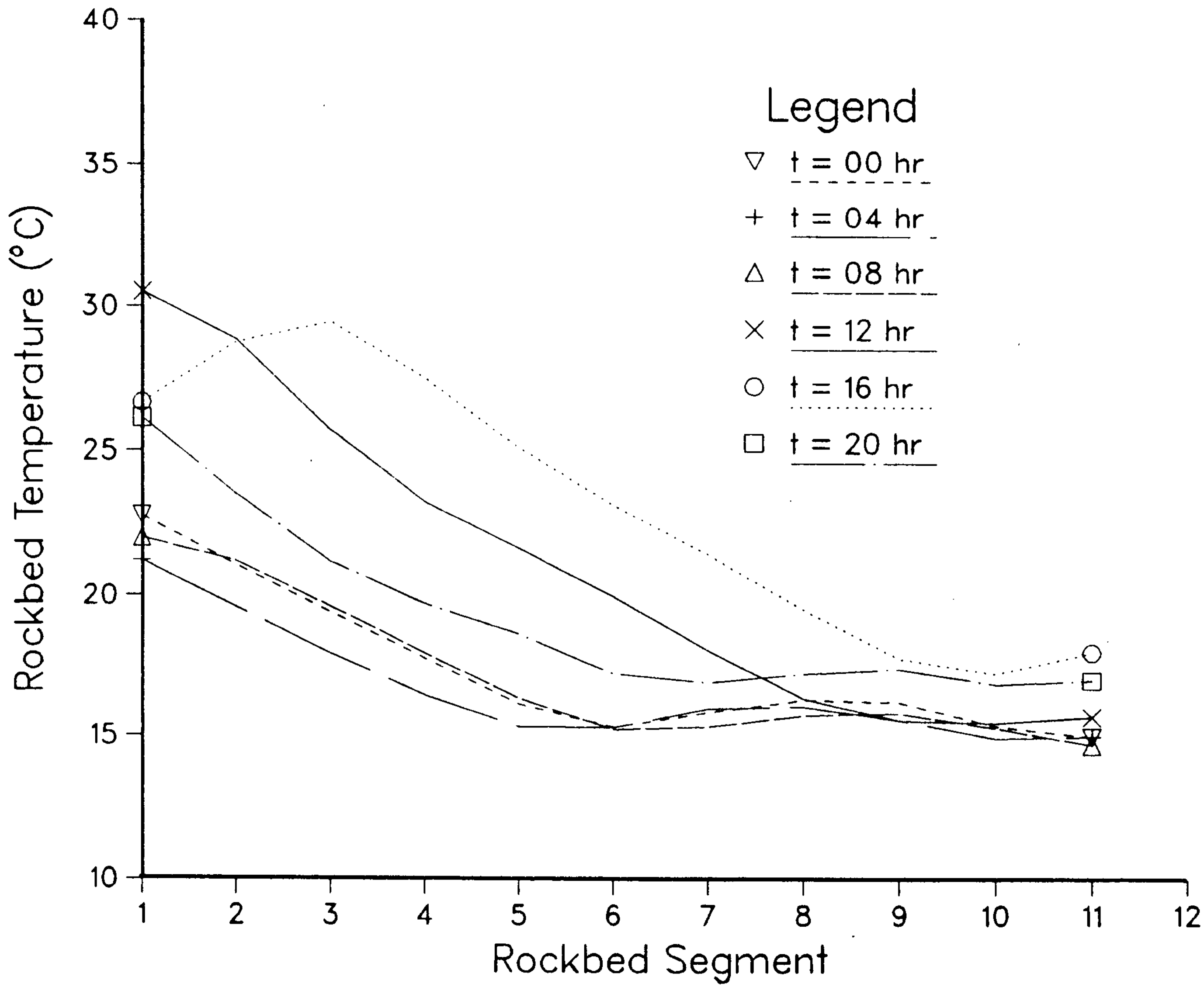

Fig. 3.10 System I - simulated results of spatial temperature distribution in the rockbed, Feb 18-24(day 3)

By fixing the inside air temperature at 18 °C at night, total daytime and nighttime energy requirement was computed to be 7650 MJ , marking a difference of 8% from the experimental value of 7080 MJ.

Case 2. Mar 25–31

Fig. 3.11 depicts the outside climatic conditions. Wind speeds were the lowest among the three weeks under study. Global solar radiation averaged 14.4 MJ m^{-2} per day, and beam radiation constitutes 70% of I_o . The second half of this week had abundant sunshine when I_o attained values of up to 800 W m^{-2} for three consecutive days. These driving forces produced simulation results of inside solar radiation, greenhouse air temperature and relative humidity and rockbed temperature profiles which are separately illustrated in Figs. 3.12 to 3.16.

Except for day 1 when solar radiation level was very low, greenhouse air temperature T_a was consistently above 30 °C during daytime hours with I_o that exceeded 500 W m^{-2}. Correspondingly, the absorber plate temperature T_q was well above T_a , and it managed to acquire a value as high as 63 °C. Predicted temperatures are in favorable agreement with measured data, and the patterns of rises and falls are similar for all temperature terms involved in the greenhouse energy balance. Some experimental data of T_c and T_p were available on day 7 when measurements were taken between 0900 and 1700 hours, and these are also indicated in Fig. 3.13. The temperature differential between T_p and T_a varies from 2 to 8 °C. While simulated leaf temperature approaches 40 °C on one occasion, measurement with the infrared thermometer indicated a value of 33 °C. As for glass cover temperature, inside and outside surfaces did not differ by more than 3 °C, and agree reasonably well with computed values.

The trend of predicted inside relative humidity appears to be in line with the actual values. Relative humidity is kept below 80 percent because of

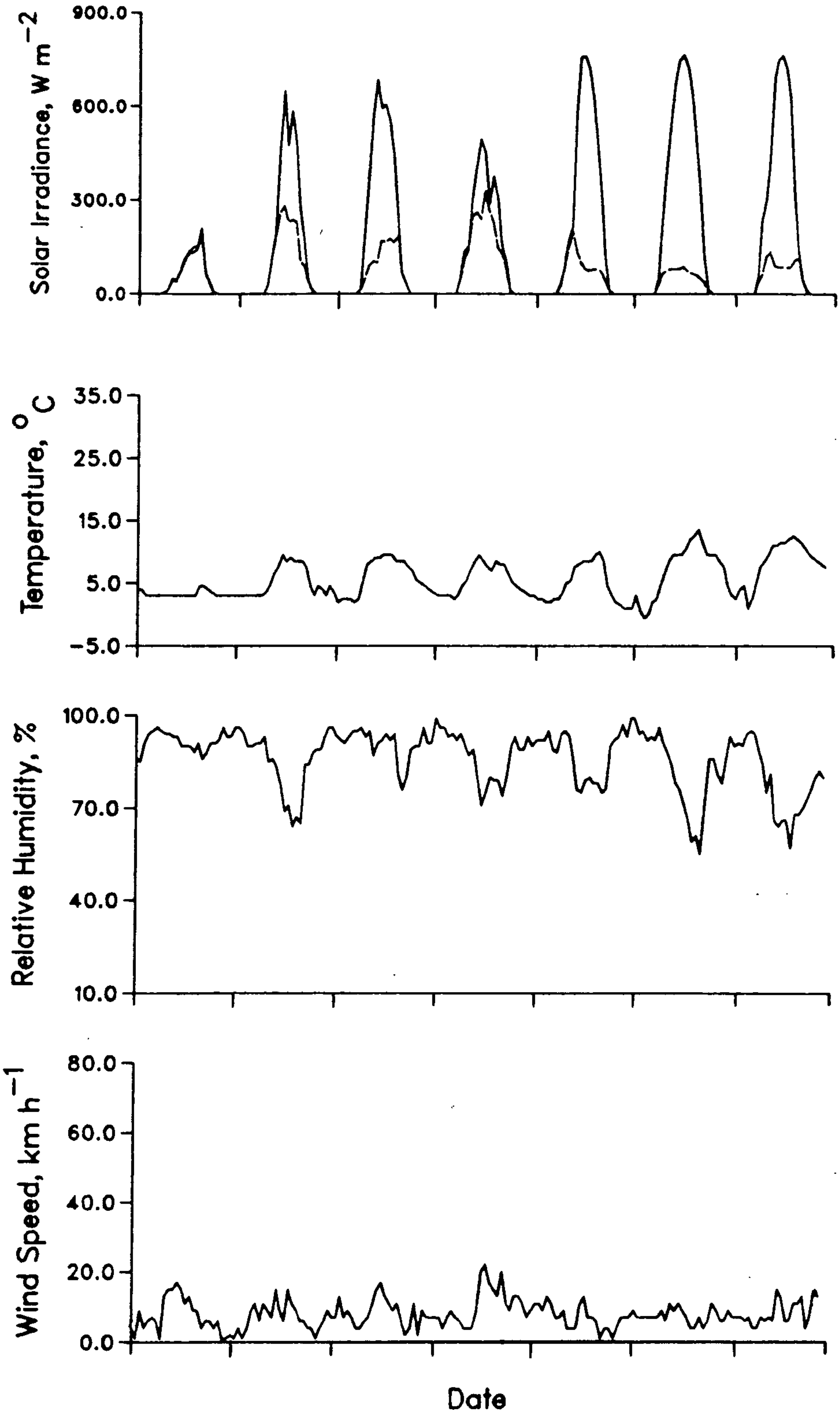

Fig. 3.11 External climatic conditions during the week of Mar 25–31, 1984

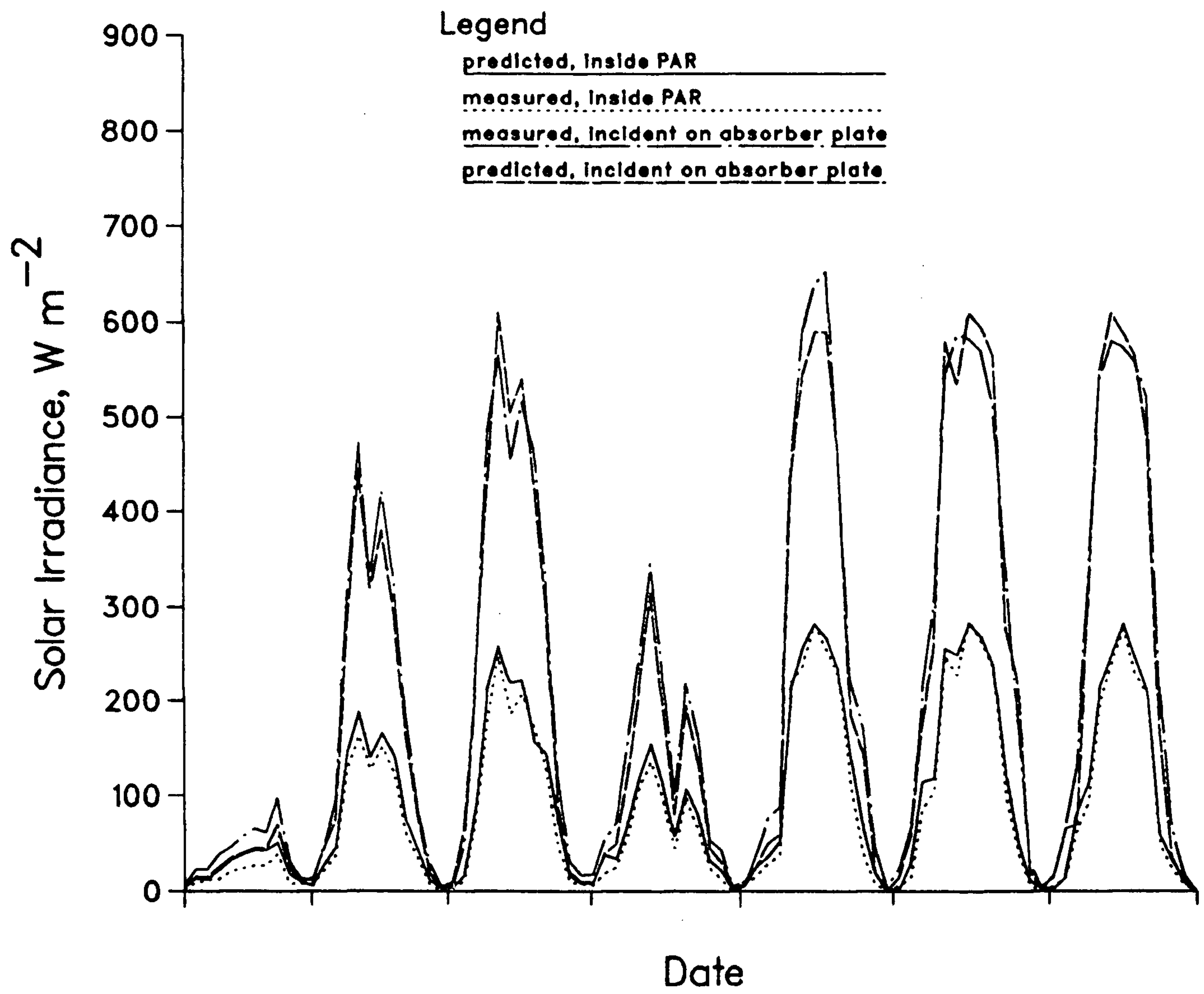

Fig. 3.12 System I - PAR at plant canopy level, Mar 25–31

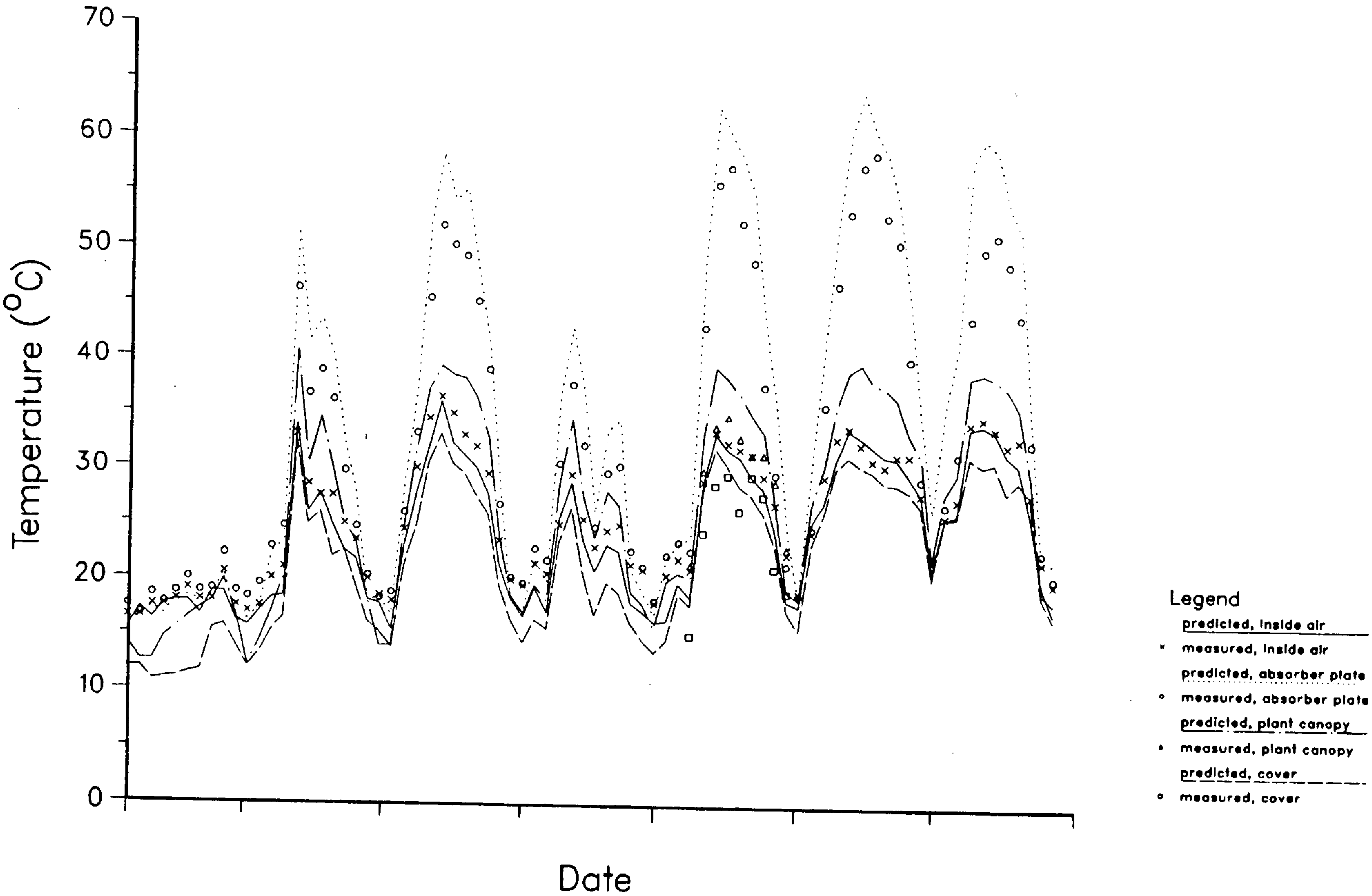

Fig. 3.13 System I – temperatures of the greenhouse thermal environment, Mar 25–31

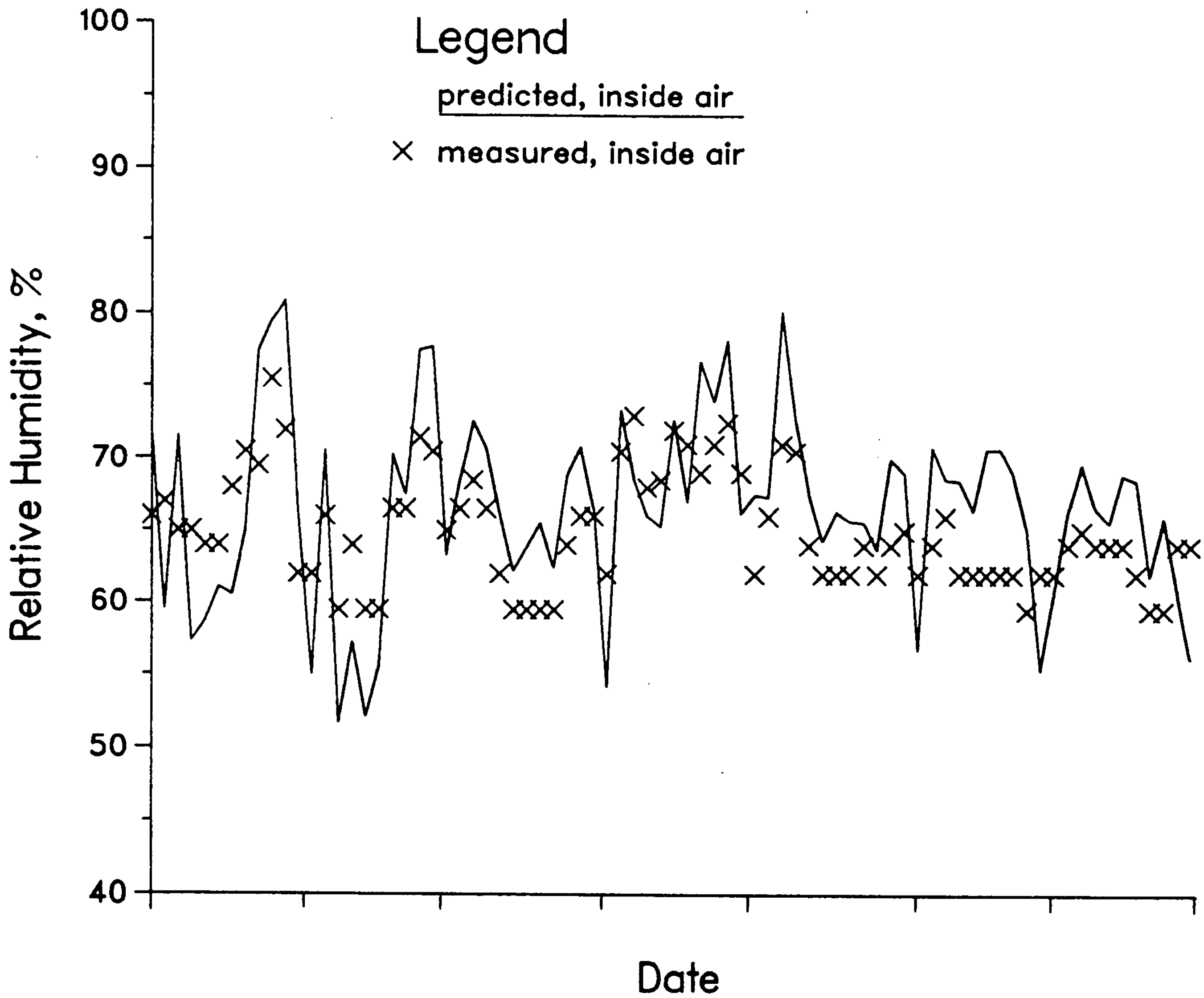

Fig. 3.14 System I - greenhouse relative humidity, Mar 25-31

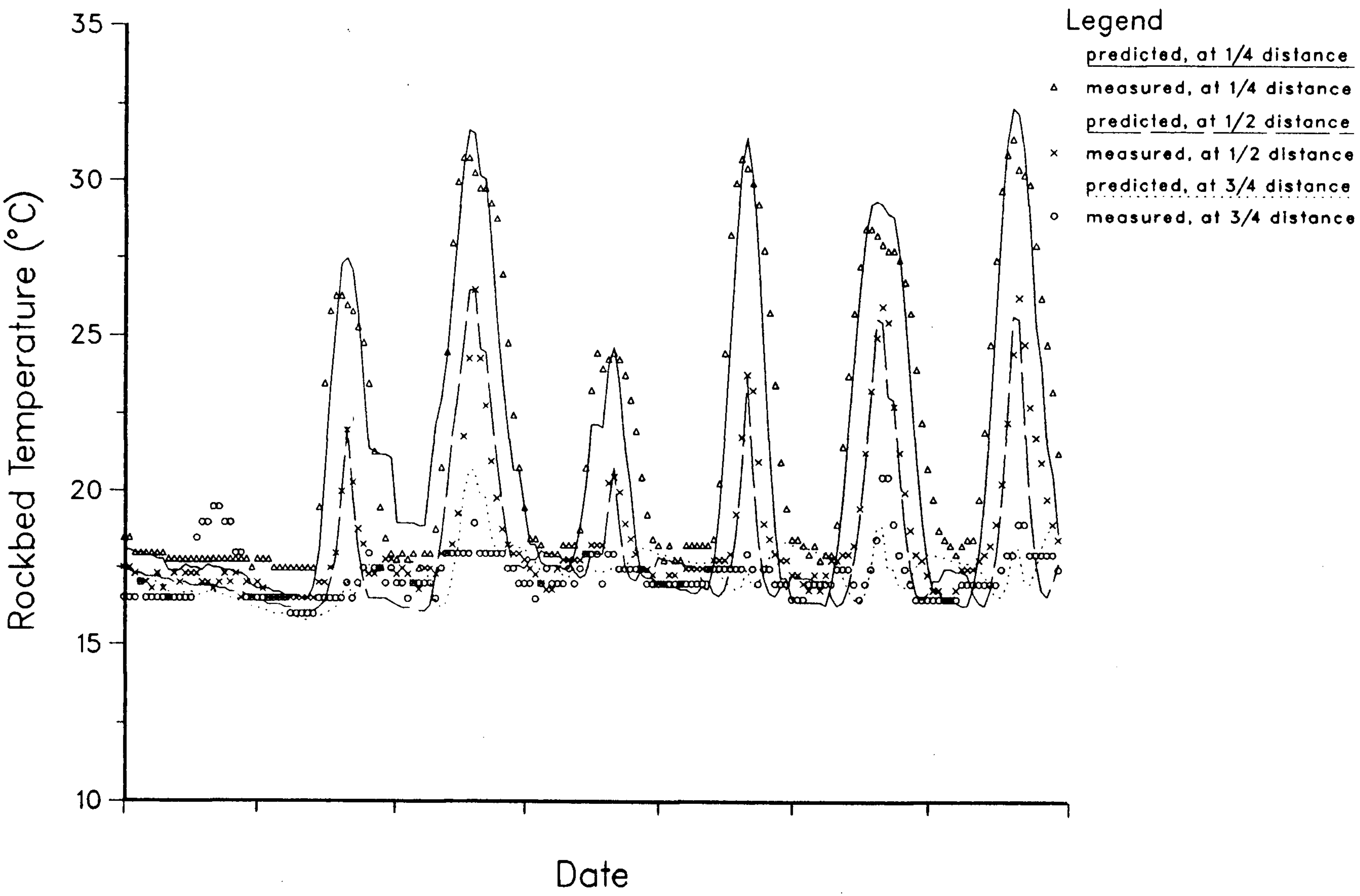

Fig. 3.15 System I – Rockbed temperatures at three sections, Mar 25–31

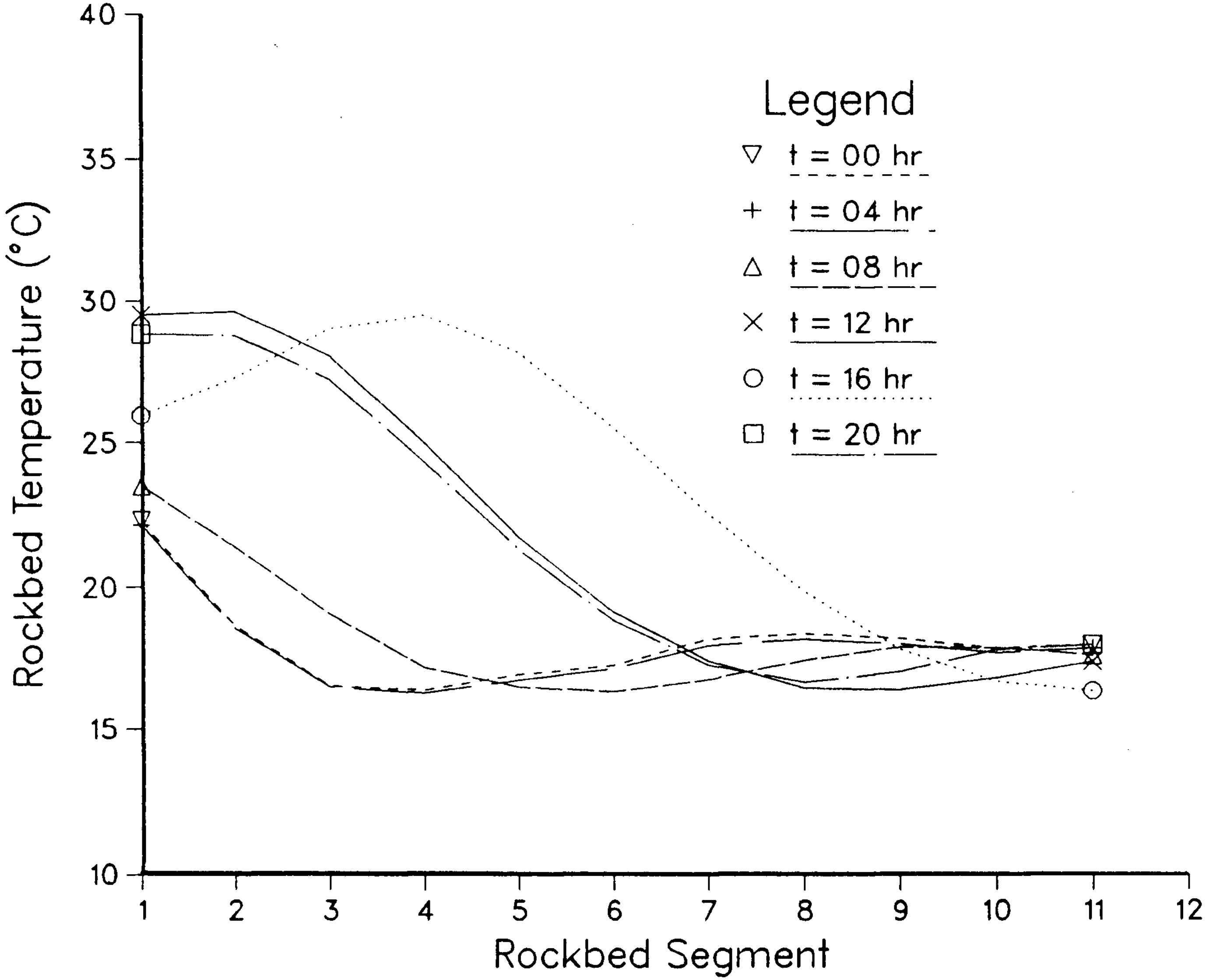

Fig. 3.16 System I - simulated results of spatial temperature distribution in the rockbed, Mar 25-31 (day 6)

ventilation, though it is chiefly for temperature control purpose. Examination of RH_a values seems to suggest that the relatively high plant temperature on days with high solar radiation level may be another factor for lower RH (below 70 percent) during those sunlit hours when stomates opened less to conserve water.

On the whole, simulated rock temperatures are rather close to measured values, exhibiting a maximum difference of 4.5 °C on day 5. Simulation started at 0000 hr of day 1 when temperatures of the rockbed ranged from 19.5 °C at one end of the storage to 16.5 °C on the other. On the days with outside solar radiation that recorded more than 500 W m^{-2}, the storage inlet temperature, T_{rsi} , during daytime charging attained peak values ranging from 30 to 33.5 °C. Higher values of T_{rsi} could not be realized due to greenhouse ventilation. In fact, the gross useful heat gain of the greenhouse acting as the solar collector was estimated to be 6320 MJ, based on convective heat transfer between the various surfaces and air. Calculations show that about 60% of this available energy is dissipated through conduction, infiltration and ventilation heat losses. Such high percentage of heat loss could be partly reduced by minimizing ventilation. However, in this week, much ventilation was required to avoid excessively high air and leaf temperatures and to ensure an adequate supply of CO_2, since no CO_2 enrichment was provided in these research greenhouses.

Computations using transient changes in rockbed temperatures returned a value of 2530 MJ as energy being stored, subsequently, 2000 MJ is recovered during 57 hours of discharging operation. Energy consumption record for this week indicated that the control house used 47.9 MJ m^{-2} whereas the solar shed required 31.9 MJ m^{-2}. The energy savings of 1870 MJ compared well with the energy discharged from the storage.

Case 3. Apr 8–14

The solar radiation of this week is characterized by the approximately equal magnitudes of the beam and diffuse components, the latter making up 54% of I_o . Other outside climatic conditions that prevailed during the period are also shown in Fig. 3.17. Discussion of results will focus on Figs. 3.18 to 3.22 in sequence.

Simulated values of inside solar radiation fall within 7% and 12% of measured values in regard to that incident on the absorber plate and the plant canopy respectively.

Like other cases presented earlier, when outside solar radiation level is at a low level of less than 200 W m^{-2}, temperatures of the various component surfaces in the greenhouse environment model are close to each other. On days with strong sunshine, the maximum temperature differentials between plant canopy and air, and absorber plate and air range from 5 to 7 °C and 13 to 22 °C respectively. By comparison with the week of Mar 25–31 (Fig. 3.13), it is readily seen that even though I_o is of the same magnitude, both T_p and T_q are less for the present week. For instance, on Mar 29, (T_p , T_q) had maximum values of (39 °C, 58 °C), but on Apr 8, they were (35 °C, 50 °C) as I_o peaked at 760 W m^{-2} on each occasion, and both days recorded total I_o = 4870 W m^{-2}. Sample outputs of model validation runs for these two days may be found in Table 3.5. Iterations during the solving of the energy and moisture balance equations indicated that for convergence to take place, values of the leaf Bowen ratio ranged from 1.3 to 1.5 on Mar 29, whereas it varied between 1.0 and 2.2 on Apr 8. The lower β value of 1.0 reflects higher transpiration rate, possibly due to a denser canopy. Furthermore, system behaviour is also influenced by the diffuse and direct composition of the global solar radiation. Whereas the diffuse radiation view factor between the cover (south roof) and the vertical absorber plate is only 0.26, the beam radiation interception factor is 0.34

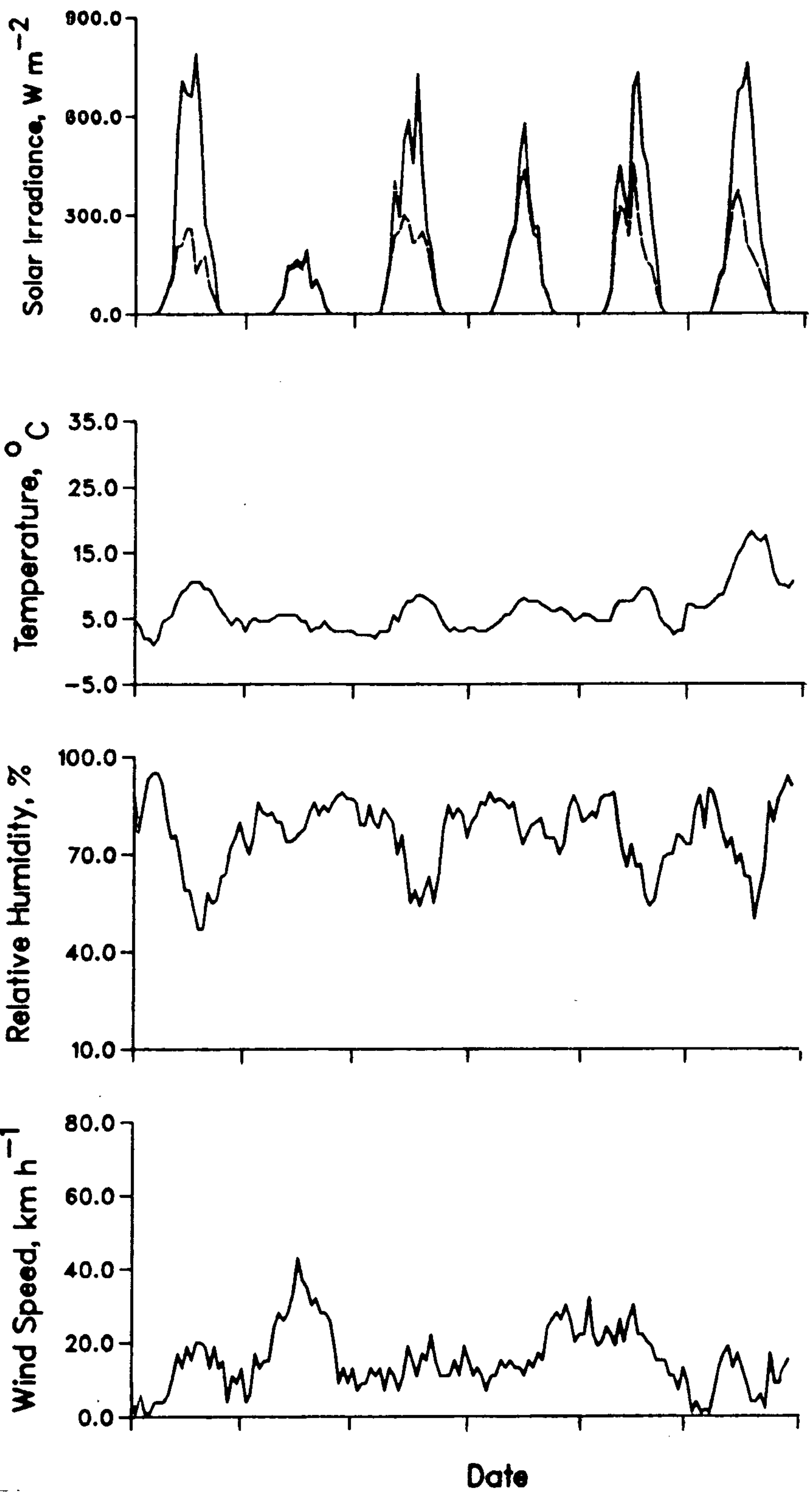

Fig. 3.17 External climatic conditions during the week of Apr 18–24, 1984

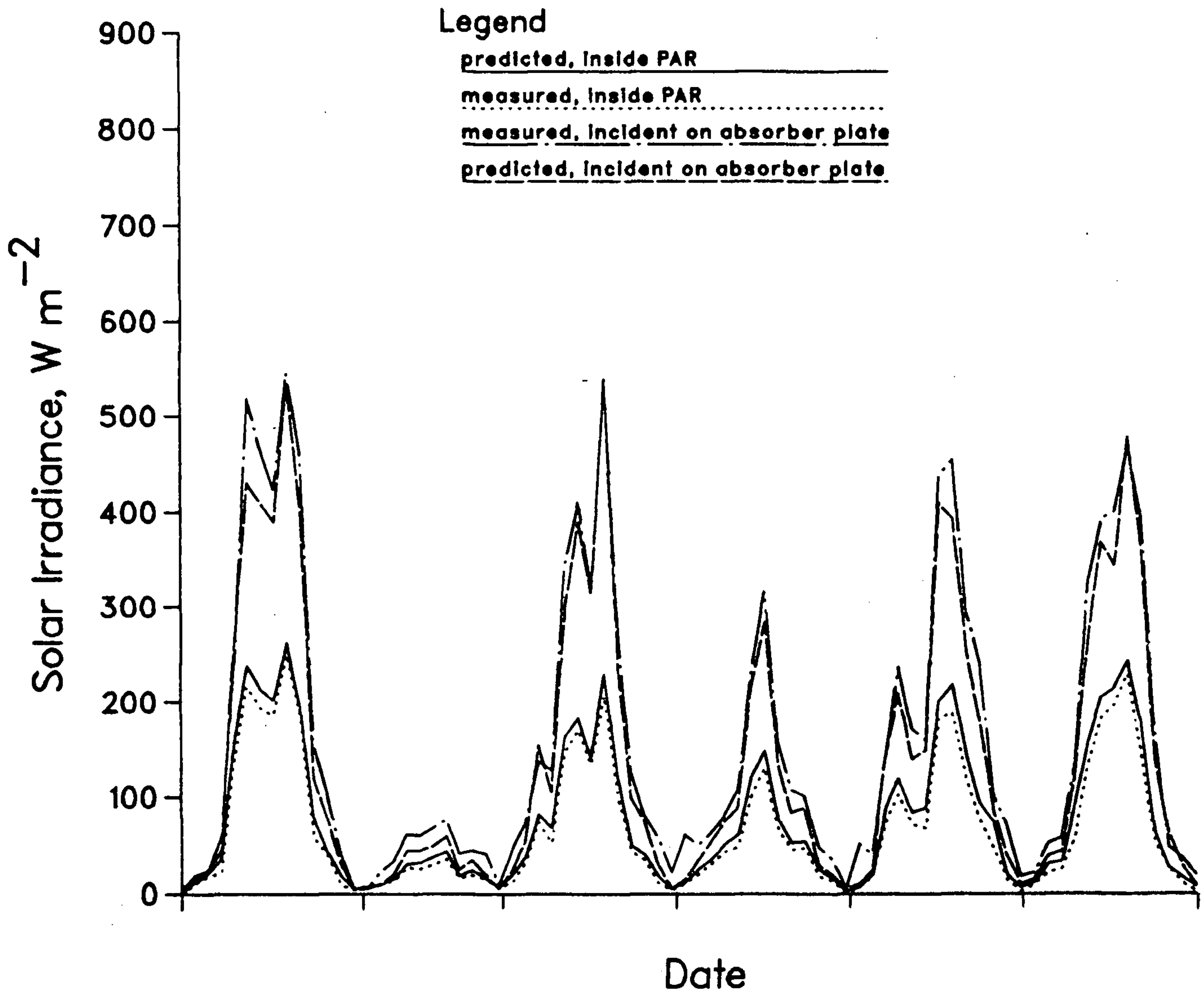

Fig. 3.18 System I - PAR at plant canopy level, Apr 8–14

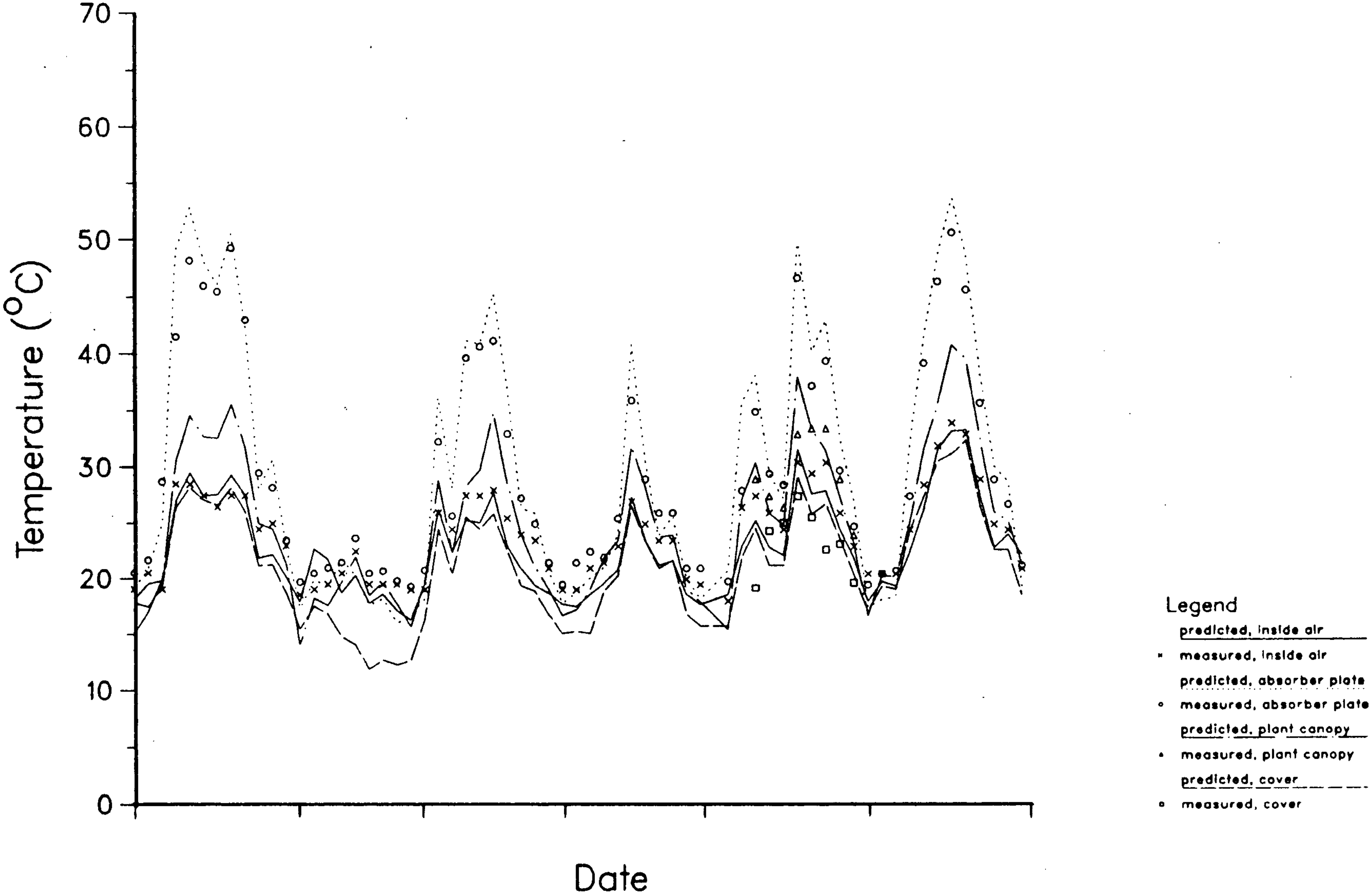

Fig. 3.19 System I – temperatures of the greenhouse thermal environment, Apr 8–14

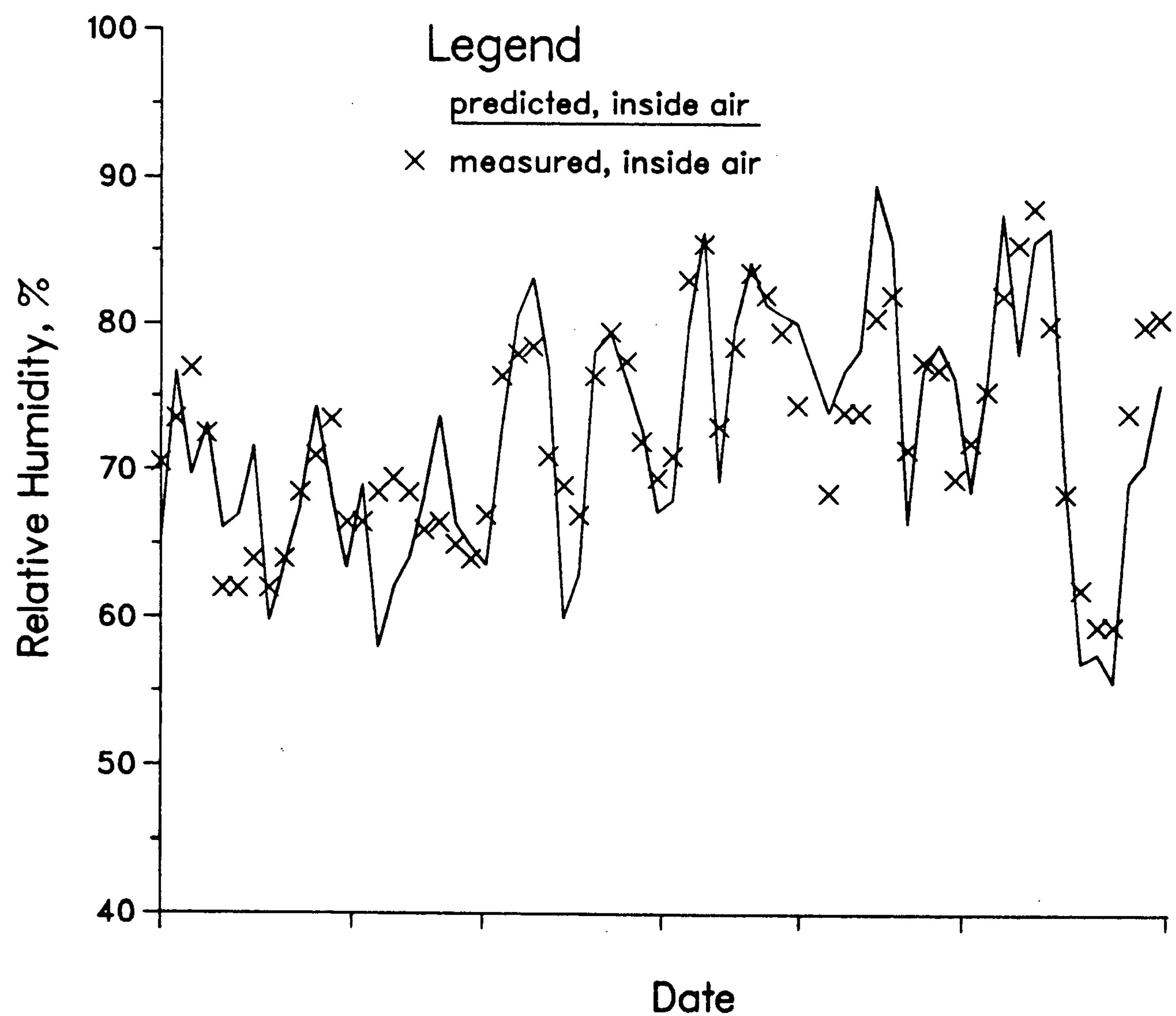

Fig. 3.20 System I - greenhouse relative humidity, Apr 8-14

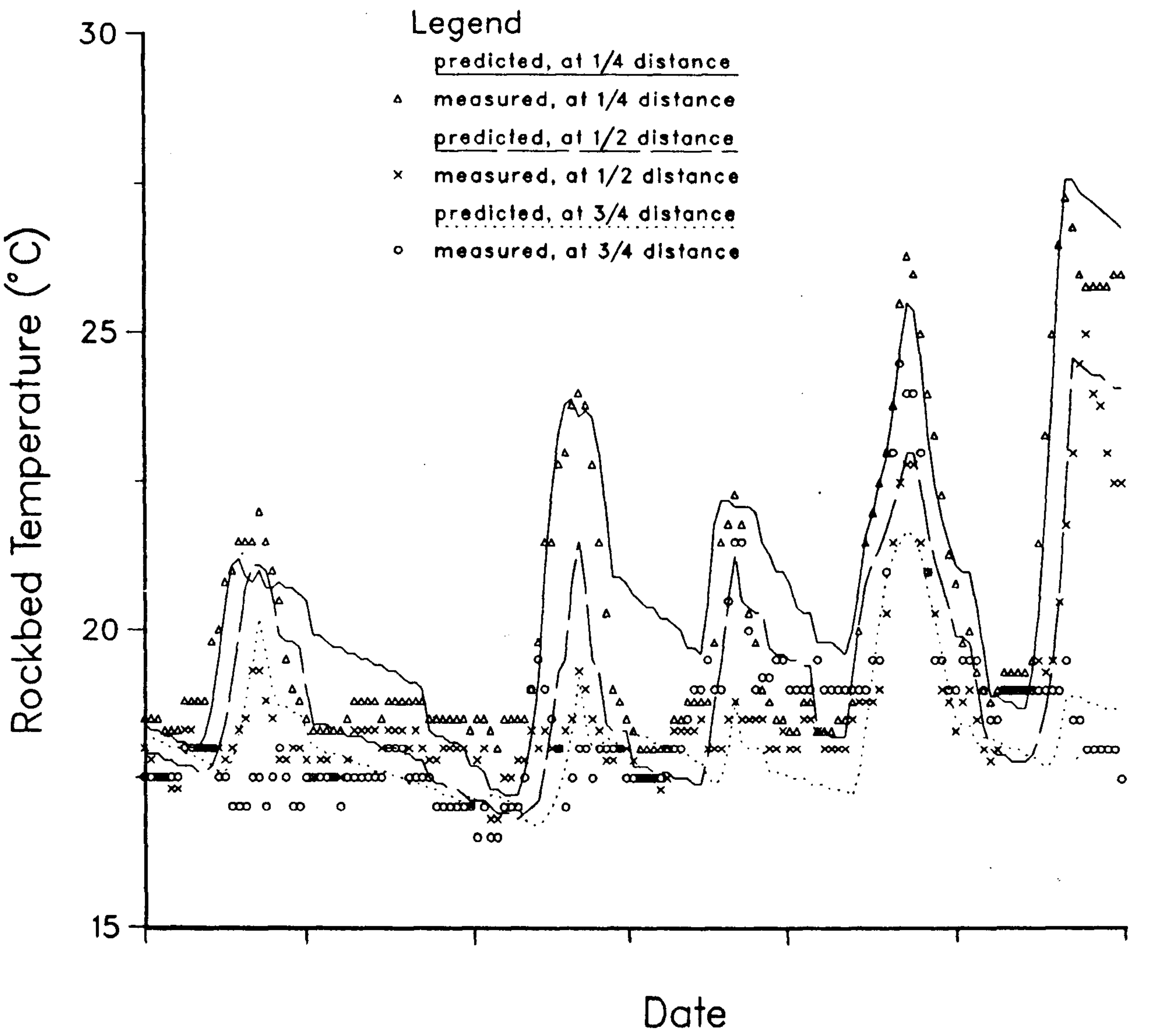

Fig. 3.21 System I – Rockbed temperatures at three sections, Apr 8–14

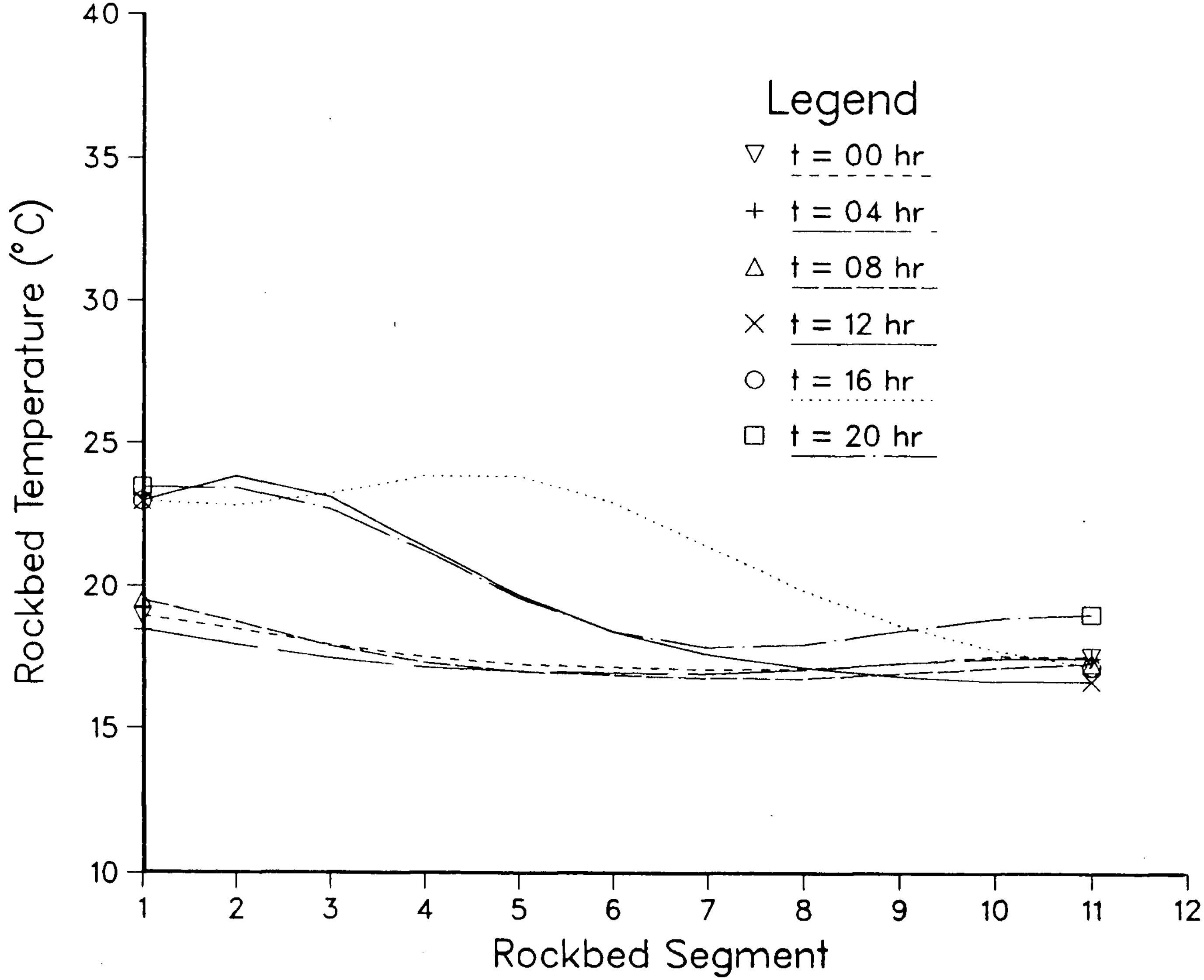

Fig. 3.22 System 1 - simulated results of spatial temperature distribution in the rockbed, Apr 8-14 (day 3)

Table 3.5 Sample outputs of model validation runs - greenhouse thermal environment

System I - Mar 29, 1984

Hour	T_p	$\tilde{T}_p$	T_a	$\tilde{T}_a$	T_g	$\tilde{T}_g$	T_c	$\tilde{T}_c$	RH_a	$\tilde{RH}_a$	U_g	U_p	U_c	N	β
7	--	20.0	20.5	16.4	22.3	22.1	--	11.7	62.0	67.5	1.8	1.7	0.8	7	1.3
8	--	20.7	22.0	19.8	23.5	23.3	--	16.8	66.0	67.3	1.5	1.4	1.3	5	1.3
9	21.5	20.2	21.0	18.5	22.7	24.0	15.1	17.8	71.0	80.2	1.5	1.5	1.3	5	1.3
10	30.0	33.3	29.0	28.9	43.0	49.3	24.4	28.3	70.5	72.6	2.3	1.8	1.6	8	1.3
11	34.0	39.4	33.5	33.3	56.0	62.9	28.7	32.0	64.0	67.6	2.6	2.0	1.7	9	1.4
12	35.0	38.3	32.5	31.9	57.5	60.5	29.6	30.4	62.0	64.3	2.4	2.0	1.6	12	1.5
13	33.0	37.0	32.0	31.2	52.5	58.5	26.4	28.6	62.0	66.3	2.4	2.0	1.5	10	1.5
14	31.5	35.1	31.5	29.5	49.0	55.1	29.5	27.8	62.0	65.7	2.3	1.9	1.5	9	1.5
15	31.5	33.5	29.5	28.4	37.7	44.0	27.7	26.2	64.0	65.6	2.3	1.8	1.5	10	1.5
16	29.0	27.2	27.0	24.6	29.7	36.4	21.2	23.3	62.0	63.7	2.0	1.7	1.5	12	1.5
17	23.0	19.2	22.5	18.3	21.5	24.9	19.0	17.5	64.0	70.0	1.6	1.5	1.3	5	1.4
18	--	18.4	19.0	17.8	18.8	18.5	--	12.6	65.0	69.0	1.1	1.1	0.4	6	1.4

System I - Apr 8, 1984

Hour	T_p	$\tilde{T}_p$	T_a	$\tilde{T}_a$	T_g	$\tilde{T}_g$	T_c	$\tilde{T}_c$	RH_a	$\tilde{RH}_a$	U_g	U_p	U_c	N	β
7	--	15.1	19.0	18.1	20.5	19.1	--	17.8	70.5	65.3	1.5	1.3	1.3	5	2.2
8	--	17.0	20.5	19.5	21.7	20.9	--	17.4	73.5	76.7	1.5	1.3	1.3	4	1.6
9	--	19.9	19.0	19.8	28.7	25.0	--	19.3	77.0	69.7	1.7	1.5	1.4	11	1.0
10	--	30.7	28.5	27.1	41.5	49.1	--	26.5	72.5	73.1	2.2	1.8	1.5	9	1.0
11	--	34.6	28.5	29.5	48.2	52.9	--	28.2	62.0	66.1	2.4	1.9	1.5	9	1.1
12	--	32.7	27.5	27.5	46.0	48.2	--	27.1	62.0	66.9	2.2	1.8	1.5	10	1.2
13	--	32.6	26.5	27.6	45.5	46.1	--	26.6	64.0	71.6	2.1	1.8	1.5	8	1.2
14	--	35.6	27.5	29.3	49.3	50.5	--	28.2	62.0	59.8	2.3	1.9	1.5	10	1.3
15	--	31.8	27.5	27.6	43.0	42.5	--	26.1	64.0	63.7	2.1	1.7	1.5	9	1.3
16	--	25.0	24.5	21.9	29.5	28.0	--	21.2	68.5	67.6	1.7	1.6	1.4	6	1.1
17	--	24.5	25.0	22.2	28.2	30.7	--	21.3	71.0	74.3	1.8	1.6	1.4	4	1.0
18	--	21.4	23.0	20.2	23.5	22.9	--	18.7	73.5	68.5	1.6	1.5	1.3	4	1.1

Symbols are defined in the 'notation' section, p.136-137 at noon at this time of the year. The shed-type greenhouse therefore captures beam radiation more effectively than diffuse radiation during most of the day. Solar radiation on Mar 29 is predominantly direct in nature (78%), by contrast, it is 40% diffuse on Apr 8. Hence, the plate is heated to a higher temperature in the former case.

As shown in Fig. 3.21, the posterior portion of the rockbed has more temperature variation in this week. On day 5, it attained a maximum value of 24 °C during charging, a mere 2 °C short of the storage inlet temperature. It may just be an incidence of erratic measured data since similar behaviour is not observed on the following day with even higher solar radiation and outdoor air temperature. Spatial temperature distribution within the rockbed is displayed in Fig. 3.22 for day 3. Although solar radiation happened to reach a high value of 730 W m^{-2}, it was a typical day with intermittent sunshine. The storage is subjected to charging for nine hours, but the inlet temperature stays relatively constant (22.5 ± 1.5 °C), resulting in little movement of the temperature front in the bed.

The week of April 8-14 was warmer and energy consumption of both the shed and the control house were less than the previous two cases. The difference in recorded supplemental heat (45.8 versus 28.6 MJ m^{-2}) implies total energy savings of 2020 MJ. This value is 260 MJ more than the predicted recovery of 1760 MJ from the storage.

3.4.2.2 System II

Case 1. Feb 18-24

Fig. 3.23 shows the solar radiation incident on an inside horizontal surface at the plant canopy level. Climatological data for this week have been given previously in Fig. 3.4. Simulation results expressed in terms of temperature and relative humidity of the greenhouse thermal environment are illustrated in

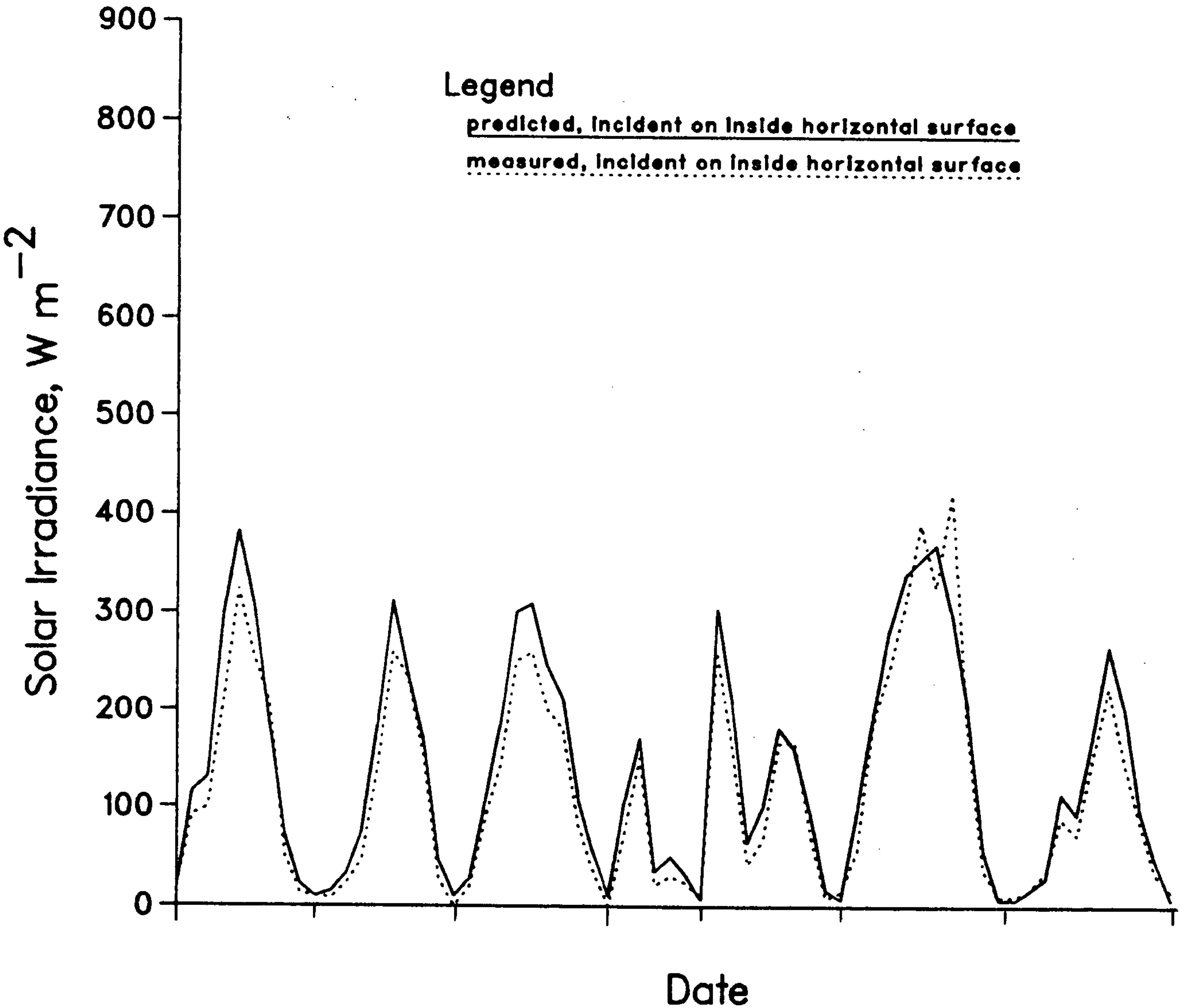

Fig. 3.23 System II - solar radiation incident at plant canopy level, Feb 18-24

Figs. 3.24 and 3.25 together with the measured points. Because of a relatively sparse crop canopy, the leaf Bowen ratio β is found to lie between 2.5 and 3.5 when the iteratively computed hourly inside air temperature and relative humidity converged with respect to measured values. Due to less transpiration heat loss, plant temperature is higher than air temperature by as much as 15 °C, and radiative heat exchange between the plant canopy and glass surface could only lower T_p by 1 to 3 °C. Gates and Benedict (1962) measured heat exchange for various broad-leaved deciduous trees under still air conditions in the laboratory. The surface temperature of Maple and Poplar leaves (characteristics dimension = 62 and 96 mm) was observed to be 9 and 15 °C higher than air temperature when energy lost through transpiration represented 10 and 20% of total energy absorbed by the plant.

Measured RH_a experienced a narrow range of 62 to 68%, whereas $\widetilde{RH}_a$ is seen to vary from 58 to 74%, suggesting that a fixed value of β could have been used for this week, but for consistency in the simulation, β was allowed to possess different values when necessary.

Simulated soil temperatures are presented in two forms. Fig. 3.26 depicts the measured temperatures along with the simulated values at three representative locations in the region near the centre of the storage. Location A coincides with the immediate neighbourhood of the upper pipe (that is, soil/pipe interface), location B is at a depth of 0.2 m between the soil surface and the upper pipe, and location C is midway between the upper and the lower pipes. For this week, the soil temperatures are seen to be bound within a narrow belt of 15 to 19 °C, due to the low-grade heat transferred from pipe air to the soil. Temperature of air at the pipe inlet varied from 18 to 23 °C, and is up to 7°C less than the daytime greenhouse air temperature. Calculated values have a mean difference of 0.9 °C from actual data. Again, like the case of the

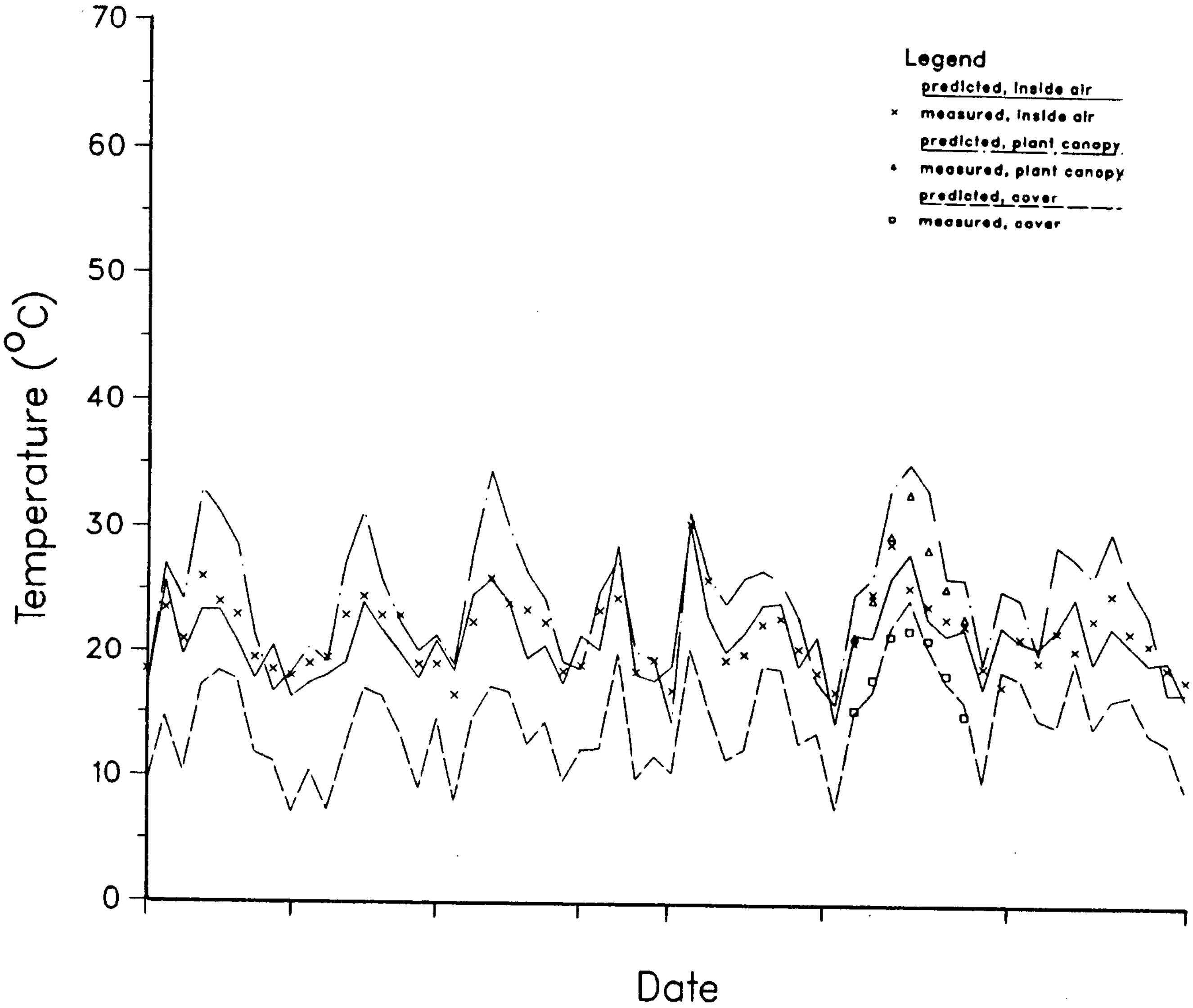

Fig. 3.24 System II – temperatures of the greenhouse thermal environment, Feb 18–24

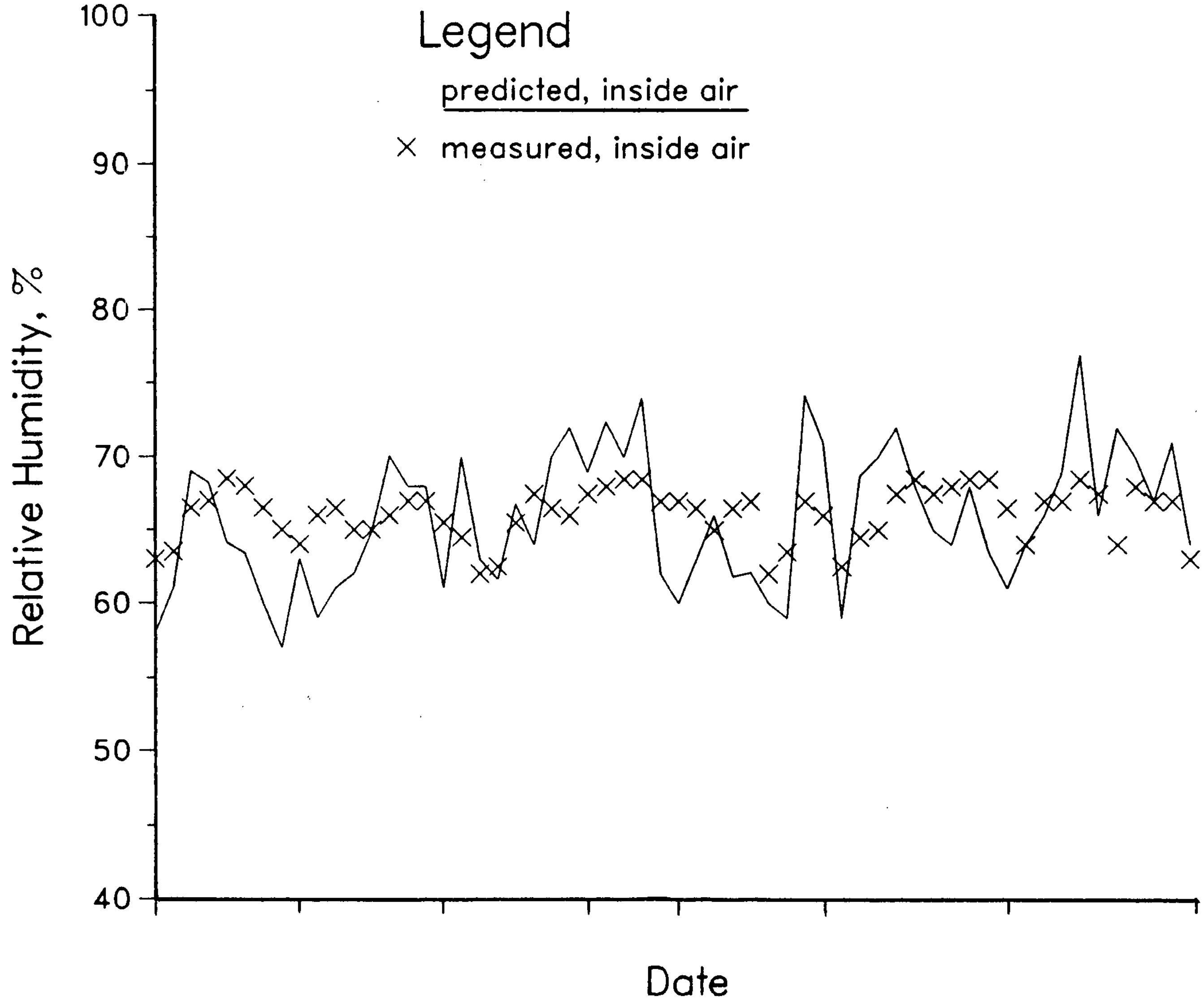

Fig. 3.25 System II - greenhouse relative humidity, Feb 18-24

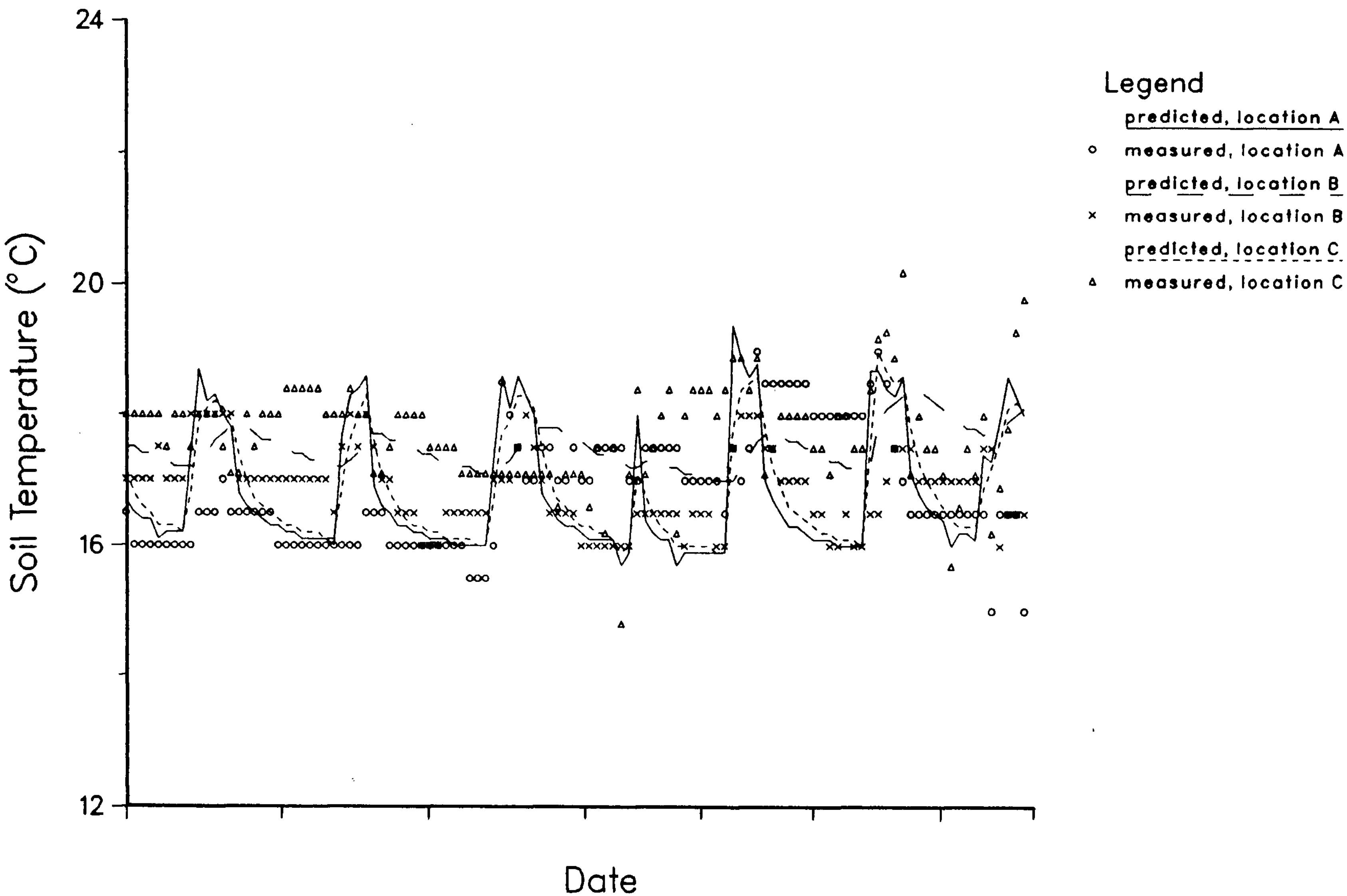

Fig. 3.26 System II - soil temperatures at three locations in the storage zone, Feb 18-24

rockbed thermal storage, the mean and standard deviation vary with the point of interest. Prediction accuracy is best with location B, whereas location C is associated with the largest discrepancy. Fig. 3.27 shows the isotherms that represent the calculated soil temperatures in the entire region near the edge of the storage. The contours were generated by a packaged computer program SCATCN (Mair, 1984). Heat loss to the ambient soil drives the temperature down to 14 °C at the insulation boundary, whereas a large portion of this region is close to 17 °C.

Predicted pipe outlet air temperature is compared with the measured data in Fig. 3.28. When storage charging takes place in the day, a temperature drop of 7.5 °C between the inlet and outlet air can be realized. At night, measured greenhouse air temperature centers upon 17 °C with a variation of 1.5 °C, and is close to T_{po} . On the whole, the prediction of T_{po} during both charging and discharging agrees reasonably well with observed values.

The difference between the soil/pipe interface and pipe air temperatures averaged 2.5 ± 2 °C, which is within 20% of the air temperature. Less difference is observed when pipe air temperature is higher. The magnitude of this temperature differential indicates that heat exchange between soil and air is quite efficient. The overall heat transfer coefficient was calculated to have a value of about 20 W m^{-2} $°C^{-1}$ most of the time. When condensation of moist air occurs, its computed value increased by up to three fold, however, no significant effect on this temperature differential was found.

Heat transferred from soil to air during 66 hours of discharging operation in this week amounts to a total of 1830 MJ, and is 11% less than the actual energy savings of 2060 MJ. Stored solar heat provided 17% of the total greenhouse heating demand.

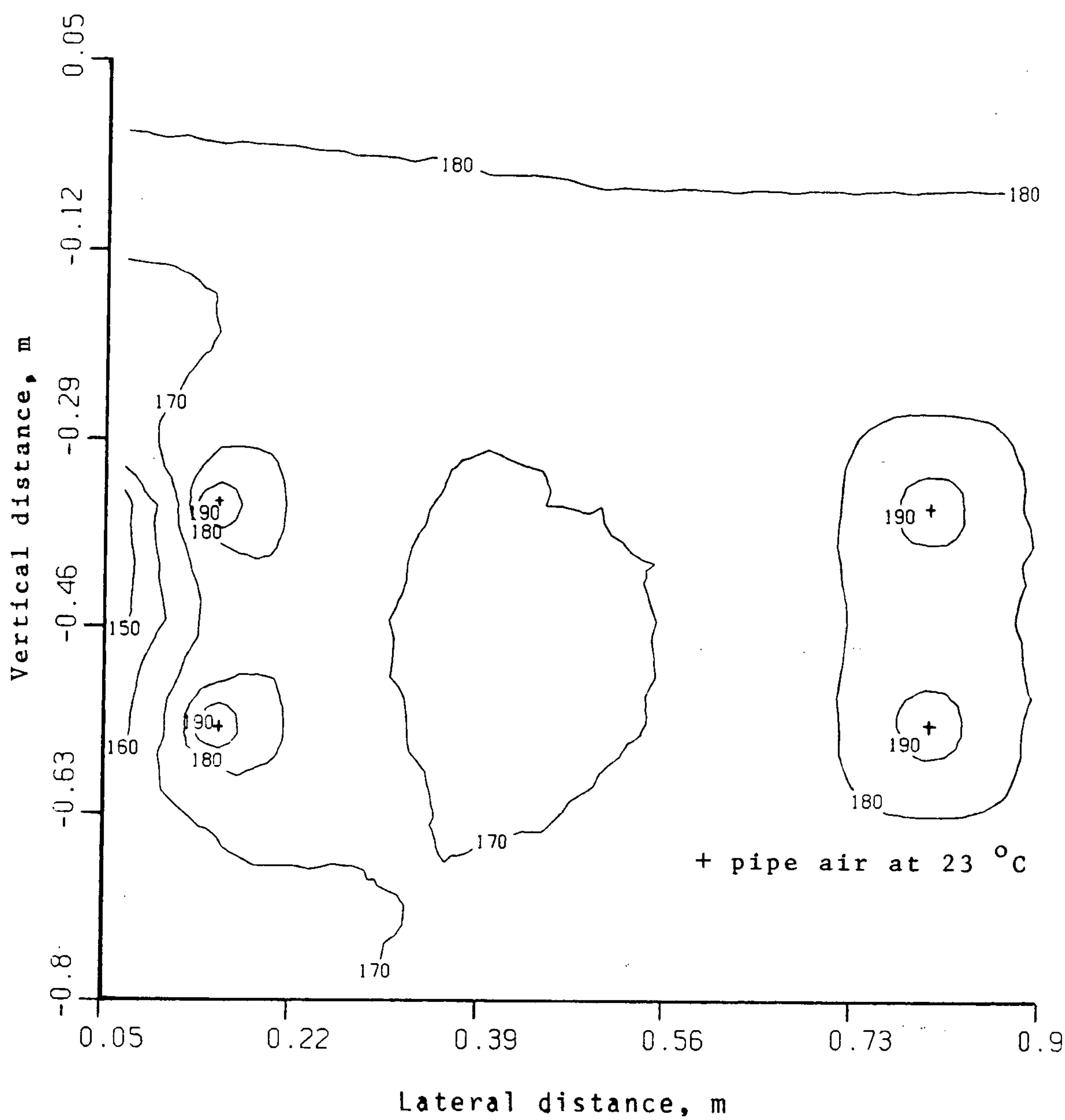

Fig. 3.27 System II - isotherms of simulated soil temperatures, Feb 18-24 (day 6, 0900 hr)

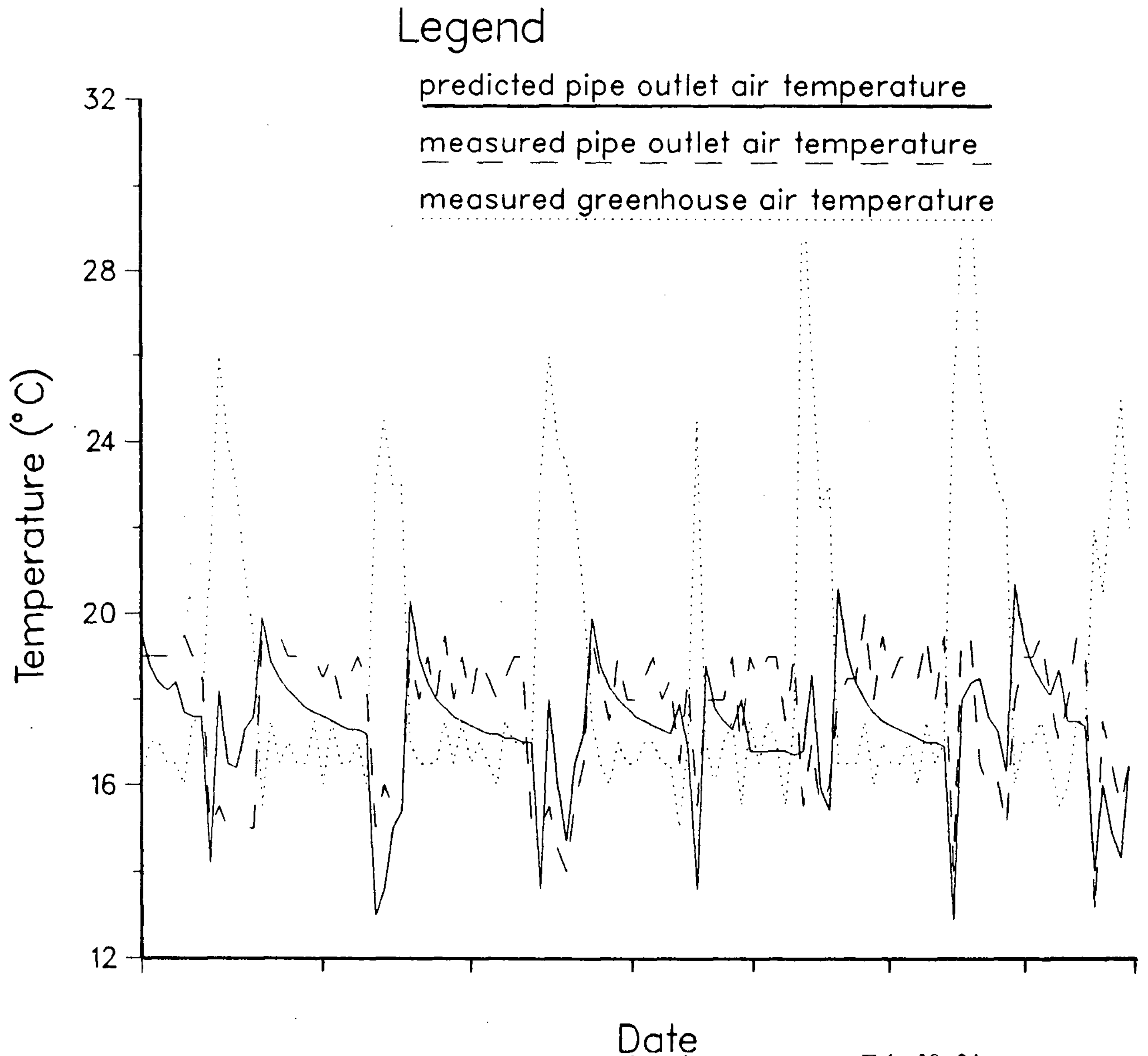

Fig. 3.28 System II - pipe outlet air temperature, Feb 18-24

Case 2. Mar 25–31

For the greenhouse thermal environment, values of measured and computed inside solar radiation, air temperature and relative humidity are plotted in Figs. 3.29, 3.30 and 3.31.

Predicted inside solar radiation is greater than the measured data on days when outside solar radiation are high and shows opposite trend on other days. The overall prediction differs 8% from the measured weekly quantity of 5540 MJ (weekly $\dot{I}_o$ = 8035 MJ).

On the days with high solar radiation, inside air temperature did not get past 30 °C, in contrast to the conditions inside the shed-type greenhouse in System I, which is 6 to 8 °C higher. This demonstrates the combined effect of absorber plate and plant cover on greenhouse temperature regime. In fact, a dense canopy by itself has already added thermal mass to the greenhouse and therefore convective heat exchange with inside air. In this aspect, Avezov et al. (1985) analyzed daily variations in T_a in a solar-heated greenhouse. With identical values of solar radiation input and outside temperature, T_a was found to be lower in the absence of plant cover than it is when plants are present, exhibiting a maximum difference of 8 °C in the early afternoon.

Again, one can observe from Fig. 3.31 that the actual relative humidity again did not vary much – between 60% and 72%, and is quite well predicted by the model. Since less natural ventilation is required for climate control in this conventional greenhouse, air movement is reduced and subsequently, plant temperature rose well above air temperature.

Soil temperatures have more variation in this week, as illustrated by the wider spreading of data points that appear in Fig. 3.32. Among the three sensor locations, location C has values that are least accurately predicted. Measured soil temperature here ranged from 14.0 to 20.8 °C and the corresponding predicted

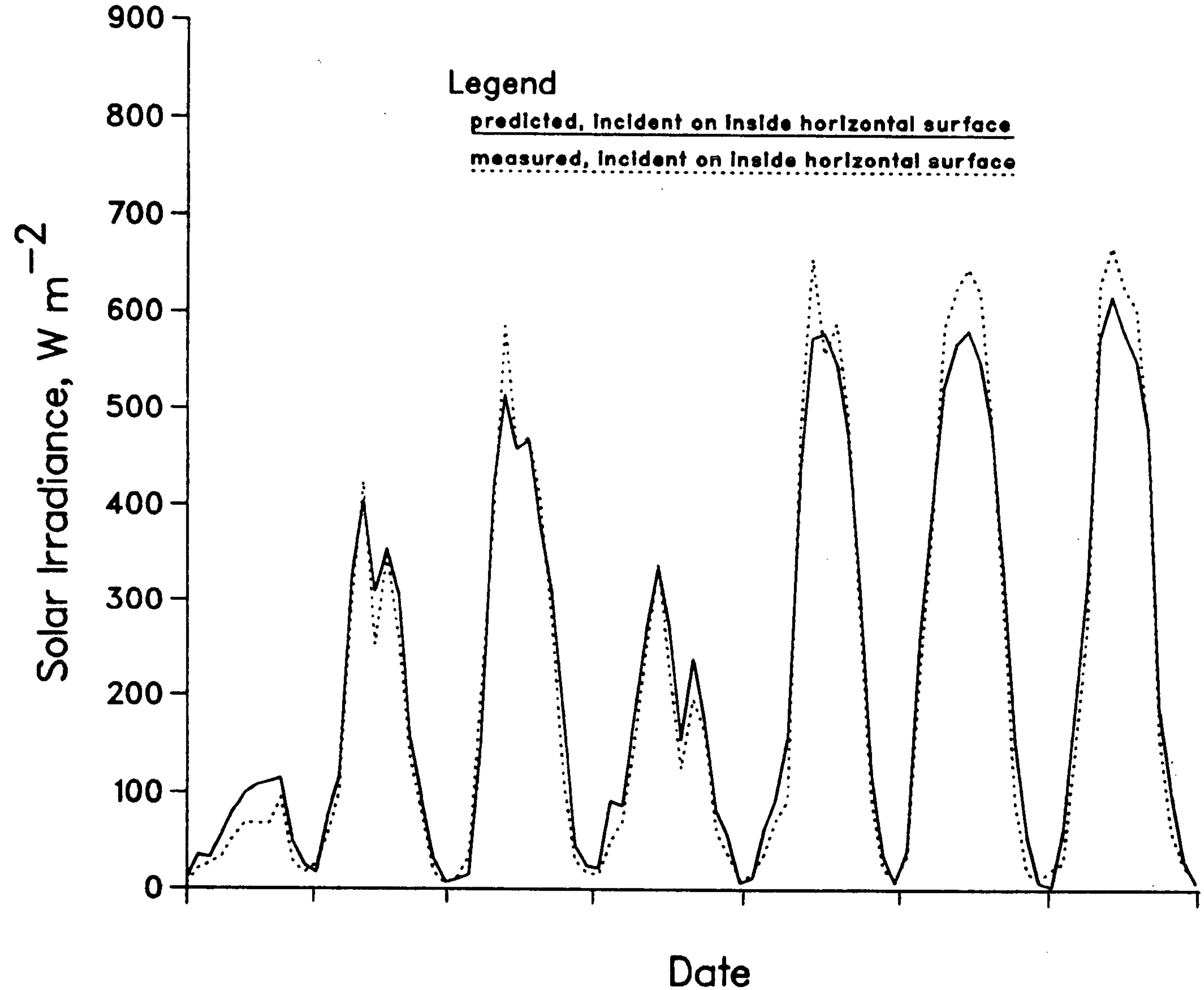

Fig. 3.29 System II - solar radiation incident at plant canopy level, Mar 25–31

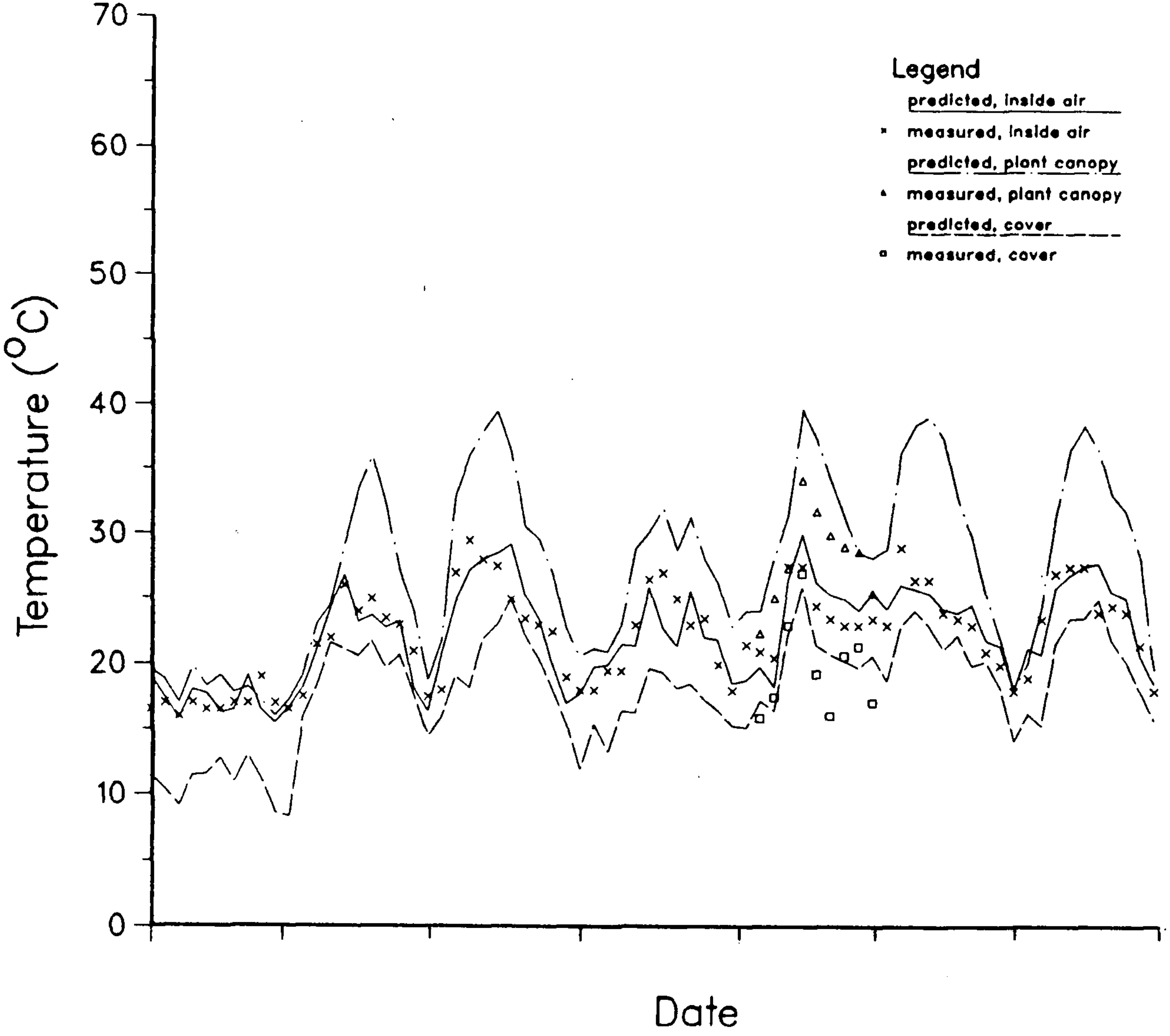

Fig. 3.30 System II – temperatures of the greenhouse thermal environment, Mar 25–31

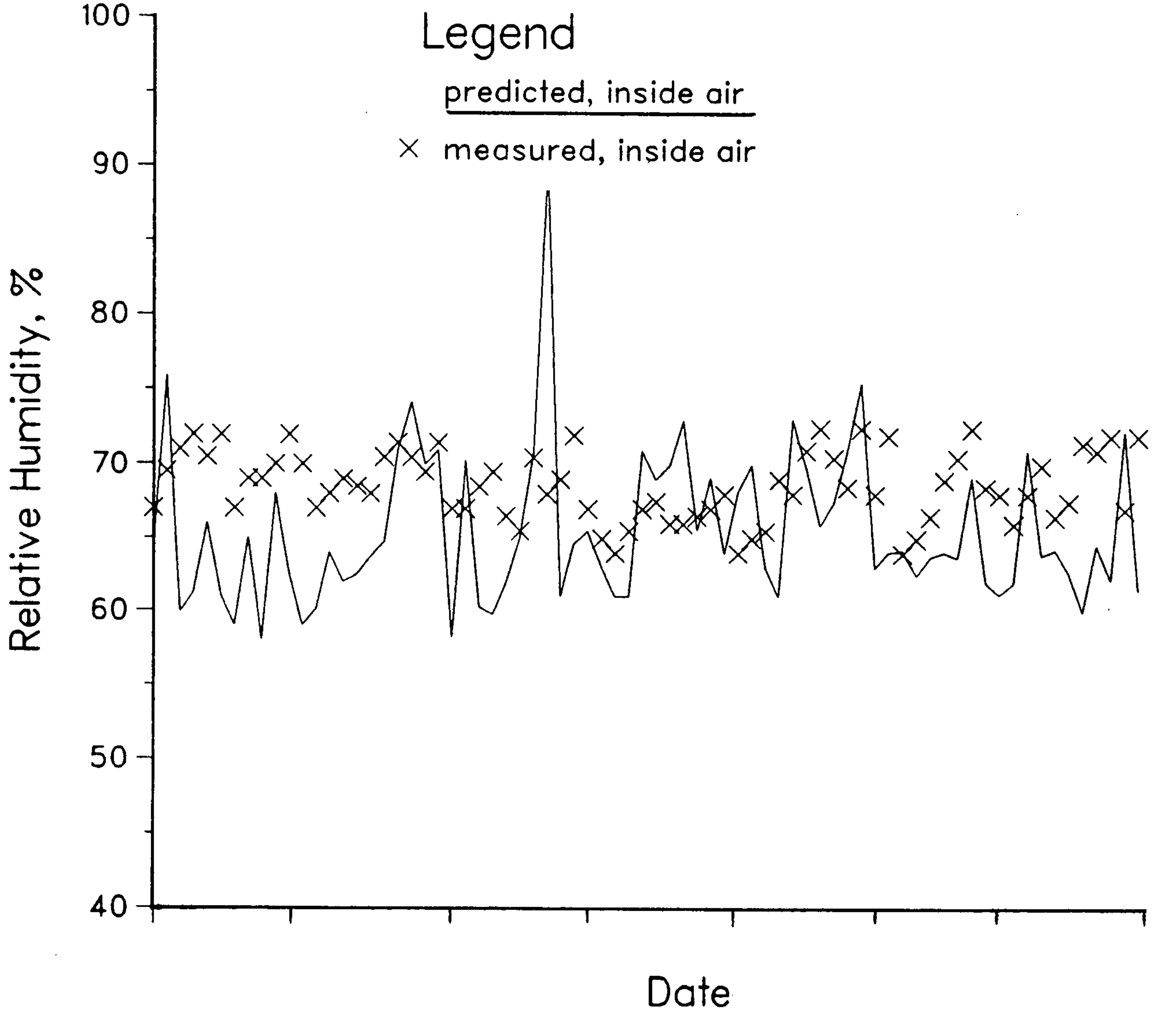

Fig. 3.31 System II - greenhouse relative humidity, Mar 25-31

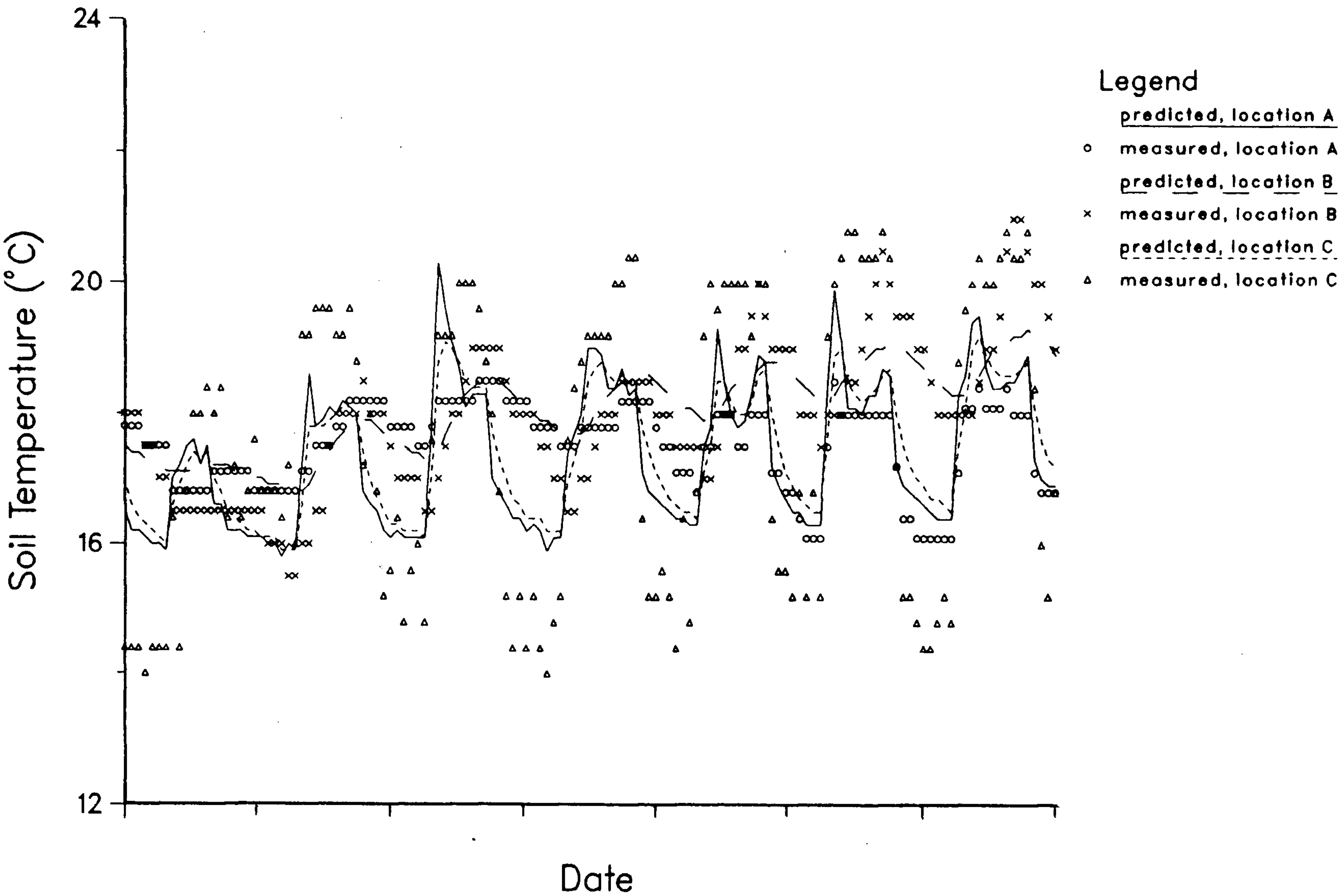

Fig. 3.32 System II – soil temperatures at three locations in the storage zone, Mar 25–31

values are 15.9 to 19.2 $^\circ$C; the maximum difference is 2.2 $^\circ$C or in percentage, 15%. The maximum difference between measured and computed results is 2.1 $^\circ$C (11%) for location A and 1.8 $^\circ$C (8%) for location B. The discrepancy can be partly explained by the unequal inlet air temperature in the pipes. Measurements indicated that air in an upper pipe had consistently higher temperature than that in a lower pipe by 0.5 to 2.0 $^\circ$C. In the simulation, however, all pipes are assumed to have uniform air temperature at the entry.

Predicted and measured pipe outlet air temperature is plotted in Fig. 3.33. The maximum difference in T_{po} and $\tilde{T}_{po}$ is 2.7 $^\circ$C for nighttime discharging mode, and 2.1 $^\circ$C with daytime charging operation. The outlet air temperature is calculated as a function of enthalpy change between inlet and outlet air due to q_s , the heat exchange per meter pipe length between air and soil. A two-dimensional model assumes q_s is the same at any cross section in the longitudinal direction, whereas in practice, q_s should be different along the pipe length. Consequently, the pipe outlet air temperature cannot be predicted very accurately, though it is better predicted than the soil temperatures.

Figs. 3.34 and 3.35 show the isotherms that represent two regions in the same cross section of the soil thermal storage. For the region near the center line, more uniform temperature distributions result in the symmetrical shapes of the contour lines, whereas thermal gradient is larger near the edge, as expected.

The model is then checked on a macroscopic basis. Supplemental energy consumption data for this week indicated that 2490 MJ was saved, or 26% of the 9580 MJ consumed by the control house. Calculated heat transfer from soil to pipe air during 70 hours of discharging totalled 2180 MJ, and is 12.5 % less than the actual energy savings. Computed quantity of heat being stored during daytime amounts to 2570 MJ, however, the concept of 'stored heat' is not appropriate for model validation as it is not as well defined as the rockbed

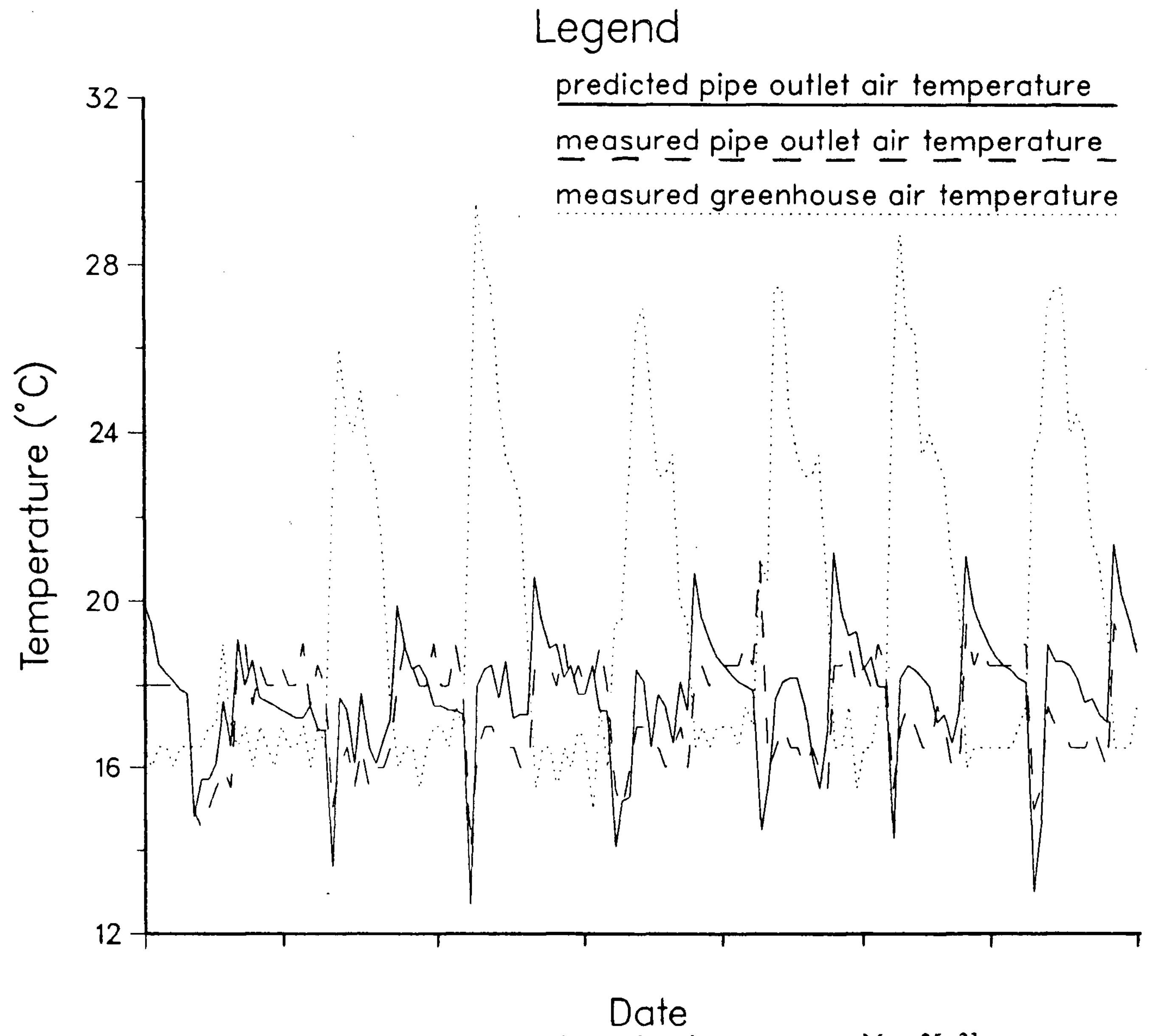

Fig. 3.33 System II - pipe outlet air temperature, Mar 25-31

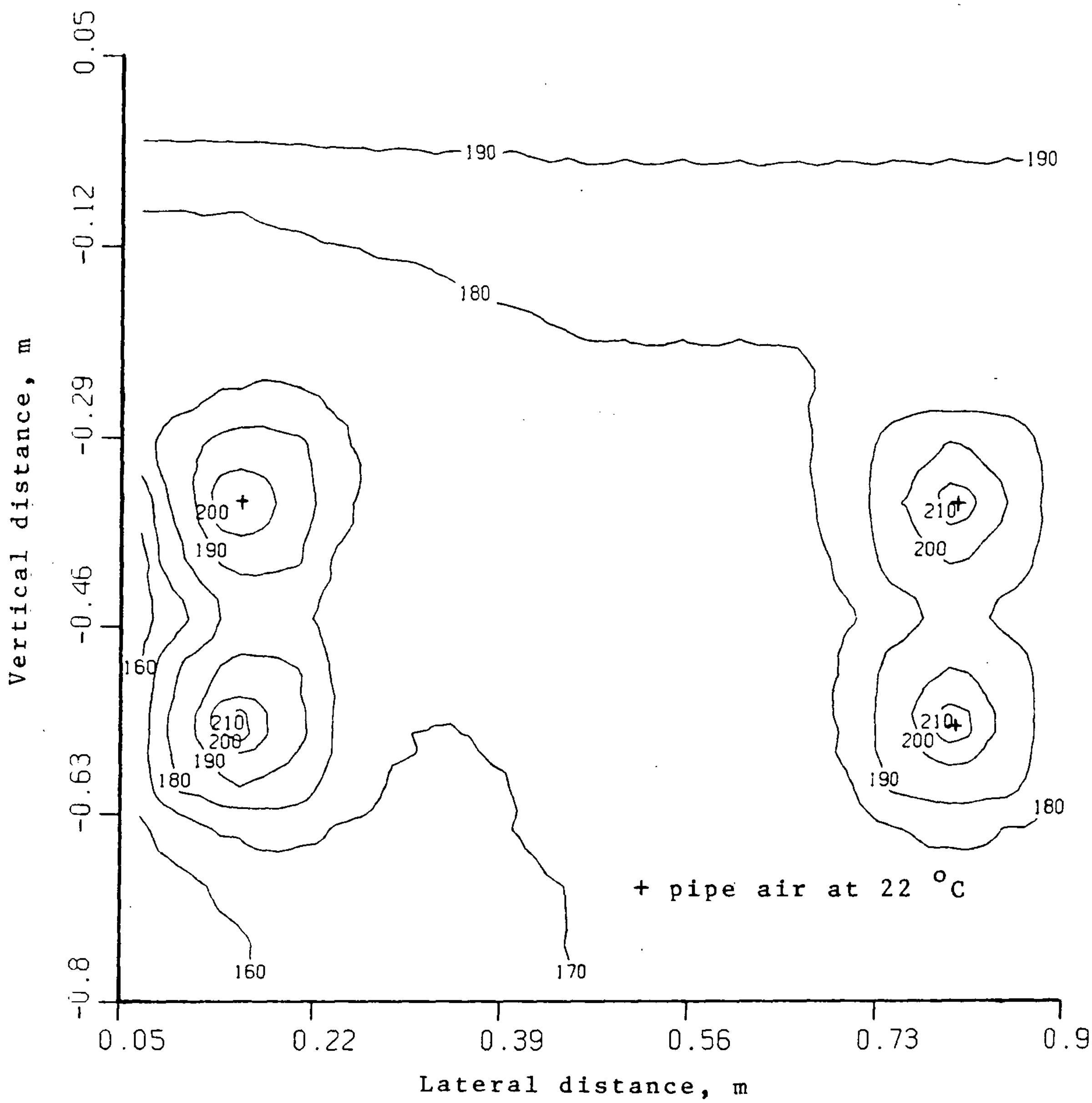

Fig. 3.35 System II - isotherms of simulated soil temperatures at the edge region, Mar 25-31 (day 6, 0900 hr)

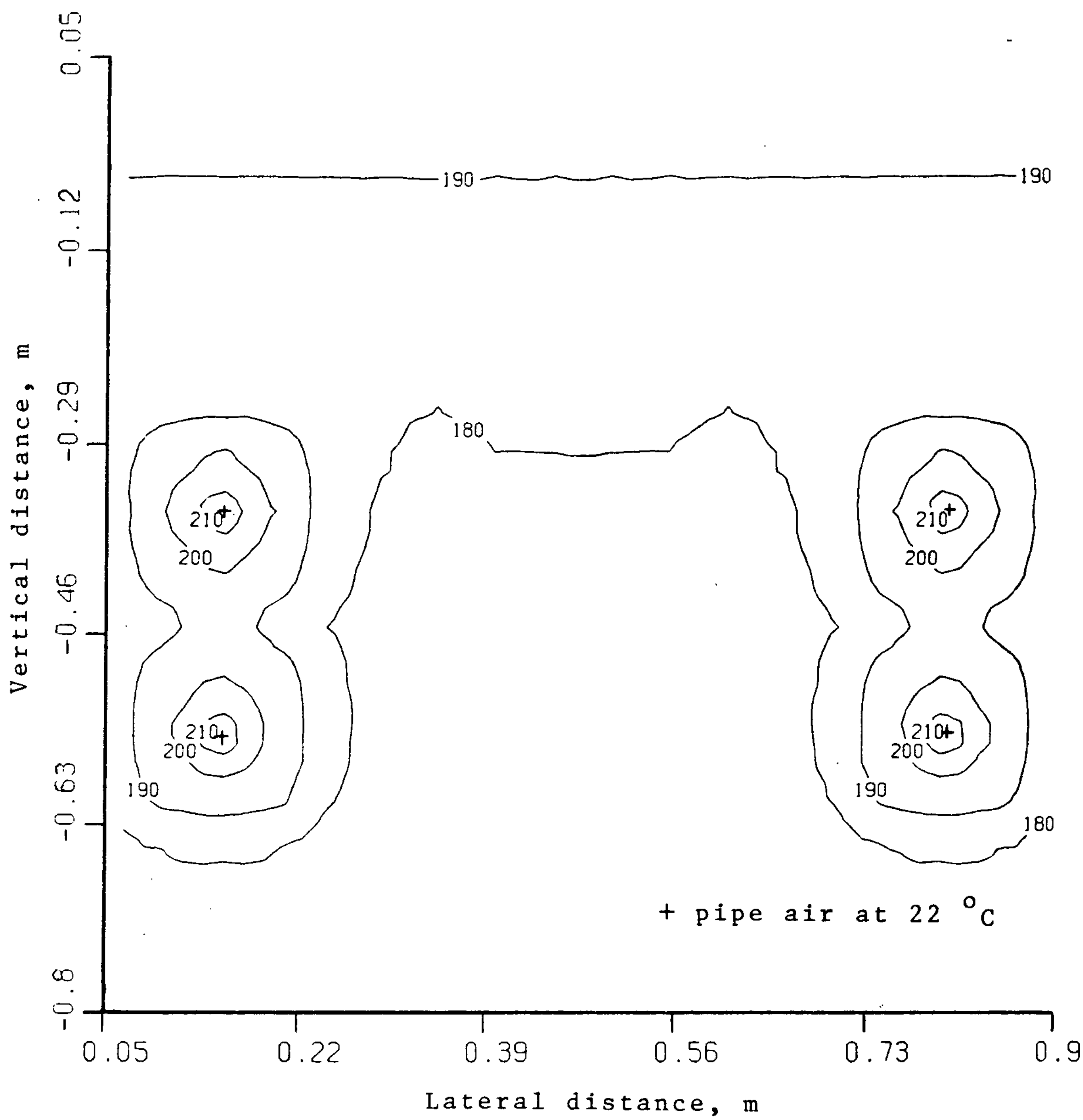

Fig. 3.34 System II - isotherms of simulated soil temperatures at the center region, Mar 25–31

thermal storage that has a closed boundary.

Case 3. Apr 8–14

This week has medium solar radiation as compared to the other two weeks. Predicted and measured inside solar radiation agrees well and is within 9% of one another, as observed from Fig. 3.36.

Fig. 3.37 demonstrates once again that plant temperature can be very close to air temperature when solar radiation is low. Predicted inside humidity is more accurate for this week, the measured values range from 59 to 73%, while prediction has a range of 55 to 75 %, as seen in Fig. 3.38.

Figs. 3.39 and 3.40 present simulated results of soil temperatures. Soil temperature has gradually increased from about 18 $^{\circ}$C in the beginning of the week to about 20 $^{\circ}$C on the last day. This pattern follows the temperature of the soil outside the storage zone. Records show that measured T_{so} was 3 to 4.5 $^{\circ}$C in the week of Feb 18–24, 6 to 6.5 $^{\circ}$C during Mar 25–31 and 6 to 7 $^{\circ}$C in the period Apr 8–14.

Predicted soil temperature is most accurate for location B, followed by locations A and then C. The difference between calculated and measured soil/pipe interface temperature is large on days 5 and 6 (more than 3 $^{\circ}$C or 15% on a few occasions). In fact, the mean difference between simulated and observed data is 1.3 $^{\circ}$C with a standard deviation of 1.1 $^{\circ}$C. When considered on an individual basis, calculated means and S.D.'s are (1.3, 0.9), (0.5, 0.4) and (2.2, 1.1) $^{\circ}$C respectively for the temperature nodes that correspond to the three thermistor locations. The pipe air temperature reached 29 $^{\circ}$C during charging, and a small dry core region could have been formed around the pipe, leading to a reduction of the soil thermal conductivity and hence a steeper temperature gradient than that computed.

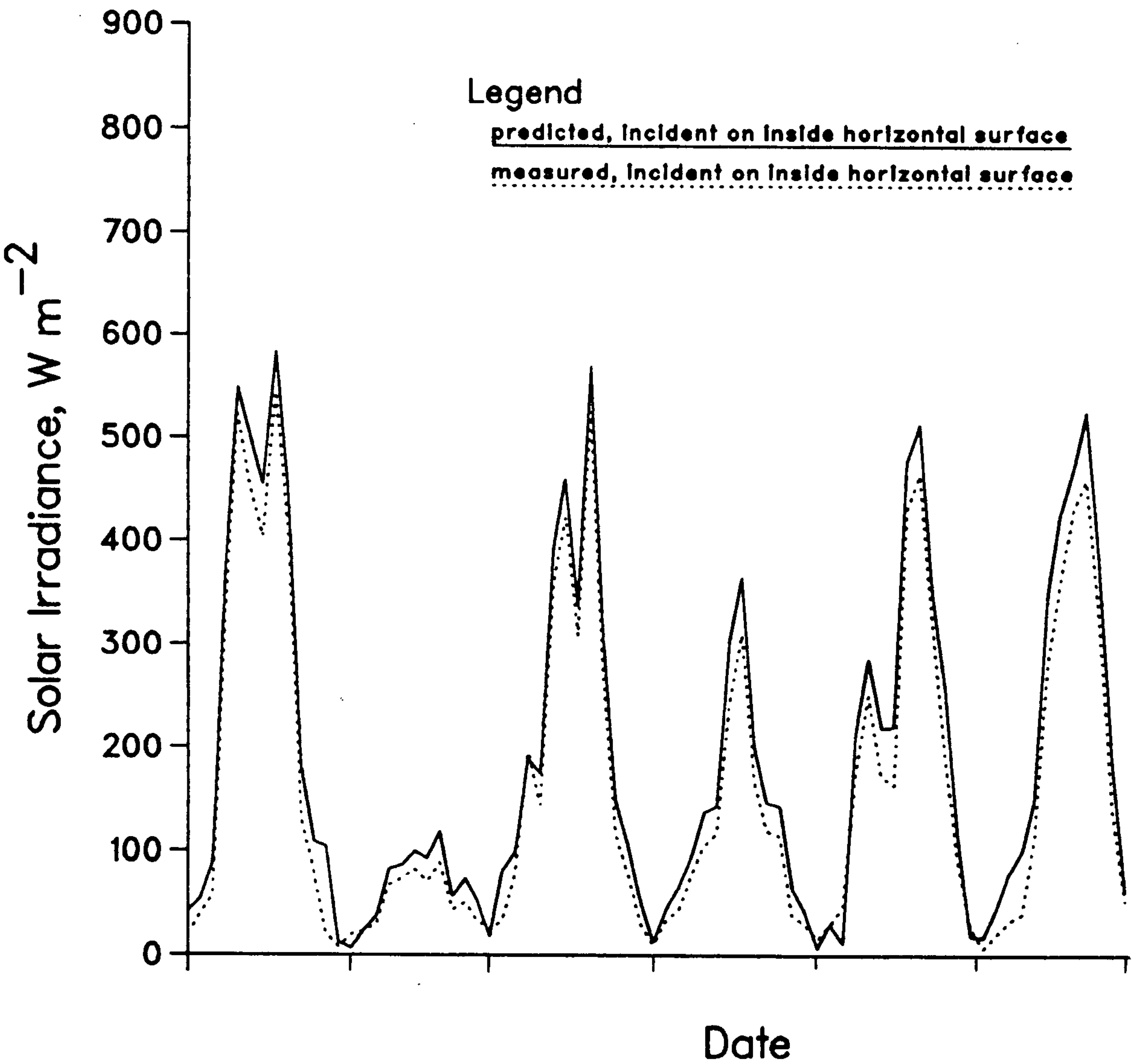

Fig. 3.36 System II – solar radiation incident at plant canopy level, Apr 8–14

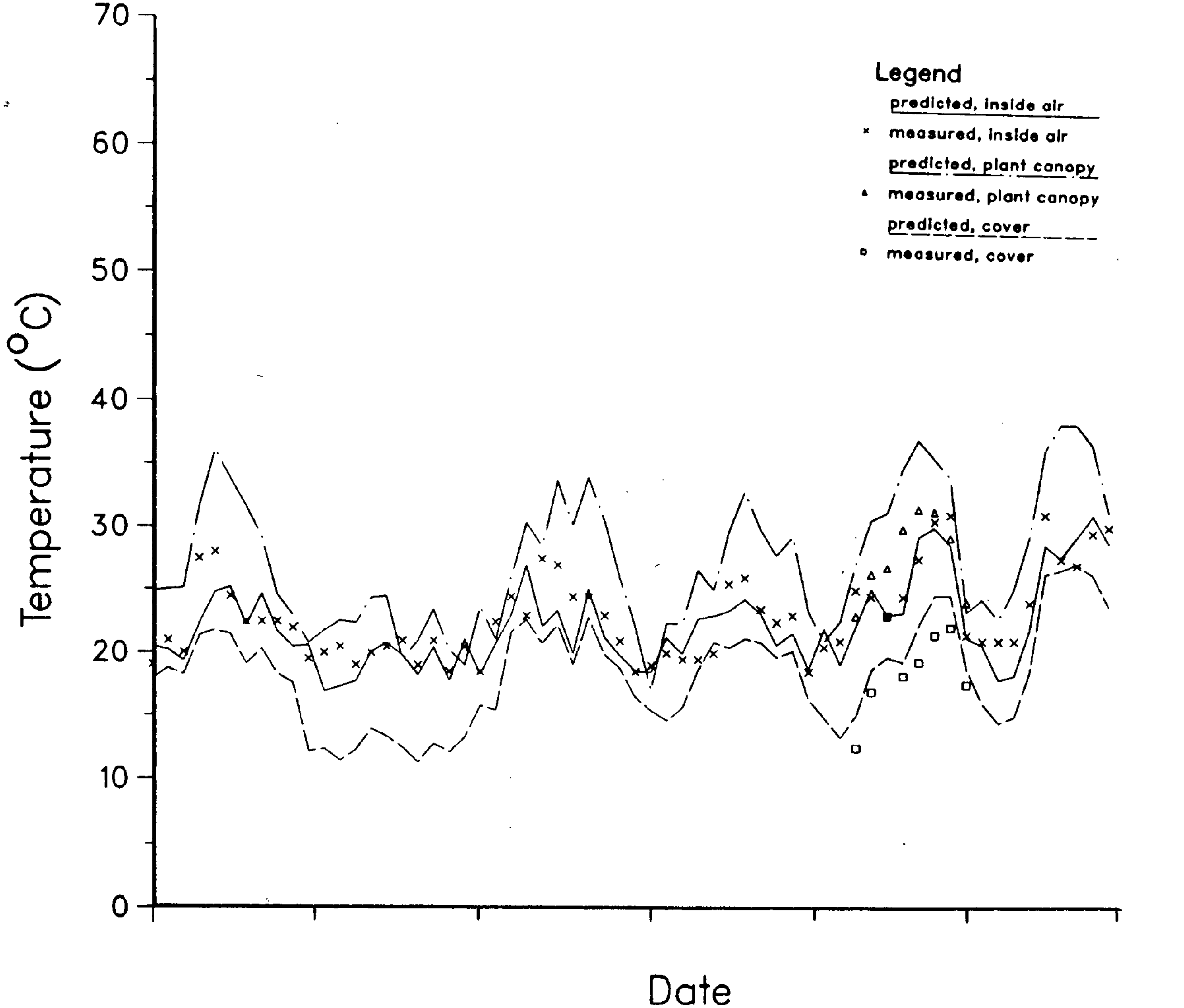

Fig. 3.37 System II – temperatures of the greenhouse thermal environment, Apr 8–14

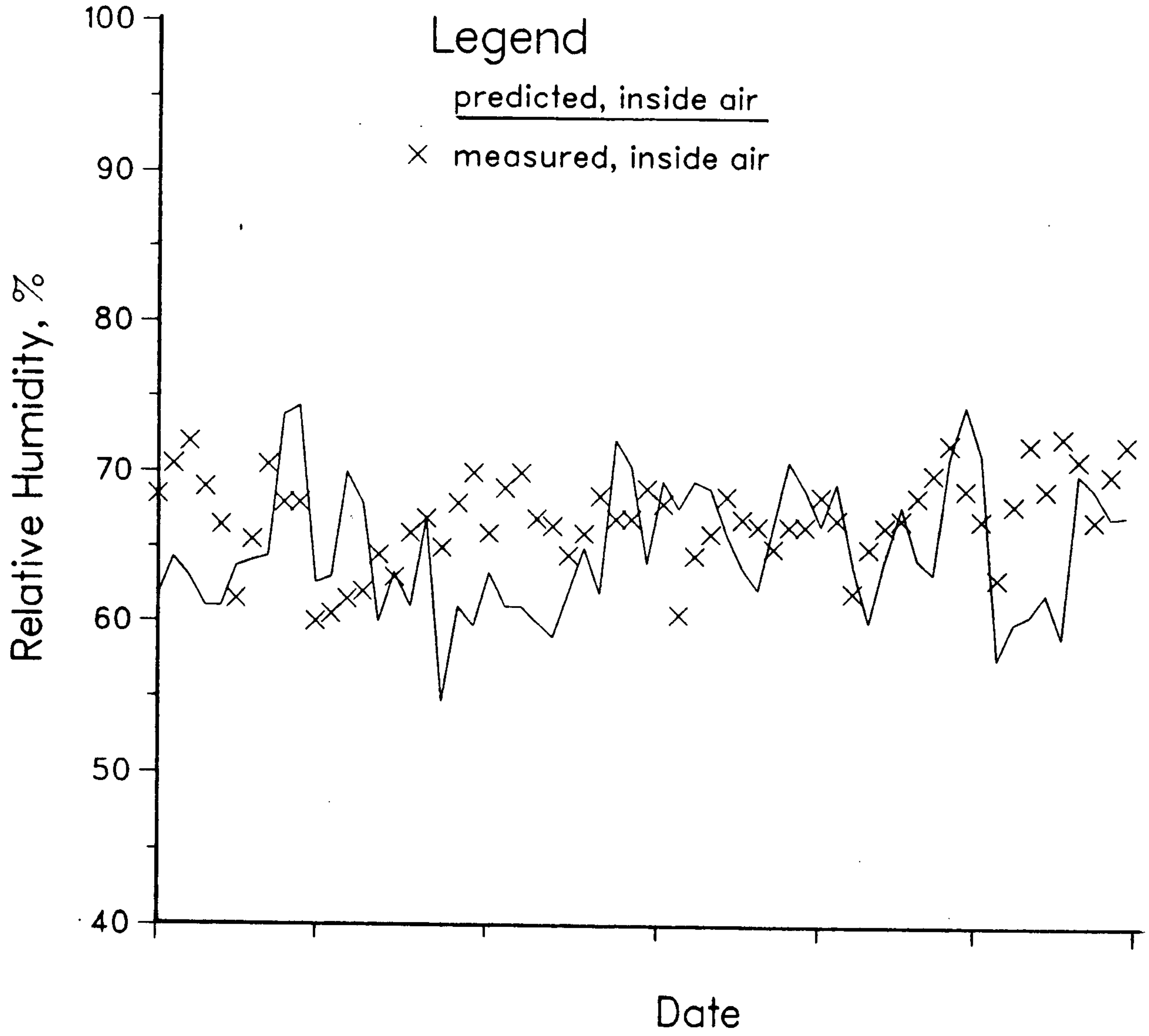

Fig. 3.38 System II – greenhouse relative humidity, Apr 8–14

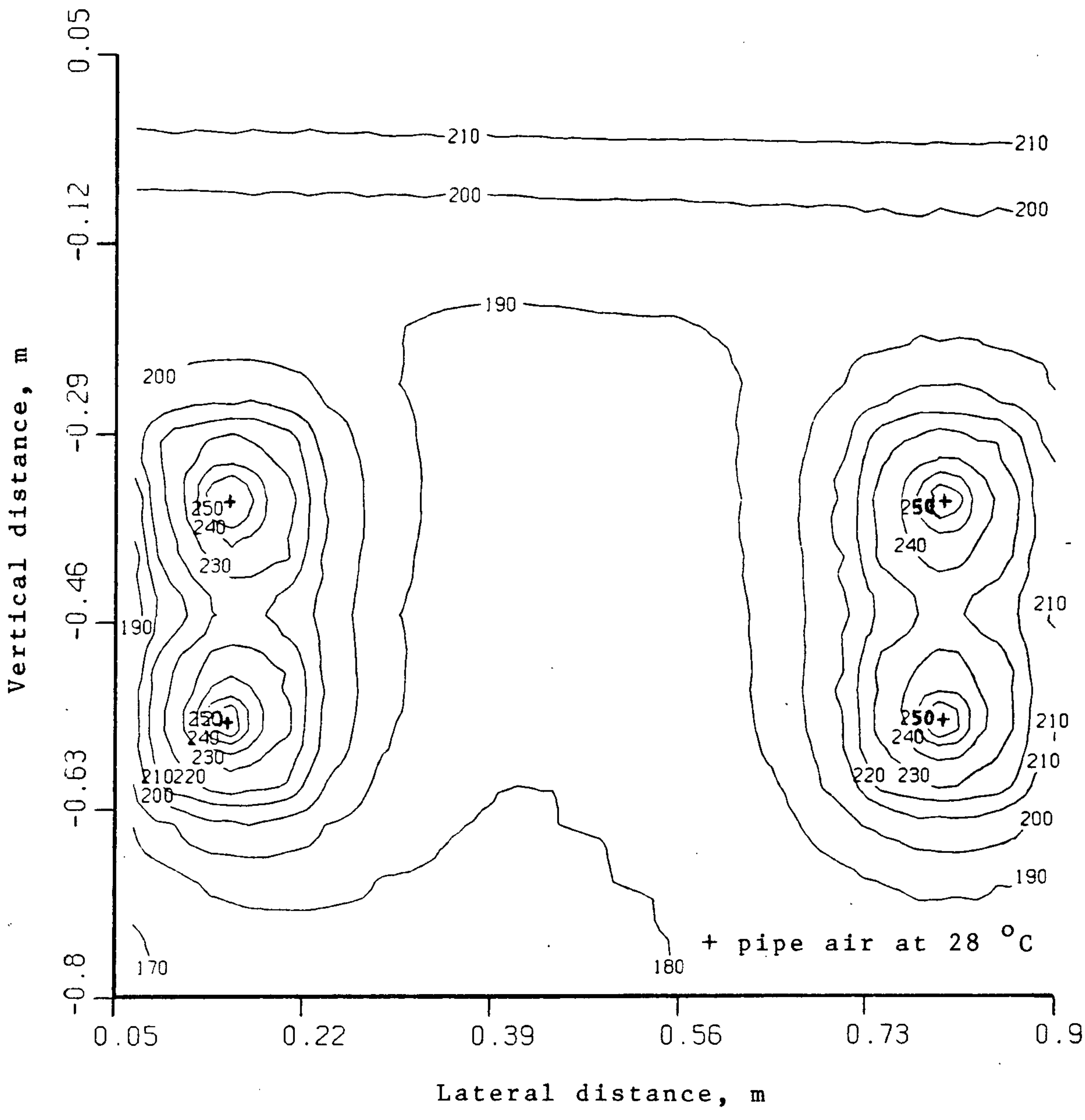

Fig. 3.40 System II - isotherms of simulated soil temperatures, Apr 8-14 (day 6, 1400 hr)

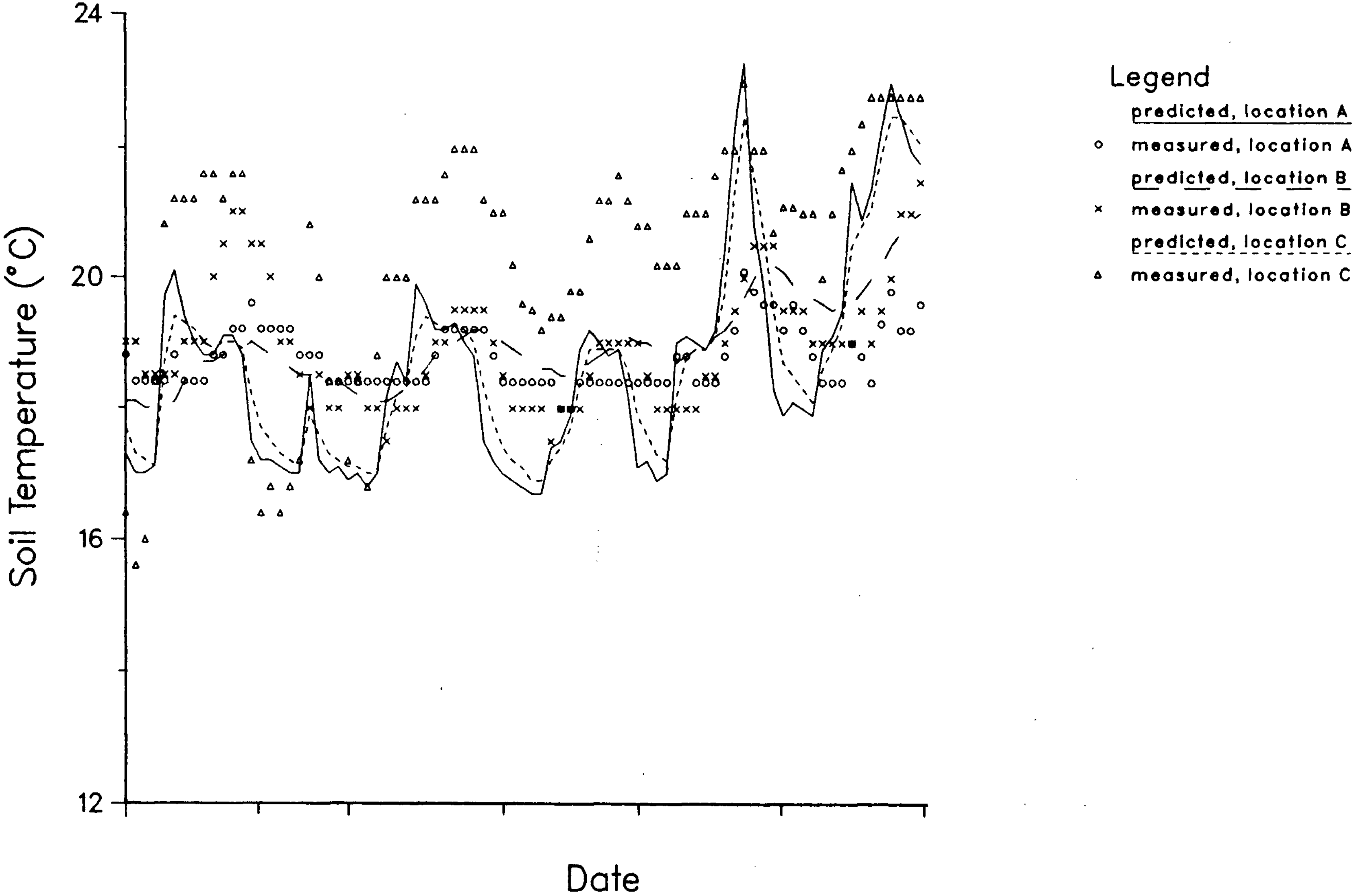

Fig. 3.39 System II - soil temperatures at three locations in the storage zone, Apr 8-14

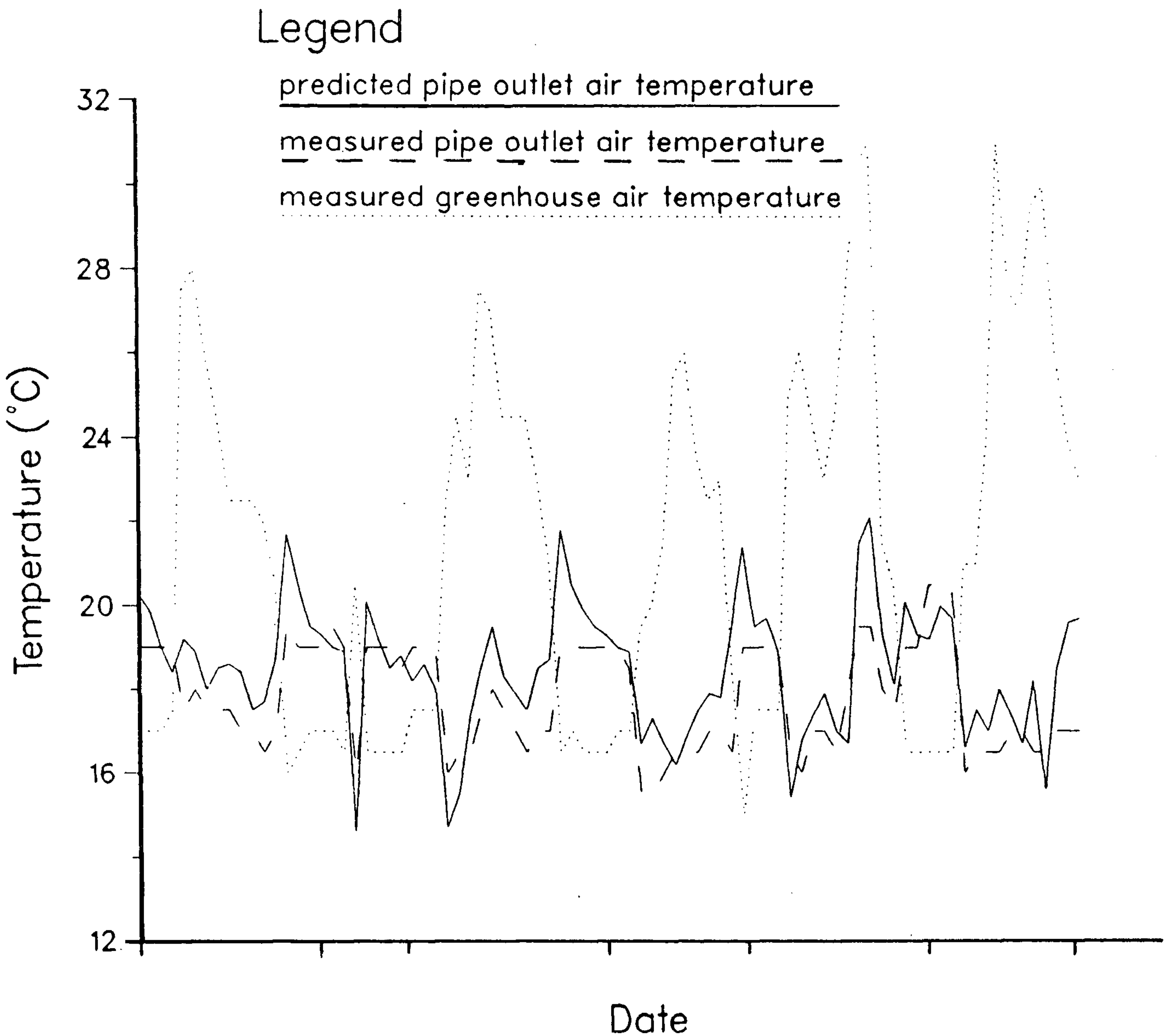

Fig. 3.41 System II - pipe outlet air temperature, Apr 8-14

Isotherms are plotted in Fig. 3.40. Soil temperature near the surface reaches 21 °C because of higher greenhouse temperature. Yet, even with a higher pipe air temperature, the lateral depth of penetration of temperature is less than three pipe diameters. In other words, the lateral pipe spacing of 0.63 m used in the experiments is sufficient to avoid undesirable influence of one pipe on the other in the same layer. On the other hand, thermal gradient is restricted in the vertical direction since the pipes are only 0.20 m apart. A larger vertical pipe spacing would be able to expand the region available for heat storage, but more insulation is required.

Lastly, energy savings due to the soil thermal storage is calculated, whereby 1910 MJ of stored heat is recovered during 34 hours of discharging operation. This value is 9.5 % higher than the actual savings of 1740 MJ which in turn is equivalent to 19% of the total weekly heating demand of 9180 MJ.

NOTATION

		Dimension
A	Area	m^2
C_s	Thermal capacity of soil	$MJ\ m^{-3}\ K^{-1}$
F_{kj}	Configuration factor between two surfaces	-
I	Hourly solar irradiance	$W\ m^{-2}$
J	Radiosity	$W\ m^{-2}$
L	Length	m
L_c	Characteristic length of cover	m
Le	Lewis number	-
M	Moisture flow rate	$kg\ s^{-1}$
N	Number of air changes	h^{-1}
NTU_c	Number of heat transfer units for rockbed thermal storage	-
P_{kj}	Beam radiation interception factor between two surfaces	-
PAR	Hourly photosynthetically active irradiance	$W\ m^{-2}$
Q	Heat flow rate	W
RH	Relative humidity	%
S	Absorbed solar radiation	W
T	Temperature	$^\circ C$
TTF	Total transmission factor	-
U	Overall heat loss coefficient	$W\ m^{-2}\ K^{-1}$
V	Volume	m^3
W	Humidity ratio	$kg\ kg^{-1}$
a_s ,b_s	Constants in soil thermal conductivity	-
c	Specific heat	$J\ kg^{-1}\ K^{-1}$
d_1, d_2	Vertical separation distances	m
h	Convective (surface) heat transfer coefficient	$W\ m^{-2}\ K^{-1}$
h_v	Convective (volumetric) heat transfer coefficient	$W\ m^{-3}\ K^{-1}$
h_D	Mass transfer coefficient	$kg\ m^{-2}\ s^{-1}$
k	Thermal conductivity	$W\ m^{-1}\ K^{-1}$
m	Mass	kg
n_c	Number of glazing covers	-
q_s	Heat transfer rate per unit length of pipe	$W\ m^{-1}$
s_1	Lateral separation distance	m
t	Time	s
u	Air velocity inside greenhouse	$m\ s^{-1}$
x,y,z	Cartesian coordinates	m
α	Solar radiation absorptance	-
β	Leaf Bowen ratio	-
ε	Thermal emittance	-
θ	Absolute temperature	$^\circ K$
θ_s	Volumetric moisture content of soil	%
λ	Latent heat of vaporization	$J\ kg^{-1}$
ν	Density	$kg\ m^{-3}$
ϑ	Thickness	m

ρ	Solar radiation reflectance	-
σ	Stefan-Boltzmann constant	W m^{-2} $°K^{-4}$
τ	Transmittance	-
∂	Differential operator	-
Δ	Difference	-

Subscripts

a	inside air
au	supplemental heat
b	beam radiation
ci	inside cover
cd	condensation
co	outside cover
d	diffuse radiation
e	transpiration
f	floor
g	glazing
h	greenhouse
i	inlet
ih	inside horizontal surface
k,j	glazing surfaces
lw	long-wave radiation
m	measured value
o	outlet, outside
oh	outside horizontal surface
p	pipe, plant canopy
q	absorber plate
r	radiative heat transfer
rs	rockbed storage
s	soil
td	transferred to storage
v	ventilation and infiltration
w	wind, pipe wall
ψ	sky
β	inclined surface

Superscript

*	saturated value
~	predicted value

Chapter 4

SIMULATION FOR LONG-TERM PERFORMANCE OF GREENHOUSE SOLAR HEATING SYSTEMS

System thermal performance is of primary concern to a designer who wants to find out what percentage of energy savings can be attained with each different design. It is necessary to carry out simulations using long-term average climatic data as the driving force. The computer models validated in chapter 3 were used to predict solar heating contributions under different climatic conditions and for varying design parameters.

The computer program was modified to make it general and flexible enough to handle a variety of inputs. From the outputs of energy recovered from storage to meet nighttime heating requirements, it is possible to find out what magnitude of design parameters in combination are required to bring about a desired level of solar contribution for different locations. The effects of design variations on crop canopy net photosynthetic rate shall be assessed and compared by means of a simple growth function.

Based upon the availability of solar radiation and ambient temperature regimes, eight Canadian and US locations were selected for the simulation experiments: Albuquerque, NM; Edmonton, ALTA; Guelph, ONT; Montreal, PQ; Nashville, TN; St. John's, NFD; Vancouver, BC and Winnipeg, MAN.

Mean (monthly average) meteorological data include the following: daily (H) or hourly (I) global solar radiation incident on an outside horizontal surface, maximum and minimum outside air temperatures (T_{max} and T_{min}), outside relative humidity or dew point temperature, wind speed, and soil temperatures at various depths. Ground albedo is needed to compute reflected diffuse radiation from the greenhouse surroundings, and mean values were cited by Iqbal (1983). Some weather stations also recorded diffuse or direct radiation in addition to global radiation, and these were used as inputs so as to reduce the error incurred by estimating either form of radiation with empirical relations. These weather data are published by Environment Canada (1983) for many Canadian locations, whereas soil temperatures were obtained from Ouellet et al. (1975). In the United States, hourly 'typical meteorological year (TMY)' data are recorded on a magnetic tape for 26 locations (National Climatic Center, 1983) so that minimal data processing is required before using them as inputs. However, soil temperature monthly normals could not be obtained and values are assumed in the simulation studies.

Design variations considered in this study pertain mainly to the greenhouse, the rockbed thermal storage and the soil thermal storage.

1. Greenhouse
   a. shape: conventional gable roof, quonset, shed-type and Brace-style (all single-span)
   b. roof tilt: 18.4°(1:4), 26.7°(1:2) and 33.7°(1:1.5)
   c. glazing material: glass, polyethylene and twin-walled acrylic
2. Rockbed thermal storage
   a. storage capacity: 0.19, 0.24 and 0.38 m^3 m^{-2} A_f
   b. air flow rate: 6, 12 and 18 L s^{-1} m^{-2} A_f
3. Soil thermal storage
   a. pipe diameter: 0.10 and 0.15 m
   b. ratio of total pipe wall area to greenhouse floor area: 0.5, 1.0 and 1.5
   c. air flow rate: 6, 12 and 18 L s^{-1} m^{-2} A_f
   d. soil type: clay, sand
   e. soil moisture content: 20% - 40%

4.1 Modification to the Simulation Method

Certain algorithms had to be rearranged for long-term simulations. Simulation starts with a minimum ventilation rate of 1.0 air change per hour, and is altered when computed inside relative humidity exceeds 85% or if the greenhouse air temperature rises above 30 °C after excess heat has been delivered to the thermal storage. The value of net useful heat gain, that is, the excess solar energy available for storage, is computed based on the criterion that the solar fan is turned on when T_a attains 22 °C or above. Predicted plant canopy temperature is the variable that links the greenhouse thermal environment model with the crop growth function. The Bowen ratio is assumed to have a 1-2-3-4 variation from September to December and a 4-3-2-1 pattern between January and May, matching the usual greenhouse cropping practices. Hourly values of climatic data must be generated when only daily values are available. Initial temperatures are needed in the thermal storage models. The rockbed is assumed initially to be at a uniform temperature of 15 °C, whereas undisturbed soil temperatures at various depths are used as initial values. The program simulates the hourly performance of the solar heating system over a typical design-day each month for the heating season which starts in September and ends in May, and its performance was assumed to be the average performance of that month. The typical day has average climatological conditions. Carnegie et al. (1982) noted that the design-day analysis leads to quite optimistic results during the colder months when large weather fluctuations are more common.

4.1.1 Solar radiation

The aim is to obtain I, and either I_b or I_d, depending on several cases.

Case 1. only hourly global radiation (I) is available

Hay's method as summarized by Iqbal (1983) may be used to compute the hourly diffuse component I_d in the following manner:

$$I' = I\{1 - \rho[\rho_a(B/N_j) + \rho_c(1 - B/N_j)]\} \tag{4.1}$$

$$I_d = I'_d + (I - I')$$

$$I'_d = (0.9702 + 1.6688u - 21.303u^2 + 51.288u^3 - 50.081u^4 + 17.551u^5)I'$$

where

$$u = I'/I_{ex}$$

where N_j is the modified daylength which excludes the fraction when the solar altitude is less than 5 °

$$N_j = \frac{1}{7.5} \arccos\left(\frac{\cos 85^o - \sin\phi \sin\delta_c}{\cos\phi \cos\delta_c}\right) \tag{4.2}$$

ρ_a and ρ_c are clear sky albedo and cloud albedo, and have values of 0.25 and 0.6 respectively. I and I_d are the global and diffuse radiations before multiple reflections between the ground and the sky. ρ is the monthly average ground albedo measured for large geographic areas.

Case 2. global and diffuse radiations (I and I_d) are both available

This is the most straight-forward situation, and no solar data processing is necessary.

Case 3. only daily global radiation (H) is available

A few correlations have to be applied in sequence to achieve our aim in this case. For locations situated between 40 °N and 40 °S, the daily diffuse radiation can be calculated from Page's correlation (1979)

$$H_d = H[1.00 - 1.13(H/H_{ex})] \tag{4.3}$$

whereas Iqbal's correlation may be used for Canadian locations

$$H_d = H[0.791 - 0.635(B/N_d)] \tag{4.4}$$

where N_d is the average daylength defined by

$$N_d = \frac{2}{15}\arccos(-\tan\phi\tan\delta_c) \tag{4.5}$$

The next step is to estimate hourly diffuse radiation from H_d using Liu and Jordan's method (1967)

$$I_d = \frac{\pi}{24} H_d \left(\frac{\cos\omega_i - \cos\omega_s}{\sin\omega_s - \omega_s(\pi/180)\cos\omega_s}\right) \tag{4.6}$$

Finally, hourly global radiation can be calculated by the expression of Collares-Pereira and Rabl (1979):

$$I = \frac{I_{ex}}{H_{ex}} H(a' + b'\cos\omega_i) \tag{4.7}$$

where

$$a' = 0.409 + 0.5016\sin(\omega_s - 60^\circ)$$

$$b' = 0.6609 - 0.4767\sin(\omega_s - 60^\circ)$$

Case 4. only the number of bright sunshine hours (m) is available

This case applied to locations where solar radiation is not routinely measured, rather, sunshine records are maintained. The correlation due to Rietveld (1978) will be adopted

$$H = H_{ex}[0.18 + 0.62(B/N_d)] \tag{4.8}$$

Thence, H_d , I_d and I are estimated as outlined in case 3 above.

For the above cases, hourly beam radiation is calculated simply as the difference between I and I_d .

Case 5. both hourly global and direct normal radiations (I and I_n) are available

This case refers to the US locations where I_n is measured by a pyrheliometer. I_b may be calculated in terms of the solar azimuth

$$I_b = I_n \cos\theta_z \tag{4.9}$$

where

$$\cos\theta_z = \sin\phi\sin\delta_c + \cos\phi\cos\delta_c\cos\omega_i$$

Then I_b is subtracted from I to get I_d .

4.1.2 Temperature

For Canadian stations, diurnal temperature patterns can be generated from daily maximum and minimum temperatures using the model of Parton and Logan (1981) that accounts for monthly variation in daylength and modified by Kimball and Bellamy (1986) to provide for a continuity in temperature between the end of the night and the beginning of the day.

daytime:

$$T = T_{min} + (T_{max} - T_{min})\sin\left[\frac{\pi(n - n_{min})}{N_d + 2a}\right] \tag{4.10}$$

where n_{min} , the hour of the lowest temperature is given by

$$n_{min} = n_{sr} + c$$

nighttime:

$$T = (T_{min} - e) + [T_{set} - (T_{min} - e)]\exp\left[\frac{-b(n - n_{ss})}{24 - N_d + c}\right] \tag{4.11}$$

where T_{set} is the temperature at sunset computed from eqn. (4.10) with $n = n_{ss}$, and n_{sr} and n_{ss} are sunrise and sunset hours. After midnight, 24 h is added to n for use in eqn. (4.11). Also,

$$e = (T_{set} - T_{min})/[\exp(b) - 1] \tag{4.12}$$

Values of a, b and c are 1.86 h, 2.20 and -0.17 h respectively. Kimball and Bellamy (1986) noted that some caution should be exercised when applying this model to desert areas. Their model is preferred over a simpler sinusoidal function first proposed by Close (1967) and subsequently used by various researchers in solar heating system simulations, such as Eldighidy and Taha (1983).

4.1.3 Relative humidity

The Canadian stations recorded outdoor relative humidity four times a day. Therefore, the cubic-spline curve fitting technique may be employed to interpolate hourly values. For this end, the program DSPLFT is used (Moore, 1981).

In the case of US locations, relative humidity is calculated from two psychrometric variables, T_{db} and T_{dp}. The psychrometric equations were similar to those used earlier in chapter 3, and are listed in Appendix B.

4.2 Parametric Study

Before the simulation results can be reduced to some simplified design tools, it is useful to carry out a parametric study to examine the effects of a number of design parameters on system thermal performance, and eventually eliminate those found to have minimal influence.

4.2.1 Greenhouse

Variations of greenhouse design parameters (construction) are confined to greenhouse shape, orientation, glazing material, roof tilt and length-to-width ratio. Table

4.1 gives the greenhouse dimensions, and associated view factors and overall heat loss coefficients.

The majority of conventional glasshouses constructed for commercial use have a roof tilt of 1:2 or 1:1.5. The steeper slope is usually found in greenhouses that are narrower than 8 m (Mastalerz, 1979), while a slope less than 1:2 is not recommended for snowfall areas; also, condensate on the inside cover surface will have a higher tendency to drip onto the plants below unless the glazing has been pre-treated with products such as the 'sun-clear solution' (Bredenbeck, 1984) that would permit filmwise condensation.

Unsymmetrical roof tilts are characteristics of the shed-type and Brace-style greenhouses. All three roof tilts (1:1.5, 1:2 and 1:3) were included in the parametric study for the south roof of the shed, while the north wall is at 90°. The roof slopes were fixed at a constant 35° (south side)/65° (north side) configuration for the Brace-style house.

Glazing materials are generally classified as transparent or translucent. Highly transparent materials are homogeneous with a planar surface and cause virtually no diffusion as light passes through them. Typical examples are glass and acrylic (plexiglas). Translucent materials may diffuse the light up to 90%. Clear polyethylene, polycarbonate, polyester and PVC film are materials that diffuse light slightly, whereas fibreglas and striated glass are much more diffusing. To maximize solar energy input for subsequent storage, fibreglass structures are not desirable. In this study, glass, polyethylene and twin-walled acrylic are considered.

The foremost requirement for computing the capture of solar radiation is the transmittance of the cover material of known refractive index ι and extinction (absorption) coefficient K. Information of ι for most glazing materials is published in handbooks.[1] However, values of K for plastics are not immediately available. This

---

[1] typical values may be found in

- User's practical selection handbook for optimum plastics, rubbers and adhesives.

Table 4.1 Greenhouse dimensions and related quantities

shape/ cover	A_f (m^2)	L:W	ξ_1	ξ_2	V (m^3)	A_{gz} (m^2)	A_{NW} (m^2)	F_{12}	F_{13}	UA W/^oC
CV/GS	200	2	26.6	26.6	650	370	0	0.86	0.09	2430
CV/DA	200	2	26.6	26.6	650	370	0	0.86	0.09	1505
SS/GS	200	2	26.6	90.0	900	355	140	0.67	0.25	2475
SS/DA	200	2	26.6	90.0	900	355	140	0.67	0.25	1590
BS/GS	200	2	35.0	65.0	930	315	160	0.66	0.24	2280
CV/GS	200	4	26.6	26.6	575	380	0	0.81	0.16	2465
CV/GS	200	8	26.6	26.6	525	410	0	0.82	0.16	2660
SS/GS	200	4	26.6	90.0	755	335	155	0.61	0.34	2325
SS/GS	200	8	26.6	90.0	650	335	180	0.62	0.35	2335
CV/GS	200	2	18.4	18.4	565	345	0	0.93	0.05	2275
CV/GS	200	2	33.7	33.7	735	395	0	0.79	0.15	2600
SS/GS	200	2	18.4	90.0	735	325	105	0.77	0.17	2235
SS/GS	200	2	33.7	90.0	1065	390	175	0.58	0.32	2740
CV/GS	500	2	26.6	26.6	1990	810	0	0.86	0.09	5500
CV/GS	1000	2	26.6	26.6	4800	1510	0	0.86	0.09	10595
SS/GS	500	2	26.6	90.0	2980	810	315	0.67	0.25	5955
SS/GS	1000	2	26.6	90.0	7600	1545	590	0.67	0.25	12015

Symbols found in this table and all other tables of chapter 4 are explained in the 'Notation' section on pages 235 to 237.

problem was resolved by determining the value of K using Fresnel's relation and Bouguer's law of attenuation as described in chapter 3, along with the measured values of direct transmittance at various incident angles (Godbey et al., 1979) for polyethylene; for acrylic, Russell (1985) suggested that the K-value is small. Using this method, K was estimated to be 400 m^{-1} and 10 m^{-1} for polyethylene and acrylic, of thickness 0.1 mm and 16mm (two 2mm sheets with 12mm air space) respectively. Also, using the total and direct transmittance values, the diffusing power of polyethylene was estimated to be 10% for an angle of incidence θ_i below 60°, and 15% when θ_i exceeds 60°.

4.2.2 Rockbed thermal storage

The rockbed storage capacity and the air flow rate are the two major design concerns. Values chosen for a particular system would govern the size of the bed and the fan to deliver the quantity of air. Table 4.2 shows the rockbed dimensions and information relevant to the heat transfer characteristics. The variables involved in these two design parameters are:

ρ_r : rock density (M_r / V_r)

ϵ : void ratio (void volume/total volume)

L_r , W_r , h_r : bed dimensions (length, width, depth)

d_r : rock size (equivalent diameter)

A storage capacity (SC_r) of 0.25 m^3 rock per m^2 collector area, which corresponds to 350 kJ m^{-2} °C $^{-1}$ was used by Beckman et al. (1977) as the standard size to develop the f-chart for solar air heating system. Also, a base air flow rate of 10 L s^{-1} m^{-2} was adopted.

---

[1](cont'd) 1976. The International Technical Information Institute, Tokyo, Japan.

- Handbook of tables for applied engineering science. Ed. R.E. Bolz and G.L. Ture. 1979. CRC Press, Inc., Florida, USA.

Table 4.2 Rockbed thermal storage variables

Greenhouse			Rockbed		SC_r		$\dot{m}$		NTU	h_v	h
A_f (m)	L_g(m)	W_g(m)	L_{rs} (m)	W_{rs} (m)	m^3/m^2	$kJ/m^2 C$	kg/s	$L/s.m^2$	-	$W/m^3 C$	$W/m^2 C$
200	20.0	10.0	6.8	8.0	0.38	800	4.5	18.7	71	3009	15.8
200	28.3	7.1	9.6	5.7	0.38	800	4.5	18.7	91	3835	20.1
200	40.0	5.0	13.5	4.0	0.38	800	4.5	18.7	116	4889	25.7
200	20.0	10.0	5.1	8.0	0.28	600	4.5	18.7	54	3009	15.8
200	20.0	10.0	3.4	8.0	0.19	400	4.5	18.7	36	3009	15.8
200	20.0	10.0	6.8	8.0	0.38	800	1.5	6.25	99	1395	7.3
200	20.0	10.0	6.8	8.0	0.28	600	1.5	6.25	75	1395	7.3
200	20.0	10.0	6.8	8.0	0.19	400	1.5	6.25	50	1395	7.3
200	20.0	10.0	6.8	8.0	0.38	800	3.0	12.5	81	2266	11.9
200	20.0	10.0	6.8	8.0	0.28	600	3.0	12.5	61	2266	11.9
200	20.0	10.0	6.8	8.0	0.19	400	3.0	12.5	40	2266	11.9
200	28.3	7.1	9.6	5.7	0.38	800	3.0	12.5	103	2888	15.2
200	40.0	5.0	13.5	4.0	0.38	800	3.0	12.5	131	3681	19.3
500	31.6	15.8	10.7	12.7	0.38	800	7.5	12.5	111	3122	16.4
1000	44.7	22.4	15.1	17.9	0.38	800	15.0	12.5	142	3980	20.9

The air flow rate determines the pressure drop ΔP in the packed bed for given ϵ, L and d values. Expressions for ΔP depend on the nature of the flow regimes. In the laminar regime, the Blake–Kozeny (Bird et al., 1960) equation gives

$$\Delta P_1 = 150 \frac{v_f \mu L_{rs}(1-\epsilon)^2}{d^2 \epsilon^3} \tag{4.13}$$

For highly turbulent flow, the Burke–Plummer (Bird et al., 1960) equation governs

$$\Delta P_2 = 1.75 \frac{v_f^2 \nu_f L_{rs}(1-\epsilon)}{d \epsilon^3} \tag{4.14}$$

whereas for flow in the transition zone, the Ergun equation (Sissom and Pitts, 1972) may be used, which is simply

$$\Delta P_3 = \Delta P_1 + \Delta P_2 \tag{4.15}$$

In the long-term simulations, the bed's depth was fixed at 1.0 m, and its width as 0.8 x house width. Other fixed quantities are ρ_r = 2400 kg m^{-3}, ϵ = 0.30 and d = 25 to 38 mm. When SC_r is specified, the bed volume and therefore the bed length can be calculated. Air flow rate is selected to give a high enough NTU value so that eqn. (2.19) is valid.

4.2.3 Soil thermal storage

Again, the key design parameters are storage capacity and air flow rate. But unlike the rockbed storage which has a fixed size, the 'size' of the soil storage is represented by the layout of the pipe network. The following factors are involved:

N_p : number of pipes

D: pipe diameter

S_p : pipe spacing

n_L : number of layers of pipe

L_p : pipe length

d_f : depth of pipe

d_i : depth of insulation material

Table 4.3 lists the various arrangements together with some heat transfer characteristics. In the simulations, the fixed variables are $n_L = 2$, L = greenhouse length, $d_f = 0.4$ m and $d_i = 1.0$ m. When the ratio of total pipe wall area to greenhouse floor area A_p / A_f and total air flow rate are specified, the number of pipes and air flow rate in each pipe can be calculated. Furthermore, for a given pipe diameter, pipe spacing is also determined.

4.2.4 Results and discussion

For long-term system thermal performance, the ultimate output from simulations is the annual solar heating fraction for the heating period from September to May. Before the simulation results are presented in this section, it is necessary to define several terms.

Two concepts are involved in defining the percentage of greenhouse heating requirements met by solar energy. Internal collection systems use the greenhouse as a passive solar collector, and admitted solar radiation could therefore counteract the whole or part of its daytime heat losses. If this solar contribution is to be explicitly recognized, then the term 'total solar contribution, s' may be defined as

$$s = \frac{\text{passive solar gain + solar heat recovered from storage}}{\text{daytime and nighttime heating load}}$$

$$= \frac{Q_{PAS} + Q_{ST}}{Q_{DL} + Q_{NL}} \tag{4.16}$$

In the program, Q_{PAS} is set equal to Q_{DL} when the passive solar gain exceeds daytime gross heating load, so that the 'passive solar gain' term does not include the portion of useful heat gain that is stored.

However, if only fuel savings is concerned, then the term 'solar heating

Table 4.3 Soil thermal storage variables

greenhouse floor area: 200 m^2 , length-to-width ratio: 2

pipe network layout (L_p = 20.0 m)				$\dot{m}$		NTU	U_p	$\dot{m}_p$
r_s	N_p	D	S_p	kg/s	L/s.m²	-	W/m²C	kg/s
1.5	46	0.10	0.35	4.5	18.7	1.40	21.8	0.10
1.0	30		0.61			1.14	27.3	0.15
0.5	14		1.55			0.75	38.2	0.32
1.5	46	0.10	0.35	1.5	6.2	2.12	11.0	0.03
1.0	30		0.61			1.83	14.6	0.05
0.5	14		1.55			1.35	23.8	0.11
1.5	30	0.15	0.53	4.5	18.7	1.04	16.4	0.15
1.0	20		0.90			0.88	20.8	0.23
0.5	10		2.31			0.63	30.5	0.45
1.5	30	0.15	0.53	1.5	6.2	1.48	7.8	0.05
1.0	20		0.90			1.31	10.4	0.08
0.5	10		2.31			1.04	16.8	0.15

fraction, f applies, and is defined as

$$f = \frac{\text{solar heat recovered from storage}}{\text{daytime net heating load + nighttime heating load}}$$

$$= \frac{Q_{ST}}{Q_{DN} + Q_{NL}} \qquad (4.17)$$

Daytime net heating load is the auxiliary heat supplied to the greenhouse when passive solar gain cannot meet the total daytime heat losses induced by transmission and ventilation (including infiltration). The f value corresponds to the energy savings achieved against a control greenhouse in research experiments. The denominator of the above expression is also directly linked to the cost of greenhouse space heating borne by the grower.

Results of the detailed parametric study are now presented. Effects of the greenhouse construction parameters will be discussed first, and followed by an examination of the influence of thermal storage design parameters on long-term system performance. Typical simulation results will be tabulated where necessary and the values of the fixed parameters used in each cluster of computer runs are also indicated in the relevant tables.

4.2.4.1 Effect of greenhouse construction parameters

The major design parameters that affect the useful heat gain of a greenhouse being used as a solar collector are the shape and glazing of the greenhouse. As mentioned earlier, embedded in the parameter 'shape' is the energy collection or absorption method. The shape SS represents method I that features a shed-type greenhouse with north wall insulation and a vertical absorber plate with high short-wave absorptivity for augmenting heat collection. Method II is implied by the shape CV where a conventional greenhouse (gable roof or quonset type) is built without modification. The curved surface of the quonset house could be approximated by polygons, but the resulting profile would complicate the determination of view factors and interception factors. Thus, the quonset shape is assumed to have straight sloping surfaces like the gable-roofed greenhouse. BS refers to energy collection method III whereby a Brace-style greenhouse having an insulated north surface and lined inside with a highly reflective material is used for energy collection.

Table 4.4 shows the simulation results for a glass greenhouse of different shapes CV, SS and BS and located at Montreal. First, we consider the greenhouse effective transmissivity. Values of τ_e typically range from 0.65 to 0.75 for an east-west aligned greenhouse and a small difference in the magnitude of inside solar radiation exists between the SS and CV greenhouses, suggesting that modification of the greenhouse shape alone cannot bring about an appreciable improvement in the effective transmissivity. At an early stage of this project, the total transmission factor (TTF) as proposed by Ben-Abdallah (1983) for comparing greenhouse solar input efficiency was calculated for some North American locations. Two representative plots for the shed-type glasshouse and the conventional glasshouse are shown in Figs. 4.1 and 4.2. It can be readily seen that TTF is well above 1.0 for the SS house in certain locations. The drastic difference in the magnitudes of TTF and τ_e of the same greenhouse points out the phenomenon that even though the solar shed can admit substantially greater amount of solar radiationat the glazing level, the loss induced by the greenhouse geometry itself on both the direct and diffuse components eventually erodes this advantage if solar radiation at the plant canopy level is considered. This argument has been substantiated with experimental evidence in chapter 3 for the location of Vancouver, and the results here show that it applies to other locations. Besides, on an equal floor area basis, the glazing area of a SS house is close to that of a CV house, and has greater volume (Table 4.1 refers). Therefore, were the absorber plate not installed in the solar shed, this modified

Table 4.4 Effect of greenhouse shape on system thermal performance

greenhouse - location: Montreal, floor area: 200 m^2, orientation: E-W, cover: glass
length-to-width ratio: 2, roof tilt: 26.6 (SS and CV)

storage - medium: rockbed, capacity: 0.38 m^3/m^2, air flow rate: 12.5 $L/s.m^2$

		Sep	Oct	Nov	Dec	Jan	Feb	Mar	Apr	May	Year
τ_e	CV	0.77	0.78	0.76	0.74	0.74	0.77	0.79	0.78	0.71	0.76
	SS	0.79	0.79	0.78	0.75	0.77	0.83	0.81	0.77	0.73	0.78
	BS	0.84	0.88	0.90	0.87	0.91	0.93	0.88	0.80	0.81	0.85
H_p [MJ]	CV	2031	1287	681	565	789	1329	1962	2512	2670	13826
	SS	2084	1304	699	573	821	1433	2012	2479	2745	14150
	BS	2216	1452	806	665	970	1605	2186	2576	2857	15333
Q_{DL} [MJ]	CV	349	774	1440	1659	1863	2299	2205	1594	711	12894
	SS	361	798	1483	1709	1917	2366	2269	1642	723	13268
	BS	306	678	1259	1450	1627	2007	1925	1394	615	11261
Q_{NL} [MJ]	CV	609	1413	2351	3992	4599	3975	2679	1512	810	21940
	SS	629	1458	2422	4112	4732	4092	2758	1557	823	22583
	BS	535	1238	2056	3489	4015	3472	2340	1321	701	19167
Q_L [MJ]	CV	958	2187	3791	5651	6462	6274	4884	3106	1521	34834
	SS	990	2256	3905	5821	6649	6458	5027	3199	1546	35851
	BS	841	1916	3315	4939	5642	5479	4265	2715	1316	30428
SLR	CV	2.11	0.59	0.18	0.10	0.12	0.21	0.40	0.80	1.76	0.40
	SS	2.09	0.58	0.18	0.10	0.12	0.22	0.40	0.77	1.77	0.40
	BS	2.63	0.76	0.24	0.13	0.17	0.29	0.51	0.94	2.17	0.50
s	CV	0.91	0.50	0.22	0.13	0.15	0.25	0.39	0.60	0.75	0.33
	SS	0.96	0.62	0.33	0.18	0.24	0.35	0.48	0.71	0.92	0.40
	BS	0.93	0.56	0.22	0.11	0.16	0.27	0.42	0.61	0.89	0.37
f	CV	0.77	0.22	0.00	0.00	0.00	0.00	0.05	0.30	0.54	0.07
	SS	0.92	0.43	0.06	0.00	0.02	0.05	0.15	0.47	0.86	0.14
	BS	0.88	0.29	0.03	0.00	0.02	0.03	0.07	0.32	0.79	0.11

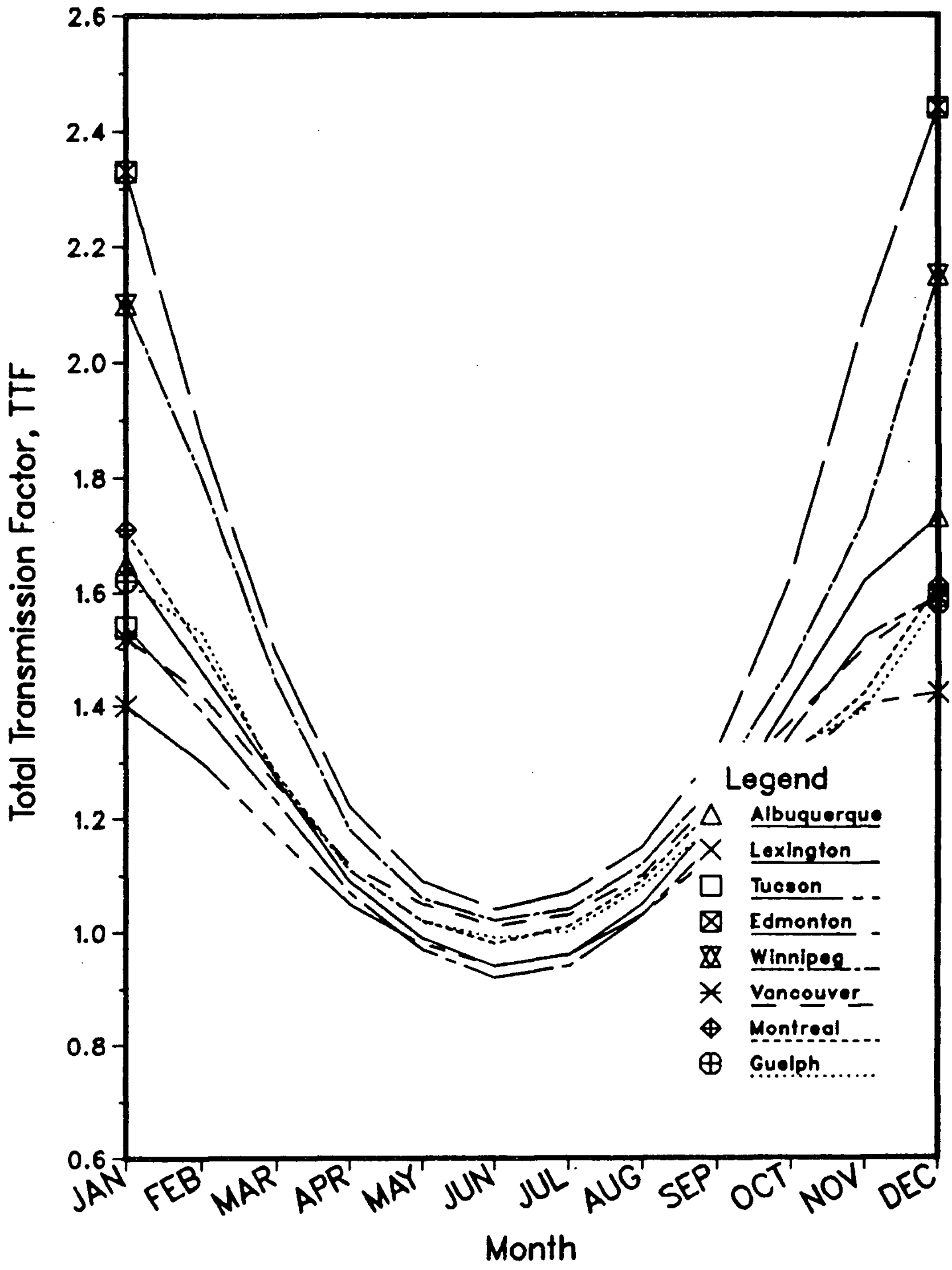

Fig. 4.1 Shed-type glasshouse - total transmission factor calculated using average solar radiation data for eight geographic locations

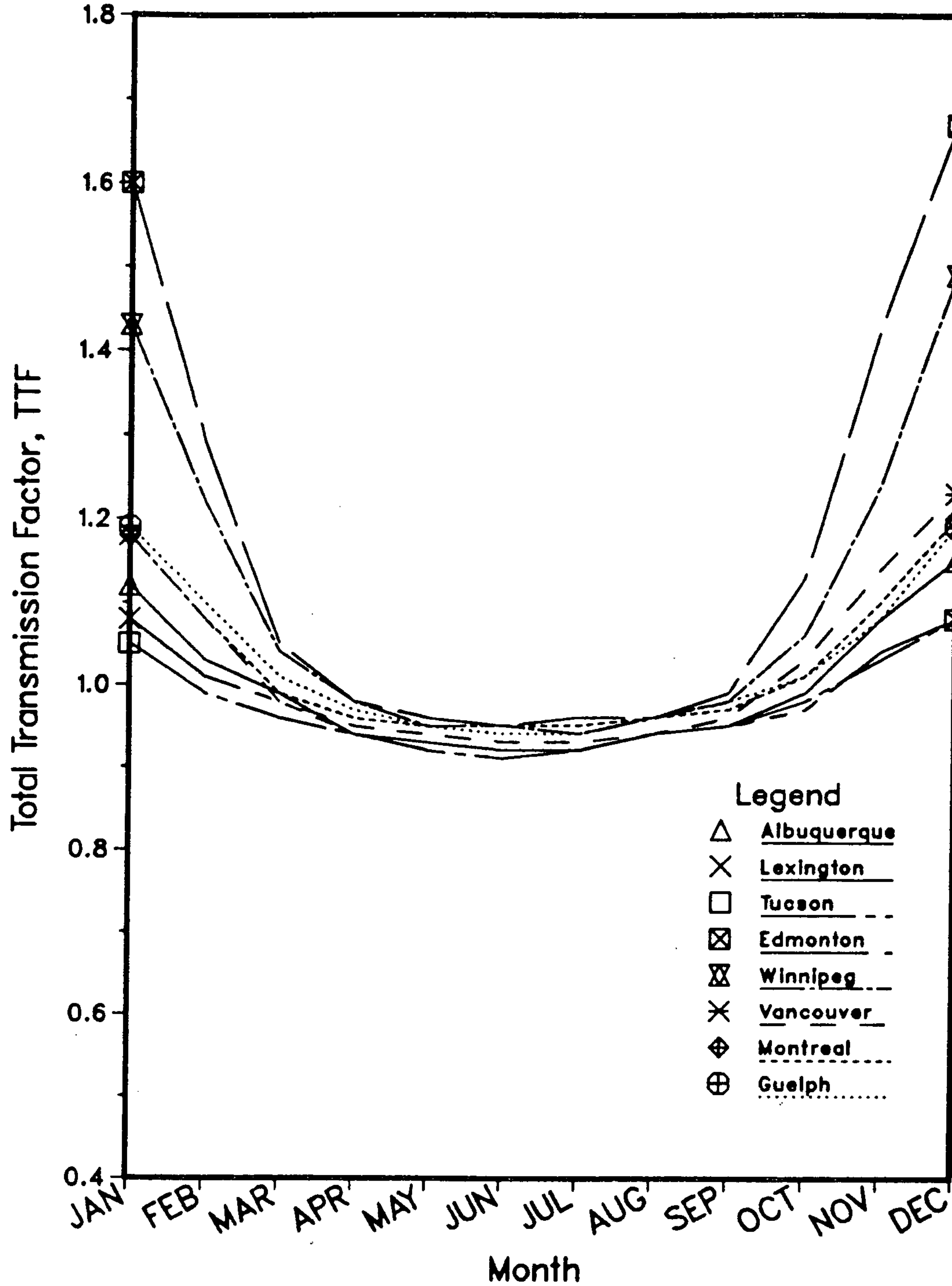

Fig. 4.2 Conventional glasshouse - total transmission factor calculated using average solar radiation data for eight geographic locations

structure would have claimed no advantage over a conventional greenhouse shape for the sake of collection. With these solar heat gain and building heat loss values, the solar load ratio (SLR) defined as the quotient of H_p , the mean daily total solar radiation incident on an inside horizontal surface at the plant canopy level divided by Q_L , the mean daily gross heating load before discounting passive solar gain was calculated for each greenhouse shape. Since the daytime setpoint temperature of the greenhouse is 22 °C while it is 17 °C at nighttime, during the warmer spring period in Montreal, daytime heating load Q_{dl} is comparable to that at night, Q_{nl} . SLR has the highest value for the BS greenhouse, while the CV and SS come very close to each other in terms of the solar load ratio. Over the heating season from September to May, the SS and CV houses admit 10% less solar radiation than the BS house, and at the same time, lose 14% more heat, since the latter has the least glazing-to-floor area ratio. To demonstrate that the better solar admission of the Brace-style greenhouse is credited primarily to the reflective aluminum foil mounted on the inside of the insulated north surface rather than the shape itself, a short-wave reflectivity of 0.05 (equal to that used for the vertical absorber plate of the SS house) was then used in the input in the simulation runs involving the BS house. It was noticed that τ_e became even less than that of the SS house.

However, when the entire solar heating system is considered, the annual total solar contribution s_y and hence the solar heating fraction f_y are more favourable for the SS greenhouse, followed by the BS and lastly the CV greenhouse collection method. As seen in Table 4.4, f_y is 0.14 for SS and 0.11 and 0.07 for CV and BS houses respectively. Expectedly, the presence of the absorber plate is beneficial for solar heat gain and collection. The reflective coating characteristics of the BS collection method permits greater luminosity, but is less effective in enhancing convective heat exchange and thus solar energy collection compared to the SS design.

The merits of the SS collection system is more obvious if the greenhouse is located in Vancouver where the fraction of heating load supplied by solar is 0.32, which is 39% more than the BS method and 60% more than the CV greenhouse collection.

The effect of cover (glazing) material on system thermal performance is next shown in Table 4.5 for a CV greenhouse located in the Vancouver area. Whereas the effective transmissivity of a polyethylene covered quonset house is close to that of a gable roof glasshouse, due in part to the assumption of a straight edge for the curved surface, it is about 10% less for a gable roof greenhouse with double acrylic cover. On the other hand, the double acrylic cover retards the rate of heat loss by about 45% relative to either glass or polyethylene. Hence, its solar load ratio is considerably higher; the annual solar heating fraction turns out to be 0.31, compared to 0.20 for a glasshouse and 0.17 for a polyethylene greenhouse in the same location. During the months of November to February, the CV collection method is the limiting factor even when glass is replaced by double acrylic. However, the impact of twin-walled acrylic material is significant in early fall and spring time, when some marked increase in solar heating fraction is sufficient to boost the annual energy savings.

Another way to compare the thermal performance of one collection method with the other is via the collection efficiency η which is defined as the percentage of inside solar radiation, H_p that is converted into useful heat gain, Q_u . Some calculated values of η based on simulated results of H_p and Q_u can be found in Table 4.6 for the SS and CV collection systems with glass or double acrylic cover. Substituting double acrylic for glass would let a SS house improve its collection efficiency by 12% whereas a CV house will be 20% more efficient. Viewing from another angle, if the SS collection system is preferred

Table 4.5 Effect of cover material on system thermal performance

greenhouse - location: Vancouver, floor area: 200 m^2 , orientation: E-W, cover: glass
shape: CV, length-to-width ratio: 2, roof tilt: 26.6

storage - medium: rockbed, capacity: 0.38 m^3/m^2 , air flow rate: 12.5 $L/s.m^2$

	cover	Sep	Oct	Nov	Dec	Jan	Feb	Mar	Apr	May	Year
τ_e	GS	0.76	0.76	0.71	0.71	0.71	0.76	0.79	0.77	0.78	0.75
	PE	0.74	0.74	0.71	0.72	0.71	0.75	0.77	0.75	0.75	0.75
	DA	0.69	0.69	0.65	0.66	0.65	0.70	0.72	0.69	0.71	0.69
H_p [MJ]	GS	2009	1122	514	318	418	863	1585	2318	2936	12064
	PE	1957	1092	507	323	423	848	1515	2221	2823	11976
	DA	1830	1029	471	296	382	777	1444	2077	2743	11032
Q_{DL} [MJ]	GS	593	875	1008	1163	1260	1401	1491	1349	1074	8075
	PE	601	884	1021	1178	1362	1513	1507	1363	1086	8160
	DA	274	413	470	552	592	677	736	667	526	4907
Q_{NL} [MJ]	GS	564	1087	1743	2023	2215	1796	1407	951	561	12463
	PE	597	1125	1804	2094	2293	1859	1456	984	582	12602
	DA	366	671	1051	1224	1324	1089	873	606	374	7578
Q_L [MJ]	GS	1157	1962	2751	3187	3475	3197	2898	2300	1635	22562
	PE	1188	2009	2825	3472	3655	3372	3013	2447	1668	23299
	DA	640	1084	1521	1776	1916	1766	1609	1273	900	12485
SLR	GS	1.74	0.57	0.19	0.10	0.12	0.27	0.55	1.01	1.80	0.54
	PE	1.65	0.54	0.18	0.09	0.12	0.25	0.50	0.91	1.69	0.51
	DA	2.86	0.95	0.31	0.17	0.20	0.44	0.90	1.63	3.05	0.88
s	GS	0.88	0.54	0.28	0.18	0.20	0.34	0.52	0.71	0.92	0.44
	PE	0.83	0.50	0.24	0.17	0.19	0.30	0.50	0.62	0.86	0.40
	DA	1.00	0.76	0.24	0.12	0.17	0.39	0.67	0.89	1.00	0.51
f	GS	0.78	0.21	0.02	0.00	0.02	0.05	0.23	0.48	0.85	0.20
	PE	0.66	0.16	0.00	0.00	0.00	0.03	0.19	0.38	0.75	0.17
	DA	1.00	0.57	0.02	0.00	0.03	0.08	0.43	0.78	1.00	0.31

Table 4.6 Collection efficiency for shed-type and conventional greenhouses with glass or double acrylic covers

greenhouse - floor area: 200 m^2 , orientation: E-W
length-to-width ratio: 2, roof tilt: 26.6

location	shape/cover		Sep	Oct	Nov	Dec	Jan	Feb	Mar	Apr	May	Year	$\eta = Q_u/H_p$
VAN	SS/GS	H_p	2116	1180	522	336	418	888	1604	2318	3020	12402	0.58
		Q_u	1215	883	289	146	237	429	930	1402	1693	7223	
	SS/DA	H_p	1983	1107	492	314	394	844	1505	2197	2818	11654	0.66
		Q_u	1184	941	328	225	319	490	1072	1496	1644	7729	
	CV/GS	H_p	2009	1122	514	318	418	863	1585	2318	2936	12064	0.33
		Q_u	804	514	113	0	0	144	485	835	1028	3920	
	CV/DA	H_p	1830	1029	471	296	382	777	1444	2077	2743	11049	0.39
		Q_u	770	547	149	0	174	202	571	896	1014	4324	
GPH	SS/GS	H_p	2208	1474	754	664	976	1693	2161	2510	2956	15396	0.48
		Q_u	1312	979	149	0	156	683	1061	1310	1746	7391	
	SS/DA	H_p	2068	1399	714	620	915	1575	2000	2353	2795	14439	0.53
		Q_u	1286	941	270	201	321	775	1117	1366	1724	7656	
	CV/GS	H_p	2152	1455	734	655	940	1609	2161	2576	3077	15359	0.27
		Q_u	996	681	0	0	0	113	464	753	1149	4106	
	CV/DA	H_p	1956	1343	675	601	868	1484	1945	2340	2794	14006	0.33
		Q_u	881	725	174	48	92	351	534	842	1011	4658	

over the CV method, a glasshouse would experience a 77% increase in efficiency while a double acrylic greenhouse would see its collection efficiency be raised by 65%.

Aside from the shape and cover material, other construction parameters investigated are: roof tilt, length-to-width ratio (L:W), orientation and floor area. Each of these variables would modify the greenhouse climate to a different extent. Simulation results are presented in turn in Tables 4.7 to 4.10.

Holding the floor area constant, as the roof tilt is lowered from 33.7° to 18.4°, the glazing area is reduced by 10% and greenhouse volume gets smaller as well, hence there is slightly less heat loss. It was found that the effective transmissivity is not appreciably affected over the range of roof slopes studied. Figs. 4.3 and 4.4 illustrate this point when monthly τ_e is plotted for the shed-type and conventional glasshouses at three locations Vancouver, Edmonton and Winnipeg. For the conventional gable roof house, τ_e increases very mildly with roof tilt during the winter months, when the effect is most obvious for Edmonton, followed by Winnipeg, while Vancouver exhibits the least variation. Similar behaviour is observed for the shed. The difference in the pattern between Vancouver and the other two locations may be explained by different composition of solar radiation received at Vancouver, as demonstrated by two indices: K_T, the ratio of global horizontal radiation to extraterrestrial radiation and K_d, the ratio of diffuse to global radiation that are depicted in Table 4.11. As shown, Vancouver has the highest K_d and the lowest K_T in the winter months, indicating the domination by the diffuse component. Coupled to the fact that direct radiation interception factor has different value from the diffuse radiation view factor, a greenhouse located at Vancouver and Winnipeg therefore differs in solar radiation capture characteristics, though the two locations are at the same latitude.

Table 4.7 Effect of greenhouse roof tilt on system thermal performance

greenhouse - location: Vancouver, floor area: 200 m^2 , orientation: E-W, cover: glass
shape: SS, length-to-width ratio: 2

storage - medium: rockbed, capacity: 0.38 m^3/m^2 , air flow rate: 12.5 $L/s.m^2$

roof tilt		Sep	Oct	Nov	Dec	Jan	Feb	Mar	Apr	May	Year
33.7	s	1.00	0.63	0.33	0.21	0.25	0.44	0.61	0.84	1.00	0.54
	f	1.00	0.44	0.10	0.05	0.06	0.16	0.32	0.68	1.00	0.31
26.6	s	1.00	0.65	0.34	0.20	0.24	0.44	0.63	0.87	1.00	0.54
	f	1.00	0.47	0.09	0.04	0.06	0.15	0.34	0.70	1.00	0.32
18.4	s	1.00	0.69	0.33	0.19	0.21	0.45	0.64	0.90	1.00	0.55
	f	1.00	0.52	0.08	0.04	0.04	0.14	0.38	0.78	1.00	0.34

other cases

location	shape/cover	roof tilt	SC_r	$\dot{m}$	s	f
GPH	SS/GS	18.4	0.38	12.50	0.45	0.17
		33.7			0.44	0.15
		18.4	0.19	6.25	0.31	0.10
		33.7			0.31	0.09
VAN	CV/GS	18.4	0.38	12.50	0.44	0.21
		33.7			0.43	0.19
		18.4	0.19	6.25	0.33	0.11
		33.7			0.33	0.11

Table 4.8 Effect of greenhouse length-to-width ratio on system thermal performance

greenhouse - location: Vancouver, floor area: 200 m^2 , orientation: E-W, shape: CV, roof tilt: 26.6, cover: double acrylic

storage - medium: rockbed, capacity: 0.38 m^3/m^2 , air flow rate: 12.5 $L/s.m^2$

	L:W	Sep	Oct	Nov	Dec	Jan	Feb	Mar	Apr	May	Year
τ_e	2	0.69	0.69	0.65	0.66	0.65	0.70	0.72	0.69	0.71	0.69
	4	0.70	0.71	0.67	0.67	0.66	0.71	0.73	0.70	0.71	0.70
	8	0.70	0.70	0.66	0.67	0.66	0.70	0.73	0.70	0.70	0.69
H_p [MJ]	2	1830	1029	471	296	382	777	1444	2077	2743	11032
	4	1850	1048	486	301	388	788	1464	2107	2743	11175
	8	1850	1033	479	301	388	777	1464	2107	2704	11103
Q_{DL} [MJ]	2	274	413	470	552	592	677	736	667	526	4907
	4	275	414	471	554	594	679	739	670	531	4927
	8	295	444	505	594	636	728	791	717	569	5278
Q_{NL} [MJ]	2	366	671	1051	1224	1324	1089	873	606	374	7578
	4	367	673	1055	1229	1329	1093	876	608	377	7607
	8	393	721	1129	1317	1423	1170	938	650	403	8145
Q_L [MJ]	2	640	1084	1521	1776	1916	1766	1609	1273	900	12485
	4	642	1087	1526	1783	1923	1772	1615	1278	908	12534
	8	688	1165	1634	1911	2059	1898	1729	1367	972	13423
SLR	2	2.86	0.95	0.31	0.17	0.20	0.44	0.90	1.63	3.05	0.88
	4	2.88	0.96	0.32	0.17	0.20	0.44	0.91	1.65	3.02	0.89
	8	2.69	0.89	0.29	0.16	0.19	0.41	0.84	1.54	2.78	0.83
s	2	1.00	0.76	0.24	0.12	0.17	0.39	0.67	1.00	1.00	0.51
	4	1.00	0.84	0.27	0.14	0.20	0.41	0.70	1.00	1.00	0.53
	8	1.00	0.82	0.28	0.17	0.22	0.41	0.69	1.00	1.00	0.49
f	2	1.00	0.57	0.02	0.00	0.03	0.08	0.43	0.78	1.00	0.31
	4	1.00	0.66	0.04	0.00	0.04	0.11	0.48	0.83	1.00	0.34
	8	1.00	0.52	0.02	0.00	0.03	0.07	0.41	0.73	1.00	0.30

Table 4.9 Effect of greenhouse orientation on system thermal performance

greenhouse - location: Vancouver, floor area: 200 m^2 , cover: glass
shape: CV, length-to-width ratio: 2, roof tilt: 26.6

storage - medium: rockbed, capacity: 0.38 m^3/m^2 , air flow rate: 12.5 $L/s.m^2$

		Sep	Oct	Nov	Dec	Jan	Feb	Mar	Apr	May	Year
τ_e	E-W	0.76	0.76	0.71	0.71	0.71	0.76	0.79	0.77	0.78	0.75
	N-S	0.56	0.58	0.58	0.62	0.60	0.60	0.60	0.63	0.66	0.62
H_p [MJ]	E-W	2009	1122	514	318	418	844	1585	2318	2936	12064
	N-S	1431	856	420	278	353	666	1204	2197	2484	9939
Q_{DL}[MJ]	E-W)	593	875	1008	1163	1260	1401	1491	1349	1074	8075
	N-S)										
Q_{NL}[MJ]	E-W)	564	1087	1743	2023	2215	1796	1407	951	561	12463
	N-S)										
Q_L [MJ]	E-W)	1157	1962	2751	3187	3475	3197	2898	2300	1635	22562
	N-S)										
SLR	E-W	1.74	0.57	0.19	0.10	0.12	0.27	0.55	1.01	1.80	0.54
	N-S	1.29	0.43	0.15	0.08	0.10	0.21	0.41	0.96	1.78	0.44
s	E-W	0.88	0.54	0.28	0.18	0.20	0.34	0.52	0.71	0.92	0.44
	N-S	0.76	0.45	0.22	0.15	0.18	0.26	0.46	0.68	0.87	0.41
f	E-W	0.78	0.21	0.02	0.00	0.02	0.05	0.23	0.48	0.85	0.20
	N-S	0.62	0.15	0.01	0.00	0.00	0.02	0.13	0.42	0.80	0.16

<u>another case - location: Albuquerque</u>

E-W	s	1.00	0.95	0.64	0.47	0.45	0.53	0.67	0.86	1.00	0.64
	f	1.00	0.90	0.31	0.24	0.18	0.22	0.40	0.76	1.00	0.35
N-S	s	1.00	1.00	0.55	0.39	0.39	0.46	0.64	1.00	1.00	0.49
	f	1.00	1.00	0.19	0.10	0.11	0.14	0.32	1.00	1.00	0.30

Table 4.10 System thermal performance for various greenhouse sizes (floor area)

greenhouse - location: Vancouver, orientation: E-W, cover: glass
shape: SS, length-to-width ratio: 2, roof tilt: 26.6

storage - medium: rockbed, capacity: 0.38 m^3/m^2 , air flow rate: 12.5 $L/s.m^2$

floor area		Sep	Oct	Nov	Dec	Jan	Feb	Mar	Apr	May	Year
200 m^2	s	1.00	0.65	0.34	0.20	0.24	0.44	0.63	0.87	1.00	0.54
	f	1.00	0.47	0.09	0.04	0.06	0.15	0.34	0.70	1.00	0.32
500 m^2	s	1.00	0.63	0.28	0.17	0.19	0.39	0.58	0.83	1.00	0.51
	f	1.00	0.41	0.06	0.02	0.03	0.12	0.28	0.61	1.00	0.29
1000 m^2	s	1.00	0.61	0.23	0.14	0.16	0.33	0.51	0.76	1.00	0.49
	f	1.00	0.40	0.04	0.00	0.02	0.09	0.24	0.53	1.00	0.27

Other cases

shape/cover	area (m^2)	s	f
CV/GS	200	0.44	0.20
	500	0.41	0.18
	1000	0.37	0.17
CV/DA	200	0.51	0.31
	500	0.48	0.29
	1000	0.45	0.27

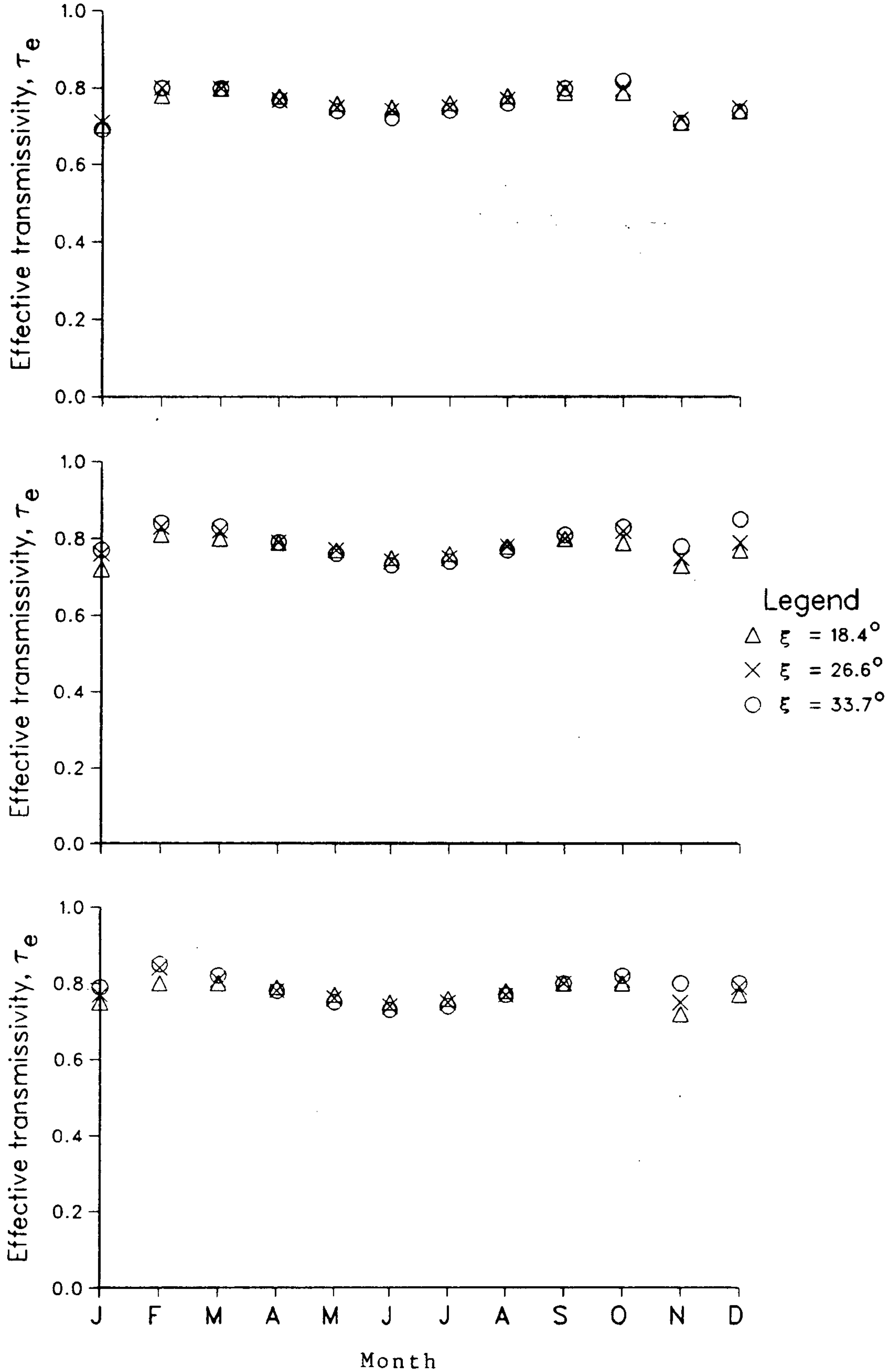

Fig. 4.3 Effective transmissivity for a shed-type glasshouse (top: VAN, middle: EDM, bottom: WNG)

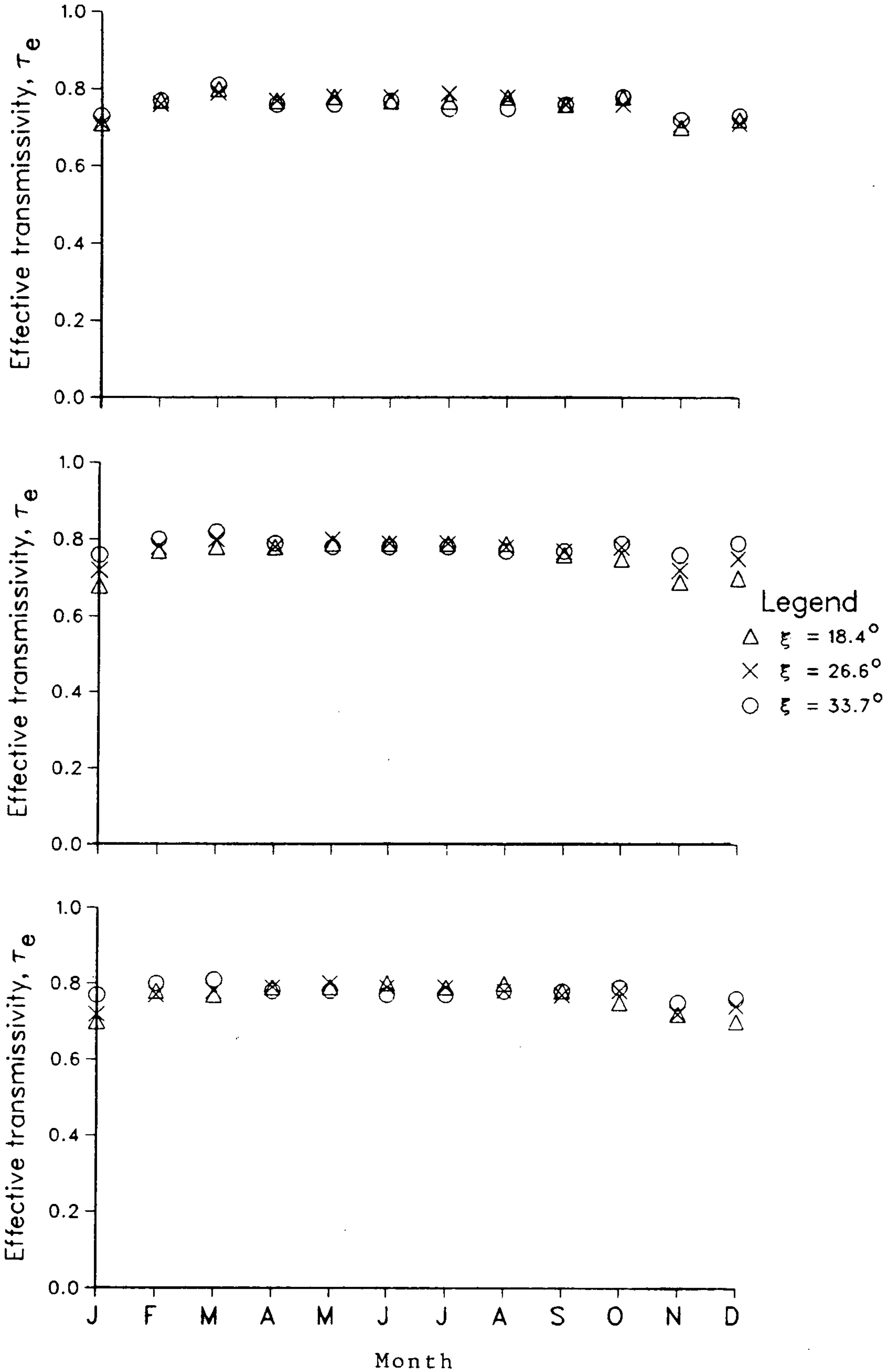

Fig. 4.4 Effective transmissivity for a conventional glasshouse (top: VAN, middle: EDM, bottom: WNG)

Table 4.11 Monthly average values of K_d and K_T

Location	Latitude °N		Feb	Apr	Jul	Oct	Dec
Edmonton	53.5	K_T	0.58	0.58	0.59	0.55	0.49
		K_d	0.39	0.39	0.38	0.42	0.47
Winnipeg	50.0	K_T	0.63	0.56	0.58	0.49	0.50
		K_d	0.34	0.41	0.39	0.47	0.47
Vancouver	49.3	K_T	0.38	0.48	0.57	0.42	0.28
		K_d	0.59	0.49	0.40	0.54	0.68
Montreal	45.5	K_T	0.50	0.49	0.52	0.43	0.37
		K_d	0.47	0.48	0.45	0.54	0.60
Guelph	43.5	K_T	0.56	0.49	0.55	0.46	0.39
		K_d	0.41	0.48	0.42	0.51	0.58
Lexington	38.0	K_T	0.41	0.48	0.52	0.51	0.37
		K_d	0.53	0.46	0.42	0.43	0.58
Albuquerque	35.1	K_T	0.66	0.71	0.70	0.70	0.63
		K_d	0.26	0.20	0.21	0.21	0.29

In terms of system thermal performance as a whole, annual solar heating fraction increases with decreasing roof slope. In fact, additional computer runs with roof tilt = 45.0° confirm that energy saving is inversely proportional to roof tilt, albeit insignificant within the range of slopes found in practice. Thus, unlike the important role of latitude-dependent collector slope in optimizing the design of flat plate solar collectors, the greenhouse geometry renders the roof tilt a minor factor in solar heating system design considerations.

Solar load ratio is essentially unchanged when L:W increases from 2 to 4, and decreases somewhat when L:W is further raised to 8, as illustrated in Table 4.8. For a 200 m^2 greenhouse, the shift in house length is from 20 m to 28 m and then 40 m, and correspondingly from 10 m to 7 m and then 5 m in width. With a high L:W ratio, the apparent advantage of relatively greater south facing glazing area is offset by the interception of less direct radiation at the gutter height level as the result of a narrower greenhouse. At the same time, heat loss increases by 8% as the L:W ratio is changed from 2 to 8. On the whole, length-to-width ratio of a greenhouse has no perceptible effect on system thermal performance for a 200 m^2 greenhouse, and it has more visible influence as the floor area expands.

Table 4.9 summarizes the difference in annual solar heating fraction attained by a greenhouse equipped with rockbed thermal storage when the structure is oriented either with its long axis lying east-west or north-south. The effective transmissivity of a greenhouse is reduced by 13% to 26% when it is moved from the E-W to N-S orientation, depending on the time of the year. The decrease in inside solar radiation is less pronounced in the winter months when diffuse radiation dominates for the Vancouver area. On the other hand, since heat loss is assumed to be independent of greenhouse orientation, the reduction in solar input is solely responsible for the 20% reduction in energy savings. For Albuquerque where direct sunlight constitutes a major part of the global solar radiation during most of the heating season, the decrease of 38% in solar heating fraction for a N-S aligned greenhouse compared to one oriented otherwise is more significant.

Lastly, greenhouse collection is studied with various floor areas. Results depicted in Table 4.10 show that it is not necessarily true for the greenhouse solar heating system to perform independently of greenhouse floor area, which might be desirable from the point of view of developing a generalized design procedure. As the floor area expands from 200 m^2 to 500 m^2 and 1000 m^2, the annual solar heating fraction is predicted to decrease from 0.32 to 0.29 and 0.27 respectively. While solar radiation transmission is unaffected by the floor area, the size of the greenhouse varies. As indicated in Table 4.1, the volume-to-floor area ratio does not stay constant with different floor areas. For the SS house, it increases from 6 to 8 when a 200 m^2 SS greenhouse is increased to 500 m^2, and a further increase to 10 occurs when the greenhouse floor area reaches 1000 m^2. The difference in house volume is expected to cause a different extent of natural ventilation, and thus affects the useful heat gain, Q_u . In fact, the collection efficiency drops from 58% to 53% when one compares the performance of a 200 m^2 house to one occupying 1000 m^2. Less difference is observed for a CV collection system. Since the shed can attain a higher inside temperature, for a given storage capacity, more ventilation is required for temperature and humidity control. With natural ventilation, the associated heat loss depends strongly on the greenhouse volume. The volume increase per unit floor area is greater in the case of a solar shed compared to the conventional greenhouse. Thus, as floor area gets larger, the efficiency of a SS system reduces more than a CV system and is reflected in the solar heating fraction.

4.2.4.2 Effect of locations

Table 4.12 presents simulation results of a SS collection system with glass cover for three locations - Vancouver, Guelph and Albuquerque that have distinctly different climatic conditions throughout the heating season from September to May. The solar radiation and outside temperature regimes of the regions represented by these locations may be classified as (low, cool), (medium, cold) and (high, cool) respectively, and their relative magnitudes are reflected by the solar load ratio. Not only is the outside solar radiation more abundant in Albuquerque, the simulated effective transmissivity for this location is also 10% higher than either Vancouver or Guelph. This is likely due to the capture of more direct sunlight; the interception factor for direct radiation is consistently higher for Albuquerque compared to the other sites. For the SS collection system, a greenhouse located at Guelph saves approximately 50% less energy than one operating at Vancouver, while the latter saves 40% less energy than Albuquerque. Results for other locations are also found in Table 4.12. It is readily seen that although the total solar contribution can exceed 0.35 in the colder regions of Canada, the annual solar heating fraction is short of 0.15. On the other hand, the solar heating fraction for Nashville is computed to be higher than that of Albuquerque, even though its characteristic solar load ratio are lower than the latter's, indicating that energy savings is not necessarily directly proportional to the solar load ratio. The nighttime temperature in September in Nashville is higher than the inside setpoint temperature, thus SLR need not be calculated for this month.

The behaviour of the solar greenhouse with a CV collection system was also studied, and results for four locations - Vancouver, Guelph, Montreal and Albuquerque are listed in Table 4.13. A reduction of the solar heating fraction ranging from 35% to 50% is realized upon comparing the thermal performance

Table 4.12 Effect of locations on system thermal performance - shed-type greenhouse

greenhouse - floor area: 200 m^2 , orientation: E-W, cover: glass
shape: SS, length-to-width ratio: 2, roof tilt: 26.6

storage - medium: rockbed, capacity: 0.38 m^3/m^2 , air flow rate: 12.5 $L/s.m^2$

	location	Sep	Oct	Nov	Dec	Jan	Feb	Mar	Apr	May	Year
τ_e	VAN	0.80	0.80	0.72	0.75	0.71	0.80	0.80	0.77	0.75	0.78
	GPH	0.79	0.79	0.77	0.74	0.81	0.81	0.80	0.76	0.73	0.77
	ALB	0.80	0.85	0.87	0.91	0.87	0.93	0.82	0.79	0.80	0.84
H_p [MJ]	VAN	2116	1180	522	336	418	888	1604	2318	3020	12402
	GPH	2208	1474	754	664	976	1693	2161	2510	2956	15306
	ALB	3552	3077	2311	1962	1937	2466	3246	4108	4688	27347
Q_{DL} [MJ]	VAN	605	892	1028	1187	1285	1430	1521	1376	1096	8409
	GPH	482	978	1735	1883	2609	2541	2504	1847	1032	12934
	ALB	22	634	1167	1579	1518	1439	1373	723	91	8546
Q_{NL} [MJ]	VAN	575	1109	1778	2064	2260	1832	1435	970	572	12984
	GPH	642	1437	2289	3564	3603	3505	2521	1456	862	20555
	ALB	0	587	1555	2180	2295	2102	1502	928	180	11329
Q_L [MJ]	VAN	1180	2001	2806	3251	3545	3262	2956	2346	1668	23015
	GPH	1124	2415	4025	5447	6212	6046	5025	3302	1894	33489
	ALB	22	1221	2722	3759	3813	3541	2875	1651	271	19875
SLR	VAN	1.79	0.59	0.19	0.10	0.12	0.27	0.54	0.99	1.81	0.54
	GPH	1.96	0.61	0.19	0.12	0.16	0.28	0.43	0.76	1.56	0.46
	ALB	161.5	2.52	0.85	0.52	0.51	0.70	1.13	2.49	15.37	1.38
s	VAN	1.00	0.65	0.34	0.20	0.24	0.44	0.63	0.87	1.00	0.52
	GPH	1.00	0.66	0.34	0.21	0.30	0.39	0.51	0.71	0.96	0.44
	ALB	1.00	1.00	0.73	0.56	0.56	0.64	0.81	0.96	1.00	0.71
f	VAN	1.00	0.47	0.09	0.04	0.06	0.15	0.34	0.70	1.00	0.32
	GPH	0.94	0.49	0.06	0.00	0.04	0.10	0.20	0.48	0.88	0.17
	ALB	1.00	1.00	0.56	0.29	0.30	0.41	0.74	0.95	1.00	0.54

Table 4.12 (continued)

Other locations

		Sep	Oct	Nov	Dec	Jan	Feb	Mar	Apr	May	Year
EDM	s	0.84	0.51	0.23	0.14	0.13	0.32	0.44	0.72	0.96	0.36
	f	0.68	0.25	0.03	0.00	0.00	0.03	0.13	0.44	0.84	0.11
	SLR	1.01	0.41	0.12	0.07	0.08	0.17	0.36	0.77	1.40	0.38
WNG	s	0.94	0.53	0.25	0.18	0.19	0.33	0.48	0.70	0.91	0.37
	f	0.82	0.30	0.03	0.00	0.00	0.04	0.13	0.42	0.74	0.10
	SLR	1.19	0.42	0.12	0.09	0.10	0.17	0.33	0.69	1.34	0.35
MTL	s	1.00	0.62	0.33	0.18	0.24	0.35	0.48	0.74	0.97	0.41
	f	0.92	0.43	0.06	0.00	0.02	0.05	0.15	0.47	0.86	0.14
	SLR	1.88	0.53	0.17	0.09	0.12	0.22	0.38	0.74	1.64	0.40
NSV	s	--	1.00	0.82	0.57	0.60	0.69	0.89	1.00	1.00	0.73
	f	--	1.00	0.77	0.38	0.40	0.52	0.84	1.00	1.00	0.58
	SLR	--	2.24	0.65	0.30	0.32	0.50	0.89	2.29	12.57	1.03

Table 4.13 Effect of locations on system thermal performance - conventional shape greenhouse

greenhouse - floor area: 200 m^2 , orientation: E-W, cover: glass
shape: CV, length-to-width ratio: 2, roof tilt: 26.6

storage - medium: rockbed, capacity: 0.38 m^3/m^2 , air flow rate: 12.5 $L/s.m^2$

		Sep	Oct	Nov	Dec	Jan	Feb	Mar	Apr	May	Year
VAN	s	0.88	0.54	0.28	0.18	0.20	0.34	0.52	0.71	0.92	0.44
	f	0.78	0.21	0.02	0.00	0.00	0.05	0.23	0.48	0.85	0.20
GPH	s	0.94	0.52	0.23	0.15	0.22	0.30	0.43	0.61	0.69	0.36
	f	0.85	0.20	0.00	0.00	0.00	0.02	0.06	0.29	0.46	0.09
YUL	s	0.91	0.50	0.22	0.13	0.15	0.25	0.39	0.60	0.75	0.33
	f	0.77	0.22	0.00	0.00	0.00	0.00	0.05	0.30	0.54	0.07
ALB	s	1.00	0.95	0.61	0.47	0.45	0.53	0.67	0.86	1.00	0.64
	f	1.00	0.90	0.31	0.24	0.18	0.22	0.40	0.76	1.00	0.35

with that of a SS collection system. Without some means to augment energy collection, the colder regions cannot save energy by more than 10% even with a relatively large rockbed storage capacity of 0.38 m^3 per m^2 greenhouse floor area.

4.2.4.3 Effect of rockbed thermal storage parameters

The dependence of system thermal performance on storage capacity (volume) is demonstrated in Table 4.14. Simulation results, expressed as the fraction of the monthly total heating load supplied by solar energy, are shown along with various heat flow quantities: Q_u , the useful heat gain; Q_{td} , the amount of heat transferred to storage during daytime; and Q_{ST} , the amount of heat subsequently recovered from storage during nighttime. Q_{ST} is the variable common to the calculation of both the monthly total solar contribution and monthly solar heating fraction.

In general, the solar heating fraction varies directly with storage capacity at any given air flow rate and the behaviour follows the law of diminishing return. For instance, f_y for a SS greenhouse located in Vancouver increases by 24% from 0.29 to 0.36 as the storage capacity is enlarged from 0.19 to 0.28 m^3 m^{-2}, whereas further expansion of the rocked volume to 0.38 m^3 m^{-2} merely leads to a change of 8% more energy savings. In early fall and late spring, excess solar heat is available for storage during most of the day. Although solar heat gain in May is more than double that in October and May is a slightly warmer month, the amount of excess solar heat available for storage is only 40% more for the May climatic conditions. Collection efficiency for the month of May is 56% compared to 75% for October. The occurence of this phenomenon in the simulation experiments is due to the seasonal variation in the leaf Bowen ratio β in accordance with the stage of plant growth. For the fall crop, Bowen ratio β is set at 2.0 in October, whereas β is assigned a value of 1.0 in May for a fully developed canopy that is transpiring more to induce less sensible heat

Table 4.14 Effect of rockbed storage capacity on system thermal performance

greenhouse - location: Vancouver, floor area: 200 m^2 , orientation: E-W, cover: glass
shape: SS, length-to-width ratio: 2, roof tilt: 26.6

storage - air flow rate: 18.75 $L/s.m^2$

storage capacity		Sep	Oct	Nov	Dec	Jan	Feb	Mar	Apr	May	Year
SC_r = 0.19	Q_u	1215	883	289	146	237	429	930	1402	1693	
	Q_{td}	710	576	198	121	193	267	539	660	662	
	Q_{ST}	575	510	155	100	141	206	517	615	572	
	s	1.00	0.66	0.35	0.18	0.25	0.45	0.59	0.71	1.00	0.53
	f	1.00	0.45	0.10	0.03	0.06	0.17	0.30	0.49	1.00	0.29
SC_r = 0.28	Q_u	1215	883	289	146	237	429	930	1402	1693	
	Q_{td}	966	697	211	122	194	363	784	1055	1087	
	Q_{ST}	575	594	182	100	143	279	726	921	572	
	s	1.00	0.77	0.36	0.19	0.25	0.49	0.67	0.86	1.00	0.60
	f	1.00	0.61	0.12	0.03	0.06	0.23	0.42	0.72	1.00	0.36
SC_r = 0.38	Q_u	1215	883	289	146	237	429	930	1402	1693	
	Q_{td}	1140	776	214	123	195	376	872	1185	1296	
	Q_{ST}	575	715	183	102	148	294	833	970	572	
	s	1.00	0.82	0.36	0.20	0.25	0.49	0.71	0.91	1.00	0.65
	f	1.00	0.72	0.12	0.04	0.06	0.24	0.49	0.78	1.00	0.39

Table 4.14 (continued)

Other cases

location	shape/cover	$\dot{m}$	SC_r	s	f
VAN	SS/GS	6.25	0.19	0.51	0.23
			0.28	0.53	0.24
			0.38	0.53	0.24
		12.50	0.19	0.49	0.27
			0.28	0.51	0.30
			0.38	0.54	0.32
	SS/DA	6.25	0.19	0.52	0.30
			0.38	0.55	0.32
		12.50	0.19	0.61	0.41
			0.38	0.66	0.44
		18.75	0.19	0.63	0.42
			0.38	0.76	0.53
	CV/DA	6.25	0.19	0.48	0.20
			0.28	0.51	0.22
			0.38	0.52	0.22
		12.50	0.19	0.44	0.23
			0.28	0.47	0.26
			0.38	0.51	0.31
GPH	SS/DA	6.25	0.19	0.47	0.20
			0.38	0.49	0.20
		12.50	0.19	0.52	0.27
			0.38	0.55	0.31
		18.75	0.19	0.54	0.29
			0.38	0.60	0.38

exchange with greenhouse air, thus useful heat gain is reduced. In some months, the quantity of heat transferred to storage during charging can be less than 50% of the useful heat gain if the storage capacity is relatively small. A portion of the latent heat could be reclaimed if condensation takes place in the rockbed. The bed temperature however may increase to a value higher than the dew-point temperature of the incoming air, consequently, excess greenhouse moisture still needs to be removed via ventilation. For the months of September and May, nighttime heat demand is less than 600 MJ per night, and in theory can be met entirely by the heat retrieved from storage.

On the other hand, in the winter, excess solar heat is only available for a fraction of the daytime hours. Under such circumstances, greenhouse collection becomes limiting and enlargement of the storage volume does not induce any improvement in energy savings. It should be noted that the amount of heat retrieved from storage during discharging may well exceed the nighttime requirement in September and May for the Vancouver climate. In calculating the monthly solar fractions, though, Q_{ST} is set equal to Q_{NL} when this situation arises so as to suppress the impossibility of f-values being greater than unity. In practice, then, this manipulation is equivalent to invoking additional venting of daytime surplus solar heat. This partly confirms the findings of Ben-Abdallah (1983) that excess solar heat accumulated inside the shed-type glasshouse can indeed supply more than its own heating demand. Nevertheless, this is only true for a short period within the heating season. Hence, in September and May when nighttime heating load is small, a large storage is bound to be wasteful. The merits of larger storage capacity lie mainly in the months of October and February through April. The rockbed storage is not designed for long-term energy storage, and collection of excessive energy would affect the subsequent thermal performance of the rockbed itself, and has to be avoided by means of appropriate computer control algorithm. In other words, dumping of excess heat is necessary so that the bed would not be cooled prematurely during the daytime.

Results of simulation runs that incorporate variation in storage capacity for other cases are also summarized in Table 4.14. When the air flow rate is relatively low (6.25 L s^{-1} m^{-2} or equivalent to 1.5 kg s^{-1} for A_f = 200 m^2), the meritorious collection potentials possessed by a SS collection system or twin-walled acrylic cover material cannot be fully utilized; solar heating fraction is found to be quite independent of storage capacity and only 5% increase in f_y may be realized for a change of SC_r from 0.19 to 0.38 m^3 m^{-2}. Increasing the air flow rate to 12.5 and 18.75 L s^{-1} m^{-2} would see this percentage increase in f_y raised to an average of 14% and 31% respectively for three different collection methods and two locations. These average values can be expected to be reasonably valid for other situations unless the collection system becomes the limiting factor.

How air flow rate affects system thermal performance can be inferred from the energy flows tabulated in Table 4.15 for a double acrylic shed-type greenhouse located at Guelph. Together with condensed results pertinent to other cases that are presented in the same table, it can be deduced that for the SS and CV methods of collection, average percentage change of annual solar heating fraction amounts to a 36% increase as flow rate is tripled from 6.25 to 18.75 L s^{-1} m^{-2}, for a fixed storage capacity of 0.19 m^3 m^{-2}. The increase in f_y jumps to 76% if a larger storage of 0.38 m^3 m^{-2} is in place. The number of runs for the Brace-style greenhouse is limited, but a consistent pattern is observed, in Vancouver and Montreal alike.

The interaction of storage capacity and air flow rate may be elaborated in greater detail. With respect to heat exchange, a lower NTU value means

Table 4.15 Effect of rockbed air flow rate on system thermal performance

greenhouse - location: Guelph, floor area: 200 m^2 , orientation: E-W, cover: double acrylic
shape: SS, length-to-width ratio: 2, roof tilt: 26.6

storage - capacity: 0.38 m^3/m^2

air flow rate		Sep	Oct	Nov	Dec	Jan	Feb	Mar	Apr	May	Year
$\dot{m}$ = 6.25	Q_u	1286	941	270	201	321	775	1117	1366	1724	
	Q_{td}	583	391	101	67	126	208	295	418	663	
	Q_{ST}	424	268	82	45	89	167	242	373	562	
	s	1.00	0.59	0.32	0.22	0.28	0.38	0.48	0.64	0.96	0.49
	f	1.00	0.39	0.06	0.02	0.04	0.09	0.17	0.38	0.93	0.20
$\dot{m}$ = 12.50	Q_u	1286	941	270	201	321	775	1117	1366	1724	
	Q_{td}	942	653	182	118	193	386	541	829	1101	
	Q_{ST}	424	539	151	82	159	357	493	736	592	
	s	1.00	0.85	0.36	0.23	0.31	0.44	0.58	0.86	1.00	0.55
	f	1.00	0.77	0.11	0.04	0.07	0.18	0.33	0.75	1.00	0.31
$\dot{m}$ = 18.75	Q_u	1286	941	270	201	321	775	1117	1366	1724	
	Q_{td}	1137	836	243	144	290	582	837	1110	1262	
	Q_{ST}	424	747	209	115	240	531	742	966	592	
	s	1.00	1.00	0.40	0.25	0.34	0.50	0.68	1.00	1.00	0.60
	f	1.00	1.00	0.16	0.06	0.11	0.27	0.48	1.00	1.00	0.40

Table 4.15 (continued)

Other cases

location	shape/cover	SC_r	$\dot{m}$	s	f
VAN	SS/GS	0.19	6.25	0.51	0.23
			12.50	0.54	0.27
			18.75	0.53	0.29
	SS/GS	0.38	6.25	0.53	0.24
			12.50	0.59	0.32
			18.75	0.60	0.39
	SS/DA	0.38	6.25	0.57	0.32
			12.50	0.66	0.44
			18.75	0.76	0.52
	BS/GS	0.38	6.25	0.39	0.15
			12.50	0.46	0.24
			18.75	0.51	0.32
	CV/DA	0.19	6.25	0.48	0.20
			12.50	0.54	0.23
			18.75	0.58	0.25
		0.38	6.25	0.42	0.22
			12.50	0.51	0.31
			18.75	0.59	0.38
GPH	SS/DA	0.19	6.25	0.47	0.20
			12.50	0.52	0.27
			18.75	0.54	0.30
MTL	BS/GS	0.38	6.25	0.29	0.08
			12.50	0.35	0.12
			18.75	0.39	0.17

more uniform distribution of heat transfer through the entire rockbed, whereas a high NTU value leads to more effective transfer in the anterior portion. Thus, the temperature rise of the bed near the air exit passage is more for the former case, which implies less temperature drop takes place between inlet and outlet. Now, as air flow rate increases, NTU decreases asymtotically, and the temperature drop diminishes more. Hence the increase in the amount of heat transferred to the storage dampens with flow rate upsurge. However, when more storage volume is used, the number of heat transfer units is sufficiently large to sustain a temperature drop that varies little with increasing flow rate. Consequently, energy savings increase more linearly with air flow rate.

4.2.4.4 Effect of soil thermal storage parameters

The volume of a soil thermal storage medium is indefinite and thus the effect of storage capacity has been investigated indirectly via the pipe heat exchange system and the soil type and its moisture content. Table 4.16 contains the simulation results that indicate how system behaviour varies with r_s , the ratio of total pipe wall area to greenhouse floor area. Again, heat flow quantities are included in the table along with annual performance indices for a typical case of a CV glasshouse located at Vancouver, followed by results of other cases. For the entire heating season, the amount of excess solar energy made available for storage adds up to 4325 MJ per day in a month, or 55% of what a SS collection system can accumulate. In December and January, virtually no energy saving can be expected. These long-term average estimations of system performance are more conservative than the observed experimental values, partly because there were few plants in the research greenhouse equipped with soil thermal storage.

The system configuration that is compatible with the research greenhouse unit is one of D = 0.10 m, $\dot{m}$ = 6.25 L s^{-1} m^{-2}, and r_s = 1.0. The

Table 4.16 Effect of pipe wall area-to-greenhouse floor area ratio on system thermal performance

greenhouse - location: Vancouver, floor area: 200 m^2, orientation: E-W, cover: glass
shape: CV, length-to-width ratio: 2, roof tilt: 26.6

storage - medium: clay soil, θ_s = 30%, air flow rate: 6.25 L/s.m^2, pipe diameter: 0.15 m

		Sep	Oct	Nov	Dec	Jan	Feb	Mar	Apr	May	Year
r_s = 0.5	Q_u	804	514	113	0	0	144	485	835	1028	
	Q_{td}	536	302	49	0	0	97	288	546	561	
	Q_{ST}	343	176	26	0	0	66	169	339	415	
	s	0.66	0.42	0.23	0.18	0.21	0.30	0.46	0.61	0.68	0.33
	f	0.54	0.16	0.00	0.00	0.00	0.02	0.11	0.29	0.57	0.09
r_s = 1.0	Q_u	804	514	113	0	0	144	485	835	1028	
	Q_{td}	518	315	57	0	0	99	281	529	530	
	Q_{ST}	352	182	28	0	0	67	180	365	443	
	f	0.70	0.42	0.25	0.18	0.22	0.30	0.46	0.62	0.71	0.34
	f	0.59	0.16	0.01	0.00	0.02	0.02	0.12	0.31	0.60	0.09
r_s = 1.5	Q_u	804	514	113	0	0	144	485	835	1028	
	Q_{td}	571	328	76	0	0	101	300	561	588	
	Q_{ST}	383	207	31	0	0	85	186	376	477	
	s	0.71	0.43	0.25	0.18	0.22	0.31	0.46	0.63	0.73	0.35
	f	0.62	0.17	0.01	0.00	0.02	0.03	0.12	0.32	0.63	0.10

Table 4.16 (continued)

Other cases

location	shape/cover	D	$\dot{m}$	r_s	s	f	NTU_p
VAN	CV/GS	0.10	6.25	0.5	0.32	0.10	1.35
				1.0	0.35	0.13	1.83
				1.5	0.36	0.14	2.12
			18.75	0.5	0.33	0.11	0.75
				1.0	0.36	0.14	1.14
				1.5	0.38	0.17	1.40
		0.15	6.25	0.5	0.34	0.09	1.04
				1.0	0.34	0.09	1.31
				1.5	0.35	0.10	1.48
			18.75	0.5	0.35	0.10	0.63
				1.0	0.36	0.11	0.88
				1.5	0.37	0.13	1.04
	CV/DA	0.10	6.25	0.5	0.33	0.19	
				1.0	0.43	0.23	
				1.5	0.50	0.25	
	SS/GS	0.10	18.75	1.0	0.49	0.24	
				1.5	0.54	0.31	
		0.15	6.25	1.0	0.42	0.17	
				1.5	0.43	0.18	
GPH	SS/GS	0.10	18.75	1.0	0.41	0.12	
				1.5	0.44	0.15	
ALB	SS/GS	0.10	18.75	1.0	0.63	0.41	
				1.5	0.72	0.56	

predicted annual solar heating fraction is 0.12, as compared to the 20% energy saving achieved with the experimental set-up in the 1983/1984 heating season. Like the case of the research shed-type greenhouse unit, the microcomputer control that was fine-tuned to monitor the energy flows should be partially credited with the improvement in system thermal performance. The simulation method used in this study cannot effectively duplicate the corrective measures taken by the microcomputer to achieve the desired greenhouse climate. Therefore the present estimates of long-term average system performance tends to be conservative.

Different combinations of pipe diameter, total flow rate and pipe wall to greenhouse floor area ratio would lead to different values of NTU_p, the number of heat transfer units for each individual pipe, defined as $U_p A_w / \dot{m}C$. An examination of the variation of NTU_p with r_s revealed that for a given greenhouse floor area and a fixed pipe diameter D, NTU_p increases with increasing r_s. As a result of the installation of more pipes the air flow rate in each pipe gets smaller, and the heat transfer coefficient from the pipe air to the pipe/soil interface is reduced. However, the decrease in U_p is more than balanced by the decrease in air flow rate. The increase in NTU_p together with the fact that more pipes are present eventually bring about an increase in the annual solar heating fraction. As r_s increases further, NTU_p shows less increment and a diminishing effect is seen in the energy savings. The algorithm used in this study gives the maximum pipe spacing for a confined floor area, and given values of r_s and D. Computer runs with a fixed number of pipes, but varying pipe spacings indicated that system thermal performance is not significantly affected as long as a S_p/D ratio of at least six is maintained. This low value can be attributed to the fact that the temperature gradient within the soil mass is not large enough to cause appreciable interaction between pipes. In other words, the influence of each pipe does not extend beyond three pipe diameters.

Furthermore, it is noted that for the case of fixed heat exchange surface area and fixed total air flow rate, the adoption of a pipe network with larger pipe diameter means less pipes are required. As a result, NTU_p simply gets smaller and exert an opposite effect on energy savings.

In order to compare the soil thermal storage with the rockbed thermal storage, simulation runs were carried out for solar heating systems that couple the SS collection method to either storage medium. For the location at Vancouver, it is found that a design configuration of $D = 0.10$ m, $r_s = 1.0$ and $\dot{m} = 18.75$ L s^{-1} m^{-2} chosen for the pipe heat exchange system would produce an annual solar heating fraction of 0.24 which can be matched by a rockbed storage with $SC_r = 0.28$ m^3 m^{-2} and $\dot{m} = 6.25$ L s^{-1} m^{-2}.

Table 4.17 shows the computed results based on inputs that involve two air flow rates, $\dot{m} = 6.25$ and 18.75 L s^{-1} m^{-2}. Computer runs carried out separately with a total flow rate of 12.50 L s^{-1} m^{-2} have shown that f_y has negligible increase over a flow rate of 6.25 L s^{-1} m^{-2}, especially when r_s is small. The average percentage change in annual solar heating fraction due to increasing flow rate is +10%, +17% and +26% respectively for values of r_s equal to 0.5, 1.0 and 1.5. From the same table, one can detect an interesting similarity in the trend of annual solar heating fraction and total heat transfer coefficient $U_t = U_p \times N_p$. For a given r_s , f_y is directly proportional to U_t , and upon ranking this coefficient in descending order, the effect of the combination of pipe diameter and total air flow rate becomes visible. A system with smaller pipe diameter coupled with higher air flow rate consistently performs better than one with larger pipe diameter and lower flow rate; as r_s increases, the difference in performance also magnifies.

Table 4.17 Effect of pipe air flow rate on system thermal performance

greenhouse - location: Vancouver, floor area: 200 m^2 , orientation: E-W
shape: CV, length-to-width ratio: 2, roof tilt: 26.6, cover: double acrylic

storage - medium: clay soil, θ_s = 30%, pipe diameter: 0.10 m,
pipe wall/greenhouse floor area ratio: 1.5

air flow rate		Sep	Oct	Nov	Dec	Jan	Feb	Mar	Apr	May	Year
$\dot{m}$ = 6.25	s	1.00	0.58	0.23	0.18	0.20	0.32	0.53	0.73	1.00	0.50
	f	1.00	0.35	0.00	0.00	0.00	0.04	0.26	0.57	1.00	0.25
$\dot{m}$ = 12.50	s	1.00	0.63	0.24	0.18	0.21	0.35	0.58	0.84	1.00	0.52
	f	1.00	0.42	0.00	0.00	0.00	0.06	0.32	0.72	1.00	0.28
$\dot{m}$ = 18.75	s	1.00	0.66	0.26	0.19	0.22	0.40	0.61	0.86	1.00	0.53
	f	1.00	0.45	0.01	0.00	0.01	0.07	0.36	0.80	1.00	0.30

Other cases

Shape/cover	r_s	D	$\dot{m}$	s	f	$U_t = U_p * N_p$
CV/GS	0.5	0.10	18.75	0.34	0.11	532
			6.25	0.32	0.10	333
		0.15	18.75	0.35	0.10	305
			6.25	0.33	0.09	168
	1.0	0.10	18.75	0.37	0.15	819
			6.25	0.36	0.13	438
		0.15	18.75	0.36	0.11	416
			6.25	0.34	0.09	208
	1.5	0.10	18.75	0.38	0.17	1003
			6.25	0.36	0.14	506
		0.15	18.75	0.37	0.13	492
			6.25	0.35	0.10	234
CV/DA	1.0	0.10	18.75	0.34	0.26	
			6.25	0.29	0.23	

In designing a pipe heat exchange system for a greenhouse of known floor area, consider the case of obtaining greater solar heating fraction by increasing the total pipe wall area. Apparently, this may be accomplished in two ways: using larger pipes while keeping the number of pipes constant, or installing more pipes but retaining the original diameter. Both approaches introduce the same additional area of pipes. Consider for the moment the case of a CV house located in Vancouver. From Table 4.17, by comparing the thermal performance of the various scenarios with the same air flow rate: (r_s = 1.0, D = 0.10, N_p = 30) with (r_s = 1.5, D = 0.15, N_p = 30) and (r_s = 1.5, D = 0.10, N_p = 46), the first approach is seen to cause a decrease in f_y and thus destroy our purpose. While this phenomenon implies that it would be more effective to increase the number of pipes than their diameter, a larger pressure drop associated with smaller pipes needs to be considered upon sizing for the solar fan.

Lastly, we examine the effect of soil type and its moisture content on energy savings. Results of simulation runs are entered in Table 4.18. Although a limited number of runs was carried out, these results suggested that system performance is not significantly affected by either parameter. In fact, even when the volumetric moisture content θ_w is raised to a fictitious value of 80% as compared to the usual saturation value of 40% for clay and sand, still no significant difference can be visualized. These results are not surprising because the thermal diffusivity of soil does not change significantly with moisture content, as indicated in Table 4.19. In the model, both the soil heat capacity C_s and thermal conductivity k_s are linear functions of moisture content; the increase in C_s with θ_w is slightly more than that of k_s. The preference of a clay soil medium over sand is due to the former's moisture holding capability, which is advantageous in keeping the soil wet from time to time.

Table 4.18 Effect of soil type/moisture content on system thermal performance

greenhouse - location: Vancouver, floor area: 200 m^2 , orientation: E-W, cover: glass
shape: CV, length-to-width ratio: 2, roof tilt: 26.6

storage - air flow rate: 18.75 $L/s.m^2$, pipe diameter: 0.10 m,
pipe wall/greenhouse floor area ratio: 1.5

soil type/ moisture content		Sep	Oct	Nov	Dec	Jan	Feb	Mar	Apr	May	Year
clay 20%	s	0.82	0.52	0.25	0.18	0.20	0.32	0.50	0.79	0.83	0.38
	f	0.70	0.23	0.01	0.00	0.00	0.04	0.19	0,54	0.71	0.16
sand 20%	s	0.89	0.54	0.25	0.18	0.20	0.33	0.53	0.82	0.92	0.40
	f	0.77	0.30	0.01	0.00	0.00	0.05	0.23	0.61	0.83	0.19

Other cases

Shape/cover	D	$\dot{m}$	r_s	type	θ_s	s	f
CV/GS	0.10	18.75	1.5	clay	20%	0.38	0.16
					30%	0.38	0.17
					40%	0.39	0.19
				sand	20%	0.39	0.19
					40%	0.40	0.21
CV/DA	0.15	6.25	1.0	clay	20%	0.34	0.17
					30%	0.35	0.18
					40%	0.36	0.19
				sand	20%	0.34	0.18
					40%	0.36	0.20

Table 4.19 Thermal properties of clay and sand

soil type	volumetric moisture content	thermal conductivity	thermal capacity	thermal diffusivity
		$W\ m^{-1}\ C^{-1}$	$MJ\ m^{-3}\ C^{-1}$	$m^2\ s^{-1}$
clay	20%	1.20	2.20	0.56
clay	40%	1.60	3.00	0.54
sand	20%	1.73	2.20	0.80
sand	40%	2.39	3.00	0.80

4.3 Sensitivity Analysis

The mathematical models contain some factors that have not been experimentally determined in detail or variables that may be calculated by different methods. This section is devoted to test the influence of these uncertainties on the system performance at large.

For the greenhouse thermal environment model, sensitivity is tested upon the following:

1. number of air changes per hour, N
2. Bowen ratio, β
3. shading factor due to structural members, f_{sh}
4. solar radiation as driving force

The rockbed storage model has been used by many researchers and the level of uncertainty of the variables involved is the least in the overall modeling process. A sensitivity test was made of the initial rockbed temperature. The same test was applied to the soil storage model, the variables of which have also been widely evaluated by many researchers.

Results of the model sensitivity testing are listed in Tables 4.20 to 4.22.

With the method of natural ventilation, it is not always possible to keep the number of air changes per hour, N, at a desirable value that is associated with the extent of vent openings. If its maximum value should differ from 10 h^{-1} as used in the parametric study, the amount of useful heat gain will be affected. For a greenhouse located at Vancouver, the annual solar heating fraction, f_y would fall by 20% if N_{max} is 20 h^{-1}. The percentage reduction in energy savings is larger for a colder region such as Guelph and may be up to 50%.

For the case of N_{max} = 10, as Bowen ratio β is altered from a 4–3–2–1 pattern to a 4–2.5–1.5–1 pattern, f_y decreases by 7% from 0.27 to 0.25, and by 17% from 0.29 to 0.24 respectively for a SS/GS system in Vancouver and a SS/DA system

Table 4.20 Sensitivity test results - ventilation rate, leaf Bowen ratio and shading factor

greenhouse - floor area: 200 m^2 , orientation: E-W, cover: glass
length-to-width ratio: 2, roof tilt: 26.6

storage - medium: rockbed, capacity: 0.38 m^3/m^2 , air flow rate: 12.5 $L/s.m^2$

location	cover/ shape	maximum number of air changes per hour	Bowen ratio	shading factor	s	f
VAN	SS/GS	20	A	0.85	0.35	0.17
		20	A	0.90	0.37	0.18
		20	A	0.95	0.38	0.19
		15	A	0.85	0.42	0.21
		10	A	0.85	0.50	0.27
		20	B	0.85	0.34	0.16
		15	B	0.85	0.33	0.20
		10	B	0.85	0.49	0.25
		20	C	0.85	0.32	0.14
		15	C	0.85	0.35	0.19
		10	C	0.85	0.40	0.24
GPH	SS/DA	20	A	0.85	0.28	0.16
		15	A	0.85	0.37	0.22
		10	A	0.85	0.50	0.29
		20	B	0.85	0.25	0.15
		15	B	0.85	0.32	0.18
		10	B	0.85	0.44	0.24

Table 4.21 Sensitivity test results - initial thermal storage temperatures

initial rockbed temperature [°C]	s	f
12.5	0.515	0.282
10.0	0.516	0.283

	initial soil temperature [°C]	s	f
clay, θ_s = 30%	12.0	0.53	0.30
	16.0		
	18.0	0.52	0.29
sand, θ_s = 30%	12.0	0.55	0.33
	16.0		
	18.0	0.53	0.31

Table 4.22 Sensitivity test results - solar radiation processing algorithm

greenhouse - location: Montreal, floor area: 200 m^2, orientation: E-W, cover: glass
length-to-width ratio: 2, roof tilt: 26.6

storage - medium: rockbed, capacity: 0.38 m^3/m^2, air flow rate: 12.5 $L/s.m^2$

	Sep	Oct	Nov	Dec	Jan	Feb	Mar	Apr	May	Year
$H_p/H\ (\tau_e)$	0.79	0.79	0.78	0.75	0.77	0.83	0.81	0.77	0.73	
	0.77	0.77	0.77	0.76	0.78	0.84	0.79	0.75	0.72	
	0.76	0.78	0.79	0.76	0.77	0.82	0.78	0.75	0.73	
H_q/H	0.72	0.85	1.00	1.13	1.14	0.91	0.79	0.61	0.49	
	0.70	0.82	0.99	1.14	1.13	0.92	0.77	0.61	0.50	
	0.70	0.83	1.02	1.14	1.11	0.89	0.76	0.61	0.50	
f	0.92	0.43	0.06	0.00	0.02	0.05	0.15	0.47	0.86	0.14
	0.89	0.43	0.06	0.00	0.02	0.06	0.14	0.45	0.87	0.13
	0.87	0.45	0.08	0.00	0.00	0.05	0.13	0.42	0.81	0.12

in Guelph. An even lower Bowen ratio throughout the growing season (3.5–2.5–1.5–0.5 pattern) practically does not affect the solar heating fraction any further.

The testing on model sensitivity to shading factor, f_{sh} , due to the structural components of the greenhouse framework shows that the percentage variation in solar heating fraction is directly proportional to the change in the value of f_{sh} . About 10% less energy savings would occur if it is a 15% shading in lieu of 5%. Less shading is actually possible with acrylic cover which requires less structural members provided that the greenhouse is located in places like Vancouver with nominal snow-cover in winter.

As for the thermal storage, results indicate that the overall model is not sensitive to initial rockbed temperature, and mildly sensitive to initial soil temperatures. Hence, the lack of soil temperature data for the U.S. locations is not expected to generate unreasonable simulation results for sites such as Albuquerque and Nashville.

Lastly, the model is tested on its sensitivity to the variation of hourly solar energy input due to different processing algorithms as presented in section 4.1.1. Results for Montreal, where records of global and diffuse solar radiations and the number of bright sunshine hours are all available, are presented in Table 4.22. Not only is the greenhouse effective transmissivity relatively unaffected by the method of solar radiation processing, but also its effect on the annual solar heating fraction is negligible. The simulation method used in this study can therefore provide reasonable estimates of the energy savings for locations where solar energy data are less complete than Montreal, in which case solar radiation processing requires more correlations other than direct computation.

4.4 Crop Canopy Photosynthesis

Various crop growth mathematical models have been reviewed in Chapter 2. Modeling of various processes involved in plant growth and eventually the final marketable yield requires a combination of mechanistic and empirical models, and thus a good deal of experimental data for curve fitting purpose. Photosynthesis provides the driving force for most of these processes, and net photosynthetic rate may be regarded as an index of primary production. The present study does not incoporate experiments for generating measured data of the variables that are needed in plant growth analysis. However, it is felt that a growth function may be developed to quantify plant response under different aerial environment in greenhouses as affected by the engineering parameters considered in the last section.

4.4.1 The simulation method

The model presented by Acock el al. (1978) is based on fitting a net photosynthesis function (eqn. 2.27) to experimental data collected at the Glasshouse Crops Research Institute, Littlehampton, U.K. Measurements of net canopy photosynthesis were taken from noon to dusk for the tomato plants, *Lycopersicon esculentum* Mill. (cv. Kingley Cross) that were placed in a controlled-environment cabinet. Air temperature was maintained at 20 $^{\circ}$C, the CO_2 concentration at 400 ppm and the vapor pressure deficit at 0.7 kPa.

The operation of a solar greenhouse alters the greenhouse temperature and moisture regimes. Though it is known that temperature exerts less influence on net photosynthesis compared to light and CO_2, the growth function shall account for temperature's role in plant response. Variation in the greenhouse relative humidity results in varying degrees of vapor pressure deficit, and thus the leaf conductance, ζ, to CO_2 transfer. However, the lack of specific experimental data results in the assumption that ζ is independent of greenhouse relative humidity. Another assumption made here is that for a given set of light and CO_2 conditions, gross photosynthesis (deducting photorespiration), P_g, is constant beyond a certain temperature that yields maximum P_g, as more dissolved oxygen is present to induce more photorespiration so as to cancel the stimulating effect of temperature on gross photosynthesis. Based on the literature review, the temperature at this point is taken as 26 °C, and the temperature-correction factor, F, is assumed to have the following value, which is light-dependent:

$$
\begin{array}{ll}
F = 1.00 & \text{PAR} < 125Wm^{-2} \\
F = 1.25 - 0.007(T_p - 26)^2 & \text{PAR} > 125Wm^{-2} \\
F = 1.25 & \text{PAR} > 125Wm^{-2} \text{ and } T_p > 26^{\circ}\text{C}
\end{array} \qquad (4.18)
$$

These expressions do not imply that PAR = 125 W m^{-2} is the light saturation level for tomatoes. It is chosen to encompass the situation when temperature has a mild effect on P_g under medium light intensities.

Together with an expression for canopy dark respiration, which combines eqn. 2.28 (Enoch and Hurd, 1977) and eqn. 2.29 (Charles-Edwards, 1981), the mathematical model used for canopy net photosynthesis is given by

$$
P_n = F\frac{\varsigma C}{K_p}\ln\left(\frac{\alpha K_p \text{PAR}_p + (1-\tau_p)\varsigma C}{\alpha K_p \text{PAR}_p \exp(-K_p L_i) + (1-\tau_p)\varsigma C}\right) - \frac{R_{do}}{K_p}[(1-\exp(-K_p L_i)]2^{(T_p-20)/10} \qquad (4.19)
$$

At 20 °C, F has a value of 1.00 regardless of light level, and $2^{(T - 20)/10}$ = 1.00, so that with the right parameters, P_n should have values that match the results obtained by Acock et al. (1978) who carried out experiments under this condition. It shall be noted that the leaf temperature is assumed to be equal to air temperature in their experiments. The parameters α, ς and K vary with L_i, and are listed in Table 4.23 along with the estimated L_i values over the two crop growing seasons. For the

Table 4.23 Crop canopy photosynthesis model parameters

	Sep	Oct	Nov	Dec	Jan	Feb	Mar	Apr
K_p	0.52	0.53	0.56	0.60	0.63	0.60	0.55	0.52
L_i	8.6	7.6	5.8	3.4	2.0	3.4	6.6	8.6
α	1.6	1.5	1.2	1.6	2.1	1.6	1.4	1.6
ζ	9.6	9.1	11.5	10.3	9.1	10.3	10.5	9.6

fall crop, plants are seeded in May/June, and a sizeable crop canopy is established by September; leaf area is assumed to decrease thereafter till December. The spring crop usually starts in November/December (later seeding if fuel price is high), and leaf area index is assumed to have reached its peak value in April. In the simulation, PAR is taken as a constant percentage (45%) of broadband (total) solar radiation.

The engineering parameters considered in the simulation study of crop performance are mainly concerned with the greenhouse solar collection method – shape, cover material and absorption means. Computer runs were carried out for the locations of Vancouver and Guelph. The computer modeling does not include the prediction of the time history of the CO_2 level within the greenhouse enclosure; rather, at the simulation stage, net photosynthesis as affected by five ambient CO_2 concentrations (210, 240, 270, 300 and 330 ppm) were calculated.

4.4.2 Results and discussion

Prior to using the average climatic conditions as inputs to the computer program, the combined effect of light and CO_2 only on net photosynthesis is evaluated by subjecting eqn. 2.27 to preliminary computer runs. Fig. 4.5 shows the variation of canopy net photosynthetic rate at 20 $^\circ C$ with PAR above the plant canopy, and CO_2 is the additional parameter. As CO_2 decreases from 330 to 240 ppm, P_n is reduced by 9.5%, 11% and 13% respectively for PAR fluxes of 90, 150 and 240 W m^{-2}. The calculated percentage decrease is less pronounced than that reported by Bauerle and Short (1984) who found it to range from 22% to 35% for a single physiologically mature tomato (cv. MR-13) leaf.

The computation is then extended to examine the effect of temperature using eqn. 4.19, and calculated results for two leaf area indices are illustrated in Figs. 4.6 and 4.7. At low PAR levels such as 90 W m^{-2}, P_g is unaffected by the range of temperatures considered, whereas R_d increases with temperature, thus P_n is noticed to

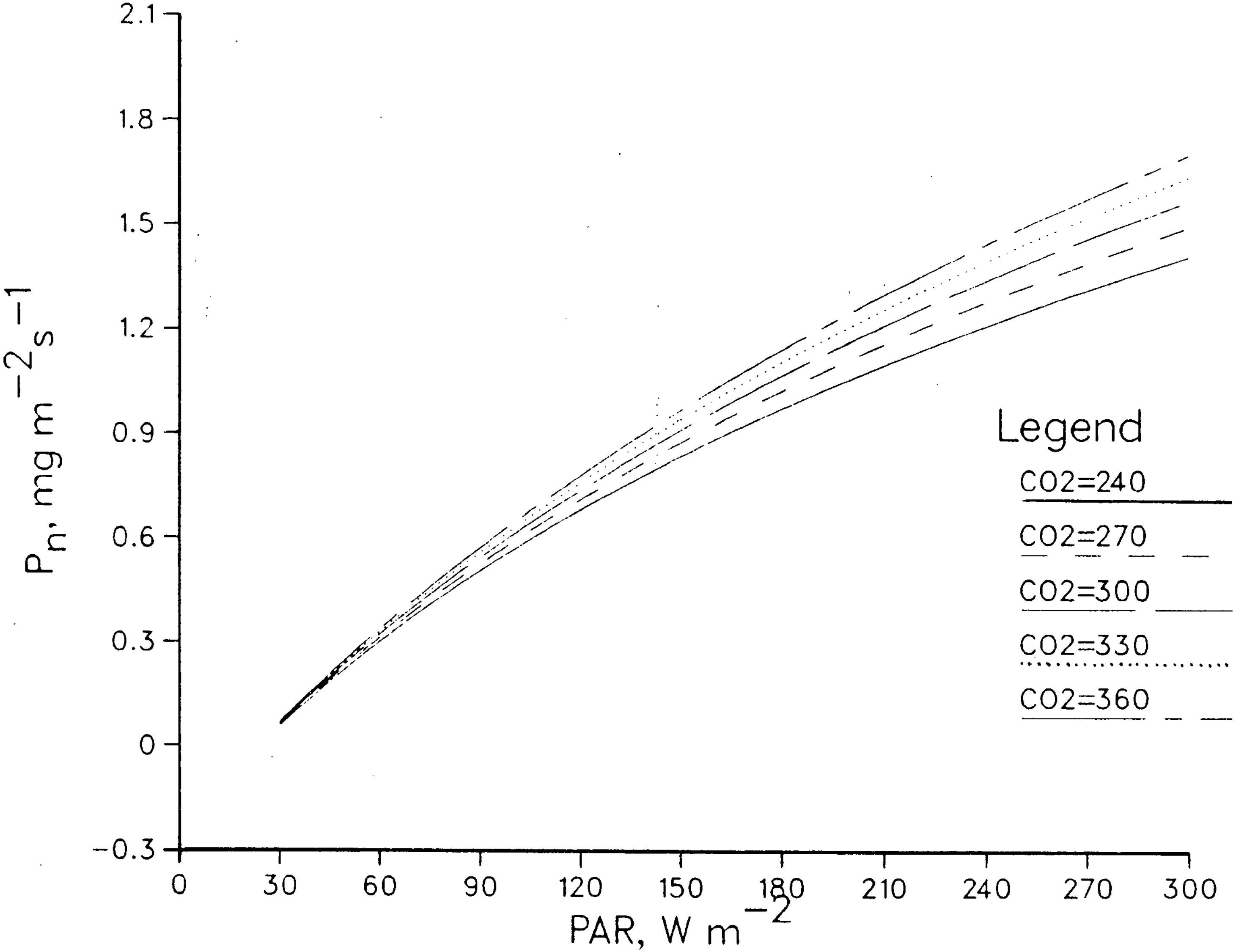

Fig. 4.5 Variation of net canopy photosynthesis with PAR and CO_2

decrease monotonically with rise in temperature. As light level increases, P_n reaches a maximum at 26 °C, falling off to about 20% less at 20 °C. Temperature exceeding 26 °C also causes less net CO_2 uptake, but to a less extent. Light intensity has a smaller influence on P_n for a relatively young plant. Comparison of Figs. 4.6 and 4.7 reveals that at low light levels, net photosynthetic rate differs less markedly between a young crop and one with a fully developed canopy. The difference becomes more obvious as PAR increases.

The crop net photosynthesis function as represented by eqn. 4.19 is then incorporated as a subroutine in the overall computer program previously used for predicting the thermal performance of the solar heating system. For each month, mean hourly results are summed up to give mean daily values of P_n (g m^{-2} d^{-1}) and subsequently total value for each growing period (kg m^{-2} $period^{-1}$). Tables 4.24 and 4.25 separately present these results for the Vancouver region and Guelph region. In each case, five solar greenhouse collection systems are studied.

For the fall period in Vancouver, P_n has a remarkable drop from 29.56 g m^{-2} d^{-1} in September to 12.56 g m^{-2} d^{-1} in October as the corresponding leaf area index changes from 8.6 to 7.6, and mean daily outside solar radiations are 13.40 MJ m^{-2} and 7.56 MJ m^{-2}. The original model (eqn. 2.27) fitted to the experimental data by Acock et al. (1978) gives P_n values that are boosted by at most 10% as L_i is increased from 5.2 to 8.6. Charles-Edwards (1981) and Ludwig et al. (1965) noted that canopy net photosynthesis (or crop metabolic rate activity) decreased appreciably only when the leaf area index was reduced below 3. The large decrease in P_n may therefore be attributed primarily to the reduction in outdoor light intensity, which in fact is the most important factor affecting photosynthesis. Fig. 4.8 sketches the mean hourly inside PAR flux density profile for the months of September through May, while the mean hourly net photosynthetic rate is depicted in Fig. 4.9. It is obvious that the trend of P_n follows that of PAR very closely. Hourly values of the

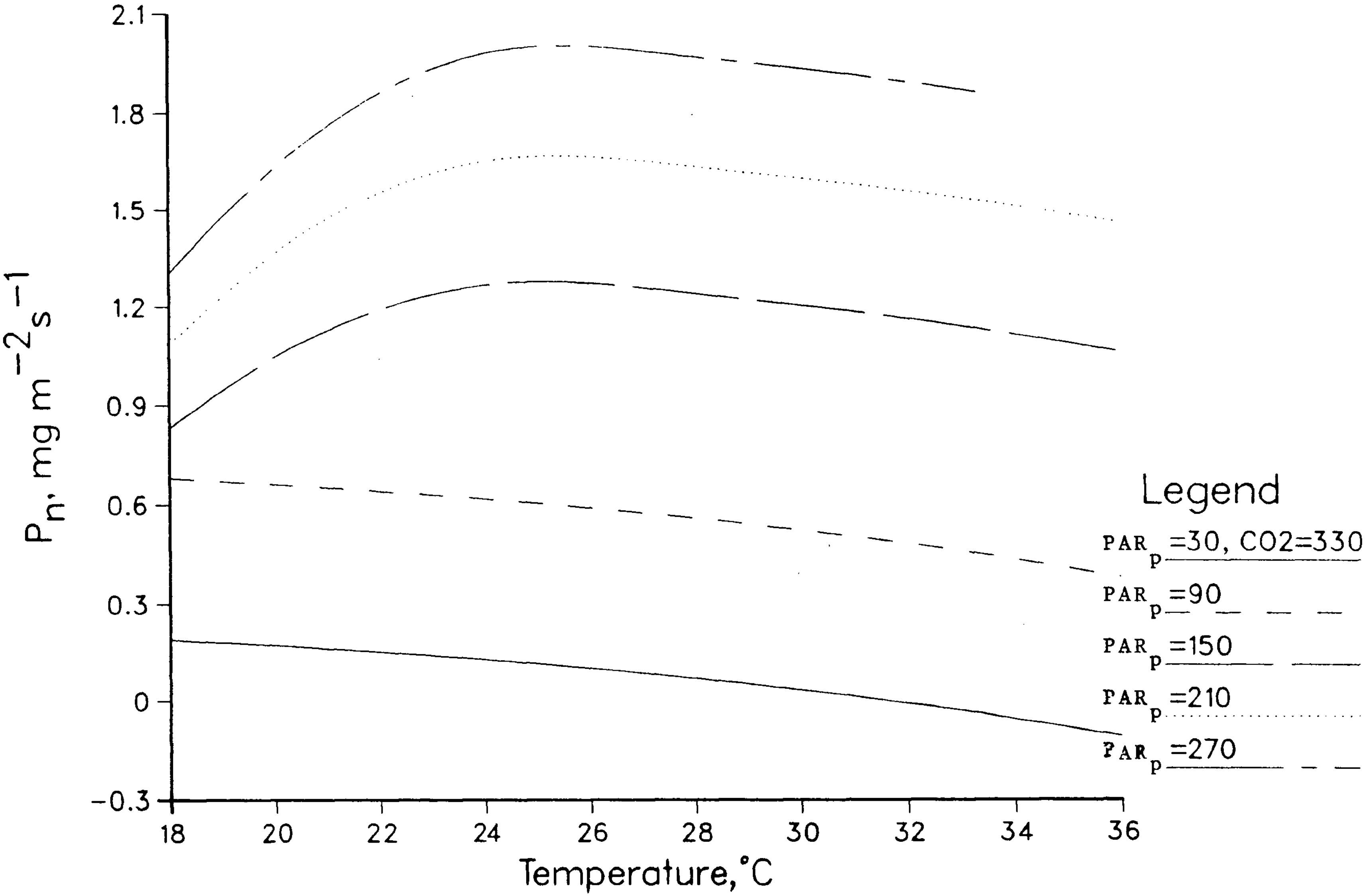

Fig. 4.6 Variation of net canopy photosynthesis (leaf area index = 8.6) with temperature and PAR

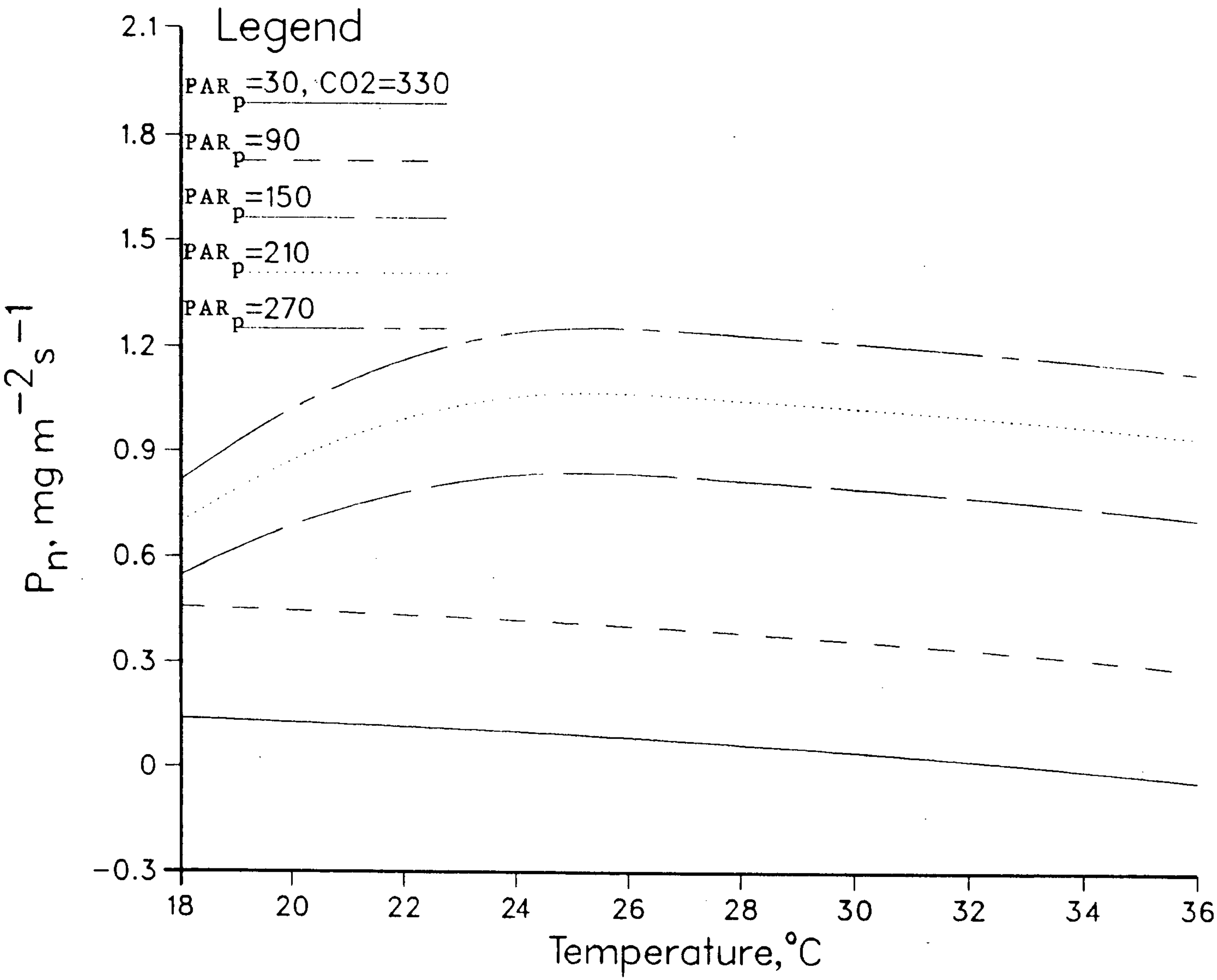

Fig. 4.7 Variation of net canopy photosynthesis (leaf area index = 2.1) with temperature and PAR

Table 4.24 monthly average daily net photosynthetic rate - Vancouver

		Sep	Oct	Nov	Dec	Period total	Jan	Feb	Mar	Apr	Period total	Annual total
Solar Greenhouse												
SS/GS	C1	29.56	12.56	6.84	3.17	1.56	2.95	9.94	23.87	33.52	2.11	3.67
	C2	27.43	11.77	6.41	3.02	1.46	2.81	9.29	22.18	31.21	1.96	3.42
	C3	24.62	10.69	5.80	2.81	1.32	2.63	8.42	19.94	28.15	1.77	3.09
SS/DA	C1	26.68	11.41	6.12	2.74	1.41	2.56	9.04	21.28	31.10	1.92	3.33
	C2	24.84	10.69	5.72	2.59	1.32	2.45	8.46	19.80	29.05	1.79	3.11
	C3	22.36	9.72	5.18	2.41	1.19	2.27	7.70	17.82	26.28	1.62	2.81
CV/GS	C1	28.33	11.74	6.66	2.95	1.49	2.99	9.29	23.54	33.23	2.07	3.56
	C2	26.32	10.98	6.26	2.81	1.39	2.84	8.68	21.85	30.92	1.93	3.32
	C3	23.69	9.97	5.65	2.59	1.26	2.66	7.88	19.62	27.90	1.74	3.00
CV/DA	C1	25.20	10.66	5.98	2.52	1.33	2.59	8.42	19.91	30.28	1.84	3.17
	C2	23.51	10.01	5.62	2.38	1.25	2.48	7.88	18.50	28.30	1.72	2.97
	C3	21.20	9.11	5.11	2.20	1.13	2.30	7.16	16.67	25.63	1.55	2.68
BS/GS	C1	31.50	17.06	8.24	3.56	1.81	3.67	11.16	26.75	35.78	2.32	4.13
	C2	29.12	15.95	7.70	3.38	1.68	3.49	10.40	24.77	33.23	2.16	3.84
	C3	25.99	14.44	6.95	3.13	1.52	3.24	9.36	22.14	29.92	1.94	3.46
Conventional Greenhouse												
CV/GS	C1	30.28	12.56	6.98	3.10	1.59	3.17	9.76	24.59	35.03	2.18	3.77
	C2	28.26	11.81	6.55	2.95	1.49	3.02	9.14	22.90	32.72	2.03	3.52
	C3	25.63	10.80	5.98	2.74	1.35	2.84	8.35	20.70	29.70	1.85	3.20

units: $g\ m^{-2}\ day^{-1}$ for monthly values
$kg\ m^{-2}\ period^{-1}$ for period total values

C1: CO_2 = 330 ppm
C2: CO_2 = 270 ppm
C3: CO_2 = 210 ppm

Table 4.25 monthly average daily net photosynthetic rate - Guelph

		Sep	Oct	Nov	Dec	Period total	Jan	Feb	Mar	Apr	Period total	Annual total
SS/GS	C1	30.49	19.26	9.97	7.56	2.02	7.85	20.88	31.75	36.36	2.91	4.93
	C2	28.30	18.00	9.29	7.13	1.88	7.34	19.12	29.20	33.77	2.68	4.56
	C3	25.34	16.27	8.39	6.48	1.69	6.66	16.85	25.92	30.38	2.39	4.08
SS/DA	C1	28.40	16.13	9.00	6.80	1.81	7.13	19.48	29.70	32.90	2.68	4.49
	C2	26.42	15.08	8.39	6.41	1.69	6.66	17.93	27.40	30.64	2.48	4.17
	C3	23.76	13.64	7.60	5.87	1.53	6.05	15.84	24.41	27.65	2.22	3.75
CV/GS	C1	29.92	18.94	9.61	7.38	1.98	7.56	19.94	31.50	37.01	2.88	4.86
	C2	27.76	17.68	8.96	6.95	1.84	7.09	18.29	28.98	34.34	2.66	4.50
	C3	24.88	15.95	8.10	6.34	1.66	6.41	16.13	25.70	30.85	2.37	4.03
CV/DA	C1	27.47	15.77	8.68	6.66	1.76	6.84	18.58	29.20	33.12	2.63	4.39
	C2	25.56	14.69	8.10	6.26	1.64	6.44	17.10	26.93	30.82	2.44	4.08
	C3	23.04	13.28	7.31	5.72	1.48	5.83	15.16	24.01	27.76	2.18	3.66
BS/GS	C1	31.93	21.28	11.41	8.86	2.20	10.19	24.26	33.48	37.26	3.16	5.36
	C2	29.56	19.76	10.58	8.28	2.05	9.50	22.10	30.67	34.56	2.91	4.96
	C3	26.39	17.78	9.50	7.49	1.83	8.57	19.37	27.11	31.07	2.58	4.41

units: $g\ m^{-2}\ day^{-1}$ for monthly values
$kg\ m^{-2}\ period^{-1}$ for period total values

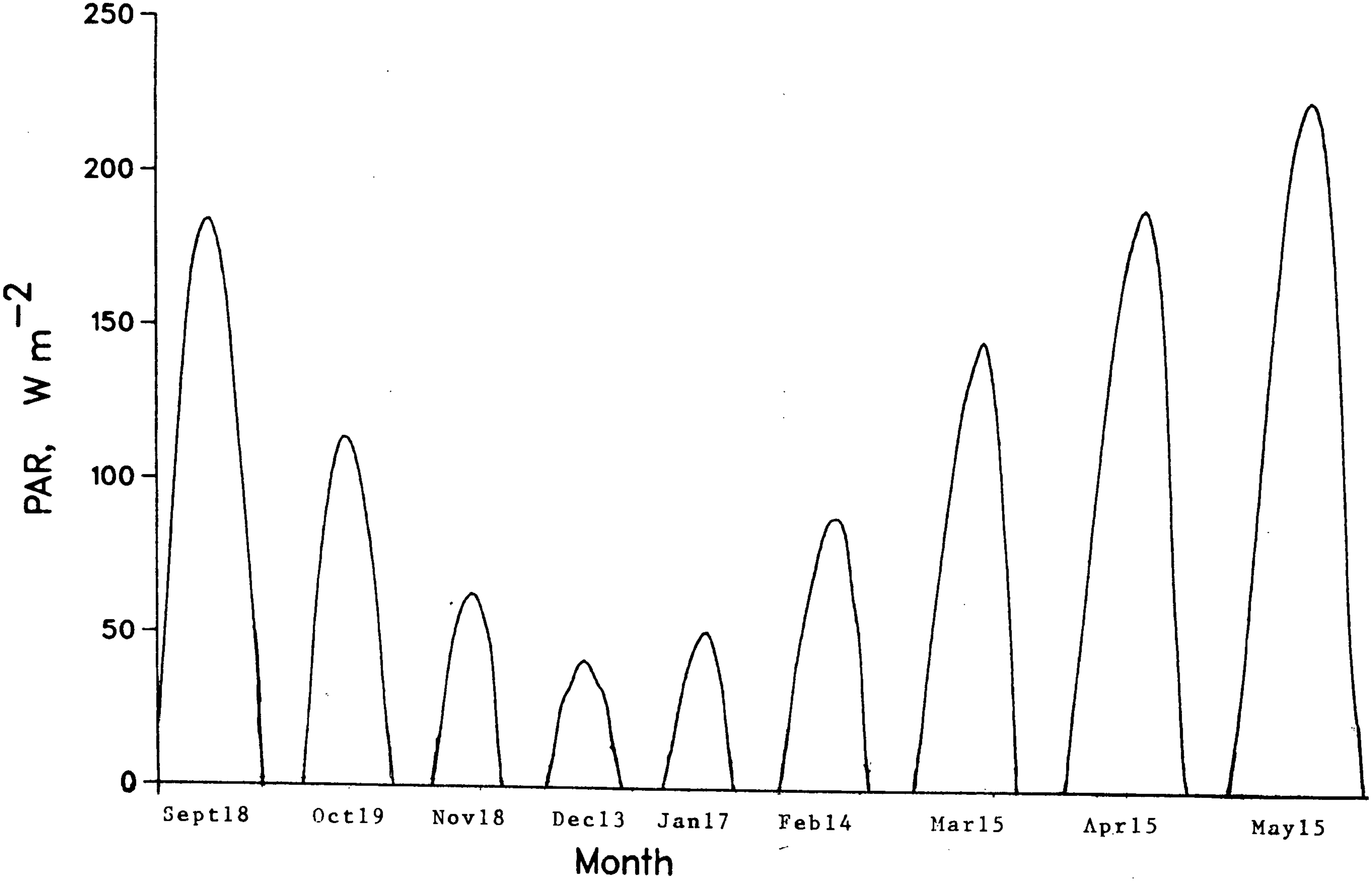

Fig. 4.8 Mean hourly inside PAR flux density on the typical design day of each month - Vancouver

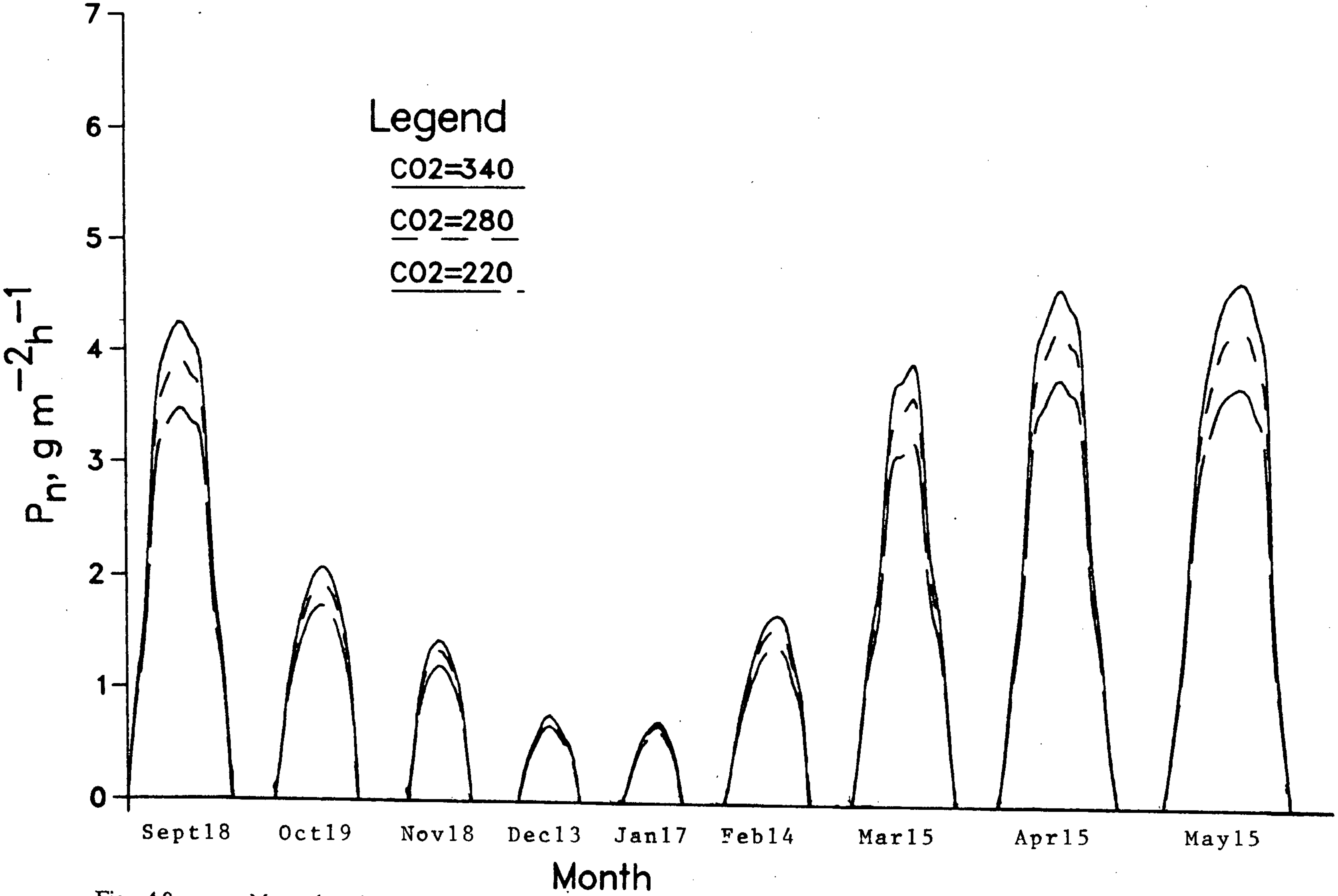

Fig. 4.9 Mean hourly net photosynthetic rate on the typical design day of each month for a greenhouse tomato crop grown in Vancouver

components (P_g and R_d) that constitute P_n are shown in Fig. 4.10 for the representative day in September. It is seen that dark respiration makes up about 30% of gross photosynthesis around noon time. Šesták (1985) commented that although the process of dark respiration is partly inhibited by light in photosynthesizing cells, some 25% of the dark rate might be preserved.

The situation is somewhat different for the same tomato plant grown 'numerically' in Guelph. Since inside PAR level is above 125 W m^{-2} d^{-1} in October, the difference between P_n in September and October is less pronounced. Vast differences in photosynthetic rate between the two locations are found in December and January when solar radiation in Guelph is about twice as much as that in Vancouver. It should be noted that the climatic data processing algorithm in the simulation program does not consider the situation when snow is present on the greenhouse roof. It is imperative that good management practice would be followed to minimize the duration of snow cover that induces static live load on the cover and blocks incoming solar radiation.

The extent of reduction in P_n with diminishing CO_2 concentration is also demonstrated by the results in Tables 4.24 and 4.25. If CO_2 is depressed from the normal 330 ppm to 210 ppm, P_n lessens by 15% to 18%. On a monthly basis, less percentage decrease occurs in the winter months for Vancouver, but this percentage is relatively more uniform from month to month for Guelph. It is simply a reaffirmation of the fact that the effect of CO_2 concentration is more significant when light is not limiting.

Comparison is next made between greenhouse collection methods, with reference to the pivotal case of CV/GS - solar collection with a conventional glasshouse and no auxiliary features for absorption. Table 4.26 lists the effective transmissivity for various greenhouse collection systems. For a glasshouse located in the Vancouver region, crop performance is slightly better with a SS/GS collection system; total P_n during the fall

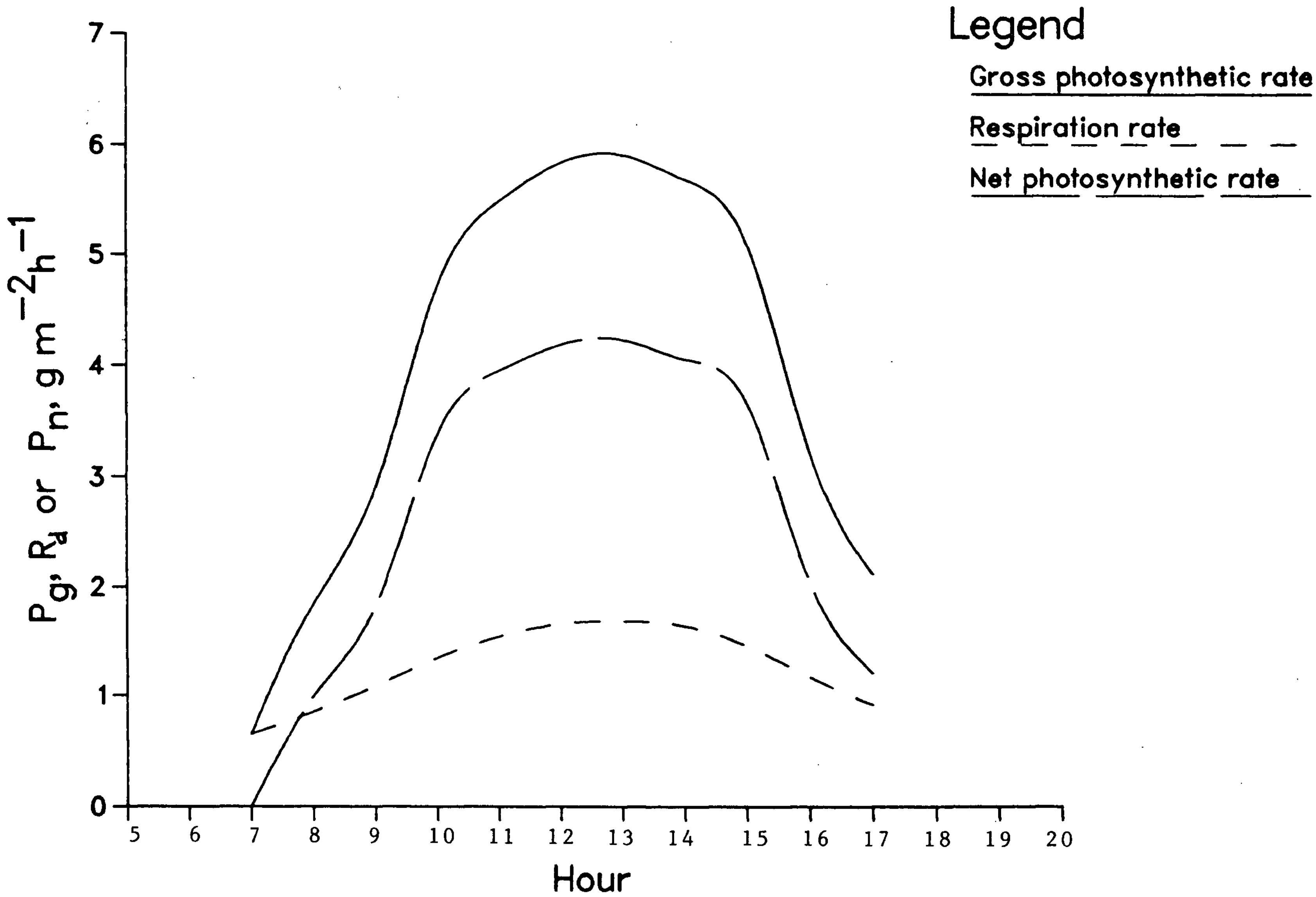

Fig. 4.10 Mean hourly rates of gross photosynthesis, respiration and net photosynthesis on the representative day in September

Table 4.26 Effective transmissivity for different collection systems

	shape/cover	Sep	Oct	Nov	Dec	Jan	Feb	Mar	Apr
Vancouver	SS/GS	0.80	0.80	0.72	0.75	0.71	0.80	0.80	0.77
	SS/DA	0.74	0.74	0.66	0.69	0.65	0.74	0.74	0.71
	CV/GS	0.76	0.76	0.71	0.71	0.71	0.76	0.79	0.77
	CV/DA	0.69	0.69	0.65	0.66	0.65	0.70	0.72	0.69
	BS/GS	0.87	0.92	0.85	0.81	0.82	0.91	0.88	0.81
Guelph	SS/GS	0.79	0.79	0.77	0.74	0.81	0.81	0.80	0.76
	SS/DA	0.72	0.73	0.71	0.68	0.74	0.75	0.73	0.70
	CV/GS	0.77	0.78	.0.75	0.73	0.78	0.77	0.80	0.78
	CV/DA	0.70	0.72	0.69	0.67	0.72	0.71	0.72	0.71
	BS/GS	0.83	0.88	0.88	0.85	0.93	0.92	0.86	0.78

is increased by 5%, and only 2% improvement is achieved for the spring growing period. Upon modifying the greenhouse to bear the BS/GS configuration (with internal reflecting surface), the plant canopy would secure a 21% (0.32 kg m^{-2}) and 12% (0.25 kg m^{-2}) increase in P_n for the fall and spring respectively. On the other hand, if one decides to use double acrylic cover (the CV/DA arrangement), a 11% reduction in net CO_2 uptake may be expected throughout the entire heating season. Similarly, if the SS/DA system is adopted, P_n would cut by 10% relative to a SS/GS system.

In general, net photosynthesis is about 35% higher in Guelph than in Vancouver. Departure from this trend lies in the BS/GS system where only 10% (fall: 0.22 kg m^{-2}, spring: 0.28 kg m^{-2}) more P_n is realized compared to the CV/GS method. It may be attributed to the months with a high leaf area index (Sept, Oct, Mar, Apr) which govern the overall performance in each growing season, when inside light level increases relatively more in Vancouver by adopting the BS/GS design.

As far as leaf temperature is concerned, the effect is coupled to light intensity (and CO_2). The BS/GS setup leads to the most inside PAR level at the top of the canopy, accordingly the temperature-correction factor F with values larger than unity is applied more frequently, and further enhance the net photosynthetic rate. For Guelph, temperature effect is insignificant in the fall, but more influential in the winter months of January and February, becoming insignificant again in later spring.

The accuracy of the absolute value of P_n cannot be verified since the model parameters are pertinent to a tomato plant not grown in Canada. Furthermore, to the knowledge of the author, there is very little information on net photosynthetic rate of greenhouse crops. Nevertheless, some endeavor was made to check with reported values of related information such as greenhouse crop yield.

Moss (1983) found that there was a direct relationship between radiation level and yield. Tomatoes grown with NFT and subject to root-zone warming had a yield of 0.845 kg m^{-2} per week in the first two weeks of picking when the average daily radiation outside was 10.3 MJ m^{-2} d^{-1} in Australia. The mean daily outside solar radiation in Vancouver is 10 MJ m^{-2} d^{-1} in March, and the computed P_n for a CV/GS system is 23.5 g m^{-2} d^{-1}. Enoch (1977) made an attempt to generalize yield, Y, from primary production, P_n . Based upon the assumption that one absorbed CO_2 molecule is used to create one molecule of dry matter (CH_2O), that 50% of this dry matter is yield, and that the total mass of yield contains 5% dry matter, a multiplication factor of 7 is estimated for greenhouse crops such as tomatoes and cucumbers. Thus for P_n = 23.5 g m^{-2} d^{-1}, the yield is roughly 1.17 kg m^{-2} per week, a reasonable value compared to Moss' findings.

Papadopalos and Jewett (1984) measured the marketable yield of tomatoes grown under glass and twin-wall PVC gable-roof greenhouses at the Agriculture Canada Harrow Research Station, Ontario. In March 1982, the yield of the three cultivars (CR-6, Vendor and MR-13) grown under glass are 0.23, 0.57 and 0.31 kg per plant, which, for a planting density of 0.281 m^2/plant can be translated to 26.0, 64.0 and 35.0 g m^{-2} d^{-1}. For the entire spring growing season, cumulative yield amounts to 21.6, 17.5 and 15.6 kg m^{-2}. The corresponding yield for those cultivars grown under twin-wall PVC are 23.3, 16.0 and 16.8 kg m^{-2}. By comparison, the simulated total P_n of 2.88 kg m^{-2} for the CV/GS system in the Guelph region results in a yield estimate of 20.2 kg m^{-2}, and that for the CV/DA system, 18.4 kg m^{-2}. In the fall growing season of 1982, cultivar CR-6 grown under PVC showed a reduction in yield compared to that grown under glass. These results suggest that crop yield may increase or decrease when grown under energy-conserving greenhouses such as the one with twin-wall PVC cover, though no conclusion may be drawn. In contrast, computed values of P_n in this study are always lower for the case of twin-wall acrylic cover material, the light transmission characteristics of which is much like twin-wall PVC.

Yield records obtained from the Saanichton research station (van Zinderen Bakker, 1986) indicated that annual tomato crop yield had an average of 17 and 20 kg m^{-2} for two (fall 1983/spring 1984 and fall 1984/spring 1985) experimental periods; the computed total (fall and spring) P_n of 3.56 kg m^{-2} (yield estimate = 25 kg m^{-2}) for the CV/GS system in the Vancouver region is therefore not an unreasonable value either. Comparing the solar shed with the control house (a conventional glasshouse without thermal storage), actual data also showed that 6% and 8% yield reduction occured during the Fall 1983/Spring 1984 growing period and Fall 1984/Spring 1985 period respectively.

Since no thermal storage is there to remove the surplus solar heat built up in a conventional greenhouse, much ventilation is needed. Also given in Table 4.24 are the simulation results of P_n , with a maximum ventilation rate of 30 air changes per hour. Comparing the values with those of the CV/GS solar heating system where less ventilation takes place to conserve captured solar energy, these net photosynthetic rates are 5% to 7% higher, due to lower greenhouse air temperature and thus plant temperature.

Aside from the temperature effect, where depletion of CO_2 occurs in a solar greenhouse such as the solar shed (SS/GS system) with less ventilation and no CO_2 enrichment, reduction in P_n can be expected. Referring to Table 4.24 again, if its concentration is allowed to drop to 280 ppm, total P_n for both growing seasons would be 3.32 kg m^{-2} for a CV/GS collection system, and 3.42 kg m^{-2} for a SS/GS system. Suppose CO_2 level can be maintained at the normal level in a conventional greenhouse with much ventilation, the associated P_n is 3.77 kg m^{-2}, which is 14% and 10% more than each of the above system. If the depletion is more severe (down to 210 ppm), the loss in primary production is increased to 26% and 22% respectively.

The actual depletion of CO_2 varies from month to month, and is a function of the total leaf area and Q_e , the amount of excess solar heat not collected and subsequently delivered to the thermal storage. A high L_i means plants consume more CO_2, and if coupled to a very small Q_e value, then ventilation must have been kept to a minimum. It is therefore expected that CO_2 will be depleted least in the winter months, and most in October and April when leaf area index is large while at the same time, collection of solar heat is to be maximized.

Therefore, for a known quantity of useful heat gain, Q_u , that can be achieved by a greenhouse solar collection system, as storage capacity increases, more heat can be collected over a longer time during the day with the right combination of air flow rate and storage capacity. Accordingly, vents will be closed for an extended period, thus more CO_2 depletion takes place. The algorithm for such a situation has not been developed in this study, and the effect of thermal storage parameters can only be described qualitatively with respect to the results of P_n for varying amount of CO_2.

The rate of CO_2 consumption in a closed system may be estimated by the following equation:

$$\Delta CO_2 = \frac{22.4 A_f P_n T}{(44)(273)V} \tag{4.20}$$

The area used in the above expression is greenhouse floor area, A_f . For the shed-type glasshouse (A_f = 117 m^2, V = 490 m^3), if P_n has a typical value of 1.0 mg m^{-2} s^{-1} at T = 30 °C and is assumed to stay constant with time, then in 15 minutes, CO_2 will drop by 120 ppm. Of course, CO_2 depletion rate is not constant in the actual situation, but this simple calculation demonstrates one important point: for collection of solar heat to be realistic such that vents are not open often, CO_2 enrichment is necessary. Willits and Peet (1987) commented that the closed-loop cooling provided by storage during the day allows sufficient additional CO_2 enrichment time over conventional ventilation systems such that significant yield increases can be expected with some greenhouse crops. For a glasshouse with tomatoes under U.K.

winter conditions, an average of 416 kg CO_2 ha^{-1} y^{-1} was used to raise the CO_2 concentration 1 ppm (Slack and Calvert, 1972). Enoch (1978) suggested that this would require 139 kg propane ha^{-1} y^{-1}.

4.5 Development of A Simplified Design Method

4.5.1 Introduction

The parametric study described in detail in section 4.2 provides some insight into the extent of variation of system thermal performance with the key design variables. The most important observation is that in most cases, both the key indices of long-term system performance, the total solar contribution and solar heating fraction are directly proportional to the dimensionless solar load ratio which represents the characteristics of the greenhouse collection system.

In developing a simplified design method for solar heating systems for greenhouses, it is desirable to have a set of generalized design curves that cover as many parameters as possible. Besides, a designer needs some guidelines to obtain the information related to the essential variables involved in the design procedure.

From the results of the parametric study, the greenhouse construction parameters that bear minimal influence on system performance have been identified to be roof slope and length-to-width ratio. On the other hand, parameters that can induce large variation in system performance by way of the solar load ratio include location and cover material. Greenhouse orientation and floor area have some measurable effect on the energy savings too. The greenhouse shape per se has no appreciable effect on solar radiation input, rather, it is the combination of the shape and the energy absorption method that would either modify the solar load ratio or enhance the heat exchange process that ultimately leads to better system performance. Storage parameters affect the system behaviour independently and do not affect the solar load ratio.

Results suggested that all the storage parameters with the exception of soil type and moisture content are significant variables, so that a family of design curves are probably required for different choices of the storage configuration.

The approach adopted here is to establish a correlation between the solar load ratio and system thermal performance. Preliminary plottings of SLR versus s and f indicated that both s and f exhibit a positive correlation with SLR and that the former shows a more definitive pattern. Moreover, 's' was found to be well correlated with 'f', as seen in Fig. 4.11. It is therefore possible to establish a set of design curves that permit s and f to be calculated in sequence. Although the solar heating fraction is of utmost concern for subsequent economic analysis of the results generated from the present study, the total solar contribution can provide complimentary information for comparing alternative designs. Hence, it is necessary to estimate both indices of system thermal performance to assist in decision making.

The simulation results in the form of s and f of a large number of runs are plotted in Figs. 4.12 and 4.13. Fig. 4.12 pertains to the SS and CV collection systems with rockbed thermal storage. Each collection method is coupled to two combinations of the storage parameters, $SC_r = 0.38$, $\dot{m} = 12.50$ and $SC_r = 0.19$ and $\dot{m} = 6.25$. These two sets of values are chosen to represent some bounds within practical consideration to the system performance with alternative storage designs. For a given collection system and storage configuration, it is realized that, by and large, variations in the following design parameters can be accomodated by a single curve that relates s to SLR: cover material, roof tilt, length-to-width ratio, orientation and floor area. Some adjustment on the annual solar heating fraction is necessary for large greenhouses. The same curve can account for the thermal performance of a particular design put to operation in regions with climatic conditions representative of the various locations covered in this study.

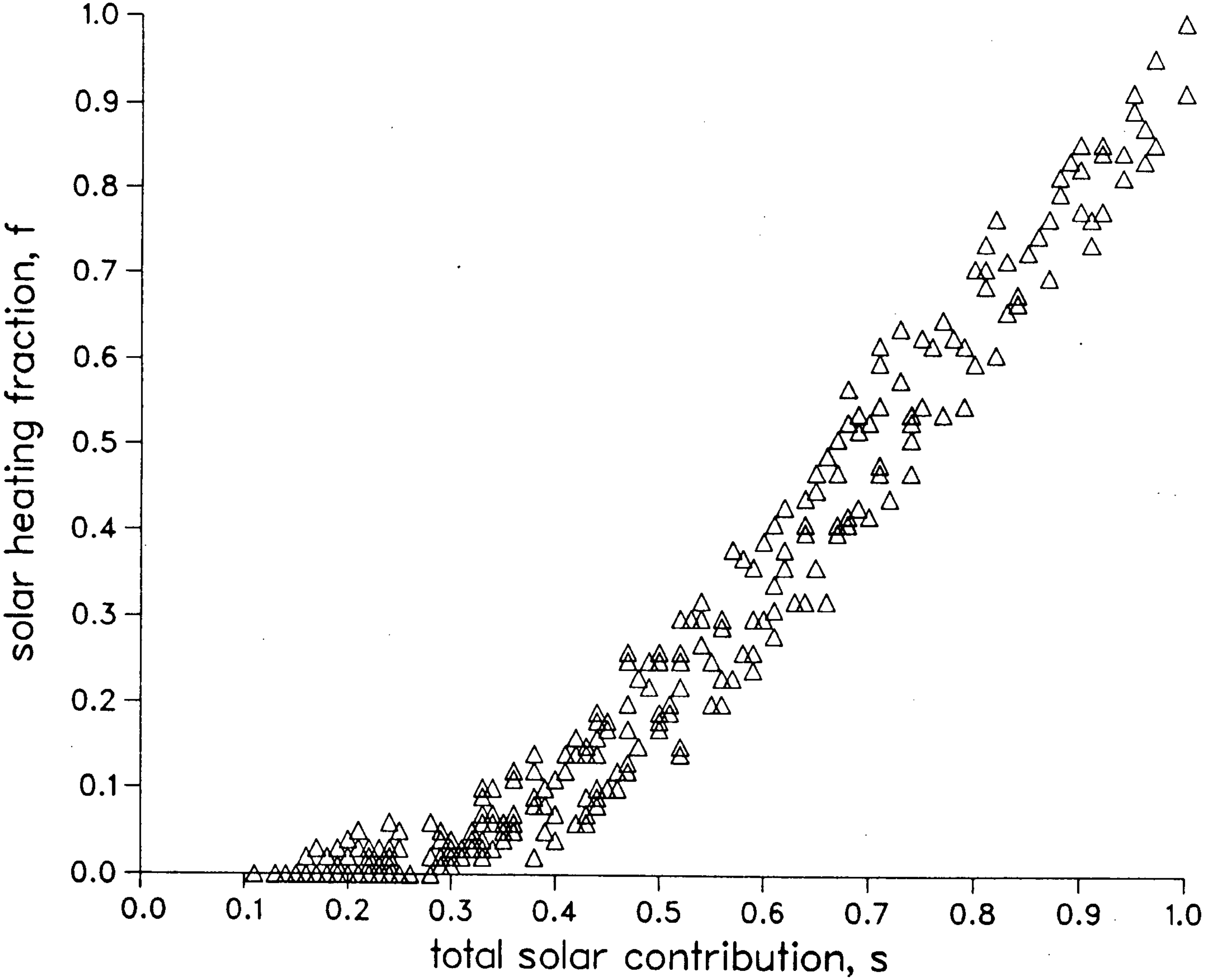

Fig. 4.11 Simulated values of solar heating fraction versus total solar contribution

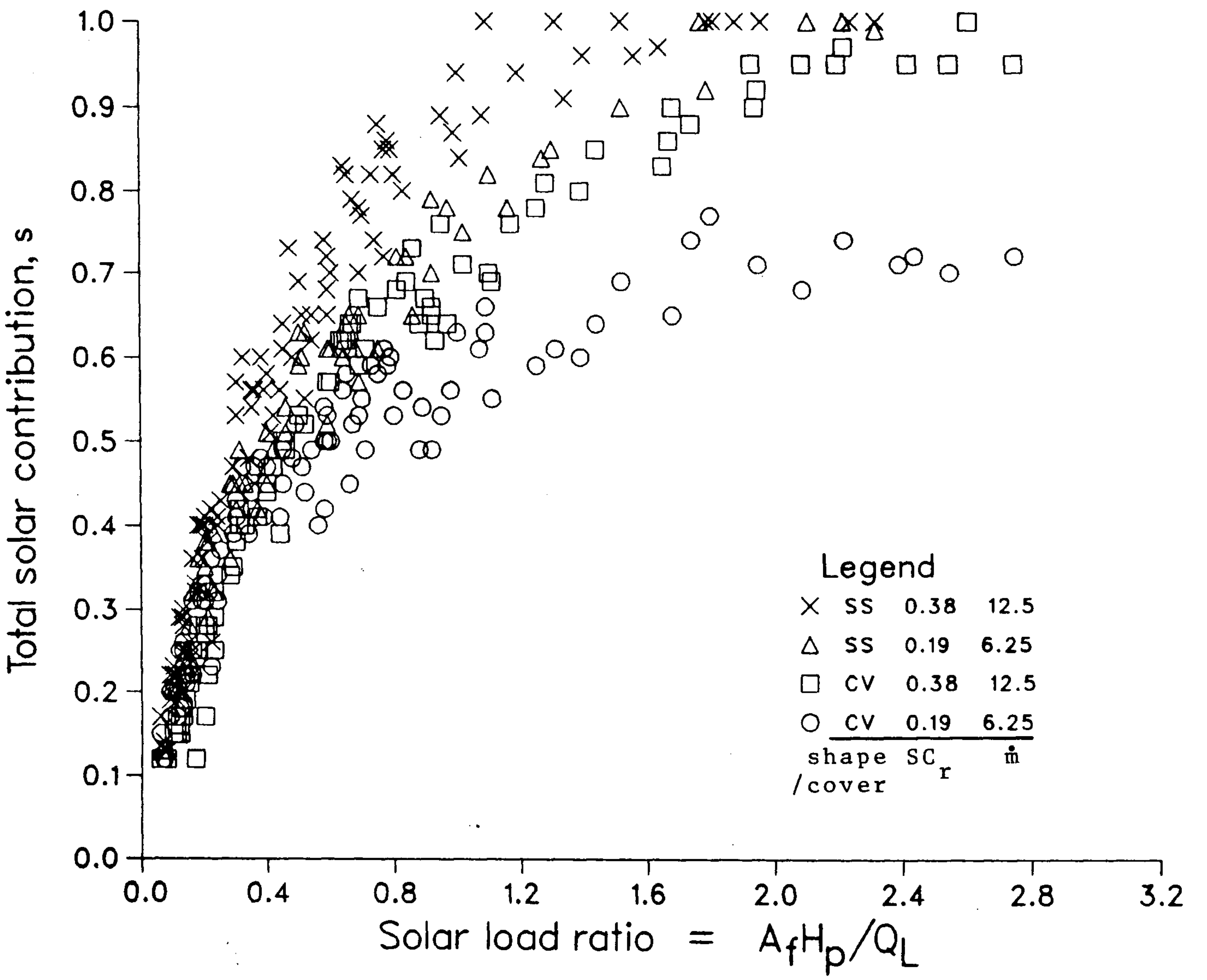

Fig. 4.12 Simulated values of total solar contribution versus solar load ratio - rockbed thermal storage

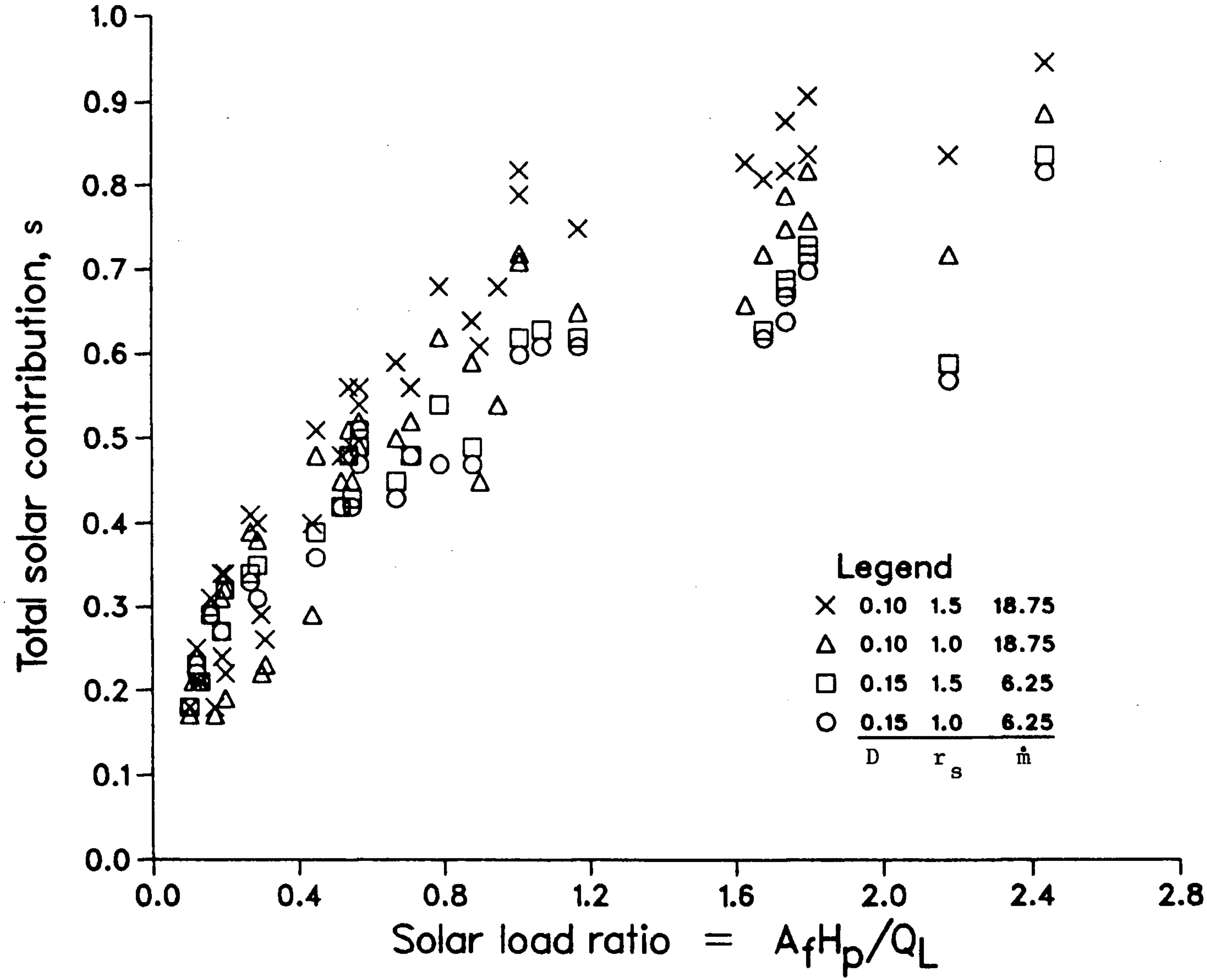

Fig. 4.13 Simulated values of total solar contribution versus solar load ratio – soil thermal storage

Total solar contribution as a function of solar load ratio is plotted in Fig. 4.13 for a CV collection system and wet soil thermal storage. Less simulation runs were executed for this solar heating system since it is not necessary to repeat the variation of those parameters that have nominal effect on system performance. Also, in view of the higher computing cost involved in the soil storage simulation, only the locations of Vancouver, Guelph and Albuquerque were included. The climatic conditions of other locations do not give rise to solar load ratios and hence solar fractions that are out of the range covered by the aforesaid locations.

4.5.2 Regression method

At this point, the performance curves that shall form the skeleton of the proposed simplified design procedure are ready to be synthesized through curve fitting. The desirable output is to produce a general empirical relation for a family of curves. However, this is only possible if the parameters of the curves can be fully quantified. The next desirable outcome is the generation of the same form of a certain equation, in which the constants (coefficients) are allowed to vary with different parameters. The situation that equations of different forms need to be fitted to these simulated data is to be avoided by all means because of possible confusion. Mathematical expressions are required since a fair amount of computational work is still expected on the part of the user though he/she is no longer required to undertake the detailed simulations carried out herewith.

For the correlation between monthly total solar contribution, s, and solar load ratio, SLR, since s has an upper limit of 1.00, the exponential form of equation is more appropriate than other forms such as hyperbolic which has an asymtotic locus, or parabolic which tends to fall off at some point. Using the packaged program NLSUM at UBC (Moore, 1981), the data points of Fig. 4.12 and 4.13 were fitted to the function

$$s = a_o + a_1 e^{b_1 \cdot \mathrm{SLR}} + a_2 e^{b_2 \cdot \mathrm{SLR}} \tag{4.21}$$

where the coefficients for each case (rockbed thermal storage and soil thermal storage) with various combinations of storage characteristics are given in Table 4.27. The value of s is insensitive to round-off of decimal points for the coefficients, except case S1, for which 5 decimal places need to be retained. For nonlinear regression analysis, the correlation index, I^2, was computed and its values are shown in Table 4.27 as well. Equation 4.21 is graphically shown in Fig. 4.14 and 4.15 for the two cases.

A polynomial function was fitted to the correlation between monthly solar heating fraction, f, and s, and results in the following quadratic equation:

$$f = -0.007 + 0.03\,s + 0.92\,s^2 \tag{4.22}$$

A slightly better fit was obtained with a cubic polynomial, however, a local minimum f occurs where s = 0.20, below and above which f begins to increase, which is unrealistic. Equation 4.22 is represented by Fig. 4.16.

4.5.3 Outline of the design procedure

The use of the design curves or the fitted equations for determining the solar heating fraction involves a number of calculation steps, as outlined below:

1. Specify location, greenhouse and thermal storage design characteristics.
2. Obtain monthly average climatic data - solar radiation [in MJ m^{-2} d^{-1}] and temperature.,
3. Calculate total glazing area, A_{gz} , as

$$A_{gz} = A_{gr} + A_{gw} + A_{ge} \tag{4.23}$$

4. The 24-hour greenhouse heating load [in MJ] is estimated by summing the hourly values,

$$Q_L = \sum_{24-hr} U_{gz} A_{gz} (T_{set} - T_o)(0.0036) \tag{4.24}$$

Table 4.27   Coefficients of equation 4.21

Case	a_o	a_1	a_2	b_1	b_2	r^2
R1	1.03	-1.00	-	-1.96	-	0.91
R2	1.15	-0.89	-0.35	-0.82	-9.18	0.92
R3	1.13	-0.71	-0.44	-0.61	-3.24	0.92
R4	0.80	-0.44	-0.39	-0.73	-6.38	0.88
S1	0.873	-2151.478	2150.697	-0.83676	-0.83657	0.95
S2	0.85	-0.76	0.06	-1.19	-9.76	0.91
S3	0.79	-0.59	-0.75	-1.00	-22.4	0.94
S4	0.77	-0.57	-1.19	-0.98	-27.6	0.93

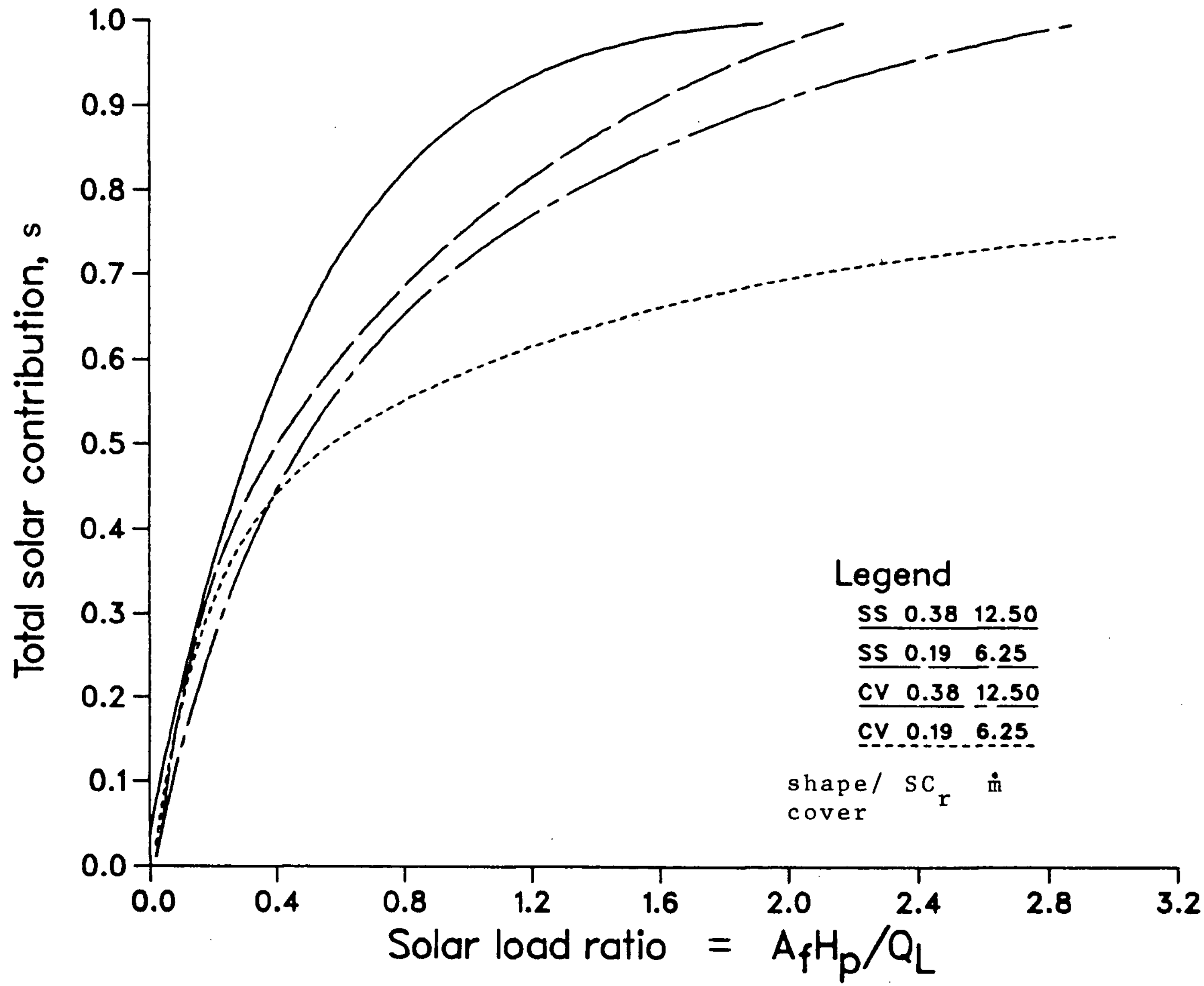

Fig. 4.14 Design curves fitted to the simulated data points of Fig. 4.12

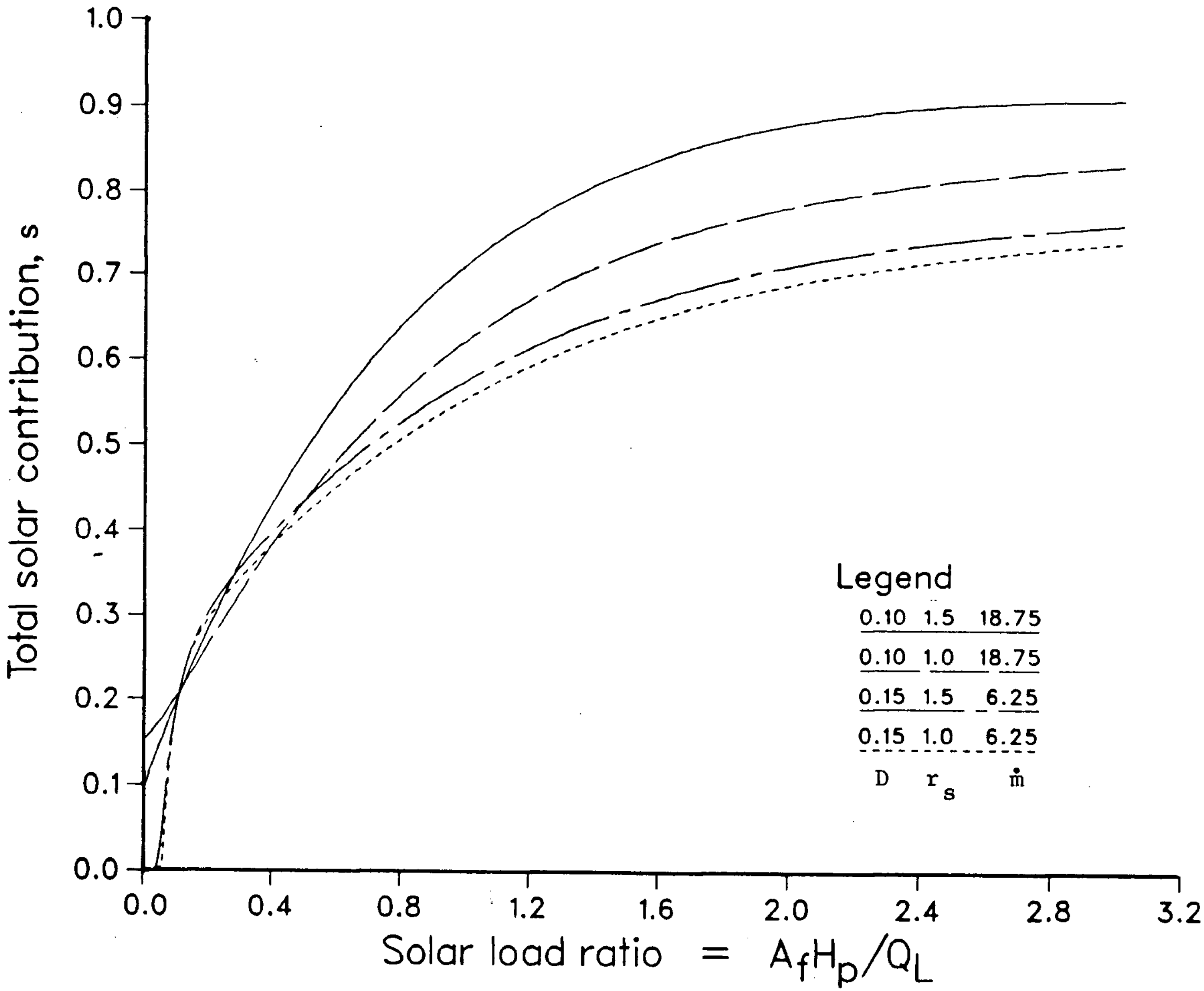

Fig. 4.15 Design curves fitted to the simulated data points of Fig. 4.13

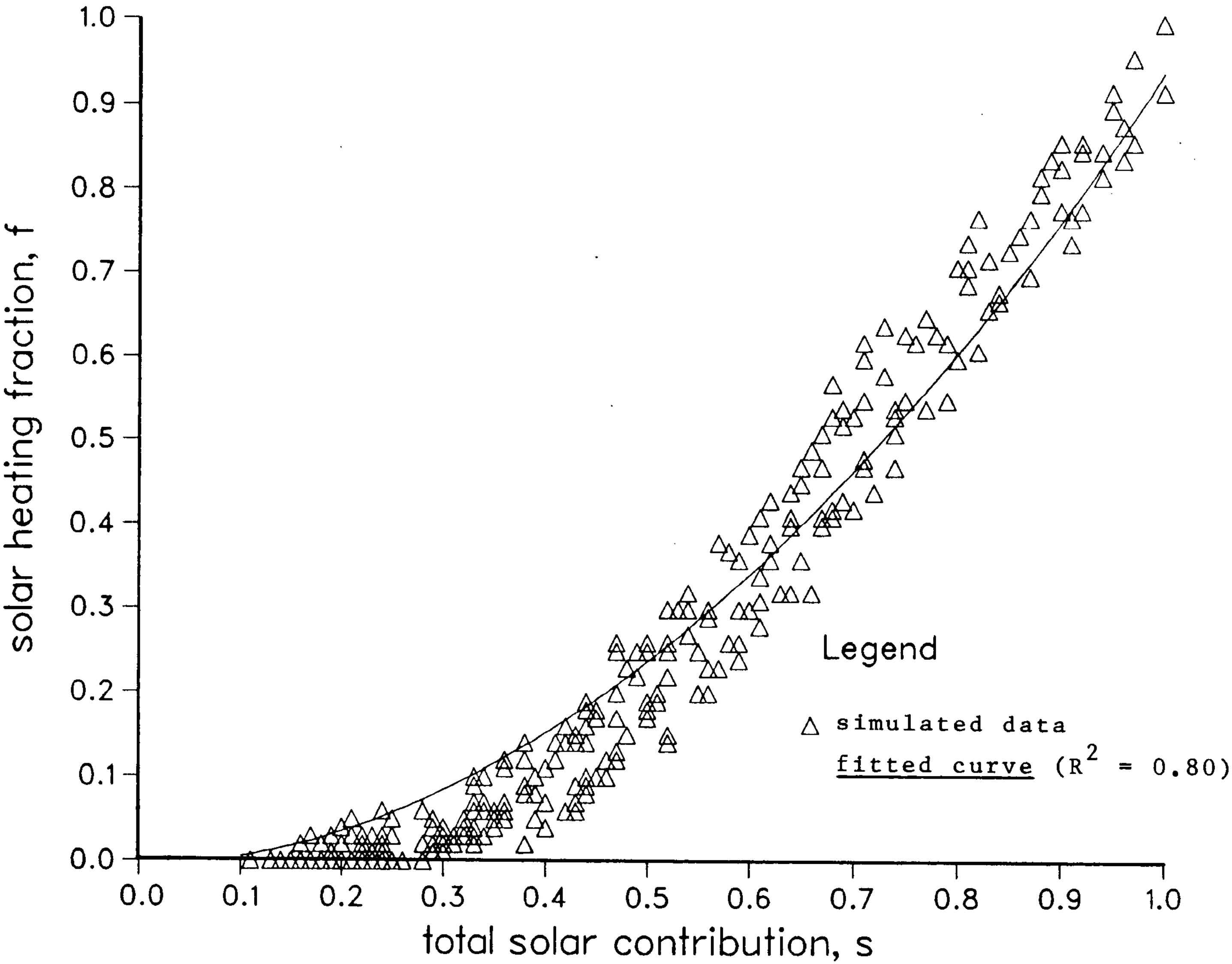

Fig. 4.16 Function fitted to the simulated data of Fig. 4.11

where T_{set} is the set-point temperature (e.g. 22 °C daytime and 17 °C nighttime), and U is the overall heat loss coefficient of the greenhouse glazing (5.7, 5.8, and 3.2 W m^{-2} K^{-1} for glass, polyethylene, and double acrylic respectively). The outside temperature, T_o, is calculated in accordance with eqns. 4.10 (daytime) and 4.12 (nighttime).

5. Determine monthly greenhouse effective transmissivity, τ_e. It is noted that τ_e does not vary much from month to month at a specific location, and for a given collection system (shape, cover and absorption means). Typical values may be found in Table 4.26. However, a computer program that only computes τ_e can be made available for users if so desired.

6. Calculate the amount of solar radiation incident on an inside horizontal surface as

$$H_p = \tau_e H \tag{4.25}$$

7. The monthly solar load ratio is then

$$\text{SLR} = A_f H_p / Q_L \tag{4.26}$$

8. From Fig. 4.14 or Fig. 4.15, obtain the corresponding monthly total solar contribution, s.

9. Estimate monthly solar heating fraction, f, from Fig. 4.16.

10. Finally, the annual solar heating fraction, f_y for the entire heating season may be computed from

$$f_y = \frac{\sum_m f\, Q_L}{\sum_m Q_L} \tag{4.27}$$

11. Design options that are not covered by the performance curves may have the reference system thermal performance estimated by the procedure outlined above, and calculated results can be modified by consulting Tables 4.28 and 4.29.

Table 4.28 Combined rockbed storage capacity and air flow rate effect on system thermal performance

greenhouse - floor area: 200 m^2 , orientation: E-W
length-to-width ratio: 2, roof tilt: 26.6

location	shape/cover	SC_r	$\dot{m}$	s	f
VAN	SS/GS	0.19	6.25	0.51	0.23
		0.38	12.50	0.59	0.32
	SS/DA	0.19	6.25	0.54	0.30
		0.38	12.50	0.66	0.44
	CV/GS	0.19	6.25	0.33	0.12
		0.38	12.50	0.37	0.20
	CV/DA	0.19	6.25	0.48	0.20
		0.38	12.50	0.61	0.31
	CV/PE	0.19	6.25	0.29	0.10
		0.38	12.50	0.34	0.17
GPH	SS/GS	0.19	6.25	0.37	0.08
		0.38	12.50	0.44	0.17
	SS/DA	0.19	6.25	0.47	0.20
		0.38	12.50	0.57	0.35
	CV/GS	0.19	6.25	0.27	0.05
		0.38	12.50	0.36	0.09
	CV/DA	0.19	6.25	0.37	0.10
		0.38	12.50	0.44	0.21
YUL	SS/GS	0.19	6.25	0.35	0.07
		0.38	12.50	0.40	0.14
	8S/GS	0.19	6.25	0.31	0.07
		0.38	12.50	0.35	0.12
	CV/DA	0.19	6.25	0.39	0.11
		0.38	12.50	0.41	0.20
ALB	SS/GS	0.19	6.25	0.57	0.28
		0.38	12.50	0.70	0.54
	CV/GS	0.19	6.25	0.43	0.20
		0.38	12.50	0.57	0.35
	CV/PE	0.19	6.25	0.41	0.17
		0.38	12.50	0.52	0.31

Table 4.29 Combined effect of soil storage pipe wall area and air flow rate on system thermal performance

greenhouse - floor area: 200 m^2 , orientation: E-W
length-to-width ratio: 2, roof tilt: 26.6

storage - medium: clay soil, θ_s = 30%

location	shape/cover	D	r_s	$\dot{m}$	s	f
VAN	SS/GS	0.10	1.5	18.75	0.54	0.31
		0.15	1.0	6.25	0.42	0.17
	CV/GS	0.10	1.5	18.75	0.38	0.17
		0.15	1.0	6.25	0.34	0.09
	CV/DA	0.10	1.5	18.75	0.53	0.30
		0.15	1.0	6.25	0.44	0.18
	CV/PE	0.10	1.5	18.75	0.32	0.14
		0.15	1.0	6.25	0.19	0.06
GPH	SS/GS	0.10	1.5	18.75	0.44	0.15
		0.15	1.0	6.25	0.39	0.09
	CV/DA	0.10	1.5	18.75	0.43	0.20
		0.15	1.0	6.25	0.37	0.13
	CV/PE	0.10	1.5	18.75	0.36	0.09
		0.15	1.0	6.25	0.28	0.05
ALB	SS/GS	0.10	1.5	18.75	0.72	0.56
		0.15	1.0	6.25	0.51	0.27
	CV/PE	0.10	1.5	18.75	0.46	0.23
		0.15	1.0	6.25	0.40	0.15

4.5.4 Example calculation

In this section, an example is given showing how the design curves can be used to determine the annual solar heating fraction during the period of September through May, for the following specifications:

location: Vancouver

greenhouse floor area: 500 m^2

length-to-width ratio: 2

wall height: 2 m

roof tilt: 26.6 $^{\circ}$

glazing: single layer glass

daytime setpoint temperature: 22 $^{\circ}$C

nighttime setpoint temperature: 17 $^{\circ}$C

By working through the steps outlined in section 4.5.3, we shall be able to come up with a set of f-values for various options provided in the design curves.

The local climatological data for Vancouver is given in Table 4.30, also shown here are the calculated monthly solar load ratio values. The fraction of the heating load supplied by solar energy during each month can then be obtained from Figs. 4.12 or 4.13, and Fig. 4.11. A small computer program as listed in appendix E has been written to facilitate the computation procedure. Users need to prepare a short list of inputs that correspond to the design specifications. The estimated system thermal performance for each design alternative is given in Table 4.31.

Table 4.30 Average local climatological data for Vancouver, and solar load ratio for a CV/GS collection system

	Sep	Oct	Nov	Dec	Jan	Feb	Mar	Apr	May
H	13.22	7.38	3.59	2.28	2.94	5.53	10.03	15.09	20.15
T_{max}	18.47	13.74	9.06	6.61	5.29	7.56	9.65	13.19	16.83
T_{min}	9.90	6.46	2.90	1.24	-0.27	0.96	2.30	4.83	7.84
τ_{ℓ}	0.76	0.76	0.71	0.71	0.71	0.76	0.79	0.77	0.78
H_p	10.05	5.61	2.55	1.62	2.09	4.20	7.92	11.62	15.72
Q_L	2838	4814	6749	7821	8528	7847	7110	5642	4008
SLR	1.77	0.58	0.19	0.10	0.12	0.27	0.56	1.03	1.96

Table 4.31 Solar heating fraction, f for eight design options

Case	Sep	Oct	Nov	Dec	Jan	Feb	Mar	Apr	May	Year
R1	0.94	0.48	0.11	0.04	0.05	0.18	0.46	0.76	0.96	0.35
R2	0.84	0.34	0.10	0.03	0.05	0.16	0.32	0.56	0.89	0.28
R3	0.78	0.33	0.07	0.02	0.03	0.13	0.32	0.55	0.83	0.26
R4	0.45	0.25	0.09	0.04	0.05	0.14	0.25	0.35	0.47	0.19
S1	0.72	0.30	0.08	0.04	0.05	0.12	0.29	0.53	0.75	0.25
S2	0.57	0.23	0.07	0.04	0.04	0.10	0.22	0.40	0.60	0.20
S3	0.47	0.22	0.09	0.04	0.05	0.12	0.21	0.34	0.49	0.18
S4	0.44	0.20	0.08	0.04	0.05	0.11	0.19	0.32	0.46	0.17

NOTATION

		Dimension
A_f	Greenhouse floor area	m^2
B	Monthly average number of bright sunshine hours	
C	CO_2 concentration	$mg\ m^{-3}$
D	Pipe diameter	m
F	Temperature-correction factor	-
F_{12}	View factor between one roof surface and plant canopy	-
F_{13}	View factor between two roof surfaces	-
H	Daily global solar radiation incident on a horizontal surface	$MJ\ m^{-2}\ d^{-1}$
I	Hourly global radiation incident on a horizontal surface	$kJ\ m^{-2}\ h^{-1}$
K	Extinction coefficient	m^{-1}
K_d	The ratio H_d/H_{ex}	-
K_T	Clearness parameter (cloudiness index) = H/H_{ex}	-
L	Length	m
L_i	Leaf area index	$m^2\ m^{-2}$
L:W	greenhouse length-to-width ratio	-
N	Number of air changes per hour	hr^{-1}
N_d	Day length	h
N_j	Modified day length	h
N_p	Number of pipes	-
NTU	Number of heat transfer units	-
P_g	Gross photosynthetic rate	$mg\ m^{-2}\ s^{-1}$
P_n	Net photosynthetic rate	$mg\ m^{-2}\ s^{-1}$
PAR	Photosynthetically active radiation	$kJ\ m^{-2}\ h^{-1}$
Q_{DL}	Daytime heating load	$MJ\ d^{-1}$
Q_{DN}	Daytime net heating load	$MJ\ d^{-1}$
Q_L	24-hour gross heating load	$MJ\ d^{-1}$
Q_{NL}	Nighttime heating load	$MJ\ d^{-1}$
Q_{PAS}	Passive solar gain	$MJ\ d^{-1}$
Q_{ST}	Solar heat recovered from storage	$MJ\ d^{-1}$
Q_{td}	Heat transferred to storage (charging)	$MJ\ d^{-1}$
Q_u	Useful heat gain	$MJ\ d^{-1}$
R_d	Dark respiration rate	$mg\ m^{-2}\ s^{-1}$
S_p	Pipe spacing	m
SC	Storage capacity	$m^3\ m^{-2}$
SLR	Solar load ratio	-
T	Temperature	$^\circ C$
TTF	Total transmission factor	-
U	Overall heat transfer coefficient	$W\ m^{-2}\ K^{-1}$
W	Width	m

ΔP	Pressure drop	$kN\ m^{-2}$
a,b,c,e	Constants used in equations 4.10 and 4.11	-
a', b'	Constants used in equation 4.7	-
a_o, a_1, a_2 b_1, b_2	Constants used in eqn. 4.21	-
d	Rock equivalent diameter	m
f	Monthly solar heating fraction	-
f_{sh}	shading factor due to greenhouse structural members	
f_y	Annual solar heating fraction	-
f_{sh}	shading factor due to greenhouse structural members	-
h	Depth	m
n	Hour	00–24
$\dot{m}$	Air flow rate	$L\ s^{-1}\ m^{-2}$
n_L	Number of layers of pipe	
r_s	Total pipe wall area to greenhouse floor area ratio	-
s	Monthly total solar contribution	-
s_y	Annual total solar contribution	-
v	Superficial fluid velocity	$m\ s^{-1}$
α	Leaf light utilization efficiency	$mg\ J^{-1}$
β	Leaf Bowen ratio	-
δ_c	Declination on characteristic days	Degrees
ϵ	Void ratio	-
ζ	Leaf conductance to CO_2 transfer	$m\ s^{-1}$
η	Collection efficiency	-
θ_s	Soil volumetric moisture content	%
θ_z	Zenith angle	Degrees
θ_i	Angle of incidence	Degrees
ι	Refractive index	-
μ	Absolute viscosity	$kg\ m^{-1}\ s^{-1}$
ν	Density	$kg\ m^{-3}$
ξ_1	slope of roof surface 1	Degrees
ξ_2	slope of roof surface 2	Degrees
ρ	Ground albedo	-
ρ_a	Cloudless sky albedo	-
ρ_c	Cloud albedo	-
τ_e	Effective transmissivity	-
τ_p	Leaf transmittance	-
ϕ	Latitude	Degrees
ω_i	Hour angle at the middle of an hour	Degrees
ω_s	Sunset-hour angle for a horizontal surface	Degrees

Subscripts

1,2,3	for pressure drop expressions
ex	extraterrestrial
f	floor,
	fluid
g	greenhouse
ge	greenhouse gable ends
gr	greenhouse roof
gz	greenhouse glazing
i	insulation
m	month
max	maximum
min	minimum
n	direct normal
o	outside
p	plant canopy,
	pipe
r	rock
rs	rockbed storage
set	setpoint
sr	sunrise
ss	sunset
w	wall
y	year

Abbreviations

BS	Brace-style greenhouse
CV	conventional gable roof or quonset greenhouse
SS	shed-type greenhouse

DA	twin-walled (double) acrylic
GS	glass
PE	polyethylene

ALB	Albuquerque
EDM	Edmonton
GPH	Guelph
MTL	Montreal
NSV	Nashville
STJ	St. John's
VAN	Vancouver
WNG	Winnipeg

Chapter 5

CONCLUSIONS AND RECOMMENDATIONS

The computer program written for predicting the thermal performance of solar heating systems for greenhouses has been made flexible to include a number of design alternatives. Design parameters include location, greenhouse characteristics and storage characteristics, most of which are allowed to have variable values. Provision is also made for the processing of climatological data that are available in different forms. A subroutine of the program was also written to deal with canopy net photosynthesis of a greenhouse tomato crop.

The combined greenhouse thermal environment - thermal storage model along with the empirical relationships and the values of constants approximated in the simulation has yielded reasonably accurate computed results compared to observed data for the two specific systems studied. Inside solar radiation and temperature are in better agreement with actual values, followed by rockbed temperatures and soil temperatures, whereas relative humidity shows more deviations from the experimental data. Nevertheless, the prediction of energy savings due to each solar heating system is within 15% of measured energy savings data.

Based on simulated data, a concise set of design curves have been obtained for estimating the long-term average thermal performance of a greenhouse solar heating system. With these curves, the annual solar heating fraction can be directly calculated knowing the average climatic conditions of a certain design location. Crop performance is also quantified for various greenhouse collection systems. A detailed economics study based on the predicted thermal and crop performances pertinent to a particular system design would then enable a designer to evaluate design alternatives in the early phase of a project.

Specific findings of this study are:

1. Accurately predicted greenhouse temperature and relative humidity cannot be

attained simultaneously as relative humidity depends on temperature.

2. Latent heat release by the moist inlet air in the rockbed storage is not significant as the calculated rockbed temperatures are not vastly different from measured values.

3. Of the greenhouse construction parameters investigated, roof tilt and length to width ratio have least influence on effective transmissivity and hence solar heating fraction. The collection method that comprises the shape, cover material and solar radiation absorption means has obvious effects. Besides, the effective transmissivity of a solar greenhouse does not vary appreciably from month to month, in contrast to the trend of the total transmission factor.

4. Solar irradiation on the plant canopy does not differ significantly, regardless of shape, unless internal reflection is increased considerably.

5. With the rockbed thermal storage, larger storage capacity is warranted only if a higher air flow rate is used. System thermal performance follows the 'law of diminishing return' with regard to air flow rate. A more linear variation is obtained, however, for the range of storage capacity investigated.

6. With the soil thermal storage, if the pipe wall-to-greenhouse floor area ratio is fixed, a system with smaller pipe diameter coupled with higher air flow rate performs better than one with larger pipe diameter and lower air flow rate. To obtain greater solar heating fraction by increasing the total pipe wall area, it is more effective to increase the number of pipes than their diameter.

7. For most (colder) regions in Canada, annual solar heating fraction lies below 10% with conventional greenhouse collection system and no auxiliary feature to augment solar .heat collection. Double-acrylic cover improves energy savings, but not significantly over the winter months either.

8. In months with more solar radiation, the crop canopy has more transpiration heat loss, which constitutes a good portion of incoming solar radiation. Collection

efficiency is therefore lower than it could otherwise achieve with a less dense canopy.

9. As far as model sensitivity is concerned, thermal performance is sensitive to the Bowen ratio and the maximum allowable ventilation rate. The model is mildly sensitive to the shading factor due to structural members. It is insensitive to initial storage temperatures, and practically so for different solar radiation processing algorithms.

10. Given the same plant and cultural practices, tomato crop canopy net photosynthetic rate is higher in the Guelph region than the Vancouver region because of better natural light conditions.

11. If CO_2 is replenished in solar greenhouses, net photosynthesis is greater for collection systems that use modified greenhouse shapes, whereby one with internal reflective surface has the best performance. However, reduction in primary production can be expected with twin-walled cover.

12. Correlations are developed for design curves that depict the relation between monthly solar load ratio and monthly total solar contribution. They are also generated for monthly solar heating fraction as a function of monthly total solar contribution.

13. There exists a value of total solar contribution, below which solar heating fraction is essentially zero.

14. The system thermal performance can be characterized by a location's solar load ratio, so that the design curves so developed are location-independent. For the Canadian locations, the solar load ratio for most months in the heating seasons is low because of medium to low solar radiation and high heating demand.

Though the design curves are presented as the final results of this study, it is by no means the only tool for evaluating alternative designs. The computer program developed by the author can indeed be used as a direct tool in design, provided that users have access to alternative solving packages for various submodels.

Possible future works are suggested in the following section. They may be divided into analytical work and experimental work.

1. analytical work

   The computer modeling and simulation method can be improved in order to get more accurate estimates of the absolute values of system thermal performance indices. Additional modeling efforts can be made within the framework of the present study. The following areas may be addressed:

   a. A transient model of the greenhouse thermal environment is needed for more precise prediction of storage charging and discharging times, and for determining when ventilation is required after surplus solar heat is collected and delivered to storage. This transient analysis can also be used for estimating the ventilation requirement for CO_2 replenishment in a solar greenhouse. The set of simultaneous nonlinear equations have to be solved at time intervals shorter than one hour, and may therefore necessitate the solving of simultaneous ordinary differential equations.

   b. Other pipe network configurations can be considered, such as vertical pipe settings. With this arrangement, the soil thermal storage may be analyzed by an axisymmetric finite element program so that the effect of pipe length can be properly assessed. This would need the assumption of no interaction between adjacent pipes, which is likely the case if space permits pipes to be separated by at least six pipe diameters.

   c. energy required by fan during the charging and discharging operations.

   d. use average hour-by-hour year-long climatological data (such as the typical meteorological year) as inputs for simulation and compare results with the present study. This method, however, is only feasible for U.S. locations at present.

e. More detailed modeling on various stages of crop growth and development, as affected by aerial environmental factors.

f. Economic modeling to assess the overall costs and benefits of alternative designs.

The scope of the study may also be expanded to cover the following cases:

a. multispan greenhouses

b. plastic covers with much light diffusive power

c. external solar collection systems

d. other sensible heat storage devices like water and solar pond

e. latent heat storage device

2. experimental work

a. The 'rate of decay tracer gas technique' can be applied to measure the ventilation rate, N, due to natural ventilation method. Accurate values of N need to be obtained for different extents of openings of the ventilation panels located at the ridge or the side. These values can then be used in the control algorithm of the microprocessor for more precise control of the requirement for ventilation of uncollected surplus solar heat. If CO_2 is used as the tracer gas, the rate of CO_2 replenishment can be measured at the same time.

b. CO_2 enrichment

experiments can be carried out to study the effect of CO_2 enrichment time on system thermal performance and crop performance, while minimizing the ventilation requirement.

c. latent heat recovery

While the collection efficiency could be improved if less ventilation takes place, humidity control is still necessary. The recovery of latent heat serves the dual purpose of removing excessive greenhouse moisture and further enhancing the collection efficiency. It is preferred that devices that accomplish this task be located inside the greenhouse rather than having moisture condensed in the storage medium, which is less effective and even undesirable.

d. The leaf Bowen ratio of greenhouse crops shall be measured during the entire heating season so that a seasonal variation pattern can be obtained under solar greenhouse climates. Alternatively, the plant resistance to water vapour diffusion can be measured. The objective is to get a more accurate relationship between transpiration and incoming solar radiation. The results would be needed for the estimation of latent heat recovery.

e. Bioassays may be done to acquire data for detailed modeling of plant growth and development.

f. If resources are available, the potential energy savings of a solar greenhouse with twin-walled cover such as acrylic or rigid PVC shall be evaluated.

Some of the above suggested experiments may be carried out in existing solar greenhouse research facilities, while others may be performed in smaller scale setups.

BIBLIOGRAPHY

Acock,B., D.A. Charles-Edwards, D.J. Fitter, D.W. Hand, L.J. Ludwig, J. Warren-Wilson and A.C. Withers. 1978. The contribution of leaves from different levels within a tomato crop to canopy net photosynthesis: an experimental examination of two canopy models. J. Exp. Bot. 29(111): 815-827.

Albright, L.D., I. Seginer and L.W. Langhans. 1979. Q-MATS as passive solar collectors. Proc. 4th Annu. Conf., solar energy for heating greenhouses and greenhouse-residence combinations, Piscataway, New Jersey, p. 61-71.

Aldrich, R.A. and J.W. White. 1973. The design and evaluation of rigid plastic greenhouses. Trans. ASAE, Vol. 16, p.994-996, 1001.

Aldrich, R.A., R.J. Downs, D.T. Krizek and L.E. Campbell. 1983. The effect of environment on plant growth. In: Ventilation of Agricultural Structures.M.A. Hellickson and J.N. Walker, (eds.). ASAE Monograph No. 6. pp. 217-254.

Amsen, M.G. 1981. Environmental conditions in different types of greenhouses. Acta Hortic. 115: 99-104.

Areskoug, M. and P. Wingstroem. 1980. Preparatory experiments on seasonal storage in earth of excess solar heat from greenhouse. Report 11, Dept. of Farm Buildings., Swedish University of Agricultural Sciences, Lund, 50 pp.

Arinze, E.A., G.J. Schoenau and R.W. Besant. 1984. A dynamic thermal performance simulation model of an energy conserving greenhouse with thermal storage. Trans. ASAE, 27(2): 508-519.

ASHRAE Handbook of Fundamentals. 1981. Publ. American Society of Heating, Refrigerating and Air-Conditioning Engineers, New York.

Avezov, R.R., Sh. K. Nigazov, A.A. Abdullaev and K. Zhomuratov. Effect of plant cover on the temperature regime of a solar heated greenhouse. Appl. Sol. Energy 21(5):47-49.

Avissar, R. and Y. Mahrer. 1982. Verification study of a numerical greenhouse microclimate model. Trans. ASAE 25(6): 1171-1720.

Balcomb, J.D. and R.D. McFarland. 1978. A simple empirical method for estimating the performance of a passive solar heated building of the thermal storage wall type. In Proc. 2nd Nat. Passive Solar Conf., p.377-382.

Bauerle, W. L. and T.H. Short. 1984. Carbon dioxide depletion effects in energy efficient greenhouses. Acta Hort. 148: 627-632.

van Bavel, C.H.M., C.J. Sadler and G.C. Heathman. 1980. Infra-red filters as greenhouse covers: Preliminary test of a model for evaluating their potential. Agricultural Energy II, p.552-557.

Beckman, W.A., S.A. Klein and J.A. Duffie. 1977. Solar heating design by the f-chart method. Wiley Interscience, New York.

Bégin, S., A. Gosselin, M.J. Trudel, P.A. Duke and R. Chagnon. 1984. Evaluation of a hemisphere solar greenhouse. Acta Hortic. 148: 745–750.

Bello, R.L. 1982. Evapotranspiration in greenhouses. Ph.D. Thesis, Geography Department, McMaster University, Hamilton, Ontario. 151 pp.

Ben-Abdallah, N. 1983. Solar heating of integrated greenhouse-animal shelter systems. Ph.D. Thesis, Dept. of Bio-Resource Engineering, The University of British Columbia, Vancouver, B.C. 565 pp.

Bird, R.B., W.E. Stewart and E.N. Lightfoot. 1960. Transport phenomena. Wiley, New York.

Blackwell, J., G. Shell and K.V. Garzoli. 1982. A simple solar energy system for greenhouse heating. Agric. Eng. Aust., 11(1): 9–16.

Bot, G.P.A. 1983. Greenhouse climate: from physical processes to a dynamic model. IMAG, Wageningen, 239 pp.

Boulard, T. and A. Baille. 1986a. Simulation and analysis of soil heat storage systems for a solar greenhouse. I. Analysis. Energy Agric. 5: 175–184.

Boulard, T. and A. Baille. 1986b. Simulation and analysis of soil heat storage systems for a solar greenhouse. II. Simulation. Energy Agric. 5: 285–293.

Bredenbeck, H. 1985. Influence of different glazing materials on the light transmissivity of greenhouses. Acta Hortic. 170:111–115.

Buitelaar, K., G.P.A.van Holsteijn, G.W.H.Wells and C.M.M.van Winden. 1984. Effects of different insulation materials in glasshouse walls on growth and production of tomatoes. Acta Hort. 148:511–517.

Businger, J.A. 1963. The glasshouse (greenhouse) climate. In: Physics of Plant Environment, p. 227–318. Ed. W.R. van Wijk. North-Holland Publ. Co., Amsterdam.

Caffell, A. and K.T. MacKay. 1981. Mud storage: a new concept in greenhouse heat storage. In: Energy conservation and use of renewable energies in the bio-industries. Ed. F. Vogt. Pergamon Press, New York, p.75–83.

Campbell, G.S. 1977. An introduction to environmental biophysics. Springer-Verlag, New York. 159 pp.

Carnegie, E.J., P. Niles and J. Pohl. 1982. Feasibility study of linking solar ponds to greenhouses. ASAE Pap. 82-4537.

Challa, H. and A.H.C.M. Schapendonk. 1984. Quantification of effects of light reduction in greenhouses on yield. Acta Hortic. 148: 501-507.

Chandra, P., L.D. Albright and N.R. Scott. 1981. A time-dependent model of the greenhouse thermal environment. Trans. Amer. Soc. Agr. Eng. 24(2):442-449.

Chandra, P. and D.H. Willits. 1981. Pressure drop and heat transfer characteristics of air-rockbed thermal storage systems. Solar Energy 27(6):547-553.

Charles-Edwards, D.A. 1981. The mathematics of photosynthesis and productivity.

Academic Press, London, 127 pp.

Chiapale, J.P., J. Damagnez and P. Denis. 1977. Modification of a greenhouse environment through the use of a collecting fluid. Proc. Int'l Sym. on controlled environment agriculture. Ed. N.H. Jensen. Tucson, Arizona, p.122-137.

Close, D.J. 1967. A design approach for solar processes. Sol. Energy, 11(2): 112-121.

Close, D.J., R.V. Dunkle and K.A. Robeson. 1968. Design and performance of a thermal storage air conditioning system. Mech. and Chem. Eng. Trans. of the Institute of Engineers, Australia. Vol. MC4, No. 1, p. 45-54.

Collares-Pereira, M. and A. Rabl. 1979. The average distribution of solar radiation and correlations between diffuse and hemispherical and between daily and hourly insolation values. Sol. Energy 22(2): 155-165.

Connellan, G.J. 1985. Performance aspects of a solar water heated greenhouse. Agric. Eng. Aust. 14(1): 18-22.

Cooper, P. I. and R. J. Fuller. 1983. A transient model of the interaction between crop, environment and greenhouse structure for predicting crop yield and energy consumption. J. Agr. Eng. Res. 28: 401-417.

Coutier, J.P. and E.A. Farber. 1982. Two applications of a numerical approach of heat transfer process within rock bed. Sol. Energy 29(6): 451-462.

Critten, D.L. 1984. The effect of geometric configuration on the light transmission of greenhouse. J. Agric. Eng. Res. 29: 199-206.

Curry, R.B. 1971. Dynamic simulation of plant growth - Part I. Development of a model. Trans. ASAE 14(5):946-949, 959.

Curry, R.B. and L.H. Chen. 1971. Dynamic simulation of plant growth - Part II. Incorporation of actual daily weather and partitioning of net photosynthate. Trans. ASAE 14(6):1170-1174.

Dale, A.C., V.M. Puri and P.A. Hammer. 1984. A special heat conserving greenhouse with solar heated soil for crop (tomato) production. Acta Hortic. 148: 731-738.

Dale, A.C., V.M. Puri and P.A. Hammer. 1980. Analysis and summary of a solar air collector-groundwater heat storage greenhouse heating system. Agric. Energy II, American Society of Agricultural Engineers, St. Joseph, MI, pp. 513-523.

van Die, P. 1980. Solar heating in greenhouses. Can. Agric. Eng. 25(2):8-10.

Draper, N.R. and H. Smith. 1981. Applied regression analysis. 2nd Ed., Wiley, New York. 709 pp.

Duffie, J.A. and W.A. Beckman. 1980. Solar Engineering of Thermal Processes. Wiley, New York, 762 pp.

Duncan, W.G. and J.D. Hesketh. 1968. Net photosynthetic rates, relative growth rate and leaf numbers of 22 races of maize grown at eight temperatures. Crop Sci 8:670-674.

Duncan, G.A., O.J. Loewer, Jr. and D.G. Colliver. 1976. Simulation of energy flows in a greenhouse: Magnitudes and conservation potential. Trans. ASAE, 24(4): 1014–1021.

Eckhoff, S.R. and M.R. Okos. 1980. Thermal storage comparison and design for rock, saturated soil and sodium sulfate decahydrate for agricultural applications. Trans. ASAE 23(3): 722–728, 734.

Edwards, R.I. and J.V. Lake. 1965. Transmission of solar radiation in a large span east-west glasshouse. J. Agric. Eng. Res. 10(2): 125–131.

Eldighidy, S.M. and I.S. Taha. 1983. Optimum mass flow rate of water in flat plate solar collector coupled with a storage tank and an organic Rankine cycle power loop. Sol. Energy 31(5): 455–461.

Elwell, D.L., M.Y. Hamdy, A.E. Ahmed, H.N. Shapiro, J.J. Parker and S.E. Johnson. 1985. Soil heating using subsurface pipes: a decade of research result at OSU/OARDC. Research Bull. 1175. The Ohio State University, Ohio Agricultural Research and Development Cebter, Wooster, Ohio. 54 pp.

Enoch, H.Z. 1978. A theory for optimalization of primary production in protected cultivation. I. Influence of aerial environment upon primary plant production, and II. Primary plant production under different outdoor light regimes. Acta Hortic. 76: 31–57.

Enoch, H.Z. and R. G. Hurd. 1977. Effect of light intensity, CO_2 concentration and leaf temperature on gas exchange of spray carnation plants. J. Exp. Bot. 28: 84–95.

Enoch, H.Z. and J.M. Sacks. 1978. An empirical model of CO_2 exchange of a C-3 plant in relation to light, CO_2 concentration and temperature. Photosynthetica 12(2):150–157.

Environment Canada, 1983. Canadian climate normals 1951–1980, Vols. 1, 2, 5, 7, 8. Atmospheric Environment Service, Downsview, Ont.

Feingold, A. 1966. Radiant-interchange configuration factors between various selected plane surfaces. Proc. Royal Society of London. Series A. Mathematical and Physical Sciences, Vol. 292, p.51-60.

Ferare, J. and K.L. Goldsberry. 1984. Environmental conditions created by plastic greenhouse covers. Acta Hortic. 148: 675–682.

Fohr, J.P. and A.R. Figueiredo. 1987. Agricultural solar air collectors: design and performances. Sol. Energy 38(5): 311–321.

France, J. and J.H.M. Thornley. 1984. Mathematical models in agriculture. Butterworths, London, 335 pp.

Froehlich, D.P., L.D. Albright, N.R. Scott and P. Chandra. 1979. Steady-periodic analysis of greenhouse thermal environment. Trans. ASAE 22: 387–399.

Fynn, R.P., T.M. Short and S.A. Shah. 1980. The practical operation and maintenance of a solar pond for greenhouse heating. Agric. Energy II, Gaastra, P. 1963. Climate control of photosynthesis and respiration. In: Environmental control of plant growth, L.T. Evans, ed. Academic Press, New York, pp. 113–140.

Garzoli, K.V. and J. Blackwell. 1973. The response of a glasshouse to high solar radiation and ambient temperature. J. Agric. Eng. Res. 18: 205–216.

Garzoli, K.V. and J. Blackwell. 1981. An analysis of the nocturnal heat loss from a single skin plastic greenhouse. J. Agric. Eng. Res. 26: 203–214.

Garzoli, K.V. and G. Shell. 1984. Performance and cost analysis of an Australian solar greenhouse. Acta Hortic. 148: 723–729.

Gates, D.M. and C.M. Benedict. 1962. Convection phenomena from plants in still air. Am. J. Bot. 50: 563–573.

Godbey, L.C., T.E. Bond and H.F. Zornig. 1979. Transmission of solar and long-wave length energy by materials used as covers for solar collectors and greenhouses. Trans. ASAE 22(5): 1137–1144.

Gosselin, A. and M. J. Trudel. 1983. Interaction between air and root temperature on greenhouse tomato. I. growth, development and yield. J. Amer. Soc. Hort. Sci. 108(6):901–905.

Hamilton, D.C. and W.R. Morgan. 1952. Radiant interchange configuration factors. NACA Tech. Note No. 2836.

Hanan, J.J., W.D. Holley and K.L. Goldsberry. 1978. Greenhouse management. Springer-Verlag, New York. 530 pp.

Hay, J.E. 1979. Calculation of monthly mean solar radiation for horizontal and inclined surfaces. Sol. Energy 23(4): 301–307.

Heinemann, P.H. and P.N. Walker. 1987. Effects of greenhouse surface heating water on light transmission. Trans. ASAE 30(1):215–220.

Hesketh, J.D. and J.W. Jones. 1980. Predicting photosynthesis for ecosystem models I. CRC Press, Boca Raton, FL., 273 pp.

Howell, J.R. 1982. A catalog of radiation configuration factors. McGraw Hill, New York. 243 pp.

Hughes, P.J., S.A. Klein and D.J. Close. 1976. Packed bed thermal storage model for solar air heating and cooling systems. J. Heat Transfer, 98: 336–337.

Hurd, R. G. 1983. Energy saving techniques in greenhouses and their effects on tomato crop. Scientific Horti. 34:94–101.

Hurd, R.G. and J.H.M. Thornley. 1974. An analysis of the growth of young tomato plants in water culture at different light integrals and CO concentrations. I. Physiological aspects and II. A mathematical model. Ann. Bot. 38:375–388, 389–400.

Ingersoll, L.R. and H.J. Plass. 1948. Theory of the ground pipe heat source for the heat pump. Trans. of the American Society Heating and Ventilating engineers, Vol.54, p.339–348.

Ingratta, F.J. and T.J. Blom. 1981. The potential of an active solar system for heating of commercial greenhouses in Ontario. In: Symp. More Profitable Use of Energy in Protected Cultivation. Acta Hortic. 115: 131-141.

Iqbal, M. 1983. An Introduction to Solar Radiation. Academic Press, Toronto, Ont., 390 pp.

Iqbal, M. and A.K. Khatry. 1976. Wind coefficients from long semi-circular greenhouses. Trans. ASAE 19:911-914.

Iqbal, M. and A.K. Khatry. 1977. Wind-induced heat transfer coefficients from greenhouses. Trans. ASAE, 20: 157-160.

Jaffrin, A. and P. Cadier. 1982. Latent heat storage applied to horticulture. Sol. Energy 28(4): 313-321.

Jakob, M. 1949. Heat Transfer. Wiley, New York, 758 pp.

Johnson, I.R., T.E. Ameziane and J.H.M. Thornley. 1983. A model of grass growth. Ann. Bot. 51:599-609.

Kendrick, J.H. and J.A. Havens. 1973. Heat transfer models for a subsurface, water pipe, soil-warming system. J. Environ. Quality, 2(2): 188-196.

Kimball, B.A. 1973. Simulation of the energy balance of a greenhouse. Agic. Meteorol. 11: 243-260.

Kimball, B.A. 1981. A versatile model for simulating many types of solar greenhouses. ASAE Pap. 81-4038.

Kimball, B.A. 1986. A modular energy balance program including subroutines for greenhouses and other latent heat devices. U.S. Department of Agriculture, Agricultural Research Services, ARS-33, 360 pp.

Kimball, B.A. and Bellamy. 1986. Generation of diurnal solar radiation, temperature, and humidity patterns. Energy in Agric. 5: 185-197.

Kindelan, M. 1980. Dynamic modeling of greenhouse environment. Trans. ASAE 23(5):1232-1239.

Klapwijk, D. 1987. Effects of light and temperature on tomato growth and production. Annual Conf., American Greenhouse Vegetable Growers Association, Aug. 11-14, Richmond, B.C.

Klein, S.A. 1977. Calculation of monthly average insolation on tilted surfaces. Solar Energy 19:325.

Klein, S.A., W.A. Beckman and J.A. Duffie. 1976. A design procedure for solar heating systems. Sol. Energy 18: 113-127.

Klein, S.A., P.I. Cooper, T.L. Freeman, D.M. Beekman, W.A. Beckman and J.A. Duffie. 1975. A method of simulation of solar processes and its applications. Sol. Energy 17(3): 29-37.

Klucher, T.M. 1979. Evaluation of models to predict insolation on tilted surfaces. Sol.

Energy 23(2): 111-114.

Kozai, T. 1977. Direct solar light transmission into single-span greenhouses. Agric. Meteorol. 18:329-338.

Kozai, T., K. Shida and I. Watanabe. 1986. Thermal performance of a solar greenhouse with water tanks for heat storage and heat exchange. J. Agric. Eng. Res. 33:141-153.

Kreith, F. and W.Z. Black. 1980. Basic Heat Transfer. Harper and Row, New York, 558 pp.

Lau, A.K. and L.M. Staley. 1984. Solar radiation transmission in greenhouses. ASAE Pap. 84-4525. 18pp.

Lawand, T.A., R. Alwand, B. Soulnier and E. Brunet. 1975. The development and testing of an environmentally designed greenhouse for colder regions. Sol. Energy 17: 307-312.

Lei, Q., M.G. Britton and J.S. Townsend. 1985. Modeling air tempering with a soil-heat sink/source. ASAE Pap. 85-4016.

Liu, B.Y.H. and R.C. Jordan. 1960. The interrelationship and characteristic distribution of direct, diffuse and total solar radiation. Sol. Energy 4: 1-9.

Liu, R.C. and G.E. Carlson. 1976. Proposed solar greenhouse design. Proc. Sol. Energy - Fuel and Food Workshop. Ed. M.H. Jensen, pp. 129-141.

Löf. G.O.G. and R.W. Hawley. 1948. Unsteady-state heat transfer between air and loose solids. Ind. Eng. Chem. 40: 1061-1070.

Ludwig, L.J., T. Saeki and L. T. Evans. 1965. Photosynthesis in artificial communities of cotton plants in relation to leaf area. I. Experiments with progressive defoliation of mature plants. Aust. J. Biol. Sci. 18:1103-1118.

Maher, M.J. and T. O'Flaherty. 1973. An analysis of greenhouse climate. J. Agric. Eng. Res. 18:197-203.

Mair, S.G. 1984. Surface visualization routines. Computing Centre, The University of British Columbia, Vancouver, B.C.

Major, P., N. Beidleman and J.F. Kreider. 1982. Direct calculation of annual solar fractions and economic optimal areas for attached-sunspaces: gh-chart. In: Proc. of the ASME solar energy division, 4th Ann. Conf., Albuquerque, NM, p.210-213.

Manbeck, H.B. and R.A. Aldrich. 1967. Analytical determination of direct visible solar energy transmitted by rigid plastic greenhouses. Trans. ASAE 10(4): 564-567, 572.

Mastelerz, J.W. 1979. The greenhouse environment. Wiley, New York. 629 pp.

McAdams, W.C. 1954. Heat Transmission. McGraw-Hill, New York.

McCormick, P.O. 1976. Performance of non-integral solar collector greenhouses. Proc. of the Solar Energy - Fuel and Food Workshop. N.H. Jensen, Ed. Environmental

Research Laboratory, The University of Arizona, Tucson. p. 51-60.

McCree, K. 1970. An equation for the rate of respiration of white clover plants grown under controlled conditions. In Prediction and measurement of photosynthetic productivity. Ed. I. Setlick. Centre for Agr, Publ. and Doc., Wageningen.

Mears, D.R., W.J. Roberts, J.C. Simpkins and P.W. Kendall. 1977. The Rutgers solar heating system for greenhouses. ASAE Pap. 77-4009.

Meyer, G.E., R.B. Curry, J.G. Streeter and H.J. Mederski. 1979. A dynamic simulator of soybean growth, development and seed yield. I. Theory, structure and validation. Res. Bull. #1113, Ohio Agricultural Research and Development Center, Wooster, Ohio.

Milburn, W.F. and R.A. Aldrich. 1979. Optimization of excess internal heat collection and thermal storage in greenhouses. ASAE Pap. 79-4026.

Milburn, W.F., R.A. Aldrich and J.W. White. 1977. Internal/External solar collectors for greenhouse heating. ASAE Pap. 77-4008.

Milby, R.V. 1973. Plastics technology. McGraw-Hill, New York. 581 pp.

Monk, G.J., L.M. Staley, J.M. Molnar and D.H. Thomas. 1983. Design, construction and performance of two earth thermal storage solar greenhouses. CSAE Pap. No. 83-405.

Monsi, M. and Y. Murata. 1970. Development of photosynthetic systems as influenced by distribution of matter. In Prediction and measurement of photosynthetic productivity.

Monteith, J.L. 1965a. Light and crop production. Field crop abstracts. 18: 213-219.

Monteith, J.L. 1965b. Light distribution and photosynthesis in field crops. Ann. Bot. N.S. 29:17-37.

Moore, C. 1981. UBC Curve - curve fitting routines. Computing Center, The University of British Columbia, Vancouver, B.C.

Moore, C. 1984. UBC NLE - zeros of nonlinear equations. Computing Centre, The University of British Columbia, Vancouver, B.C.

Morris, L.G., F.E. Neale and J.D. Postlethwaite. 1956. The transpiration of glasshouse crops, and its relationship to the incoming solar radiation. J. Agric. Eng. Res. (1): 111-122.

Moss, G.I. 1983. Root-zone warming of tomatoes in nutrient-film as means of reducing heating requirements. J. Hort. Sci. 58(1): 103-109.

Mumma, S.D. and W.C. Marvin. 1976. A method of simulating the performance of a pebble bed thermal energy storage and recovery system. ASME Pap. 76-HT-73.

Nagaoka, M. and K. Takahashi. 1983. Effect of multivariable control of environmental factors on the growth and yield of glasshouse tomatoes. Bull. series A #11, Veg. and Ornm. crops Res. Stn.

National Climatic Center. 1979. Climatic Atlas of the United States. Asheville, North Carolina.

National Climatic Center. 1981. Typical Meteorological Year, Hourly solar radiation - surface meteorological observations. User's manual TD-9734. Asheville, North Carolina.

Nicol, T. 1987. UBC MOL1D - The method of lines solution of partial differential equations in one spatial dimension. Computing Center, The University of British Columbia, Vancouver, B.C.

Nishina, H. and T. Takakura. 1984. Greenhouse heating by means of latent heat storage units. Acta Hortic. 148: 751-754.

Nobel, P.S. 1974. Introduction to biophysical plant physiology. Freeman and Co., San Francisco, 488pp.

Ouellet, C.E., R. Sharp and D. Chaput. 1975. Estimated monthly normals of soil temperature in Canada. Agrometeorological Research Service, Canada Department of Agriculture. Tech. Bull. 85, Ottawa, Ont.

Paez, A., H. Hellmers and B.R. Strain. 1984. CO_2 enrichment and water stress interaction on growth of two tomato cultivars. J. Agr. Sci. (UK) 102:687-693.

Page, J.K. 1964. The estimation of monthly mean values of daily total short-wave radiation on vertical and inclined surfaces from sunshine records for latitudes 40 °N - 40 °S. Proc. UN Conf. New Sources of Energy, Vol. 4, pp. 378-390.

Pallas, J. E., Jr. 1965. Transpiration and stomatal opening with changes carbon dioxide content of the air. Science 147:171-173. Vegetable Workshop Bulletin.

Papadopoulos, A. P. and T.J. Jewett. 1984. Comparative tomato growth, development and yield in twin-wall PVC panel and single glass greenhouse. Acta Hortic. 148:611-618.

Pappas, S.L. and C.R. Freberg. 1949. Heat transfer of buried pipe in clay or sand. Heating and Ventilating, Vol. 46, p. 85-86.

Parker, B.F., T.C. Bridges, L.R. Walton and D.G. Colliver. 1983. Design equations for particle bed heat storages. Trans. ASAE, 26(5): 1482-1485.

Parker, J.J., M.Y. Hamdy, R.B. Curry and W.L. Roller. 1981. Simulation of buried warm water pipes beneath a greenhouse. Trans. ASAE, 24(4): 1022-1025, 1029.

Portales, B., M. Martin, M. Le Ray and R. Torguet. 1982. Experimentation of the heating of greenhouses with solar energy stored in subsoil in the north of France. Energex '82 Conf. Proc. Vol. I, F.A. Curtis, Ed. Aug. 23-29, Regina, Saskatchewan. p.381-384.

Puri, V.M. 1981. Nomographs for design optimization of greenhouse-rock storage-collector system. ASAE Pap. 81-4043.

Puri, V.M. 1984. Performance curves for earth tube heat exchangers. ASAE Pap. 84-4537.

Riaz, M. 1978. Transient analysis of packed-bed thermal storage systems. Sol. Energy 21:123-128.

Rietveld, M.R. 1978. A new method for estimating the regression coefficient in the formula relating solar radiation to sunshine. Agric. Meteorol. Vol. 19, p.243-252.

Rijtema,P.E. 1969. Derived meteorological data: transpiration. Misc. reprints 67. I.C.W. Wageningen.

Robbins, F.V. and C.K. Spillman. 1977. Solar radiation transmission through two transparent covers. Trans. ASAE 23(5):1224-1231.

Robbins, F.V. and C.K. Spillman. 1980. Computer modeling of a ventilated Trombe wall - with actual performance results. Sol. Energy 25:207-213.

Rotz, C.A., R.A. Aldrich and J.W. White. 1979. Computer predicted energy savings through fuel conservation systems in greenhouses. Trans. ASAE, 22(2): 362-366, 369.

Russell, R.W.J. 1985. An analysis of the light transmittance of twin-walled materials. J. Agric. Eng. Res. Vol. 31, p.31-53.

Saeki, T. 1960. Interrelationships between leaf amount, light distribution and total photosynthesis in a plant community. Bot. Mag. Tokyo 73: 55-63.

Saez, A.E. and B.J. McCoy. 1982. Dynamic response of a packed bed thermal storage system - a model for solar air heating. Sol. Energy 29(3): 201-206.

Salisbury, F.B. and C.W. Ross. 1978. Plant physiology. Wadsworth, London, 422 pp.

Santamouris, M. and C.C. Lefas. 1986. Thermal analysis and computer control of hybrid greenhouses with subsurface heat storage. Energy Agric. 5:161-173.

Schumann, T.E.W. 1929. Heat transfer: liquid flowing through a porous prism. J. Franklin Inst. 208: 405-416.

Sears, F.W. and M.W. Zemansky. 1960. College Physics. Addison-Wesley, Reading, MA, 1024 pp.

Seginer, I. and L.D. Albright. 1983. Greenhouse operation for best aerial environment. Final research report. Technion Israel Inst. of Tech., Agri. Eng. Dept., Haifa, and Cornell Univ., Agr. Eng. Dept., Ithaca, New York.

Seginer, I. and N. Levav. 1971. Models as tools in greenhouse climate design. Agricultural Engineering Dept. Publ. #115. Technion - Israel Institute of Technology, Haifa, 88 pp.

Seginer, I. and A. Livne. 1978. Effect of ceiling height on the power requirement of forced ventilation in greenhouses: a computational study. IBM Israel Scientific Center, Haifa.

Sésták, Z. 1985. Gas exchange and dry matter accumulation during leaf development. in Photosynthesis during leaf development. DR W. Junk Publishers, Dordrecht, The Netherlands.

Shah, S.A., T.H. Short and R.P. Fynn. 1981. Modeling and testing a salt gradient solar pond in Northeast Ohio. Sol. Energy, 27:393-401.

Sherry, W.J., J.W. White, F.W. Schmidt, and G.A. Sanders. 1980. Energy conservation and solar energy utilization for greenhouses. Ag. Energy II, American Society of Agricultural Engineers, St. Joseph, MI, pp. 513-523.

Short, T.H. and J.I. Montero. 1984. A comparison of solar heated greenhouses in Wooster, Ohio (USA) and Malaga (Southern Spain). Acta Hortic. 148: 805-813.

Sibley, K.J. and G.S.V. Raghavan. 1984. Heat transfer coefficients for air flow in plastic corrugated drainage tubes. Can. Agric. Eng. 26(2): 177-180.

Siegel, R. and J.R. Howell. 1969. Thermal Radiation Heat Transfer, II. NASA Sp-164, Washington, D.C., 285 pp.

Simpkins, J.C., D.R. Mears and W.J. Roberts. 1976. Reducing heat losses in polyethylene covered greenhouses. Trans. ASAE 19: 714-719.

Sissom, L.E. and D.R. Pitts. 1972. Elements of transport phenomena. McGraw Hill, New York. 814 pp.

Slack, G. and A. Calvert. 1972. Control of carbon dioxide concentration in glasshouses by use of conductimetric controllers. J. Agric. Eng. Res. 17:107-115.

Smith, C.V. and H.G. Kingham. 1971. A contribution to glasshouse design. Agric. Meteorol. 8: 447-468.

Smith, I.E., M.J. Savage and P. Mills. 1984. Shading effects on greenhouse tomatoes and cucumbers. Acta Hortic. 148: 491-500.

Soribe, F.I. and R.B. Curry. 1973. Simulation of lettuce growth in an air-supported plastic greenhouse. J. Agr. Eng. Res. 18:133-140.

Staley, L.M., J.M. Molnar and G.J. Monk. 1982. First year performance of a shed-type solar greenhouse. In: Conference Proc. Energex '82, Vol. II, University of Regina, Saskatchewan.

Staley, L.M., J.M. Molnar and G.J. Monk. 1984. A comparative study of solar energy capture, use and conservation in conventional, solar shed, rock storage and wet earth thermal storage units. Third year report for Agriculture Canada, Sidney, B.C., 106 pp.

Swinbank, W.C. 1963. Long-wave radiation from clear skies. Quart. J. Royal Meteorol. Soc. 89: 89-94.

Takakura, T., K.A. Jordan and L.L. Boyd. 1971. Dynamic simulation of plant growth and environment in the greenhouse. Trans ASAE 14(5):964-971.

Takami, S. and Uchijima. 1977. A model for the greenhouse environment as affected by mass and energy exchange of a crop. J. Agric. Meteorol. 33(3): 117-127.

Telkes, M. 1977. Solar energy storage. In: Applications of solar energy for heating and cooling of buildings. R.C. Jordan and B.Y.H. Liu, (eds.). ASHRAE, Publ. GRP-170, New York.

Ting, K.C. and G.A. Giacomelli. 1987. Solar photosynthetically active radiation transmission through greenhouse glazings. Energy Agric. 6(4):1-12.

Turkewitsch, A. and E. Brundrett. 1979. Light levels in insulated greenhouses. Joint Meeting ASAE/CSAE, 24-27 June, University of Manitoba, Winnipeg, Man. Pap. 79-4023.

Walker, J.N. 1965. Predicting temperatures in ventilated greenhouses. Trans. ASAE, 8(3): 445-448.

Walker, J.N., R.A. Aldrich and T.H. Short. 1983. Quantity of air flow for greenhouse structures. In: Ventilation of Agricultural Structures. M.A. Hellickson and J. N. Walker, (eds.). ASAE Monograph No. 6.

Walker, P.N. and D.C. Slack. 1970. Properties of greenhouse covering materials. Trans. ASAE, Vol. 13, p. 682-684.

Welles, G.W.H., G.P.A. van Holsteyn, S.V.D. Berg and K. Buitelaar. 1983. In Horticultural Abstracts 1983 issue.

Went, F.W. 1945. Plant growth under controlled conditions. V. The relation between age, light, variety and thermoperiodicity of tomatoes. Am. J. Bot. 32: 469-479.

White, H.C. and S.A. Korpela. 1979. On the calculation of the temperature distribution in a packed bed for solar energy applications. Sol. Energy, Vol. 23, p.141-144.

Whittle, R.M. and W.J.C. Lawrence. 1960. The climatology of glasshouses, II. Ventilation. J. Agric. Eng. Res. 5(1): 36-41.

Wilhelm, L.R. 1976. Numerical calculations of psychrometric properties in S.I. units. Trans. ASAE 19: 318-321, 325.

Willits, D.H., P. Chandra and C.H. Miller. 1980. A solar energy collection /storage system for greenhouses: observed and simulated performance. Agric. Energy II, pp. 524-530.

Willits, D.H., P. Chandra and M.M. Peet. 1985. Modeling solar energy storage systems for greenhouses. J. Agric. Eng. Res. 32: 73-93.

Willits, D.H. and M.M. Peet. 1987. Factors affecting the performance of rockstorages as solar energy collection/storage systems for greenhouses. Trans. ASAE, 30(1): 221-232.

Wilson, G.E., D.R. Price, L.D. Albright, N.R. Scott, R.W. Langhans and P. Chandra. 1977. Experimental results of a greenhouse solar collection and modular gravel storage system. In: Proc. 2nd Annu. Conf. Heating Greenhouses, Cleveland, OH, pp. 256-285.

Wilson, G.E., D.R. Price and R.W. Langhans. 1977. Increasing the effectiveness of the greenhouse as a solar collector. ASAE Pap. No. 77-4527.

van Winden, C.M.M., J.A.M. van Uffelen and G.W.H. Welles. 1984. Comparison of effect of single and double glass greenhouses on environmental factors and production of vegetables. Acta Hort. 148:567-573.

de Wit, C.T. 1967. Photosynthesis of leaf canopies. Ag. Res. report 663, I.B.S., Wageningen.

Wittwer, S.H. and S. Honma. 1979. Greenhouse tomatoes, lettuce and cucumbers. Michigan State University Press, East Lansing, Michigan.

van Zinderen Bakker, E. 1986. Personal Communication. Section head - plant physiology. Agriculture Canada Saanichton Research and Plant Quarantine Station, Sidney, B.C.

APPENDICES

A. Direct radiation interception factor and diffuse radiation view factor

B. Psychrometric equations

C. Listing of computer program *OVERALL*

D. Sensors and their locations

E. Listing of computer program *DESIGN*

Appendix C

```
C
C   . *OVERALL* to simulate long-term average performance of solar
C     heating systems for greenhouses, with rockbed or soil thermal
C     storage.
C
C     by Anthony K. Lau
C
C     units:
C
C        3: input data
C        5: outputs - greenhouse characteristics, including solar radiation
C                      interception factor and view factor
C        6:         - greenhouse temperatures, relative humidity, storage outlet
C                     temperature, useful heat gain, heat transferred to/from storage,
C                     effective transmissivity, solar load ratio, solar heating fractions
C        7:         - absorbed solar radiations, heat transfer coefficients,
C                     amounts of transpiration and condensation
C        8:         - net photosynthetic rate
C
      IMPLICIT REAL*8(A-H, O-Z)
      COMMON/DATA/TOUT, RHT(24), VW, RHSET
      COMMON/ENV/ CL, BOWEN
      COMMON/GEOM/GHL,GHW,BH,WH, RTILT1,RTILT2,S1,S3, GVOL
      COMMON/GROWTH/RK,RLAI,TAUC,EFLITE,TRANSM,RDO, PN(10)
      COMMON/INDEX/I, J
      COMMON/HEAT/TMAX(12), TMIN(12), HEATLD, QSUP, QPASS
      COMMON/LOGIC/FOR3, ALIGN
      COMMON/MAT/THCRC, RKCRC, RKP, THPIPE
      COMMON/OCCUR/ICALL, ICAL
      COMMON/OUT/RHINS, TRPN, TRSP, SUMQU, TPOUT, QTRAN, PN1
      COMMON/PROP/RHOP, ALPP, RHOG, RKG, THG, TAULW, EPC, EPP
      COMMON/PSYC/TDP, TC,TP, RH,WA, WCSAT,WPSAT,WOUT, TIN
      COMMON/RADIAN/PSI,RDELC(12),RLAT,RWI(24),RBDN,RGAM(6),RBETA(6)
      COMMON/ROCK/STCAP, FRATE, TINIT, RHOR
      COMMON/SOILV/TS(6),TSOUT(12),VMC,C1,C2,DIA,DPIPE,DINS,VSEP,RAREA, TRATE,DT,TF,LAYER,NL,NP
      COMMON/SOLAR/HBT, HDT, HPS, HBS, SCO, SCI, SP, SB
      COMMON/SUN/SR,SS, DA, WS, IRISE, ISET
      COMMON/SYSTEM/INSN, ISTDEV
      COMMON/TRMT/TAUD2, ALPD2, TAUA, TAUB2, ALPB2
      COMMON/VENT/NAE, NAEMAX
      COMMON/VIEW/F1P,FP1, F3P,FP3, FGP,FPG, F13,F31, F3G,FG3, ANGLE,RL,RN
c
      DIMENSION DBETA(6), DGAM(6)
      DIMENSION DELC(12), E(12), DWI(24)
      DIMENSION SUNHR(12), BSUNHR(12), RHO(12)
      DIMENSION RHO1(12),RHO7(12),RH13(12),RH19(12),VW(12)
      DIMENSION H(12,24), HD(12,24), HB(12,24), D(12), DBAR(12)
      DIMENSION F(6), P(6), REFLEC(6)
      DIMENSION SPN(10), WPN(10), FPN(10)
      LOGICAL INSN, ALIGN
C
C   READ INPUTS
C
C    Group 1 inputs: climatic data
C
      READ(3,18)IRUN, NFM, NLM
18    FORMAT(5I6)
      READ(3,16) DLAT
      READ(3,15) (DELC(I), I=1,12)
      READ(3,15) (E(I), I=1,12)
      READ(3,15) (RHO(I), I=1,12)
      READ(3,15) (SUNHR(I), I=1,12)
15    FORMAT(15F10.0)
      READ(3,18) IAVSOL
      IF (IAVSOL .EQ. 2)GOTO 5
      IF (IAVSOL .EQ. 3)GOTO 6
      DO 70 I=1, 12
       READ (3,16) (H(I,J), J=4,21)
70    CONTINUE
      GOTO 6
5     READ(3,16) (DBAR(I), I=1, 12)
6     READ(3,16) (TMAX(I), I=1,12)
      READ(3,16) (TMIN(I), I=1,12)
      READ(3,16) (RHO1(I), I=1,12)
      READ(3,16) (RHO7(I), I=1,12)
      READ(3,16) (RH13(I), I=1,12)
      READ(3,16) (RH19(I), I=1,12)
      READ(3,16) (VW(I), I=1,12)
16    FORMAT(20F6.0)
C
```

```
C    Group 2 inputs: greenhouse thermal environment parameters
C
      READ(3,17)INSN
17    FORMAT(L1)
      READ(3,18) ISTDEV
      READ(3,18) NAEMAX
      READ(3,12)NS, RLWR, AP, WH, TILT1, TILT2
      READ(3,12)NC, RKL, RI, RHO1, RHO3, THG, RKG, TAULW, SHADE
12    FORMAT(I6, 10F6.0)
      READ(3,16)(DGAM(I), I=1,NS)
      READ(3,16)(DBETA(I), I=1, NS)
      READ(3,16)RHOP, ALPP, APFACT, ALPB
      READ(3,16)CW1, CW2, CW3
      IF (ISTDEV .EQ. 1)GOTO 1
      IF (ISTDEV .EQ. 2)GOTO 2
C
C    Group 3A inputs: rockbed thermal storage parameters
C
1     READ(3,16)STCAP, FRATE, TINIT, RHOR
      GOTO 3
C
C    Group 3B inputs: soil thermal storage parameters
C
2     READ(3,12)NL, TF, DT
      READ(3,12)LAYER, DIA, DPIPE, VSEP,  DINS , RAREA, TRATE
      READ(3,16)VMC, C1, C2
      READ(3,16)THCRC, RKCRC, THPIPE, RKP
      READ(3,16) (TS(I), I=1,6)
3     READ(3,16) (TSOUT(I), I=1,12)
C
C    Group 4 inputs: crop growth function parameters
C
      READ(3,16) TRANSM, RDO
C
C   Constants
C
      PI=3.14159
      HSC=4.921
      RHOCLR = 0.25
      RHOCLD = 0.6
      CPA = 1012.5
      RHOA = 1.204
      ICALL = 0
      ALIGN = .TRUE.
C
      RDO = RDO * 1.D-3
      DO 160 KL=1, 5
       FPN(KL) = 0.
       WPN(KL) = 0.
160   CONTINUE
C
C   Conversion to radians
C
      RLAT = DLAT * PI/180.
      Q1 = DSIN(RLAT)
      Q2 = DCOS(RLAT)
      RTILT1 = TILT1 * PI/180.
      RTILT2 = TILT2 * PI/180.
      DO 90 I=1,12
       RDELC(I) = DELC(I) * PI/180.
```

```
      BSUNHR(I) = SUNHR(I)/30.
90    CONTINUE
      DO 80 I = 1, NS
       RGAM(I) = DGAM(I) * PI/180.
       RBETA(I) = DBETA(I) * PI/180.
80    CONTINUE
C
C    sum up hourly global solar radiation to obtain daily value
C
      IF (IAVSOL .NE. 1)GOTO 83
      DO 40 I=1, 12
       D(I) = 0.
       DO 50 J=4, 21
        D(I) = D(I) + H(I,J)
50     CONTINUE
40    CONTINUE
C
83    RKL2 = RKL * 0.5
      NC2 = NC * 0.5
      NNC = NC
      IF (NC .EQ. 1)NC2 = NC
      GHW = DSQRT(AP/RLWR)
      GHL = AP/GHW
C
      IF(TILT1 .EQ. 90.)T21 = 1./DTAN(RTILT2)
      IF(TILT2 .EQ. 90.)T21 = 1./DTAN(RTILT1)
      IF(TILT2 .NE. 90.)T21 = 1./DTAN(RTILT1) + 1./DTAN(RTILT2)
      BH = GHW/T21
      S1 = BH/DSIN(RTILT1)
      S3 = BH/DSIN(RTILT2)
      AC1 = S1*GHL
      AC3 = S3*GHL
      AB = 0.
      IF(INSN)AB = AC3
      AG = BH * GHW * 0.5
      GVOL = (AG + WH*GHW) * GHL
C
C    set ALIGN = .FALSE. for N-S oriented gnhse
C
      IF (DBETA(1) .GT. 80.) ALIGN = .FALSE.
C
      CALL FDFSE
C
C    Print - echoed inputs and others
C
      IF (ISTDEV .EQ. 1) WRITE(6,34) IRUN
      IF (ISTDEV .EQ. 2) WRITE(6,35) IRUN
34    FORMAT(/'RR',I5/)
35    FORMAT(/'RS',I5/)
      WRITE(5,61)DLAT
61    FORMAT(/'Latitude =', F10.2/)
      WRITE(5,62)(DGAM(I), I=1, NS)
62    FORMAT(/'Surface azimuth:     ', 10F10.0)
      WRITE(5,63)(DBETA(I), I=1, NS)
63    FORMAT(/'Surface tilt:      ', 10F10.1/)
C
      IF (INSN) WRITE(5,64) RHO3
64    FORMAT(/'Insulated 3rd (North-facing) Surface, RHO =',F10.2/)
      WRITE(5,51)
51    FORMAT(/'     LWR      GHL      GHW      BH       WH   TILT1   TILT2   SHADE   NAEMAX'/)
```

```
      WRITE(5,65)RLWR, GHL,GHW,BH,WH,TILT1,TILT2,SHADE, NAEMAX
65    FORMAT(8F7.2, I7)
      WRITE(5,52)
52    FORMAT(/'    AC1    AC3     AB     AP     AG'/)
      WRITE(5,66)AC1,AC3,AB,AP,AG
66    FORMAT(5F7.1)
      WRITE(5,53)
53    FORMAT(/'    F1P    FP1    F3P    FP3    FGP    FPG    F13    F31    F3G    FG3'/)
      WRITE(5,67)F1P,FP1,F3P,FP3,FGP,FPG,F13,F31,F3G,FG3
67    FORMAT(10F7.3)
C
C    diffuse irradiance transmittance (angle of incidence = 60 deg)
C
      AINCD = PI/3.
      TAUD = TRANS(AINCD, RKL, NC,  RI)
      TAUD2 = TRANS(AINCD, RKL, NC2, RI)
      ALPD2 = 1. - TAUA
C
C    OUTERMOST DO-LOOP (10) FOR ALL MONTHS (index I)
C
      DO 10 IK = NFM, NLM
       IF (IK .GT. 12) I = IK - 12
       IF (IK .LE. 12) I = IK
       ICAL = 0
C
C    read other crop parameters from month to month
C
       READ(3,16)BOWEN, RK, RLAI, TAUC, EFLITE
C
       CALL RISET
C
       CALL SPLINE(RHO1, RHO7, RH13, RH19, I)
C
       T1 = BSUNHR(I)/DA
C
       VW(I) = VW(I) * 1000./3600.
       HW = CW1 + CW2 * (VW(I) ** CW3)
C
       WRITE(6,32)I
       WRITE(7,32)I
       WRITE(8,32)I
32     FORMAT(/100('*')/ 'Month =', I5)
C
       TAUC = TAUC * 1.D-3
       EFLITE = EFLITE * 1.D-3
       DO 170 KA = 1,5
        SPN(KA) = O.
170    CONTINUE
C
       WRITE(5,58)
58     FORMAT(/'    HR HPARIN     TP     F  PG340    RC  PN220  PN250  PN280  PN310  PN340'/)
       IF (INSN) GOTO 26
       WRITE(6,41)
41     FORMAT(/'HR NAE  BOWEN    TCO    TCI    TP   RHIN   TIN    SP   TRPN    %SP  TPOUT  QTRAN
       WRITE(7,43)
43     FORMAT(/' HR    SCO    SCI    SP    HCA    HPA   TRPN    %SP   CONDS'/)
       GOTO 27
26     WRITE(6,42)
42     FORMAT(/'HR NAE  BOWEN   TCO    TCI    TP    TB   RHIN    TIN    SP    SB   TRPN    %SP
       WRITE(7,44)
```

```
44     FORMAT(/' HR     SCO     SCI     SP     SB     HCA     HPA     HBA     TRPN     %SP'/)
C
27     Q11 = DCOS(WS)
       Q12 = DSIN(WS)
       Q5 = DSIN(RDELC(I))
       Q6 = DCOS(RDELC(I))
       IF (IAVSOL .EQ. 1)GOTO 8
C
C    daily diffuse radiation on outside horizontal surface for IAVSOL .NE. 1
C
        T34 = Q12 - WS*Q11
        DHBAR = 24.*HSC*E(I)*Q2*Q6*T34/PI
        IF (IAVSOL .EQ. 3)DBAR(I) = DHBAR * (0.18+0.62*T1)
        RKT = DBAR(I)/DHBAR
        T31 = 0.409 + 0.5016 * DSIN(WS - PI/3.)
        T32 = 0.6609 - 0.4767 * DSIN(WS - PI/3.)
C
        IF (DLAT .GT. 40.)GOTO 7
         CH1 = 1.0
         CH2 = 1.13
         GOTO 9
7        CH1 = 0.958
         CH2 = 0.982
9      DDBAR = (CH1 - CH2*RKT) * DBAR(I)
       RA1 = DDBAR/DBAR(I)
C
8      THPS = 0.
       THBS = 0.
       SUMHD = 0.
       SUMQU = 0.
       SUMQTD = 0.
       SUMQTN = 0.
       SUMNL = 0.
       SUMDL = 0.
       SUMPN = 0.
       SUMQSP = 0.
       SUMQP = 0.
C
C    OUTER DO LOOP (20) FOR HOURS (index J)
C
       IR1=IRISE + 1
       IR24 = IRISE + 24
       DO 20 JA = IR1, IR24
        IF (JA .LE. 24) J = JA
        IF (JA .GT. 24) J = JA - 24
         DWI(J) = (12 - J)*15. + 7.5
         RWI(J) = DWI(J) * PI/180.
         Q7 = DSIN(RWI(J))
         Q8 = DCOS(RWI(J))
         T33 = Q8 - Q11
         HEXT = HSC * E(I)* Q6 * Q2 * T33
C
         SCO = 0.
         SCI = 0.
         HPS = 0.
         HBS = 0.
C
         IF (J .GT. IRISE .AND. J .LT. ISET .AND. H(I,J) .LE. 0.01 .AND. IAVSOL .EQ. 1)GOTO 20
         IF (JA .GE. ISET)GOTO 25
C
```

```
C    Compute daytime hourly TOUT using Kimball and Bellamy's model
C
C         T18 = PI * (J - IHRMIN)
C         T19 = (TMAX(I) - TMIN(I)) * DSIN(T18/T20)
C         TOUT = TMIN(I) + T19
         CALL NTLOAD(JA)
         SUMDL = SUMDL + HEATLD
         IF (IAVSOL .EQ. 1)GOTO 81
C
C    hourly diffuse radiation - Liu and Jordan's method, and hence
C    hourly global radiation - Collares and Rabl's method
C    for IAVSOL .NE. 1
C
          HD(I,J) = DDBAR * PI * T33/(24. * T34)
          H(I,J) = HEXT * DBAR(I) * (T31 + T32*Q8)/DHBAR
          IF (J .GT. IRISE .AND. J .LT. ISET .AND. H(I,J) .LE. 0.01)GOTO 20
          GOTO 82
C
C    hourly diffuse radiation on horizontal surface (Hay's method)
C
81       T2 = RHOCLR * T1
         T3 = RHOCLD * (1.-T1)
         T4 = RHO(I) * (T2+T3)
         HPI = H(I,J) * (1.-T4)
         T5 = HPI/HEXT
         T6 = 1.6688*T5
         T7 = 21.303*(T5**2)
         T8 = 51.288*(T5**3)
         T9 = 50.081*(T5**4)
         T10 = 17.551*(T5**5)
         T11 = 0.9702 + T6 - T7 + T8 - T9 + T10
         HDPI = HPI * T11
         HD(I,J) = HDPI + H(I,J) - HPI
82       IF (HD(I,J) .LT. 0.)HD(I,J) = 0.
         SUMHD = SUMHD + HD(I,J)
C
C    hourly beam radiation on horizontal surface
C
         HB(I,J)= H(I,J) - HD(I,J)
         IF(HB(I,J) .LT. 0.)HB(I,J)=0.
C
C    INNER DO LOOP (30) FOR ALL CONTRIBUTING SURFACES  (index K)
C
        DO 30 K=1, NS
        IF (.NOT. (ALIGN))GOTO 84
         IF(K .EQ. 3 .AND. INSN)GOTO 30
         IF (K .EQ. 1)AREA = AC1
         IF (K .EQ. 3)AREA = AC3
         IF (K .EQ. 2 .OR. K .EQ. 4)AREA = AG
         GOTO 89
84       IF (K .EQ. 1 .OR. K .EQ. 3) AREA = AG
         IF (K .EQ. 2) AREA = AC1
         IF (K .EQ. 4) AREA = AC3
C
89       Q3 = DSIN(RBETA(K))
         Q4 = DCOS(RBETA(K))
         Q9 = DSIN(RGAM(K))
         Q10 = DCOS(RGAM(K))
C
C    hourly radiation on tilted surface (calc RB for each surface)
```

```
C
        UP21=((Q1*Q4) - (Q2*Q3*Q10)) * Q5
        UP22=((Q2*Q4) + (Q1*Q3*Q10)) * Q6 * Q8
        UP23=Q6 * Q3 * Q9 * Q7
        RBUP = UP21 + UP22 + UP23
        RBDN = (Q1*Q5) + (Q2*Q6*Q8)
        RB = RBUP/RBDN
        IF(RB .LT. O.)RB = O.
C
C    beam radiation
C
        HBT = HB(I,J) * RB
C
C    sky (anisotropic model), and ground reflected diffuse radiation
C
        FA = 1. - (HD(I,J)/H(I,J))**2
        F1 = 1. + FA*(DSIN(RBETA(K)/2.)**3)
        F2 = 1. + FA*(RBUP**2)*((1. - RBDN**2)**1.5)
        HST = 0.5 * HD(I,J) * (1. + DCOS(RBETA(K))) * F1 * F2
        HRT = 0.5 * H(I,J) * RHO(I) * (1. - DCOS(RBETA(K)))
        HDT = HST + HRT
C
C    Angle of incidence for beam radiation
C
        AINCB = DARCOS(RBUP)
        TAUB = TRANS(AINCB, RKL, NC,  RI)
        TAUB2 = TRANS(AINCB, RKL, NC2, RI)
        ALPB2 = 1. - TAUA
        IF (TAUB .LT. O.) TAUB = O.
        IF (TAUB2 .LT. O.) TAUB2 = O.
        IF (ALPB2 .LT. O.) ALPB2 = O.
C
C    Total (beam & diffuse) transmitted irradiance thru surface
C
        FRB = 1.
        IF (THG .LT. 0.001 .AND. AINCB .LT. 1.047)FRB = 0.90
        IF (THG .LT. 0.001 .AND. AINCB .GE. 1.047)FRB = 0.85
        HTB = TAUB*HBT * FRB * SHADE
        HTD = ( TAUD*HDT + TAUB*HBT*(1.-FRB)*TAUD ) * SHADE
C
C    Extend onto horizontal (Plant canopy) surface using results from
C     *FBEAM* and *FDFSE* (%BEAM and %DIFFUSE solar rad reaching it)
C
        IF (RB .GT. O.)CALL FBEAM
        IF (RB .LE. O.)GOTO 24
         GOTO 88
C
C    SURFACE NOTATION:
C
C      1,3: South and North faces
C      2,4: East and West faces
C
24      IF (K .NE. 3) REFLEC(1) = RHO3
        IF (K .EQ. 3) REFLEC(1) = RHO1
        REFLEC(2) = RHOP
        DO 110 II=1, 4
         P(II) = O.
110     CONTINUE
        GOTO 29
C
```

```
88      IF ((ALIGN .AND. K.EQ.1) .OR. (.NOT.(ALIGN) .AND. K.EQ.2))GOTO 21
        IF ((ALIGN .AND. K.EQ.3) .OR. (.NOT.(ALIGN) .AND. K.EQ.4))GOTO 22
        IF ((ALIGN .AND. (K.EQ.2 .OR. K.EQ.4)) .OR. (.NOT.(ALIGN) .AND. (K.EQ.1 .OR. K.EQ.3)))GOTO 23
21      F(1) = F1P
        F(2) = F13
        F(3) = F3P
        P(1) = P1P
        P(2) = P13
        WRITE(5,79)I,J,K, (P(M), M=1, 4)
79      FORMAT(3I5, 10F7.2)
        REFLEC(1) = RHO3
        IF(.NOT.(INSN)) GOTO 29
        F(4) = F13
        F(5) = F1P
        F(6) = FP3
        P(3) = P13
        P(4) = P1P
        REFLEC(2) = RHOP
        GOTO 29
22      F(1) = F3P
        F(2) = F31
        F(3) = F1P
        P(1) = P3P
        P(2) = P31
        REFLEC(1) = RHO1
        GOTO 29
23      F(1) = FGP
        F(2) = FG3
        F(3) = F3P
        P(1) = PGP
        P(2) = PG3
        REFLEC(1) = RHO3
        WRITE(5,79)I,J,K, (P(M), M=1, 4)
        IF(.NOT.(INSN))GOTO 29
        F(4) = FG3
        F(5) = FGP
        F(6) = FP3
        P(3) = PG3
        P(4) = PGP
        REFLEC(2) = RHOP
        GOTO 29
29      DO 60 L = 1,6
         IF(P(L) .LT. O.)P(L) = O.
         IF(P(L) .GT. 1.)P(L) = 1.
         IF(F(L) .LT. O.)F(L) = O.
         IF(F(L) .GT. 1.)F(L) = 1.
60      CONTINUE
        T15 = HTB * P(1)
        T16 = HTD * F(1)
        T17 = (HTB*P(2) + HTD*F(2)) * F(3) * REFLEC(1)
        IF ((INSN .AND. K .EQ. 3)  .OR.  (.NOT.(INSN)))GOTO 28
        T12 = HTB * P(3)
        T13 = HTD * F(4)
        T14 = (HTB*P(4) + HTD*F(5)) * F(6) * REFLEC(2)
        HBS = (T12 + T13 + T14) * AREA/AB + HBS
28      HPS = (T15 + T16 + T17) * AREA/AP + HPS
C
        CALL SCOVER (AREA)
C
30      CONTINUE
```

```
C
      SCO = SCO + RHOP*HPS*AP*FPC*TAUD2*ALPD2
      SCI = SCI + RHOP*HPS*AP*FPC*ALPD2
      SP = HPS * AP * ALPP
      SB = HBS * AB * ALPB
      IF (SCO .LT. O.  .OR.  SCI .LT. O.  .OR.  SP .LT. O.)GOTO 20
C
C   convert [MJ/hr] to [W = J/s]
C
      SCO = SCO * 1.D6/3600.
      SCI = SCI * 1.D6/3600.
      SP = SP * 1.D6/3600.
      SB = SB * 1.D6/3600.
      THPS = THPS + HPS
      THBS = THBS + HBS
C
      CALL NLE
      SUMQTD = SUMQTD + QTRAN
      SUMQSP = SUMQSP + QSUP
      SUMQP = SUMQP + QPASS
C
      CALL PSRATE
C
      DO 150 KN = 1, 5
       SPN(KN) = SPN(KN) + PN(KN)
150   CONTINUE
      GOTO 20
C
C   Calculations for nite-time hours only
C
25    CALL NTLOAD (JA)
      SUMNL = SUMNL + HEATLD
      TIN = 17.
      IF (ISTDEV .EQ. 2)CALL LTSOIL
      IF (ISTDEV .EQ. 1)CALL LTROCK
      SUMQTN = SUMQTN + DABS(QTRAN)
C
20    CONTINUE
C
      IF (IAVSOL .EQ. 1) THBAR = D(I)
      IF (IAVSOL .NE. 1) THBAR = DBAR(I)
      TCF = THPS/THBAR
      TCFB = THBS/THBAR
      X1 = THPS * AP/SUMNL
      X2 = THPS * AP/(SUMDL+SUMNL)
      FM1 = (SUMQP + SUMQTD)/(SUMDL + SUMNL)
      FM2 = SUMQTD/(SUMQSP + SUMNL)
      IF (FM1 .GT. 1.)FM1 = 1.
      IF (FM2 .GT. 1.)FM2 = 1.
      IF (FM1 .LT. O.) FM1 = O.
      IF (FM2 .LT. O.) FM2 = O.
      SUMA = SUMDL + SUMNL
      SUMB = FM1 * SUMA
      SUMC = SUMQSP + SUMNL
      SUMD = FM2 * SUMC
      WRITE(7,69)IRUN, X1,X2,FM1,FM2, SUMA,SUMB,SUMC,SUMD
69    FORMAT(I5, 10F10.2)
      FYUP1 = FYUP1 + SUMB
      FYUP2 = FYUP2 + SUMD
      FYDN1 = FYDN1 + SUMA
```

```
      FYDN2 = FYDN2 + SUMC
      WRITE(6,45)
45    FORMAT(/'monthly:  QU[MJ] QTD[MJ] QTN[MJ] QDL[MJ] QNL[MJ]    HBAR     TCF     TCFB      X1       X2       FM1       FM2'/)
      WRITE(6,33)SUMQU, SUMQTD, SUMQTN, SUMDL, SUMNL, D(I), TCF, TCFB, X1, X2, FM1, FM2
33    FORMAT(8X, 5F8.0, 10F8.2)
C
      IF (IAVSOL .NE. 1) WRITE(9,77)DBAR(I), SUMHD, DDBAR
      IF (IAVSOL .EQ. 1) WRITE(9,77)D(I), SUMHD
      WRITE(9,76)I, (HD(I,J), J=4,21)
77    FORMAT(5F7.2)
76    FORMAT(I3, 20F7.2)
C
      IF (I .GE. 9) GOTO 91
      DO 140 KK=1, 5
       WPN(KK) = WPN(KK) + SPN(KK)
140   CONTINUE
      GOTO 93
91    DO 120 KM=1, 5
       FPN(KM) = FPN(KM) + SPN(KM)
120   CONTINUE
93    WRITE(8,49)
49    FORMAT(/'monthly:     PN220   PN250   PN280   PN310   PN340'/)
      WRITE(8,78) (SPN(KJ), KJ=1, 5)
78    FORMAT(8X, 10F8.2)
10    CONTINUE
      FY1 = FYUP1/FYDN1
      FY2 = FYUP2/FYDN2
      WRITE(6,31)FY1, FY2
31    FORMAT(/100('*')//'Annual solar heating fractions =', 2F10.2)
      WRITE(8,56)
56    FORMAT(/100('*')/'  FPN220  FPN250  FPN280  FPN310  FPN340  WPN220  WPN250  WPN280  WPN310  WPN340'/)
      WRITE(8,71)(FPN(KK), KK=1,5), (WPN(KK), KK=1,5)
71    FORMAT(20F8.2)
C
      IF (ISTDEV .EQ. 1)GOTO 4
      WRITE(5,39)TRATE
39    FORMAT(/'total mass flow rate for soil storage [kg/s] =', F10.2/)
      GOTO 85
4     FRAP = FRATE * 1000./(AP * RHOA)
      WRITE(5,38)FRATE, FRAP
38    FORMAT(/'total mass flow rate for rock storage [kg/s] =', F10.2, '     or [L/s.m2] = ', F6.1)
85    STOP
      END
C
C    FUNCTION SUBPROGRAM *TRANS* for solar radiation transmittance
C
      FUNCTION TRANS(X, RKL, NC,  RI)
      IMPLICIT REAL*8(A-H, O-Z)
      COMMON/TRMT/TAUD2, ALPD2, TAUA, TAUB2, ALPB2
      AREF=DARSIN(DSIN(X)/RI)
      DIFF=AREF-X
      ADD=AREF+X
      RHOPD=(DSIN(DIFF)**2)/(DSIN(ADD)**2)
      RHOPL=(DTAN(DIFF)**2)/(DTAN(ADD)**2)
      TAUR=0.5 * ((1-RHOPD)/(1+(2*NC-1)*RHOPD) +
     &  (1-RHOPL)/(1+(2*NC-1)*RHOPL))
      TAUA=DEXP(-RKL * NC/DCOS(AREF))
      TRANS=TAUR*TAUA
      RETURN
      END
```

```
C
C    SUBROUTINE *SPLINE* to fit cubic spline to RHOUT data(4 values per day)
C
      SUBROUTINE SPLINE(RHO1, RHO7, RH13, RH19, I)
      IMPLICIT REAL*8(A-H, O-Z)
      COMMON/DATA/TOUT, RHT(24), VW, RHSET
      DIMENSION X(4), Y(4), DY(4), W(58), XX(24), YY(24), YY1(24), YY2(24)
      DIMENSION RHO1(15), RHO7(15), RH13(15), RH19(15)
      DO 10 J=1,4
       X(J) = DFLOAT(J-1) * 6. + 1.
       DY(J) = 2.
10    CONTINUE
      Y(1)=RHO1(I)
      Y(2)=RHO7(I)
      Y(3)=RH13(I)
      Y(4)=RH19(I)
      S=0.
      CALL DSPLFT(X,Y,DY,S,4,W, &99)
      DO 30 K=1,19
       XX(K)=DFLOAT(K)
30    CONTINUE
      CALL DSPLN(XX,YY,YY1,YY2, 19, &99)
      DO 50 L=1,19
       RHT(L) = YY(L)
50    CONTINUE
99    RETURN
      END
C
C   SUBROUTINE *RISET* to compute sunrise and sunset hours
C
      SUBROUTINE RISET
      IMPLICIT REAL*8(A-H, O-Z)
      COMMON/RADIAN/PSI,RDELC(12),RLAT,RWI(24),RBDN,RGAM(6),RBETA(6)
      COMMON/SUN/SR,SS, DA, WS, IRISE, ISET
      COMMON/INDEX/I, J
      PI = 3.14159
      WS = DARCOS(-DTAN(RLAT) * DTAN(RDELC(I)))
      DWS = WS * 180./PI
      DA = DWS * 2./15.
      SR = 12. - DWS/15.
      SS = SR + DA
      IRISE = DINT(SR + 0.5)
      ISET = DINT(SS + 0.5)
      RETURN
      END
C
C    SUBROUTINE *FBEAM* to compute beam radiation interception factors
C
      SUBROUTINE FBEAM
      IMPLICIT REAL*8(A-H, O-Z)
      COMMON/BEAM/NS, K, P1P, P3P, PGP, P13, P31, PG3
      COMMON/GEOM/GHL,GHW,BH,WH, RTILT1,RTILT2,S1,S3, GVOL
      COMMON/INDEX/I, J
      COMMON/LOGIC/FOR3, ALIGN
      COMMON/RADIAN/PSI,RDELC(12),RLAT,RWI(24),RBDN,RGAM(6),RBETA(6)
      LOGICAL FOR3, ALIGN
C
      PI = 3.14159
      BH2 = BH * 0.5
      ALPHA = DARSIN(RBDN)
```

```
      ALPHA2 = PI*0.5 - ALPHA
      FOR3 = .FALSE.
C
C    solar azimuth angle
C
      PSIUP = DSIN(ALPHA) * DSIN(RLAT) - DSIN(RDELC(I))
      PSIDN = DCOS(ALPHA) * DCOS(RLAT)
      PSI = DARCOS(PSIUP/PSIDN)
C
C    For Surfaces #1 and #3, use function subprogram *FB12*
C        Surfaces #2 and #4, use function subprogram *FB34*
C
      IF ((ALIGN .AND. K.EQ.1) .OR. (.NOT.(ALIGN) .AND. K.EQ.2))GOTO 1
      IF ((ALIGN .AND. K.EQ.3) .OR. (.NOT.(ALIGN) .AND. K.EQ.4))GOTO 2
      IF ((ALIGN .AND. (K.EQ.2 .OR. K.EQ.4)) .OR. (.NOT.(ALIGN) .AND. (K.EQ.1 .OR. K.EQ.3)))GOTO 3
1     P1P = FB12(GHW, GHL, BH, K, ALPHA)
      FOR3 = .TRUE.
      P13 = FB12(BH, GHL, GHW, K, ALPHA2)
      SUP1 = 1. - P1P
      SUP2 = 1. - P13
      IF (P13 .GT. SUP1)P13 = DMIN1(SUP1,SUP2)
      RETURN
2     P3P = FB12(GHW, GHL, BH, K, ALPHA)
      P31 = 1. - P3P
      IF (P3P .LE. 0.) P31 = 0.
      RETURN
3     PGP = FB34(GHW, GHL, BH2, K, ALPHA)
      FOR3 = .TRUE.
      PG3 = FB34(BH2, GHL, GHW, K, ALPHA2)
      SUP1 = 1. - PGP
      SUP2 = 1. - PG3
      IF (PG3 .GT. SUP1)PG3 = DMIN1(SUP1,SUP2)
      RETURN
      END
C
C    FUNCTION *FB12* for roof
C
      FUNCTION FB12(A, B, C, N, ELEV)
      IMPLICIT REAL*8(A-H, O-Z)
      LOGICAL FOR3, ALIGN
      COMMON/GEOM/GHL,GHW,BH,WH, RTILT1,RTILT2,S1,S3, GVOL
      COMMON/RADIAN/PSI,RDELC(12),RLAT,RWI(24),RBDN,RGAM(6),RBETA(6)
      COMMON/LOGIC/FOR3, ALIGN
C
      THETA = PSI - RGAM(N)
      EX = C/DTAN(ELEV)
      CR1 = DABS(EX * DSIN(THETA))
      CR2 = DABS(EX * DCOS(THETA))
      W1 = C/DTAN(RTILT1)
      IF (FOR3) W1 = A
      AX = W1 + CR2
      IF(CR1 .GE. B)GOTO 1
      IF(CR1 .LT. B)GOTO 2
1     IF(N .EQ. 1)FB12 = B/(2.*CR1)
      IF(N .EQ. 3)FB12 = 0.
      RETURN
2     IF(AX .GT. A)GOTO 3
      IF(AX .LE. A)GOTO 4
3     IF(N .EQ. 3)GOTO 1
      T1 = (A**2) * CR1
```

```
      T2 = 2. * AX
      T3 = (A * B) - T1/T2
      FB12 = T3/(B * AX)
      RETURN
4     FB12 = 1. - CR1/(2.*B)
      RETURN
      END
C
C    FUNCTION *FB34* for gable ends
C
      FUNCTION FB34(A, B,C, N,ELEV)
      IMPLICIT REAL*8(A-H, O-Z)
      LOGICAL FOR3, ALIGN
      COMMON/GEOM/GHL,GHW,BH,WH, RTILT1,RTILT2,S1,S3, GVOL
      COMMON/RADIAN/PSI,RDELC(12),RLAT,RWI(24),RBDN,RGAM(6),RBETA(6)
      COMMON/LOGIC/FOR3, ALIGN
C
      THETA = PSI - RGAM(N)
      EX = C/DTAN(ELEV)
      CR1 = DABS(EX * DSIN(THETA))
      CR2 = DABS(EX * DCOS(THETA))
      W1 = C/DTAN(RTILT1)
      IF (FOR3) W1 = A
      AX = W1 + CR1
      IF(CR2 .LT. B)GOTO 1
      IF(CR2 .GE. B)GOTO 7
1     IF(AX .GT. A)GOTO 2
      IF(AX .LE. A)GOTO 3
2     IF(CR1 .LE. W1)FB34 = 1. - 0.5*CR1/A
      IF(CR1 .GE. A)FB34 = 0.5*A/CR1
      IF(CR1 .GT. W1 .AND. CR1 .LT. A)GOTO 5
      RETURN
3     FB34 = 1.
      RETURN
5     T1 = (CR1 - W1)**2
      FB34 = 1. - T1/(A*CR1)
      RETURN
7     T1 = 0.5*(B**2)*DTAN(THETA)
      T2 = (A*B) - T1
      FB34 = T2/(A*CR2)
      RETURN
      END
C
C    SUBROUTINE *FDFSE* to compute diffuse radiation view factors
C
      SUBROUTINE FDFSE
      IMPLICIT REAL*8(A-H, O-Z)
      COMMON/AREAS/AB, AP, AC1, AC3, AG, APFACT
      COMMON/GEOM/GHL,GHW,BH,WH, RTILT1,RTILT2,S1,S3, GVOL
      COMMON/VIEW/F1P,FP1,F3P,FP3,FGP,FPG,F13,F31,F3G,FG3, ANGLE,RL,RN
      PI=3.14159
      EPSLN = PI - (RTILT1 + RTILT2)
      F1P = F12(GHW, GHL,S1, RTILT1)
      FP1 = F1P * AC1/AP
      F3P = F12(GHW, GHL, S3, RTILT2)
      FP3 = F3P * AC3/AP
      FPG = (1. - FP1 - FP3) * 0.5
      FGP = FPG * AP/AG
      F13 = F12(S3, GHL, S1, EPSLN)
      F31 = F13 * AC1/AC3
```

```
      F3G = (1. - F31 - F3P) * 0.5
      FG3 = F3G * AC3/AG
      RETURN
      END
C
C     FUNCTION *F12* called by FDFSE
C
      FUNCTION F12(A, B, C, PHI)
      IMPLICIT REAL*8(A-H, O-Z)
      EXTERNAL G
      COMMON/VIEW/F1P,FP1, F3P,FP3, FGP,FPG, F13,F31, F3G,FG3, ANGLE,RL,RN
C
      PI = 3.14159
      ANGLE = PHI
      RL = C/B
      RN = A/B
      RLS=RL**2
      RNS=RN**2
      T1 = (RL - RN*DCOS(PHI))/(RL*DSIN(PHI))
      T2 = DATAN(T1) * RNS
      T3 = (RN - RL*DCOS(PHI))/(RL*DSIN(PHI))
      T4 = DATAN(T3) * RLS
      T5 = (0.5*PI - PHI) * (RNS+RLS)
      T6 = RN * RL * DSIN(PHI)
      T7 = -(T2+T4+T5+T6) * DSIN(2*PHI) * 0.25
      T8 = RNS + RLS - 2*RN*RL*DCOS(PHI)
      T9 = RLS*(T8+1)/((1+RLS)*T8)
      T10 = T9 ** RLS
      T11 = (1+RNS)*(1+RLS)/(T8+1)
      T12 = (1./DSIN(PHI))**2 + (1./DTAN(PHI))**2
      T13 = T11 ** T12
      T14 = DLOG(T13*T10) * (DSIN(PHI)**2) * 0.25
      T15 = (1+RNS)/(T8+1)
      T16 = T15 ** (DCOS(PHI)**2)
      T17 = RNS/T8
      T18 = DLOG(T17*T16) * (DSIN(PHI)**2) * RNS * 0.25
      T19 = DATAN(1./DSQRT(T8))
      T20 = DSQRT(T8) * T19
      T21 = RN * DATAN(1./RN) - T20
      T22 = RL - RN*DCOS(PHI)
      T23 = DSQRT(1. + RNS*(DSIN(PHI)**2))
      T24 = DATAN(T22/T23)
      T25 = DATAN(RN*DCOS(PHI)/T23)
      T26 = T23 * (T25 + T24)
      T27 = 0.5 * RN * DSIN(PHI) * DSIN(2*PHI) * T26
      T28 = RL * DATAN(1./RL)
      AREA = CADRE (G, 0., RL, 0.00001, 0.0001, ERROR)
      T33 = AREA * DCOS(PHI)
      F12 = (T7 + T14 + T18 + T21 + T27 + T28 + T33)/(PI*RL)
      RETURN
      END
C
C     FUNCTION *G* as required by *F12*
C
      FUNCTION G(X)
      IMPLICIT REAL*8(A-H, O-Z)
      COMMON/VIEW/F1P,FP1, F3P,FP3, FGP,FPG, F13,F31, F3G,FG3, ANGLE,RL,RN
      T29 = DSQRT(1. + (X**2) * (DSIN(ANGLE)**2))
      T30 = DATAN (X * DCOS(ANGLE)/T29)
      T31 = RN - X*DCOS(ANGLE)
```

```
      T32 = DATAN (T31/T29)
      G = T29 * (T32 + T30)
      RETURN
      END
C
C    SUBROUTINE 'SCOVER' to compute absorbed solar rad by cover
C     outer and inner surfaces
C
      SUBROUTINE SCOVER (AREA)
      IMPLICIT REAL*8(A-H, O-Z)
      COMMON/AREAS/AB, AP, AC1, AC3, AG, APFACT
      COMMON/INDEX/I, J
      COMMON/PROP/RHOP, ALPP, RHOG, RKG, THG, TAULW, EPC, EPP
      COMMON/SOLAR/HBT, HDT, HPS, HBS, SCO, SCI, SP, SB
      COMMON/TRMT/TAUD2, ALPD2, TAUA, TAUB2, ALPB2
      T1 = AREA * HBT * ALPB2
      T2 = AREA * HDT * ALPD2
      SCO = T1 + T2  + SCO
      T3 = AREA * HBT * TAUB2 * ALPB2
      T4 = AREA * HDT * TAUD2 * ALPD2
      SCI = T3 + T4  + SCI
      RETURN
      END
C
C    SUBROUTINE 'NLE' to solve the system of nonlinear heat and mass balance
C      equations
C
      SUBROUTINE NLE
      IMPLICIT REAL*8(A-H, O-Z)
      EXTERNAL FCN
      COMMON/AREAS/AB, AP, AC1, AC3, AG, APFACT
      COMMON/COVER/NNC
      COMMON/CONV/CW1, CW2, CW3, HW, HCA, HPA, HBA
      COMMON/DATA/TOUT, RHT(24), VW, RHSET
      COMMON/ENV/ CL, BOWEN
      COMMON/INDEX/I, J
      COMMON/HEAT/TMAX(12), TMIN(12), HEATLD, QSUP, QPASS
      COMMON/OUT/RHINS, TRPN, TRSP, SUMQU, TPOUT, QTRAN, PN1
      COMMON/PROP/RHOP, ALPP, RHOG, RKG, THG, TAULW, EPC, EPP
      COMMON/PSYC/TDP, TC,TP, RH,WA, WCSAT,WPSAT,WOUT, TIN
      COMMON/SOLAR/HBT, HDT, HPS, HBS, SCO, SCI, SP, SB
      COMMON/SUN/SR,SS, DA, WS, IRISE, ISET
      COMMON/SYSTEM/INSN, ISTDEV
      COMMON/VENT/NAE, NAEMAX
      DIMENSION X(10), F(10), ACCEST(10)
      LOGICAL INSN, NEWY, NEWA, NEWB
C
C    Initialization of unknown (X) values
C
      IF (INSN) AC = AC1
      IF (.NOT. (INSN))AC = AC1 + AC3
      NAEMIN = 2
      JM = (IRISE+ISET) * 0.5
      IF (J .LE. JM) JN = J
      IF (J .GT. JM) JN = 24 - J
      SLOPE = 2.*(NAEMAX - NAEMIN)/(ISET-IRISE)
      BINCPT = NAEMIN - (SLOPE*IRISE)
      NAE = DINT(SLOPE*JN + BINCPT + 0.5)
      X(1) = 15.
      X(2) = 15.
```

```
      X(3) = 8000.
      X(4) = 15.
      X(5) = 70.
      X(6) = 15.
      X(7) = 450.
      X(8) = 450.
      X(9) = 450.
      ERR = 0.1
      IF (INSN) N = 6
      IF (.NOT. (INSN)) N = 5
      MAXIT = 50
      CL = 0.10
C
      CALL NDINVT (N, X, F, ACCEST, MAXIT, ERR, FCN, &2)
C
C   Print outputs
C
      IF (.NOT. (INSN))HBA = 0.
      SUMH = HPA*AP*2. + HCA*AC + HBA*AB*2.
      TIN = 22. + X(3)/SUMH
      X(3) = X(3) * 3600. * 1.D-6
      IF (X(3) .GT. 0.)GOTO 1
       QSUP = DABS(X(3))
       QPASS = HEATLD + X(3)
       GOTO 9
1      QPASS = HEATLD
       QSUP = 0.
9     SUMQU = SUMQU + X(3)
      TP = X(4)
      IF (ISTDEV .EQ. 1) GOTO 5
      IF (ISTDEV .EQ. 2) GOTO 6
       RETURN
C
5      CALL LTROCK
       GOTO 8
6      CALL LTSOIL
8     IF (INSN) GOTO 3
       WRITE(6,10)J, NAE,BOWEN, X(1),X(2), X(4), X(5), TIN, SP, TRPN, TRSP, TPOUT, QTRAN, X(3)
       WRITE(7,20)J, SCO, SCI, SP, HCA, HPA, TRPN, TRSP
       RETURN
3      WRITE(6,50)J, NAE,BOWEN, X(1),X(2), X(4), X(6), X(5),  TIN, SP, SB, TRPN, TRSP, TPOUT, QTRAN, X(3)
       WRITE(7,30)J, SCO, SCI, SP, SB, HCA, HPA, HBA, TRPN, TRSP
20     FORMAT(I3, 3F7.0, 10F7.2)
30     FORMAT(I3, 4F7.0, 10F7.2)
10     FORMAT(2I3, 6F7.1, F7.0, 2F7.2, 3F7.1)
50     FORMAT(2I3, 7F7.1, 2F7.0, 2F7.2, 3F7.1)
2      RETURN
      END
C
C   SUBROUTINE *FCN* called by *NLE* for evaluation of X's and F's
C
      SUBROUTINE FCN(X, F)
      IMPLICIT REAL*8(A-H, O-Z)
      COMMON/AIR/CPA, RHOA, FRMASS
      COMMON/AREAS/AB, AP, AC1, AC3, AG, APFACT
      COMMON/BEAM/NS, K, P1P, P3P, PGP, P13, P31, PG3
      COMMON/COVER/NNC
      COMMON/CONV/CW1, CW2, CW3, HW, HCA, HPA, HBA
      COMMON/DATA/TOUT, RHT(24), VW, RHSET
      COMMON/ENV/ CL, BOWEN
```

```
      COMMON/GEOM/GHL,GHW,BH,WH, RTILT1,RTILT2,S1,S3, GVOL
      COMMON/INDEX/I, J
      COMMON/OUT/RHINS, TRPN, TRSP, SUMQU, TPOUT, QTRAN, PN1
      COMMON/PROP/RHOP, ALPP, RHOG, RKG, THG, TAULW, EPC, EPP
      COMMON/PSYC/TDP, TC,TP, RH,WA, WCSAT,WPSAT,WOUT, TIN
      COMMON/SOLAR/HBT, HDT, HPS, HBS, SCO, SCI, SP, SB
      COMMON/SYSTEM/INSN, ISTDEV
      COMMON/VENT/NAE, NAEMAX
      COMMON/VIEW/F1P,FP1, F3P,FP3, FGP,FPG, F13,F31, F3G,FG3, ANGLE,RL,RN
      DIMENSION X(10), F(10)
      LOGICAL INSN
C
      IF (INSN) AC = AC1
      IF (.NOT. (INSN))AC = AC1 + AC3
      EPB = 0.91
      EPC = 0.95
      EPP = 0.95
      UB = 0.6
      RLEWIS = 0.89
      RHOV = RHOA * GVOL
      RLATNT = 2.45D+6
      TC = X(2)
      TP = X(4)
      RH = X(5)
      TB = X(6)
      RJB = X(7)
      RJP = X(8)
      RJC = X(9)
      T28 = 0.
C
      CALL PSY1
C
C     Convective heat transfer coefficients
C
      CALL FORCE(HFPA, HFCA, AC)
      HCA = 1.52 * DABS(22. - X(2)) ** 0.333 + HFCA
      HPA = 1.9 * (DABS(X(4)-22.)/CL) ** 0.25 + HFPA
      IF(.NOT. (INSN))GOTO 2
      HBA = 1.52 * DABS(22. - X(6))**0.333  + HFPA
C
C     Cover outside surface temperature, X(1)
C
2     T1 = SCO
      T2 = HW * AC * (TOUT - X(1))
      IF (NNC .EQ. 1) RHCHR = 0.
      IF (NNC .EQ. 2) RHCHR = 0.16666667
      RST = NNC*THG/RKG + RHCHR
      T3 = AC * (X(2) - X(1))/RST
      T51 = SKYRAD (TCO, EPC, AC)
      F(1) = T1 + T2 + T3  + T51
C
C     Cover inside surface temp, X(2)
C
      T4 = SCI
      T5 = HCA * AC * (22. - X(2))
      T6 = -T3
C
      CALL PSY2
C
      T7 = RLATNT * HCA * AC * (RLEWIS**0.67) * (WA - WCSAT)/CPA
```

```
      IF (X(2) .GT. TDP .OR. T7 .LT. O.)T7 = O.
      T22 = THRAD(TC, RJC, AC, EPC)
      IF(.NOT. (INSN))T22 = O.
      F(2) = T4 + T5 + T6 + T7 + T22
C
C   Useful heat gain (greenhouse air), X(3)
C
      T8 = HCA * AC * (X(2) - 22.)
      T9 = HPA * AP *  (X(4) - 22.) * 2.
      IF (.NOT. (INSN))GOTO 1
      T28 = HBA * AB * (X(6) - 22.)  * 2.
1     T12 = RHOV * CPA * NAE * (TOUT - 22.)/3600.
      F(3) = T8 + T9  + T28 + T12 - X(3)
C
C   Plant canopy temp, X(4)
C
      T13 = SP
      T14 = T9
      T15 = DABS(T14/BOWEN)
      IF (WPSAT .LT. WA) T15 = O.
      TAU = TAULW
      IF (T7 .LT. O.) TAU = TAULW * O.5
      T20 = SKYRAD(TP, EPP, AP) * TAU
      T23 = THRAD(TP, RJP, AP, EPP)
      IF(.NOT. (INSN))T23 = O.
      T21 = T20 + T23
      F(4) = T13 - T14 - T15  + T21
C
C   Greenhouse relative humidity, X(5)
C
      T16 = T15/RLATNT
      T17 = T7/RLATNT
      T18 = RHOV * NAE * (WA - WOUT)/3600.
      F(5) = T16 - T17 - T18
C
C   Convert Transpiration from kg/sec to mm/hr; also calculate
C    condensation in kg/sec
C
      CONDS = T17
      TRPN = T16 * 3600./AP
      IF (T13 .EQ. O.)GOTO 5
      TRSP = T15/T13
C
5     IF(.NOT. (INSN))RETURN
C
C   Absorber plate temp, X(6)
C
      T24 = SB
      T25 = THRAD(TB, RJB, AB, EPB)
      T26 = HBA * AB * (22. - X(6))  * 2.
      T27 = UB * AB * (TOUT - X(6))
      F(6) = T24 + T25 + T26 + T27
C
C   Radiosity, X(7), X(8), X(9) for surfaces (q,p,ci,) or (3,2,1)
C
      F(7) = X(7) - T25/AB - F3P*X(8) - F31*X(9)
      F(8) = X(8) - T21/AP - FP1*X(9) - FP3*X(7)
      F(9) = X(9) - T22/AB - F13*X(7) - F31*X(8)

      RETURN
```

```
      END
C
C    FUNCTION SUBPROGRAMS for psychrometrics
C
      FUNCTION PRESS(T)
      IMPLICIT REAL*8(A-H, O-Z)
      IF (T .GT. 373. .OR.  T .LT. 173.) RETURN
      IF (T .LE. 273.) GOTO 1
      IF (T .GT. 273.) GOTO 2
2      T1 = -7511.52/T
       T2 = 0.024 * T
       T3 = 1.1655E-5 * (T ** 2)
       T4 = 1.281E-8 * (T ** 3)
       T5 = 2.1E-11 * (T ** 4)
       T6 = 12.151 * DLOG(T)
       Y = T1 + 89.631 + T2 - T3 - T4 + T5 - T6
       PRESS = DEXP(Y)
       RETURN
1      T1 = -6238.64/T
       T2 = 0.3444 * DLOG(T)
       Y = 24.278 + T1 - T2
       PRESS = DEXP(Y)
       RETURN
       END
C
      FUNCTION HUMID(PS)
      IMPLICIT REAL*8(A-H, O-Z)
      HUMID = 0.622 * PS/(101.3 - PS)
      RETURN
      END
C
      FUNCTION ENTLPY(T,W)
      IMPLICIT REAL*8(A-H, O-Z)
      ENTLPY = 1.006*T + W*(2501. + 1.775*T).
      RETURN
      END
C
      FUNCTION PVAP(W)
      IMPLICIT REAL*8(A-H, O-Z)
      PVAP = 101.3/(1. + 0.622/W)
      RETURN
      END
C
C    SUBROUTINE *PSY2* to compute WCSAT, WPSAT, WOUT, TDP
C
      SUBROUTINE PSY2
      IMPLICIT REAL*8(A-H, O-Z)
      COMMON/DATA/TOUT, RHT(24), VW, RHSET
      COMMON/INDEX/I, J
      COMMON/PSYC/TDP, TC,TP, RH,WA, WCSAT,WPSAT,WOUT, TIN
      IF (J .GT. 19) J = 19
      RHOUT = RHT(J)
      TPK = TP + 273.
      TCK = TC + 273.
      TUK = TOUT + 273.
      PPSAT = PRESS(TPK)
      PCSAT = PRESS(TCK)
      PUSAT = PRESS(TUK)
      WPSAT = HUMID(PPSAT)
      WCSAT = HUMID(PCSAT)
```

```
      PVOUT = RHOUT * PUSAT/100.
      WOUT = HUMID(PVOUT)
      RETURN
      END
C
C    SUBROUTINE *PSY1* to compute psychrometrics for greenhouse air
C
      SUBROUTINE PSY1
      IMPLICIT REAL*8(A-H, O-Z)
      COMMON/DATA/TOUT, RHT(24), VW, RHSET
      COMMON/PSYC/TDP, TC,TP, RH,WA, WCSAT,WPSAT,WOUT, TIN
      TINK = 295.
      PSAT = PRESS(TINK)
      IF (RH .GT. 100.) RH=100.
      PV = RH*PSAT/100.
      IF (PV .LE. O.)GOTO 1
      IF (TINK .GT. 273.)TDP = 6.983 + 14.38*DLOG(PV) + 1.079*(DLOG(PV)**2)
      IF (TINK .LE. 273.)TDP = 5.994 + 12.41*DLOG(PV) + 0.4273*(DLOG(PV)**2)
      WA = HUMID (PV)
1     RETURN
      END
C
C    FUNCTION *SKYRAD* to compute thermal radiation exchange between
C    a component surface and sky
C
      FUNCTION SKYRAD (T, EMIS, AREA)
      IMPLICIT REAL*8(A-H, O-Z)
      COMMON/DATA/TOUT, RHT(24), VW, RHSET
      COMMON/BEAM/NS, K, P1P, P3P, PGP, P13, P31, PG3
      COMMON/GEOM/GHL,GHW,BH,WH, RTILT1,RTILT2,S1,S3, GVOL
      COMMON/VIEW/F1P,FP1, F3P,FP3, FGP,FPG, F13,F31, F3G,FG3, ANGLE,RL,RN
      BOLTZ = 5.6697D-8
      FCS = (1. + DCOS(RTILT1)) * 0.5
      TSKY = 0.0552 * (TOUT+273.) ** 1.5
      IF (TSKY .LT. O.  .OR.  T .LT. -273.)GOTO 1
      T1 = AREA * BOLTZ *  ((TSKY**4.) - (T+273.)**4.)
      T2 = (1. - EMIS)/EMIS + 1./FCS
      SKYRAD = T1/T2
 1    RETURN
      END
C
C    FUNCTION *THRAD* to compute thermal radiation exchange among surfaces
C
      FUNCTION THRAD(T, R, A, E)
      IMPLICIT REAL*8(A-H, O-Z)
      BOLTZ = 5.6697D-8
      TK = T + 273.
      T1 = A * E * (R - BOLTZ*(TK**4))
      T2 = 1. - E
      THRAD = T1/T2
      RETURN
      END
C
C    SUBROUTINE *FORCE* to compute the component of HCA/HPA due to forced convection
C
      SUBROUTINE FORCE (FP, FC, AC)
      IMPLICIT REAL*8(A-H, O-Z)
      COMMON/AREAS/AB, AP, AC1, AC3, AG, APFACT
      COMMON/BEAM/NS, K, P1P, P3P, PGP, P13, P31, PG3
      COMMON/ENV/ CL, BOWEN
```

```
      COMMON/GEOM/GHL,GHW,BH,WH, RTILT1,RTILT2,S1,S3, GVOL
      COMMON/VENT/NAE, NAEMAX
      PLNTHT = 1.5
      AFR = AC/3.
      IF (NAE .LT. 1)NAE = 1
      UM = GVOL * NAE/(AFR * 3600.)
      UP = UM * (PLNTHT*AP/GVOL)**(0.6667)
      FC = 5.2 * DSQRT(UM/S1)
      FP = 5.2 * DSQRT(UP/CL)
      RETURN
      END
C
C    SUBROUTINE *PSRATE* to compute net photosynthetic rate for tomato plants
C
      SUBROUTINE PSRATE
      IMPLICIT REAL*8(A-H, O-Z)
      COMMON/GROWTH/RK,RLAI,TAUC,EFLITE,TRANSM,RDO, PN(10)
      COMMON/INDEX/I, J
      COMMON/OUT/RHINS, TRPN, TRSP, SUMQU, TPOUT, QTRAN, PN1
      COMMON/PSYC/TDP, TC,TP, RH,WA, WCSAT,WPSAT,WOUT, TIN
      COMMON/SOLAR/HBT, HDT, HPS, HBS, SCO, SCI, SP, SB
      DIMENSION CD(10)
      TR = 20.
      Q = 2.
      HPARIN = HPS * 1.D6 * 0.45/3600.
      IF (HPARIN .LT. 125.) EFF = 1.00
      IF (HPARIN .GE. 125.  .AND.  TP .GT. 26.) EFF=1.25
      IF (HPARIN .GE. 125.  .AND.  TP .LE. 26.) EFF=1.25 - 0.007*((TP-26.)**2)
      T2 = EFLITE * RK * HPARIN
      T11 = DEXP(-RK * RLAI)
      T4 = T2 * T11
      RD1 = RDO * (1. - T11)/RK
      T8 = (TP - TR)/10.
      RC = RD1 * (Q ** T8)
      DO 10 IJ=1, 5
       CD(IJ) = 220. + (IJ - 1)*30.
       CD(IJ) = CD(IJ) * 1.83
       T1 = TAUC * CD(IJ)/RK
       T3 = (1.-TRANSM) * TAUC * CD(IJ)
       T5 = (T2+T3)/(T4+T3)
       T6 = DLOG(T5)
       PG = T1 * T6 * EFF
       PN(IJ) = PG - RC
       IF (PN(IJ) .LT. O.) PN(IJ) = 0.
10    CONTINUE
      WRITE(5,11)J, HPARIN, TP, EFF,PG, RC, (PN(K), K=1,5)
11    FORMAT(I7, F7.0, F7.1, F7.2, 10F7.3)
      RETURN
      END
C
C    SUBROUTINE *LTSOIL* to compute amount of heat transferred
C     to soil (daytime) and recovered from soil (nighttime)
C
      SUBROUTINE LTSOIL
      IMPLICIT REAL*8(A-H, O-Z)
      COMMON/AIR/CPA, RHOA, FRMASS
      COMMON/AREAS/AB, AP, AC1, AC3, AG, APFACT
      COMMON/BEAM/NS, K, P1P, P3P, PGP, P13, P31, PG3
      COMMON/GEOM/GHL,GHW,BH,WH, RTILT1,RTILT2,S1,S3, GVOL
      COMMON/INDEX/I,J
```

```
      COMMON/MAT/THCRC, RKCRC, RKP, THPIPE
      COMMON/OCCUR/ICALL, ICAL
      COMMON/OUT/RHINS, TRPN, TRSP, SUMQU, TPOUT, QTRAN, PN1
      COMMON/PAR/FUW, HP, UP, UI, BII
      COMMON/PSYC/TDP, TC,TP, RH,WA, WCSAT,WPSAT,WOUT, TIN
      COMMON/RADIAN/PSI,RDELC(12),RLAT,RWI(24),RBDN,RGAM(6),RBETA(6)
      COMMON/SOILV/TS(6),TSOUT(12),VMC,C1,C2,DIA,DPIPE,DINS,VSEP,RAREA, TRATE,DT,TF,LAYER,NL,NP
      COMMON/SUN/SR SS, DA, WS, IRISE, ISET
      COMMON/TEMP/T(100,350)
      DIMENSION T1(100,350), NODE(20)
      DIMENSION MP(5),MPP(5),MPM(5), LC(20),LCP(20),LCM(20)
      IF ((J .LE. IRISE .OR. J .GE. ISET)  .OR.  TIN .GT. 22.) GOTO 5
       TPOUT = 99.
       QTRAN = 0.
       RETURN
5     NF = NL - 15
      IF (ICALL .NE. 0)GOTO 4
C
C    calculate Cs [J/m**3 C]  and  ks [W/m C]
C
      CS = (0.315 + VMC) * 4.18 * 1.D6
      RKS = C1*VMC + C2
      RKW = RKS
      RKD = RKS
      PI = 3.14159
C
C    calculate the number of pipes (total 2 layers) required,
C     for given 'total pipe area-to-floor area' ratio, floor area,
C     and greenhouse length-to-width ratio
C
      APIPE = PI * DIA * GHL
      NP = DINT(RAREA * AP/APIPE)/LAYER
      FRMASS = TRATE/(NP*LAYER)
      NPHALF = NP * 0.5
      HSEP = (GHW - NP*DIA)/(NP-1)
      RSP = HSEP/DIA
C
C    Calculate thermal diffusivity and Fourier number
C
      DX=DIA * 0.5
      IX = DINT(HSEP/DX + 0.5)
      IY = DINT((VSEP - DIA)/DX + 0.5)
      IDP = DINT(DPIPE/DX + 0.5)
      INSD = DINT(DINS/DX + 0.5)
      INSDP1 = INSD + 1
      DO 30 KI=1, LAYER
       MP(KI) = IDP + (KI-1)*(IY+2)
       MPP(KI)=MP(KI) + 1
       MPM(KI)=MP(KI) - 1
30    CONTINUE
      ALPHAW=RKW/CS
      ALPHAD=RKD/CS
      FUW=ALPHAW*DT/(DX**2)
      FUD=ALPHAD*DT/(DX**2)
C
      CALL TXPIPE
      XNTU = (UP*APIPE)/(FRMASS*CPA)
      BIP=UP*DX/RKW
C
      HI = 6.13
```

```
      UI = 1./(1./HI + THCRC/RKCRC)
      BII=UI*DX/RKW
C
C   Establish stability criteria. If any of them is violated
C   an error message will be printed and program will exit
C
      CR1 = FUW * (2. + BII)
      CR2 = FUW * (2. + BIP)
      CR3 = FUW * (3. + BIP)
      CR4 = FUW
      CR5 = 3.*FUW + FUD
      IF(CR1 .GT. 0.5)CALL ERROR (1,CR1, &2)
      IF(CR2 .GT. 0.5)CALL ERROR (2,CR2, &2)
      IF(CR3 .GT. 0.75)CALL ERROR(3,CR3, &2)
      IF(CR4 .GT. 0.25)CALL ERROR(4,CR4, &2)
      IF(CR5 .GT. 1.0)CALL ERROR (5,CR5, &2)
      WRITE(5,33)CR1,CR2,CR3,CR4,CR5
33    FORMAT('stability criteria, CR1 to CR5 =', 5F7.2/)
C
C   Calculate Y as a function of damping depth based on daily cycle
C   and take 3 times damping depth as where perturbation is
C   insignificant (less than 5%) ; also calc NX, NY etc.
C
      DAMP = DSQRT(2. * ALPHAW/7.3D-5)
      DAM = 3.*DAMP
      Y = DAM + DPIPE + VSEP*(LAYER-1) + DX
      X = GHW * 0.5 + DAM
      INX = DINT(DAM/DX + 0.5)
      INXM1 = INX - 1
      NX = DINT (GHW/(DX*2) + 0.5) + INX + 1
      NY = DINT ((Y/DX) + 0.5) + 1
      NXM1 = NX - 1
      NYM1 = NY - 1
      NM = (NX - INX) * 0.5
C
      WRITE(5,55)
55    FORMAT(/'        X         Y     DINS      DIA   DPIPE     VSEP     HSEP  FRMASS     XNTU    RAREA'/)
      WRITE(5,35)X,Y,DINS,DIA,DPIPE, VSEP, HSEP, FRMASS, XNTU, RAREA
      WRITE(5,56)
56    FORMAT(/'          VMC          KW          KD          CS     ALPHAW     ALPHAD          FUW          FUD' /)
      WRITE(5,36)VMC, RKW, RKD, CS, ALPHAW, ALPHAD, FUW, FUD
      WRITE(5,57)
57    FORMAT(/'NX(#NODES)   NY(#NODES)'/)
      WRITE(5,37)NX,NY
      WRITE(5,52)
52    FORMAT(/'  NP/LAYER    NPHALF     LAYER'/)
      WRITE(5,37)  NP, NPHALF, LAYER
37    FORMAT(5I10)
36    FORMAT(F10.1, 2F10.3, 3E10.2, 2F10.3)
35    FORMAT(10F8.2)
C
C   After ther 1st hour, initial soil temperatures just equal last
C   hour's final computed T's at time = TF (hence skip initialization)
C
      DO 10 M=1,NY
       YD = M*DX
       DO 20 N=1,NX
        IF (M .LT. INSD .AND. N .LT. INX)GOTO 20
        IF (YD .GE. 0.   .AND.  YD .LE. 0.05)T(M,N) = TS(1)
        IF (YD .GT. 0.05  .AND.  YD .LE. 0.15)T(M,N) = TS(2)
```

```
      IF (YD .GT. 0.15  .AND.  YD .LE. 0.35)T(M,N) = TS(3)
      IF (YD .GT. 0.35  .AND.  YD .LE. 0.75)T(M,N) = TS(4)
      IF (YD .GT. 0.75  .AND.  YD .LE. 1.25)T(M,N) = TS(5)
      IF (YD .GT. 1.25)T(M,N) = TS(6)
20   CONTINUE
10  CONTINUE
C
4   TPIPE = TIN
    STORE=0.
    TIME=0.
99  CONTINUE
    TRANS1 = 0.
    TRANS3 = 0.
C
C   Compute nodal temperatures at time=t+dt (through variable FUW)
C
    DO 60 M=1, NY
     DO 70 N=1, NX
      IF(M .EQ. 1)GOTO 81
      IF(M .GT. 1  .AND. M .LE. INSD)GOTO 84
      IF(M .GT. INSD .AND. M .LT. NY)GOTO 87
      IF(M .EQ. NY)GOTO 89
C
C   surface nodes, facing greenhouse (M=1)
C
81    IF (N .LT. INX)GOTO 93
      IF (N .EQ. INX)GOTO 82
      IF (N .EQ. NX)GOTO 83
       T1(M,N) = SURF(1,0,1,2, TIN,BII,FUW,M,N)
       GOTO 70
C
C   surface (left and right corner nodes)
C
82     T1(M,N) = SURF(0,0,2,2, TIN,BII,FUW,M,N)
       GOTO 70
83     T1(M,N) = SURF(2,0,0,2, TIN,BII,FUW,M,N)
       GOTO 70
C
C   interior nodes (M = 2 TO M = INSD)
C
84    IF(M .LT. INSD .AND. N.LT.INX)GOTO 93
      IF(M .EQ. INSD .AND. N.LT.INX)GOTO 88
      IF(N .EQ. INX)GOTO 85
      IF(N .EQ. NX)GOTO 86
       T1(M,N) = SOIL(1,1,1,1, FUW,M,N)
       GOTO 70
93    T1(M,N)=0.
      GOTO 70
C
C   insulation boundary nodes (AT N=INX, M=1 TO M=INSD; and N=1, M=INSD TO M=NY:  dT/dx = 0)
C
85     T1(M,N) = SOIL(0,1,2,1, FUW,M,N)
       IF(M .EQ. INSD)T1(M,N) = SOIL(1,1,1,1, FUW,M,N)
       GOTO 70
C
C   symmetry boundary nodes (AT N=NX,  M=1 TO M=NY,  dT/dx = 0)
C
86     T1(M,N) = SOIL(2,1,0,1, FUW,M,N)
       GOTO 70
C
```

```
C     interior nodes (M = INSD TO M = NYM1)
C
87        IF(N .EQ. 1)GOTO 85
          IF(N .EQ. NX)GOTO 86
           T1(M,N) = SOIL(1,1,1,1, FUW,M,N)
           GOTO 70
C
C     boundary nodes (AT M = INSD, N=1 TO N=INX)
C
88         T1(M,N) = SOILA(1,0,1,1, FUW,FUD,M,N)
           IF(N .EQ. 1) T1(M,N) = SOILA(0,0,2,1, FUW,FUD,M,N)
           GOTO 70
C
C     bottom boundary nodes (dT/dy = 0,  M=NY)
C
89        IF(N .EQ. 1)GOTO 91
          IF(N .EQ. NX)GOTO 92
           T1(M,N) = SOIL(1,2,1,0, FUW,M,N)
           GOTO 70
C
C     bottom (left and right corner nodes)
C
91        T1(M,N) = SOIL(0,2,2,0, FUW,M,N)
          GOTO 70
92        T1(M,N) = SOIL(2,2,0,0, FUW,M,N)
          GOTO 70
70      CONTINUE
60     CONTINUE
C
C     Modify T1(M,N) for nodes adjacent to Pipes
C
       NI=2+INX
       DO 190 KJ=1, LAYER
C        K=1
        M = MP(KJ)
        DO 160 K = 1, 4
        LC(K)=NI + (K-1)*IX
        LCM(K) = LC(K) - 1
        LCP(K) = LC(K) + 1
        DO 180 N=INX, NX
         IF (K .GT. 4)GOTO 190
         IF(N .EQ. LC(K))GOTO 3
          GOTO 180
C
C     side nodes in the order of ML, MR, UM, BM
C
3          T1(M,N)=TPIPE
           T1(M,N-1)=PIPE(1.,2., 2,1,0,1, TPIPE,BIP,M,N-1)
           T1(M,N+1)=PIPE(1.,2., 0,1,2,1, TPIPE,BIP,M,N+1)
           T1(M-1,N)=PIPE(1.,2., 1,2,1,0, TPIPE,BIP,M-1,N)
           T1(M+1,N)=PIPE(1.,2., 1,0,1,2, TPIPE,BIP,M+1,N)
           TADD = T1(M,N-1)+T1(M-1,N)+T1(M,N+1)+T1(M+1,N)
           TDIF = 4.*TPIPE - TADD
           TRANS1 = TRANS1 + TDIF
C
C     corner nodes in the order of UL, BR, BL, UR
C
           T1(M-1,N-1)=PIPE(0.667, 1.333, 2,2,1,1, TPIPE,BIP,M-1,N-1)
           T1(M+1,N+1)=PIPE(0.667, 1.333, 1,1,2,2, TPIPE,BIP,M+1,N+1)
           T1(M+1,N-1)=PIPE(0.667, 1.333, 2,1,1,2, TPIPE,BIP,M+1,N-1)
```

```
        T1(M-1,N+1)=PIPE(0.667, 1.333, 1,2,2,1, TPIPE,BIP,M-1,N+1)
        K = K + 1
        LC(K) = NI + (K-1)*IX
        LCM(K) = LC(K) - 1
        LCP(K) = LC(K) + 1
180     CONTINUE
160    CONTINUE
190   CONTINUE
      IF (LC(K) .GT. NX)IP = K - 1
      IF (LC(K) .LE. NX)IP = K
C
C   Calculate amount of heat transferred during dt
C
      TRANS1 = TRANS1 * UP * DIA * DT * NP/(1.D6 * 4. * LAYER)
      TRANS2 = UI * (NX-INX)*DX * (TIN - T1(1,NM)) * DT/1.D6
      TRAN = TRAN + TRANS1 + TRANS2
      ICALL = 1
C
C  Increment time until spefified time limit is reached (3600 sec)
C
      IF(TIME .GE. TF)GOTO 1
       TIME=TIME+DT
       DO 80 M=1,NY
       DO 90 N=1,NX
        T(M,N)=T1(M,N)
90     CONTINUE
80    CONTINUE
      GOTO 99
C
C   outputs at time=TF (end of final time step in an hour)
C
C     - soil temperatures (15 specified columns  [C])
C     - Heat transferred, QTRAN  [MJ/hr]
C     - Pipe air outlet temperature, TPOUT  [C]
C
1     QTRAN = TRAN * (GHL - 1.)
      IF((J .LE. IRISE .OR. J .GE. ISET) .AND. QTRAN .GT. 0.) QTRAN = 0.
      T5 = DABS(QTRAN*1.D6)/(CPA*TRATE*3600.)
      IF(J .LE. IRISE .OR. J .GE. ISET) TPOUT = TPIPE + T5
      IF(J .GT. IRISE .AND. J .LT. ISET)TPOUT = TPIPE - T5
C
2     RETURN
      END
C
C  FUNCTION SUBPROGRAM *PIPE* to compute nodal temperature at T+DT
C     for corner and side nodes in the vicinity of a pipe
C
      FUNCTION PIPE(A1,A2, IC1,IC2,IC3,IC4, TE,BI,M,N)
      IMPLICIT REAL*8(A-H, O-Z)
      COMMON/TEMP/T(100,350)
      COMMON/PAR/FUW, HP, UP, UI, BII
      PIPE=A1*FUW*(IC1*T(M,N-1) +IC2*T(M-1,N) +IC3*T(M,N+1) +IC4
     & *T(M+1,N)  +2*BI*TE) + (1 - 4*FUW - A2*FUW*BI)*T(M,N)
      RETURN
      END
C
C     FUNCTION SUBPROGRAM *SURF* for surface convective nodes
C
      FUNCTION SURF(IC1,IC2,IC3,IC4, TE,BI,FU,M,N)
      IMPLICIT REAL*8(A-H, O-Z)
```

```
      COMMON/TEMP/T(100,350)
      SURF=FU*(IC1*T(M,N-1) + IC2*T(M-1,N) + IC3*T(M,N+1) + IC4*T(M+1,N) + 2.*BI*TE)
     &   + ( 1 - 4.*FU - 2.*FU*BI)*T(M,N)
      RETURN
      END
C
C     FUNCTION SUBPROGRAM *SOIL* for no-flow boundary nodes and interior nodes
C
      FUNCTION SOIL(IC1,IC2,IC3,IC4, FU,M,N)
      IMPLICIT REAL*8(A-H, O-Z)
      COMMON/TEMP/T(100,350)
      SOIL=FU*(IC1*T(M,N-1) + IC2*T(M-1,N) + IC3*T(M,N+1) + IC4*T(M+1,N)) +
     &    (1 - 4.*FU) * T(M,N)
      RETURN
      END
C
C     FUNCTION SUBPGM *SOILA*  for boundary nodes along depth of
C     insulation
C
      FUNCTION SOILA(IC1,IC2,IC3,IC4, FUW,FUD,M,N)
      IMPLICIT REAL*8(A-H, O-Z)
      COMMON/INDEX/I, J
      COMMON/SOILV/TS(6),TSOUT(12),VMC,C1,C2,DIA,DPIPE,DINS,VSEP,RAREA, TRATE,DT,TF,LAYER,NL,NP
      COMMON/TEMP/T(100,350)
      SOILA = (1 - 3.*FUW - FUD)*T(M,N) + (FUD * TSOUT(I)) + FUW *
     & (IC1*T(M,N-1) + IC2*T(M-1,N) + IC3*T(M,N+1) + IC4*T(M+1, N))
      RETURN
      END
C
C      calculate mass flow rate per pipe and convective heat
C      transfer coefficient
C
      SUBROUTINE TXPIPE
      IMPLICIT REAL*8 (A-H, O-Z)
      COMMON/AIR/CPA, RHOA, FRMASS
      COMMON/GEOM/GHL,GHW,BH,WH, RTILT1,RTILT2,S1,S3, GVOL
      COMMON/MAT/THCRC, RKCRC,  RKP, THPIPE
      COMMON/PAR/FUW, HP, UP, UI, BII
      COMMON/SOILV/TS(6),TSOUT(12),VMC,C1,C2,DIA,DPIPE,DINS,VSEP,RAREA, TRATE,DT,TF,LAYER,NL,NP
      PI=3.14159
      VIS = 18.5D-6
      PR = 0.71
      RKA = 0.0254
      EX = 0.3
      REY = FRMASS/(VIS * DIA)
      RNU = 0.023 * (REY**0.8) * (PR**EX)
      HP = RNU * RKA/DIA
      UP = 1./(1./HP + THPIPE/RKP)
      RETURN
      END
C
C     SUBROUTINE *ERROR* to print error messages
C
      SUBROUTINE ERROR(ICODE, A, *)
      IMPLICIT REAL*8(A-H, O-Z)
      WRITE(5,1)ICODE, ICODE, A
 1    FORMAT('Stability criterion #',I1,' violated. CR',I1,' =', F10.2)
      RETURN 2
      END
C
```

```
C    SUBROUTINE *LTROCK* to compute the amount of heat transferred to/from
C     rockbed thermal storage
C
      SUBROUTINE LTROCK
      IMPLICIT REAL*8 (A-H, O-Z)
      COMMON/AIR/CPA, RHOA, FRMASS
      COMMON/AREAS/AB, AP, AC1, AC3, AG, APFACT
      COMMON/GEOM/GHL,GHW,BH,WH, RTILT1,RTILT2,S1,S3, GVOL
      COMMON/EQN/C4,C5,C6, TPIN, IMODE
      COMMON/INDEX/I, J
      COMMON/OCCUR/ICALL, ICAL
      COMMON/RKOUT/ICOUT
      COMMON/PSYC/TDP, TC,TP, RH,WA, WCSAT,WPSAT,WOUT, TIN
      COMMON/ROCK/STCAP, FRATE, TINIT, RHOR
      COMMON/SOILV/TS(6),TSOUT(12),VMC,C1,C2,DIA,DPIPE,DINS,VSEP,RAREA,TRATE,DT,TF,LAYER,NL,NP
      COMMON/SUN/SR,SS, DA, WS, IRISE, ISET
      DIMENSION UZ(1,31), XM(31), MORD(1,3), TOUT(2), A(31)
      ICOUT = 1
C
      IMODE = 0
      IF (TIN .GT. 22.  .AND.  TIN .LE. 40.) IMODE = 1
      IF (J .LE. IRISE  .OR.  J .GE. ISET) IMODE = 2
      TPIN = TIN
C
      IF (ICALL .NE. 0)GOTO 1
      RKR = 0.93
      CPR = 880.
      RDIA = 0.0315
      VOID = 0.3
      US = 0.4
      BEDH = 1.
      BEDW = GHW * 0.8
      AP = GHL*GHW
      ASVR = 190.5
C
      ROCKWT = 0.5 * STCAP * AP * 1000./CPR
      VOLRK = ROCKWT/RHOR
      STAP = 2. * VOLRK/AP
      VOLBED = VOLRK/(1. - VOID)
      ACS = BEDH * BEDW
      BEDL = VOLBED/ACS
      T1 = FRATE*0.5/(ACS*RDIA)
      HV = 650. * (T1**0.7)
      RNTU = HV*VOLBED/(FRATE*0.5*CPA)
      HS = HV/ASVR
      BIR = HS * (RDIA*0.5)/RKR
      RNTUC = RNTU/(1. + 0.2*BIR)
      AS = 2.*(BEDW*BEDH) + 2.*(BEDL*BEDH) + (BEDL*BEDW)
      UA = US * AS
      T3 = RHOR * CPR * ACS * (1. - VOID)
      C4 = 3.6D3 * FRATE*0.5 * CPA/T3
      C5 = 3.6D3 * UA/(BEDL*T3)
      C6 = 3.6D3 * RKR * ACS/T3
C
      WRITE(5,65)
65    FORMAT(/' MCr/Ap    RNTU      HV      HS     RHOR    BEDW     BEDL  m3RK/m2AP'/)
      WRITE(5,15)STCAP, RNTU, HV, HS, RHOR, BEDW, BEDL, STAP
15    FORMAT(3F8.0, 10F8.2)
C
1     NPDE = 1
```

```
      NPTS = 31
      KEQN = 2
      KBC = 2
      METH = 0
      EPS = 0.0001
      MORD(1,1) = 2
      MORD(1,2) = 4
      MORD(1,3) = 0
      TINT = 0.
      TLAST = 1.
      MOUT = 0
      TOUT(1) = TLAST
      KMOL = 0
C
      IF (ICALL .EQ. 0) GOTO 3
       BACKSPACE 2
       READ(2,11) (A(IK), IK=1,31)
11     FORMAT(31F7.0)
C
3     DX = BEDL/(NPTS - 1)
      DO 10 IK = 1, NPTS
       XM(IK) = DFLOAT(IK-1) * DX
       IF (ICALL .EQ. 0) UZ(1,IK) = TINIT
       IF (ICALL .NE. 0) UZ(1,IK) = A(IK)
10    CONTINUE
      CALL MOL1D(NPDE,NPTS,KEQN,KBC,METH,EPS,MORD,TINT,TLAST,MOUT,TOUT,UZ,
     *    XM, KMOL)
C
      ICALL = 1
      RETURN
      END
C
      SUBROUTINE PDE(UT, U, UX, UXX, FX, T, XM, IX, NPDE)
      IMPLICIT REAL*8(A-H, O-Z)
      DIMENSION U(1,31), UT(1,31), UX(1,31), UXX(1,31), FX(1,31), XM(31), A(31)
      COMMON/AIR/CPA, RHOA, FRMASS
      COMMON/EQN/C4,C5,C6, TPIN, IMODE
      COMMON/INDEX/I, J
      COMMON/OUT/RHINS, TRPN, TRSP, SUMQU, TPOUT, QTRAN, PN1
      COMMON/ROCK/STCAP, FRATE, TINIT, RHOR
      COMMON/SOILV/TS(6),TSOUT(12),VMC,C1,C2,DIA,DPIPE,DINS,VSEP,RAREA, TRATE,DT,TF,LAYER,NL,NP
      COMMON/SUN/SR,SS, DA, WS, IRISE, ISET
      COMMON/RKOUT/ICOUT
      IF (IMODE .EQ. 0)FDIR = 0.
      IF (IMODE .EQ. 1)FDIR = -1.
      IF (IMODE .EQ. 2)FDIR = 1.
      DO 20 IJ = 1,31
       UT(1,IJ) = FDIR*C4*UX(1,IJ) + C5*(TSOUT(I)-U(1,IJ)) + C6*UXX(1,IJ)
20    CONTINUE
      IX = 31
      IF (T .GE. 1. .AND.  ICOUT .EQ. 1)GOTO 1
       RETURN
1      WRITE(2,10) (U(1,K), K=1,31)
10     FORMAT(31F7.2)
       IF (IMODE .EQ. 0) GOTO 5
       QTRAN = FRATE * CPA * (U(1,1) - U(1,31)) * 3600./1.D6
       IF (QTRAN .LT. 0.) QTRAN = 0.
       IF(J .LE. IRISE .OR. J .GE. ISET) TPOUT = U(1,1)
       IF(J .GT. IRISE .AND. J .LT. ISET)TPOUT = U(1,31)
       ICOUT = 2
```

```
       RETURN
5      QTRAN = 0.
       TPOUT = 99.
       RETURN
      END
C
      SUBROUTINE FUNC(F, U, UX, UXX, T, X, IX, NPDE)
      IMPLICIT REAL*8(A-H, O-Z)
      DIMENSION F(1), U(1), UX(1), UXX(1)
      RETURN
      END
C
      SUBROUTINE BNDRY(T, UL, AL, BL, CL, UR, AR, BR, CR, NPDE)
      IMPLICIT REAL*8(A-H, O-Z)
      COMMON/EQN/C4,C5,C6, TPIN, IMODE
      DIMENSION UR(1), AR(1), BR(1), CR(1), UL(1), AL(1), BL(1), CL(1)
      AL(1) = 0.
      BL(1) = 0.
      CL(1) = 0.
      IF(IMODE .EQ. 0)RETURN
      IF(IMODE .EQ. 1)GOTO 1
      IF(IMODE .EQ. 2)GOTO 2
1     AL(1) = 1.
      BL(1) = 0.
      CL(1) = TPIN
      RETURN
2     AR(1) = 1.
      BR(1) = 0.
      CR(1) = TPIN
      RETURN
      END
C
C    SUBROUTINE *NTLOAD* to compute outside temperatures using Kimball and Bellamy's
C     modified Parton and Logan's equation, and thus hourly heat load
C
      SUBROUTINE NTLOAD (JA)
      IMPLICIT REAL*8 (A-H, O-Z)
      COMMON/AREAS/AB, AP, AC1, AC3, AG, APFACT
      COMMON/COVER/NNC
      COMMON/CONV/CW1, CW2, CW3, HW, HCA, HPA, HBA
      COMMON/DATA/TOUT, RHT(24), VW, RHSET
      COMMON/GEOM/GHL,GHW,BH,WH, RTILT1,RTILT2,S1,S3, GVOL
      COMMON/HEAT/TMAX(12), TMIN(12), HEATLD, QSUP, QPASS
      COMMON/OCCUR/ICALL, ICAL
      COMMON/PROP/RHOP, ALPP, RHOG, RKG, THG, TAULW, EPC, EPP
      COMMON/RADIAN/PSI,RDELC(12),RLAT,RWI(24),RBDN,RGAM(6),RBETA(6)
      COMMON/SUN/SR,SS, DA, WS, IRISE, ISET
      COMMON/SYSTEM/INSN, ISTDEV
      COMMON/INDEX/I, J
      LOGICAL INSN
C
      IF (ICAL .NE. 0) GOTO 3
      A = 1.86
      B = 2.2
      C = -0.17
      PI = 3.14159
      TIN = 17.
C
C    overall heat transfer coefficients of glazing, insulated wall and perimeter
C
```

```
      IF (NNC .EQ. 1) RHRHC = 0.
      IF (NNC .EQ. 2) RHRHC = 0.166667
      RGLAZE = 0.12063 + NNC*THG/RKG + RHRHC + 1./HW
      UGLAZE = 1./RGLAZE
      RNW = 0.12063 + 2.8148 + 0.4587 + 1./HW
      UNW = 1./RNW
      UPERIM = 1.39
      NAEV = 1.0
C
      IF (.NOT. (INSN))GOTO 1
       AC = AC1
       AW = WH * GHL
       ANW = (S3 + WH/DSIN(RTILT2)) * GHL
       GOTO 2
1      AC = AC1 + AC3
       AW = 2. * (WH * GHL)
       ANW = 0.
2     AGB = 2. * GVOL/GHL
      PERIM = (GHW+GHL) * 2.
      UA = UGLAZE*(AGB + AC + AW) + UNW*ANW + UPERIM*PERIM + 0.373*GVOL*NAEV
C
      IR = IRISE - 1
      IS = ISET + 1
3     IHRMIN = DINT(IRISE + C)
      T1 = PI * (ISET - IHRMIN)
      T6 = DA + 2.*A
      T2 = (TMAX(I) - TMIN(I)) * DSIN(T1/T6)
      TSET = TMIN(I) + T2
      D1 = TSET - TMIN(I)
      D2 = DEXP(B) - 1.
      DISP = D1/D2
C
      IF (JA .LT. ISET)GOTO 5
      T3 = -B * (JA - ISET)/(24. - DA + C)
      T4 = TSET - (TMIN(I) - DISP)
      T5 = T4 * DEXP(T3)
      TOUT = (TMIN(I) - DISP) + T5
      GOTO 6
5     T18 = PI * (JA - IHRMIN)
      T19 = (TMAX(I) - TMIN(I)) * DSIN(T18/T6)
      TOUT = TMIN(I) + T19
6     IF (JA .GT. ISET) TIN = 17.
      IF (JA .LT. ISET) TIN = 22.
      HEATLD = UA * (TIN - TOUT) * 3600./1.D6
      ICAL = 1
      RETURN
      END
```

Appendix A

Direct radiation interception factor and diffuse radiation view factor

The expressions for P_{kj} and F_{kj} are derived, or otherwise extracted from the literature.

A. P_{kj}

ψ = solar azimuth angle
γ = surface azimuth angle
$\theta = \psi - \gamma$
α = solar elevation angle
ξ = surface tilt angle
L = length of the greenhouse
W = width of the greenhouse
h = distance from plant canopy (gutter height) level to ridge

If $\theta = 90^o$, then direct radiation from the sun is at grazing incidence to the receiving surface. If $|\theta| > 90^o$, then direct radiation does not impinge onto the receiving surface in such a way as to transmit into the house. For the situation $|\theta| < 90^o$, then there are a few possible situations.

For an east-west oriented greenhouse

I. South Roof

Fig. A1.1 shows the projection onto the plant canopy level of a gable-roof type greenhouse, as direct sunlight enters through the south roof. Alternative configurations are shown in Fig. A1.2, where plans of the horizontal surface area covered by the direct radiation are indicated. In each of the cases, the total area of the ground covered by direct radiation entering through the south roof is equal to area $AXYB$.

Case 1.

$$|AP| \geq W$$
$$|PX| < L$$

where

$$AP = W_1 + h \cot\alpha \cos\theta$$
$$PX = h \cot\alpha \sin\theta$$

note: for CV house, $W_1 = W/2$, and for SS and BS, $W_1 = W$

$$P_{kp} = \frac{\text{area}ANFB}{\text{area}AXYB}$$

Let$AE = W, EF = L$

since:

$$\begin{aligned}
\text{area}ANFB &= \text{area}AEFB - \text{area}AEN \\
\text{area}AEFB &= AE.EF \\
\text{area}AEN &= \frac{1}{2}AE.EN \\
\text{area}AXYB &= AP.EF \\
EN/PX &= AE/AP,
\end{aligned}$$

hence:

$$\begin{aligned}
EN &= AE.PX/AP \\
\text{area}AEN &= \frac{1}{2}AE^2.PX/AP
\end{aligned}$$

from which:

$$P_{kp} = \frac{WL - \frac{1}{2}\left(\frac{W^2 h \cot\alpha \sin\theta}{W_1 + h\cot\alpha\cos\theta}\right)}{L(W_1 + h\cot\alpha\cos\theta)}$$

Special case:

at noon, $\psi = 0$, therefore $\theta = 0$

CV:

$$P_{kp} = \frac{2}{1 + \tan\xi\cot\alpha}$$

SS, BS:

$$P_{kp} = \frac{1}{1 + \tan\xi\cot\alpha}$$

The interception factor, P_{kq}, for the SS vertical absorber plate acting as the receiving surface may be derived in a similar manner, thus

$$P_{kq} = \frac{hL - \frac{1}{2}\left(\frac{h^2 W_1 \tan\alpha \sin\theta}{h + W_1 \tan\alpha \cos\theta}\right)}{L(h + W_1 \tan\alpha \cos\theta)}.$$

Case 2.

$$|PX| \geq L$$

$$P_{kp} = \frac{\text{area}ANB}{\text{area}AXYB}$$

since:

$$BN/QX = AB/AQ,$$
$$AB = EF, QX = AP, AQ = PX,$$
$$\text{area}ANB = \frac{1}{2}AB.BN$$

hence:

$$BN = AB.QX/AQ$$
$$\text{area}ANB = \frac{1}{2}AB^2.QX/AQ$$

from which:

$$P_{kp} = \frac{L}{2h\cot\alpha\sin\theta}$$

Similarly

$$P_{kq} = \frac{L}{2W_1\tan\alpha\sin\theta}$$

Case 3.

$$|AP| < W$$
$$|PX| < L$$

The situation of $|AP| < W$ would not occur in a the SS type house. For other house types,

$$P_{kp} = \frac{\text{area}AXNB}{\text{area}AXYB}$$

since:

$$\text{area}AXNB = \text{area}APNB - \text{area}APX$$
$$\text{area}APNB = AB.AP$$
$$\text{area}APX = \frac{1}{2}AP.PX$$

hence:

$$P_{kp} = 1 - \frac{h}{2L}\cot\alpha\sin\theta$$

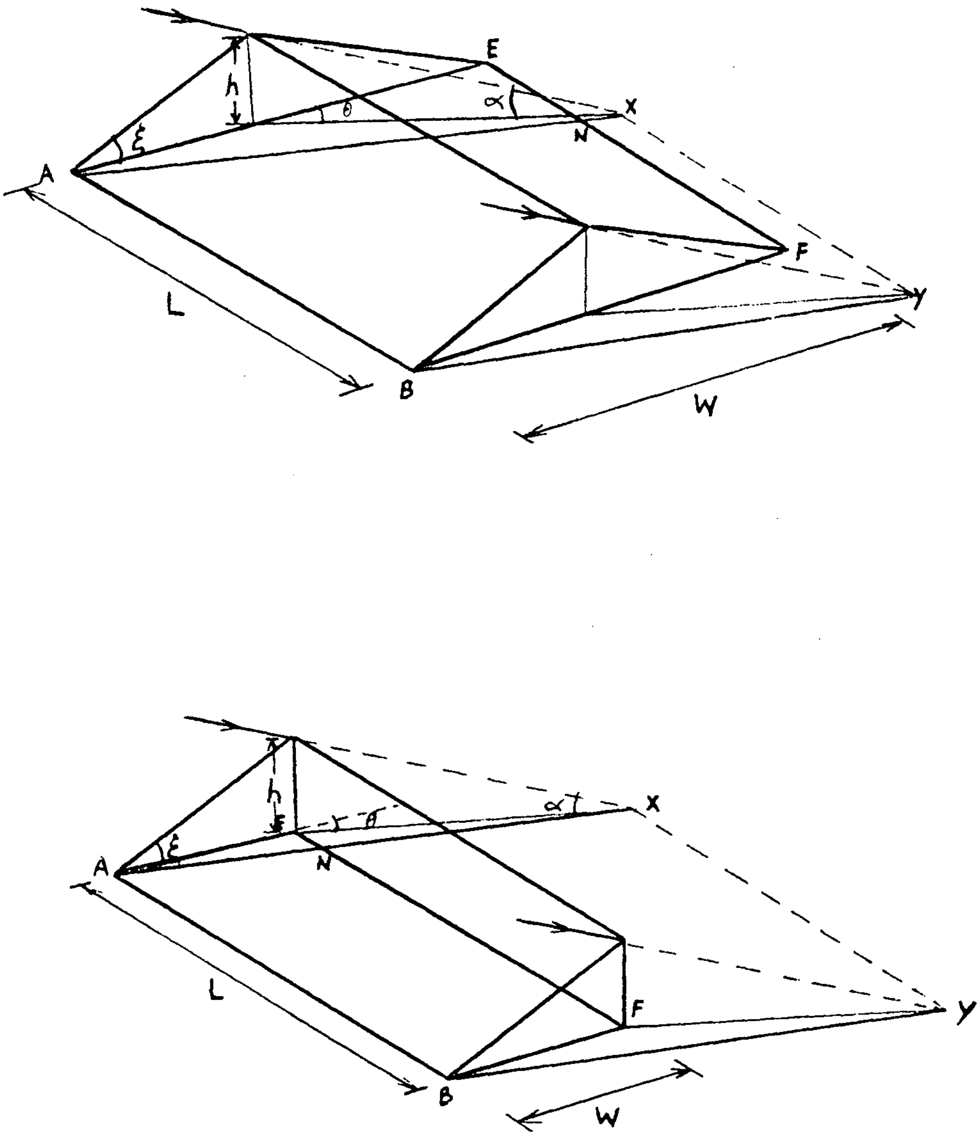

Fig. A1.1 Direct sunlight through south roof
above: CV shaped greenhouse
below: SS shaped greenhouse

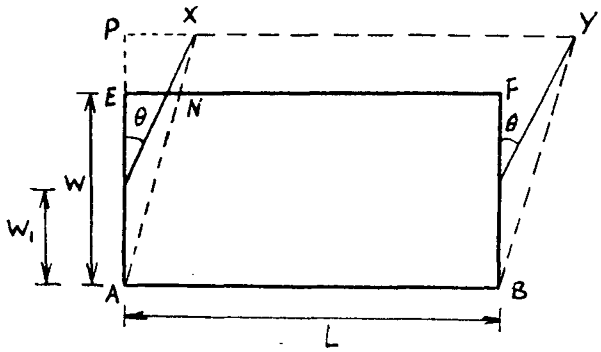

CV shape

Case 1

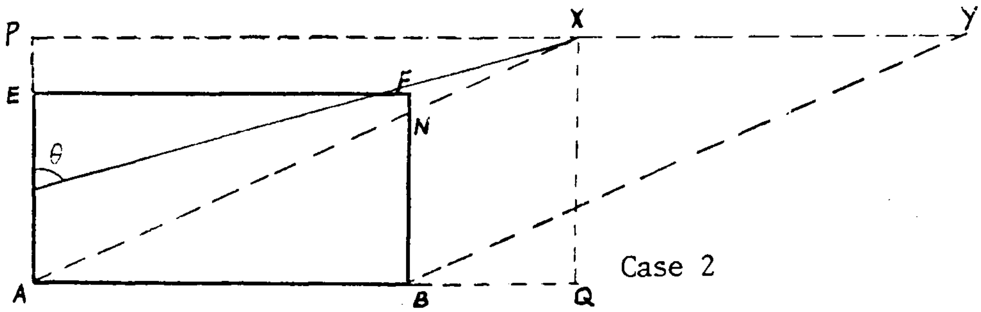

Case 2

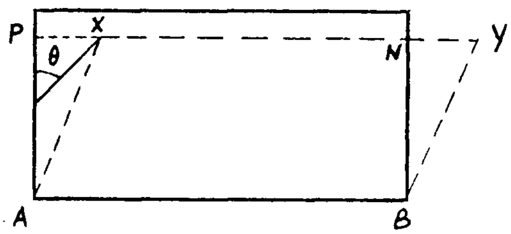

Case 3

Fig. A1.2 Intersection of direct sunlight through roof surface facing the sun (south roof) and the plane at the gutter height (plant canopy) level. Alternative configurations.

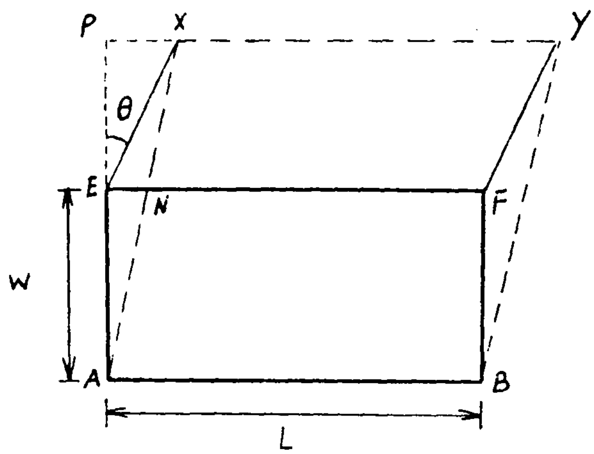

SS shape

Case 1

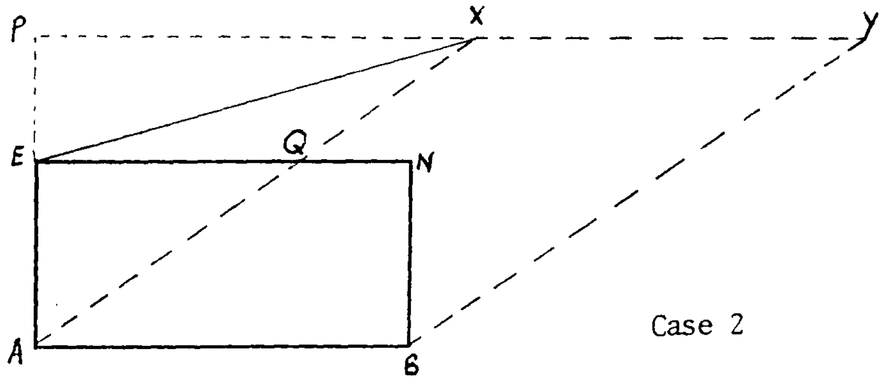

Case 2

II. North Roof

This only applies to the CV house. Referring to Fig. A1.3 which shows the projection of direct radiation onto the plant canopy level as it enters through the north roof, $P_{kp} = 0$ if

$$|MP| \geq W_1$$

or

$$|PX| \geq L$$

Since the projection of the end point of the ridge lies outside the floor area in these situations, only one principal case shall be considered:

$$|MP| < W_1$$

$$|PX| < L$$

$$P_{kp} = \frac{\text{area}XEFP}{\text{area}XEFY}$$

Again, let $AE = W, EF = L$

since:

$$\text{area}XEFP = \text{area}XEFY - \text{area}FPY$$

$$\text{area}XEFY = EF.FP$$

$$FN = W_1 - h \cot \alpha \cos \theta$$

$$FPY = \frac{1}{2} FP.PY$$

$$PY = h \cot \alpha \sin \theta$$

hence:

$$\text{area}FPY = \frac{1}{2}(W_1 - h \cot \alpha \cos \theta)(h \cot \alpha \sin \theta)$$

from which:

$$P_{kp} = 1 - \frac{h}{2L} \cot \alpha \sin \theta$$

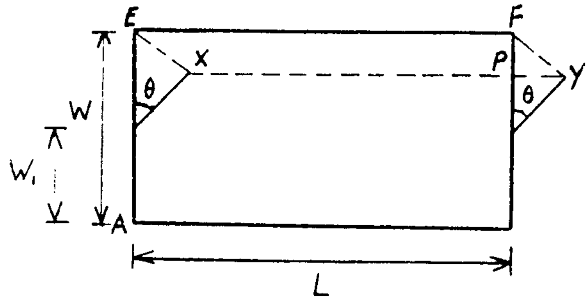

Fig. A1.3 Intersection of direct sunlight through roof surface facing away from the sun (north roof) and the plane at the gutter height level.

III. East and West Gable Ends

The development of criteria for the alternative situations where direct sunlight enters through the end walls follows in a similar manner. As Smith and Kingham (1971) did in their analyses, it was assumed that an end wall might be regarded as being of rectangular dimensions W and $h/2$ for the portion above the gutter height level.

Case 1.

$$|AP| < W_1$$
$$|PY| < L$$

where

$$AP = h_1 + h\cot\alpha\sin\theta$$
$$PY = h_1\cot\alpha\cos\theta$$
$$h_1 = h/2$$

For the CV house, this situation implies the entire projection of direct sunlight lies within the greenhouse floor area, hence $P_{kp} = 1.0$

Otherwise

$$P_{kp} = \frac{\text{area}AENY}{\text{area}AEXY}$$

since:

$$\text{area}AENY = \text{area}AEXY - \text{area}ENX$$
$$\text{area}AEXY = AE.EN$$
$$\text{area}ENX = \frac{1}{2}EN.NX$$
$$NX = AP, EN = PY$$

hence:

$$\text{area}ENX = \frac{1}{2}(h_1\cot\alpha\cos\theta)(h_1\cot\alpha\sin\theta)$$

from which:

$$P_{kp} = 1 - \frac{h_1}{2W_1}\cot\alpha\sin\theta$$

Similarly,

$$P_{kq} = 1 - \frac{W_1}{2h_1} \tan\alpha \sin\theta$$

Case 2.

$$|AP| \geq W_1$$
$$|PY| < L$$

SS:

$$P_{kp} = \frac{\text{area}AEN}{\text{area}AEXY}$$

since:

$$\text{area}AEXY = AE.EY = W_1(h_1 \cot\alpha \cos\theta)$$
$$\text{area}AEN = \frac{1}{2}AE.EN$$
$$AE = W_1, EN = AE \cot\theta$$

hence:

$$P_{kp} = \frac{1}{2}\frac{W_1 \tan\alpha}{h_1 \sin\theta}$$

Similarly,

$$P_{kq} = \frac{1}{2}\frac{h_1 \cot\alpha}{W_1 \sin\theta}$$

CV:

$$P_{kp} = \frac{\text{area}AEQNY}{\text{area}AEXY}$$

since:

$$\text{area}AEQNY = \text{area}AEXY - \text{area}QNX$$
$$\text{area}QNX = \frac{1}{2}(h_1 \cot\alpha \sin\theta - W_1)^2 \cot\theta$$
$$QN = PX \cot\theta$$
$$PX = h_1 \cot\alpha \sin\theta - W_1$$

hence:

$$\text{area}QNX = \frac{1}{2}QN.NX$$

from which:

$$P_{kp} = 1 - \frac{\text{area}QNX}{\text{area}AEXY}$$

$$= 1 - \frac{(h_1 \cot\alpha \sin\theta - W_1)^2}{2W_1 h_1 \cot\alpha \sin\theta}$$

Case 3.

$$|PY| \geq L$$

SS:

$$P_{kp} = \frac{\text{area}AEFN}{\text{area}AEXY}$$

since:

$$\text{area}AEFN = \text{area}AEFB - \text{area}ANB$$
$$\text{area}AEFB = AE.AB = WL$$
$$\text{area}AEXY = AE.PY = Wh_1 \cot\alpha \cos\theta$$
$$\text{area}ANB = \frac{1}{2}AB.BN$$
$$BN = AB \tan\theta$$

hence:

$$\text{area}ANB = \frac{1}{2}L^2 \tan\theta$$

from which:

$$P_{kp} = \frac{WL - \frac{1}{2}L^2 \tan\theta}{Wh_1 \cot\alpha \cos\theta}$$

CV:

$$P_{kp} = \frac{\text{area}AEQNR}{\text{area}AEXY}$$

since:

$$\text{area}AEQNR = \text{area}ACNB - \text{area}ECQ - \text{area}ABR$$

$$\text{area}ACNB = WL$$

$$\text{area}ECQ = \frac{1}{2}EC.CQ$$

$$\text{area}ABR = \frac{1}{2}AB^2 \tan\theta$$

$$CQ = EC \cot\theta$$

$$BR = AB \tan\theta$$

hence:

$$\text{area}ECQ = \frac{1}{2}EC^2 \cot\theta$$

$$\text{area}ABR = \frac{1}{2}AB.BR$$

and

$$P_{kp} = \frac{WL - \frac{1}{2}(W_1^2 \cot\theta + L^2 \tan\theta)}{W_1 h_1 \cot\alpha \cos\theta}$$

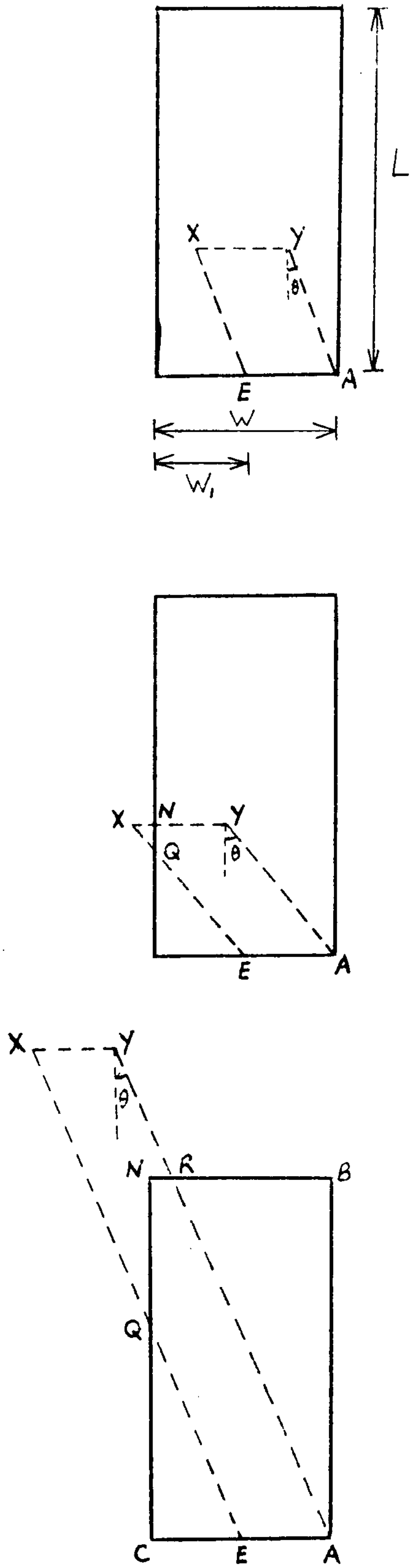

CV shape

Case 1

Case 2

Case 3

Fig. A1.4 Intersection of direct sunlight through either gable end and the plane at the gutter height level

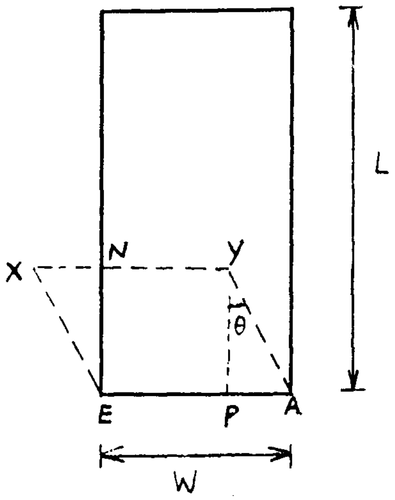

SS shape

Case 1

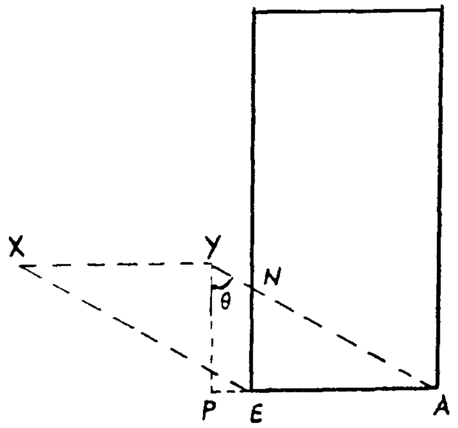

Case 2

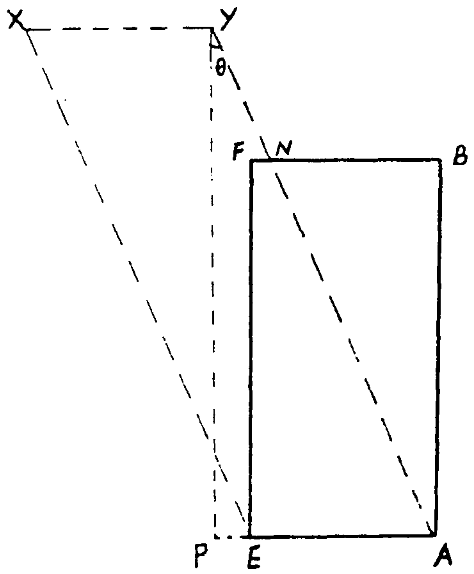

Case 3

B. F_{kj}

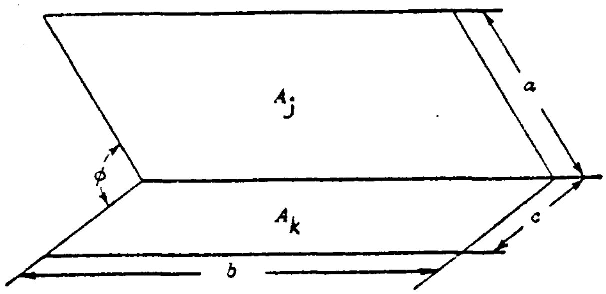

$L = c/b$; $N = a/b$.

$$
\begin{aligned}
F_{k-j} = {} & \\
\frac{1}{\pi L} \Bigg[\!\Bigg[& -\tfrac{1}{4}\sin 2\Phi \left[NL\sin\Phi + (\tfrac{1}{2}\pi - \Phi)(N^2+L^2) + L^2\tan^{-1}\left(\frac{N - L\cos\Phi}{L\sin\Phi}\right) + N^2\tan^{-1}\left(\frac{L - N\cos\Phi}{N\sin\Phi}\right)\right] \\
& + \tfrac{1}{4}\sin^2\Phi \ln\left\{\left[\frac{(1+N^2)(1+L^2)}{1+N^2+L^2-2NL\cos\Phi}\right]^{\operatorname{cosec}^2\Phi+\cot^2\Phi} \left[\frac{L^2(1+N^2+L^2-2NL\cos\Phi)}{(1+L^2)(N^2+L^2-2NL\cos\Phi)}\right]^{L^2}\right\} \\
& + \tfrac{1}{4}N^2\sin^2\Phi \ln\left[\left(\frac{N^2}{N^2+L^2-2NL\cos\Phi}\right)\left(\frac{1+N^2}{1+N^2+L^2-2NL\cos\Phi}\right)^{\cos^2\Phi}\right] + L\tan^{-1}\frac{1}{L} \\
& + N\tan^{-1}\left(\frac{1}{N}\right) - \sqrt{(N^2+L^2-2NL\cos\Phi)}\cot^{-1}\sqrt{(N^2+L^2-2NL\cos\Phi)} \\
& + \tfrac{1}{2}N\sin\Phi\sin 2\Phi\sqrt{(1+N^2\sin^2\Phi)}\left[\tan^{-1}\left(\frac{N\cos\Phi}{\sqrt{(1+N^2\sin^2\Phi)}}\right) + \tan^{-1}\left(\frac{L - N\cos\Phi}{\sqrt{(1+N^2\sin^2\Phi)}}\right)\right] \\
& + \cos\Phi\int_0^L \sqrt{(1+z^2\sin^2\Phi)}\left[\tan^{-1}\left(\frac{N - z\cos\Phi}{\sqrt{(1+z^2\sin^2\Phi)}}\right) + \tan^{-1}\left(\frac{z\cos\Phi}{\sqrt{(1+z^2\sin^2\Phi)}}\right)\right] dz \Bigg]\!\Bigg].
\end{aligned}
$$

(source: Feingold, 1966)

Appendix B

<u>Psychrometrics</u>:The following equations are used in the calculation of psychrometric properties that are carried out at various parts of the simulation.

1. saturation vapor pressure

   for $-40^{o}C \leq t_{db} \leq 0^{o}C$

$$P_{w,s} = exp[89.63121 - 7511.52/T + 0.02399897T - 1.1654551(10^{-5})T^2 - 1.2810336(10^{-8})T^3 + 2.0998405(10^{-11})T^4 - 12.150799\ ln\ T]$$

   for $0^{o}C \leq t_{db} \leq 120^{o}C$

$$P_{w,s} = exp[24.2779 - 6238.64/T - 0.344438\ ln\ T]$$

   where $T = t + 273.16$

2. actual vapor pressure

$$P_w = (RH)(P_{w,s})/100$$

   note: long-term U.S. weather data gives t_{dp} rather than RH. In this case, P_w is solved as a root of the quadratic shown in item 5 below.

3. humidity ratio

$$W = 0.622P_w/(P_{atm} - P_w)$$

$$W^* = 0.622P_{w,s}/(P_{atm} - P_{w,s})$$

4. enthalpy

$$h = 1.006t_{db} + W(2501 + 1.775t_{db})$$

   for $-50^{o}C \leq t_{db} \leq 110^{o}C$

5. dew-point temperature

   for $-50^{o}C \leq t_{db} \leq 0^{o}C$

$$t_{dp} = 5.994 + 12.41\ ln\ P_w + 0.4273(ln\ P_w)^2$$

   for $0^{o}C \leq t_{db} \leq 50^{o}C$

$$t_{dp} = 6.983 + 14.38\ ln\ P_w + 1.079(ln\ P_w)^2$$

Appendix D

Appendix D - Data acquisition equipment

Solar radiation - sensor locations are shown in Fig. A4.1

variable	device	model
outside global radiation	silicon photodiode pyranometer	Li-Cor LI-200SB
outside diffuse radiation	ditto, with shadow band	2010 S
transmitted radiation	photovoltaic pyranometer	Rho-Sigma RS-1008
inside PAR	photosynthetic irradiance sensor	Li-Cor LI-190SEB

Temperature - sensor locations are shown in Figs. A4.2, A4.3

greenhouse air temperature	thermistors or T-type thermocouples	Fenwal UUA-33J1 or Omega PR-T-24
absorber plate temperature		
storage inlet and outlet temperatures		
rockbed temperatures		
soil storage temperatures		
plant canopy temperature	Infrared thermometer	
greenhouse cover temperature		

<u>Others - sensor locations are shown in Fig. A4.2</u>

charging and discharging air flow rates	hot wire anemometer	Flowtronic 55B1 (AC-powered)
energy consumption	hot water flow meters	A.B. Svensk Varmematning SVMK-241-047-3
relative humidity	wet and dry bulb thermometers	

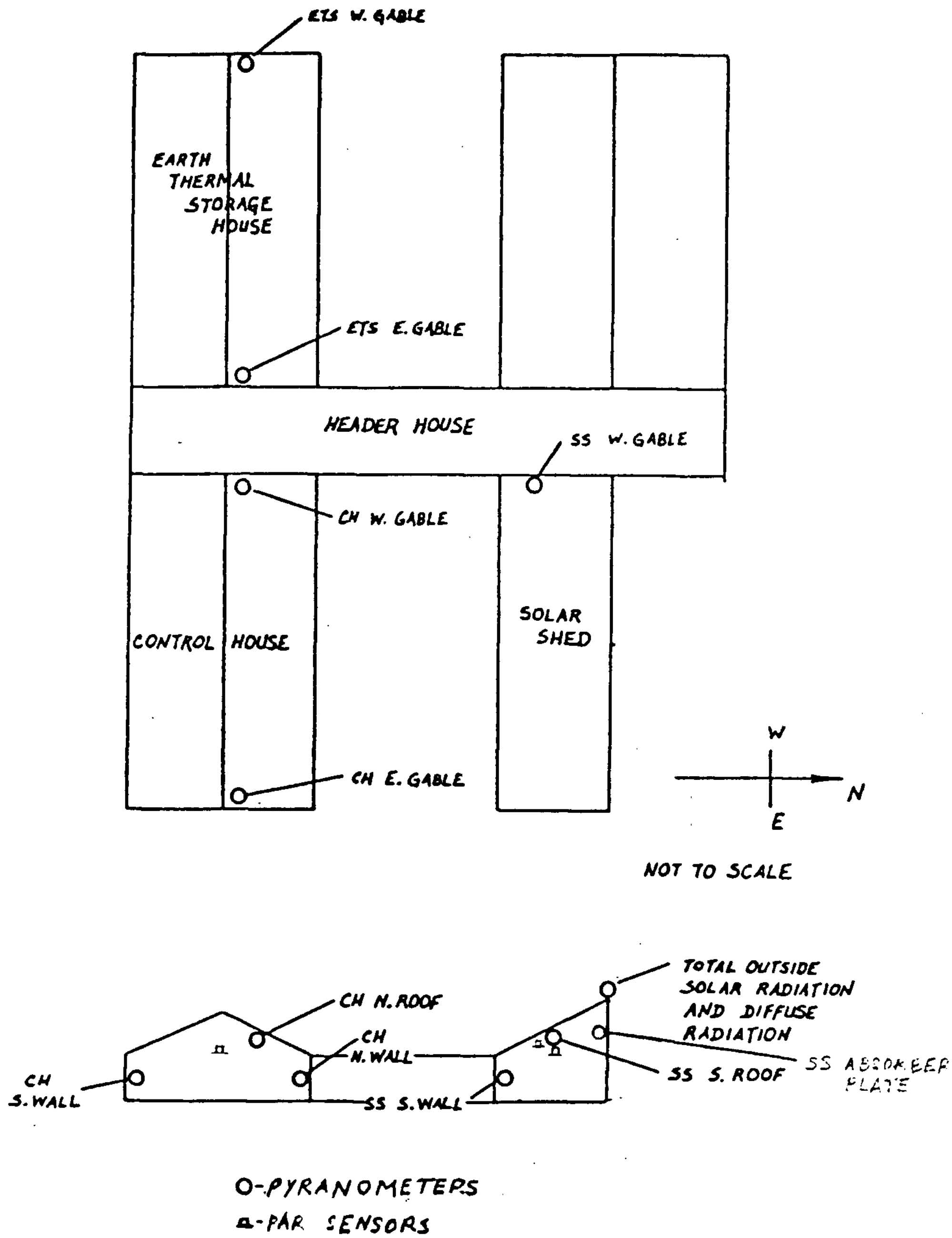

Fig. A4.1 Layout of research greenhouses at Agriculture Canada Saanichton Station and locations of solar radiation sensors

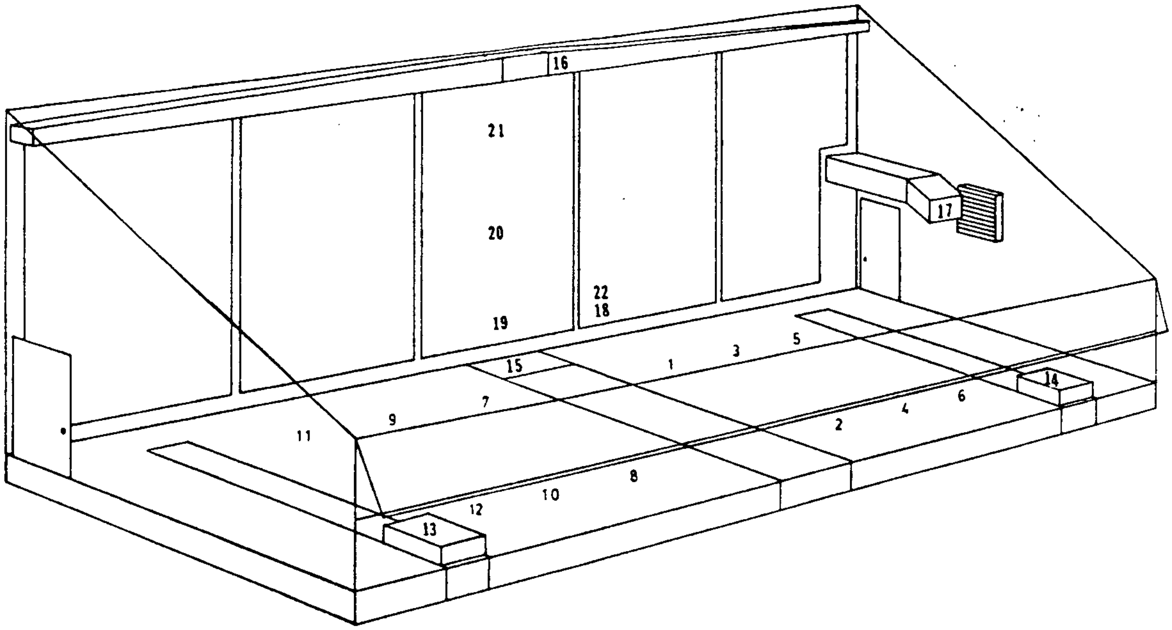

sensor

1-6	rockbed temperatures (east storage chamber)
7-12	rockbed temperatures (west storage chamber)
	1,4,5; 8,9,12: at a depth of 0.36 m 2,3,6; 7,10,11:at a depth of 0.76 m
13,14	storage outlet air temperature
15	storage inlet (central plenum) temperature
16	peak collecting duct air temperature
17	heating duct outlet temperature
18	greenhouse air temperature at gutter height level
19-21	absorber plate temperatures
22	relative humidity at plant canopy level

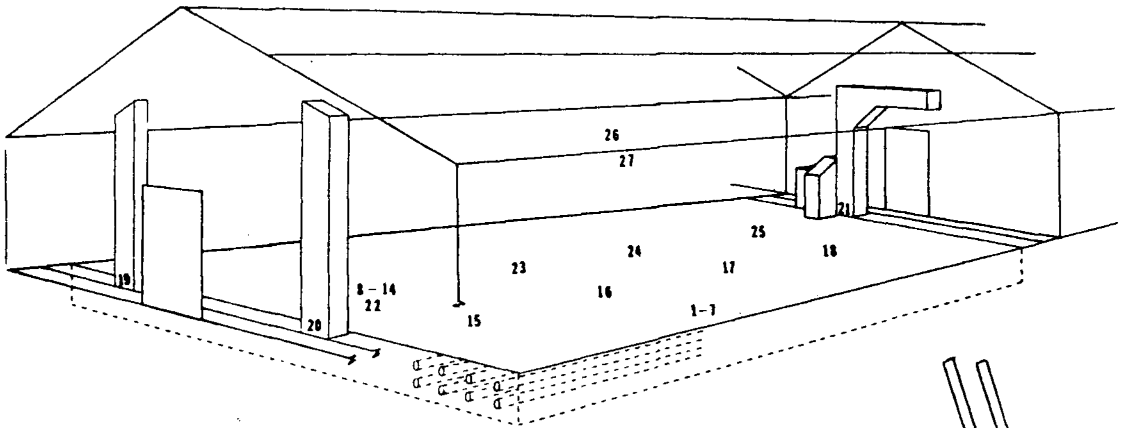

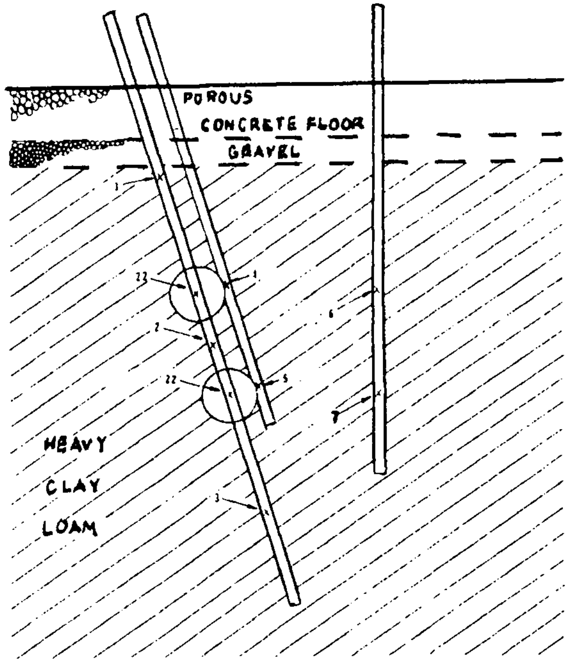

sensor

1-7	soil temperatures near edge region
8-14	soil temperatures near center region
15-18	soil temperatures along the pipe's longitudinal axis
19,20	pipe inlet air temperature
21	pipe outlet air temperature
22-25	pipe air temperature
26	greenhouse air temperature at gutter height level
27	relative humidity at plant canopy level

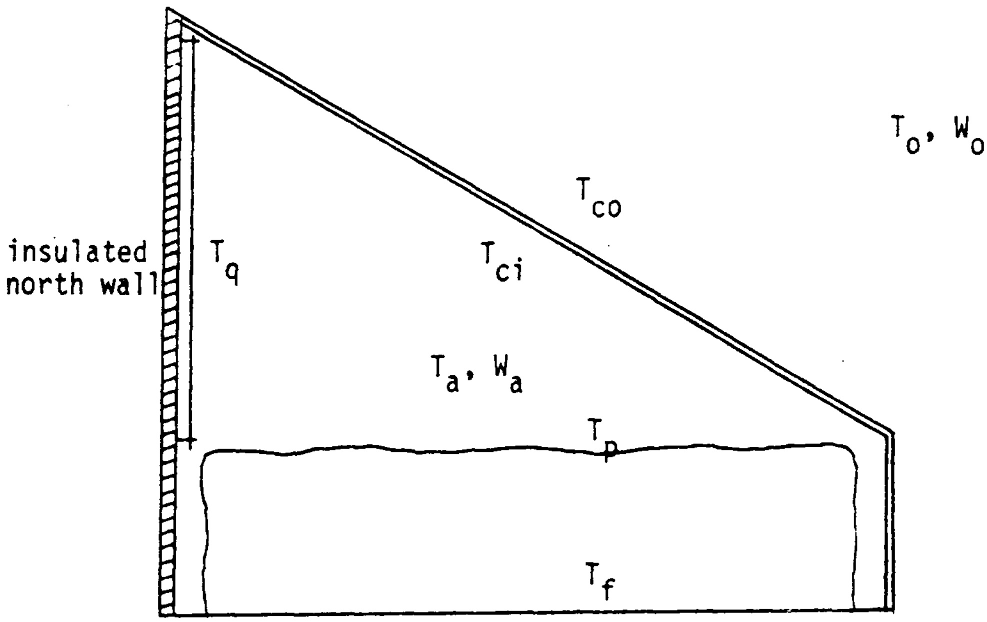

a: inside air
ci: inside surface of greenhouse cover
co: outside surface of greenhouse cover
f: greenhouse floor
p: plant canopy
q: vertical absorber plate

Fig. A6.1 Greenhouse thermal environment model - temperatures and humidity ratio

Appendix E

```
C
C    *DESIGN* to generate annual solar contribution and solar
C    heating fraction using the simplified design procedure (Lau, 1987)
C
C    by Anthony K. Lau
C
C      inputs: latitude
C              monthly declination angle
C              mean daily outside global solar radiation
C              mean daily maximum outside air temperature
C              mean daily miminum outside air temperature
C              greenhouse floor area, length-to-width ratio, roof tilts, wall height
C              overall heat loss coefficient
C              conventional greenhouse (CV) collection method (T or F)
C              thermal storage device (1 for rockbed, 2 for soil)
C              design alternatives (1, 2, 3, 4 for each storage device)
C
      IMPLICIT REAL*8 (A-H, O-Z)
      COMMON/CALL/ICAL
      COMMON/INDEX/I,J
      COMMON/HEAT/TMAX(12), TMIN(12), DTD(12), DTN(12), TOUT(20,30)
      COMMON/SUN/SR,SS, DA(12), IRISE(12), ISET(12)
      COMMON/RADIAN/RDELC(12),RLAT
      DIMENSION DELC(12), IR(12), IS(12), TMX(12), TMN(12)
      DIMENSION H(12),S(12),SP(12),TAUE(12),TAU(12), SLR(12),FS(12),FM(12)
      DIMENSION QDY(12), QNT(12), QTL(12), QL(12), QDL(12), QNL(12)
      LOGICAL CV
      READ(4,16) DLAT
      READ(4,16) (DELC(I), I=1,12)
      READ(4,16) (H(I), I=1,12)
      READ(4,16) (TAUE(I), I=1,12)
      READ(4,16) (TMAX(I), I=1,12)
      READ(4,16) (TMIN(I), I=1,12)
      READ(4,16) AP, RLWR, WH, TILT1, TILT2, UGLAZE
      READ(4,17) CV
      READ(4,15) ISTDEV
      READ(4,15) ICASE
15    FORMAT(I1)
16    FORMAT(15F8.0)
17    FORMAT(L1)
C
      GHW = DSQRT(AP/RLWR)
      GHL = AP/GHW
      PI = 3.14159
      RLAT = DLAT * PI/180.
      RTILT1 = TILT1 * PI/180.
      RTILT2 = TILT2 * PI/180.
      DO 90 I=1,12
       RDELC(I) = DELC(I) * PI/180.
90    CONTINUE
C
      IF(TILT1 .EQ. 90.)T21 = 1./DTAN(RTILT2)
      IF(TILT2 .EQ. 90.)T21 = 1./DTAN(RTILT1)
      IF(TILT2 .NE. 90.)T21 = 1./DTAN(RTILT1) + 1./DTAN(RTILT2)
      BH = GHW/T21
      S1 = BH/DSIN(RTILT1)
      S3 = BH/DSIN(RTILT2)
      AC1 = S1*GHL
      AC3 = S3*GHL
      AG = BH * GHW * 0.5
```

```
      GVOL = (AG + WH*GHW) * GHL
      UNW = 0.29
      UPERIM = 1.39
      NAEV = 1.0
C
      IF (CV) GOTO 3
       AC = AC1
       AW = WH * GHL
       ANW = (S3 + WH/DSIN(RTILT2)) * GHL
       GOTO 5
3      AC = AC1 + AC3
       AW = 2. * (WH * GHL)
       ANW = 0.
5     AGB = 2. * GVOL/GHL
      AGLAZE = AC + AW + AGB
      PERIM = (GHW+GHL) * 2.
      UA = UGLAZE*AGLAZE + UNW*ANW + UPERIM*PERIM + 0.373*GVOL*NAEV
C
      IF (ISTDEV .EQ. 1) GOTO 8
      IF (ISTDEV .EQ. 2) GOTO 9
8     IF (ICASE .EQ. 1) GOTO 81
      IF (ICASE .EQ. 2) GOTO 82
      IF (ICASE .EQ. 3) GOTO 83
      IF (ICASE .EQ. 4) GOTO 84
9     IF (ICASE .EQ. 1) GOTO 91
      IF (ICASE .EQ  2) GOTO 92
      IF (ICASE .EQ. 3) GOTO 93
      IF (ICASE .EQ. 4) GOTO 94
C
81    AO =1.03
      A1 = -1.00
      A2 = 0.
      B1 = -1.96
      B2 = 0.
      GOTO 6
82    AO =1.15
      A1 = -0.89
      A2 = -0.35
      B1 = -0.82
      B2 = -9.18
      GOTO 6
83    AO =1.13
      A1 = -0.71
      A2 = -0.44
      B1 = -0.61
      B2 = -3.24
      GOTO 6
84    AO =0.80
      A1 = -0.44
      A2 = -0.39
      B1 = -0.73
      B2 = -6.38
      GOTO 6
C
91    AO =0.87335
      A1 = -2151.4783
      A2 = 2150.6968
      B1 = -0.83676
      B2 = -0.83657
      GOTO 6
```

```
92    AO =0.854
      A1 = -0.759
      A2 = 0.055
      B1 = -1.19
      B2 = -9.762
      GOTO 6
93    AO =0.791
      A1 = -0.588
      A2 = -0.752
      B1 = -1.002
      B2 = -22.4
      GOTO 6
94    AO =0.771
      A1 = -0.574
      A2 = -1.185
      B1 = -0.976
      B2 = -27.64
C
6     DO 10 IK = 9, 17
       ICAL = 0
       DTD(I) = 0.
       DTN(I) = 0.
       IF (IK .GT. 12) I = IK - 12
       IF (IK .LE. 12) I = IK
C
       CALL RISET
C
       IR1=IRISE(I) + 1
       IR24 = IRISE(I) + 24
       DO 20 JA = IR1, IR24
        IF (JA .LE. 24) J = JA
        IF (JA .GT. 24) J = JA - 24
        CALL NTLOAD (JA)
20     CONTINUE
C
       QDL(I) = DTD(I) * UA * 3600./1.D6
       QNL(I) = DTN(I) * UA * 3600./1.D6
       QL(I) = QDL(I) + QNL(I)
10    CONTINUE
C
      DO 40 IK = 9, 17
       IF (IK .GT. 12) GOTO 1
        IJ = IK
        I = IJ - 8
        GOTO 2
1       IJ = IK - 12
        I = IK - 8
2      IR(I) = IRISE(IJ)
       IS(I) = ISET(IJ)
       TMX(I) = TMAX(IJ)
       TMN(I) = TMIN(IJ)
       QDY(I) = QDL(IJ)
       QNT(I) = QNL(IJ)
       QTL(I) = QL(IJ)
C
       TAU(I) = TAUE(IJ)
       S(I) = H(IJ)
       SP(I) = S(I) * TAU(I)
       SLR(I) = AP * S(I) * TAU(I)/QTL(I)
       FS(I) = AO + A1*DEXP(B1*SLR(I)) + A2*DEXP(B2*SLR(I))
```

```
      IF (SLR(I) .LE. O.) FS(I) = O.
      FM(I) = -O.007 + O.03*FS(I) + O.92*(FS(I)**2)
      IF (FS(I) .GT. 1.) FS(I) = 1.
      IF (FS(I) .LT. O.) FS(I) = O.
      IF (FM(I) .GT. 1.) FM(I) = 1.
      IF (FM(I) .LT. O.) FM(I) = O.
      SUMQ = SUMQ + QTL(I)
      SUMS = SUMS + (FS(I) * QTL(I))
      SUMM = SUMM + (FM(I) * QTL(I))
40    CONTINUE
      FSY = SUMS/SUMQ
      FMY = SUMM/SUMQ
C
      WRITE(5,61) DLAT
61    FORMAT(/'LATITUDE =', F10.2/)
      WRITE(5,63)
63    FORMAT(/'GHL       GHW      AP     RLWR     GVOL    TILT1    TILT2       UA       CV  ISTDEV    ICASE'/)
      WRITE(5,29)GHL,GHW,AP,RLWR,GVOL,TILT1,TILT2, UA, CV, ISTDEV,ICASE
29    FORMAT(F5.1, F8.1, 3F8.O, 2F8.1, F8.O, L8, 2I8)
      WRITE(5,62)
62    FORMAT(/5X,'     Sep     Oct     Nov     Dec     Jan     Feb     Mar     Apr     May')
      WRITE(5,22) (IR(I),  I=1, 9)
      WRITE(5,23) (IS(I),  I=1, 9)
      WRITE(5,24) (TMX(I), I=1, 9)
      WRITE(5,25) (TMN(I), I=1, 9)
      WRITE(5,26) (QDY(I), I=1, 9)
      WRITE(5,27) (QNT(I), I=1, 9)
      WRITE(5,28) (QTL(I), I=1, 9)
      WRITE(5,31) (S(I), I=1, 9)
      WRITE(5,32) (TAU(I), I=1, 9)
      WRITE(5,36) (SP(I), I=1, 9)
      WRITE(5,33) (SLR(I), I=1, 9)
      WRITE(5,34) (FS(I), I=1, 9)
      WRITE(5,38) (FM(I), I=1,9)
      WRITE(5,35) FSY, FMY
21    FORMAT(I5, 9F8.2)
22    FORMAT(/'IRISE', 9I8)
23    FORMAT('ISET ', 9I8)
24    FORMAT(/'TMAX ', 9F8.2)
25    FORMAT('TMIN ', 9F8.2)
26    FORMAT(/'QDL  ', 9F8.O)
27    FORMAT('QNL  ', 9F8.O)
28    FORMAT('QL   ', 9F8.O)
31    FORMAT(/'HBAR ', 9F8.2)
32    FORMAT('TAU  ', 9F8.2)
36    FORMAT('HP   ', 9F8.2)
33    FORMAT(/'SLR  ', 9F8.2)
34    FORMAT(/'FS   ', 9F8.2)
38    FORMAT(/'FM   ', 9F8.2)
35    FORMAT(/'annual fs, fm =', 2F10.3)
      STOP
      END
```

```
C
C  SUBROUTINE *RISET* to compute sunrise and sunset hours
C
      SUBROUTINE RISET
      IMPLICIT REAL*8(A-H, O-Z)
      COMMON/INDEX/I, J
      COMMON/SUN/SR,SS, DA(12), IRISE(12), ISET(12)
      COMMON/RADIAN/RDELC(12),RLAT


      PI = 3.14159
      WS = DARCOS(-DTAN(RLAT) * DTAN(RDELC(I)))
      DWS = WS * 180./PI
      DA(I) = DWS * 2./15.
      SR = 12. - DWS/15.
      SS = SR + DA(I)
      IRISE(I) = DINT(SR + 0.5)
      ISET(I) = DINT(SS + 0.5)
      RETURN
      END
C
C   SUBROUTINE *NTLOAD* to compute daily gross heating load
C
      SUBROUTINE NTLOAD (JA)
      IMPLICIT REAL*8 (A-H, O-Z)
      COMMON/CALL/ICAL
      COMMON/INDEX/I,J
      COMMON/HEAT/TMAX(12), TMIN(12), DTD(12), DTN(12), TOUT(20,30)
      COMMON/SUN/SR,SS, DA(12), IRISE(12), ISET(12)
C
      IF (I .GT. 5) IJ = I - 8
      IF (I .LE. 5) IJ = I + 4
      A = 1.86
      B = 2.2
      C = -0.17
      PI = 3.14159
      IHRMIN = DINT(IRISE(I) + C)
      T1 = PI * (ISET(I) - IHRMIN)
      T6 = DA(I) + 2.*A
      T2 = (TMAX(I) - TMIN(I)) * DSIN(T1/T6)
      TSET = TMIN(I) + T2
      D1 = TSET - TMIN(I)
      D2 = DEXP(B) - 1.
      DISP = D1/D2
      IF (J .GE. IRISE(I) .AND. J .LT. ISET(I))GOTO 5
C
       T3 = -B * (JA - ISET(I))/(24. - DA(I) + C)
       T4 = TSET - (TMIN(I) - DISP)
       T5 = T4 * DEXP(T3)
       TOUT(IJ, J) = (TMIN(I) - DISP) + T5
       TIN = 17.
       DTN(I) =  (TIN - TOUT(IJ, J)) + DTN(I)
       GOTO 6
5      T18 = PI * (J - IHRMIN)
       T19 = (TMAX(I) - TMIN(I)) * DSIN(T18/T6)
       TOUT(IJ, J) = TMIN(I) + T19
       TIN = 22.
       DTD(I) =  (TIN - TOUT(IJ, J)) + DTD(I)
6      RETURN
      END
```